TECHNISCHE UNIVERSITÄT WIEN
Vienna | Austria

DISSERTATION

Towards an improved mechanistic understanding of oxygen exchange kinetics on mixed conducting electrodes in solid oxide cells

ausgeführt zum Zwecke der Erlangung des akademischen Grades eines Doktors der technischen Wissenschaften unter der Leitung von

Univ.-Prof. Dipl.-Phys. Dr. Jürgen Fleig
E164 - Institute of Chemical Technologies and Analytics

eingereicht an der Technischen Universität Wien
Fakultät für Technische Chemie

von

Dipl. Ing. Christoph Riedl, BSc.
Mat-Nr.: E01425448

Wien, im August 2022

Christoph Riedl

Die approbierte gedruckte Originalversion dieser Dissertation ist an der TU Wien Bibliothek verfügbar.
The approved original version of this doctoral thesis is available in print at TU Wien Bibliothek.
TU WIEN Bibliothek Your knowledge hub

Funding Acknowledgements:
This work was supported by the Austrian Science Fund (FWF) project P31165-N37.

Eidesstattliche Erklärung:
Ich erkläre an Eidesstatt, dass die vorliegende Arbeit nach den anerkannten Grundsatzen für wissenschaftliche Abhandlungen von mir selbstständig erstellt wurde. Alle verwendeten Hilfsmittel, insbesondere die zugrunde gelegte Literatur, sind in dieser Arbeit genannt und aufgelistet. Die aus den Quellen wörtlich entnommenen Stellen sind als solche kenntlich gemacht. Das Thema dieser Arbeit wurde von mir bisher weder im In- noch Ausland einer Beurteilerin/einem Beurteiler zur Begutachtung in irgendeiner Form als Prüfungsarbeit vorgelegt. Diese Arbeit stimmt mit der von den Begutachterinnen/Begutachtern beurteilten Arbeit ueberein.
Ich nehme zur Kenntnis, dass die vorgelegte Arbeit mit geeigneten und dem derzeitigen Stand der Technik entsprechenden Mitteln (Plagiat-Erkennungssoftware) elektronisch-technisch überprüft wird. Dies stellt einerseits sicher, dass bei der Erstellung der vorgelegten Arbeit die hohen Qualitätsvorgaben im Rahmen der geltenden Regeln zur Sicherung guter wissenschaftlicher Praxis "Code of Conduct" an der TU Wien eingehalten wurden. Zum anderen werden durch einen Abgleich mit anderen studentischen Abschlussarbeiten Verletzungen meines persönlichen Urheberrechts vermieden.

Christoph Riedl

Die approbierte gedruckte Originalversion dieser Dissertation ist an der TU Wien Bibliothek verfügbar.
The approved original version of this doctoral thesis is available in print at TU Wien Bibliothek.
TU Bibliothek Your knowledge hub WIEN

Abstract

Solid oxide fuel cells (SOFCs) and solid oxide electrolysis cells (SOECs) are among the most promising technologies for sustainable energy conversion, as they offer the possibility of highly efficient power or hydrogen generation. For a broader commercialization of SOFCs and SOECs, reduction of the operation temperature from high (750 °C-1000 °C) to intermediate (450 °C-600 °C) temperatures is one of the most important goals. For SOFCs the reduction of oxygen at the cathode still poses one of the major bottlenecks, as this process is highly temperature activated and thus lower operation temperatures cause significantly higher resistive losses. This work is focused on revealing factors which influence the oxygen exchange reaction (OER) kinetics and, in addition, on improving the mechanistic understanding of the OER on SOFC cathode materials. These valuable insights are of high importance to support knowledge driven electrode improvement. While in real SOFCs porous electrodes are applied, in our model studies, measurements were conducted on thin film electrodes deposited by pulsed laser deposition on single crystalline electrolyte substrates. Most measurements were conducted with *in-situ* PLD impedance spectroscopy (*i*-PLD), which is a unique technique developed in our research group, allowing to characterize pristine electrode surfaces directly after growth inside the chamber of the PLD. As a major advantage, a high stability of the oxygen exchange is usually observed during *i*-PLD measurements, which allows us to draw far reaching mechanistic conclusions. Moreover, our *i*-PLD technique enables modification of the electrode surface (e.g. with sub-monolayer amounts of dopants) while simultaneously tracking the electrochemical performance of the electrode. As model electrodes perovskite-type ($La_{0.6}Sr_{0.4}FeO_{3-\delta}$ (LSF), $La_{0.6}Co_{0.4}FeO_{3-\delta}$ (LSC), $SrTi_{0.3}Fe_{0.7}O_{3-\delta}$ (STF)) and CaF_2-type ($Pr_{0.1}Ce_{0.9}O_{2-\delta}$ (PCO)) thin film electrodes were used.

The first two studies presented in this thesis dealt with the effect of platinum on the oxygen exchange kinetics of LSF. Platinum was sputter-deposited on top of the electrode surface and doped as Pt^{4+} into the LSF electrode (doping level ~1%). The effect of platinum in these two application forms was very different. On LSF electrodes decorated with platinum nanoparticles, measurements revealed a significant drop of the polarization resistance (e.g. a drop from 125 Ωcm^2 to ~2 Ωcm^2 was observed at 0.25 mbar O_2 and 600 °C) and, most interestingly, also a drastic change of the oxygen partial pressure dependence on the polarization resistance was found, which indicates a change of the rate limiting step. In contrast, platinum doped into LSF electrodes as Pt^{4+} revealed "just" a performance boost of about a factor of 2-3. In this

Die approbierte gedruckte Originalversion dieser Dissertation ist an der TU Wien Bibliothek verfügbar.
The approved original version of this doctoral thesis is available in print at TU Wien Bibliothek.
TU WIEN Bibliothek Your knowledge hub

study, the performance was compared using an innovative multi-layer technique, which allowed to grow differently composed electrodes on the same substrate, excluding almost any reason for sample scattering. Here, results show that the OER mechanism with and without Pt remained unchanged. This indicates that an increase of the oxygen vacancy concentration at the electrode surface due to a slight enlargement of the unit cell is responsible for the observed performance boost.

In the third study, impedance measurements comparing polarization resistances of electrodes, measured by conventional *ex-situ* techniques and *i*-PLD measurements on the same electrode, revealed a severe difference in the electrode performances. Here, additional ambient pressure X-ray photoelectron spectroscopy results showed that minor amounts of sulfur contaminations present during *ex-situ* measurements in the measurement gas adsorb on the electrode surface and lead to the observed strong performance loss.

For the fourth study, *i*-PLD measurements enabled tracking of the electrochemical performance of epitaxial LSF electrodes during growth. An unusual increase of the oxygen exchange resistance was found during growth. Using HR-TEM measurements a decrease of the unit cell volume over electrode thickness was found. This indicates a decrease of the oxygen vacancy concentration which explains the increase of the electrode resistance. Also defect thermodynamic calculations support this interpretation.

In the last study, effects of surface decoration with binary oxides on the polarization resistance of PCO10 electrodes were investigated with *i*-PLD. While acidic oxides (TiO_2, SnO_2) led to an increase of the polarization resistance, basic oxides (SrO, CaO) led to a strong decrease of the polarization resistance. Possible reasons were discussed by measuring the surface potential and the surface electron concentration during AP-XPS measurements.

To conclude, with this work it was possible to strongly deepen the mechanistic understanding of the oxygen exchange reaction on mixed conducting electrodes, especially by investigating the interplay between electrode defect chemistry and oxygen exchange kinetics.

Die approbierte gedruckte Originalversion dieser Dissertation ist an der TU Wien Bibliothek verfügbar.
The approved original version of this doctoral thesis is available in print at TU Wien Bibliothek.
TU WIEN Bibliothek Your knowledge hub

Kurzfassung

Festoxid-Brennstoffzellen (SOFCs) und Festoxid-Elektrolysezellen (SOECs) sind vielversprechende Technologie für eine nachhaltige Energieumwandlung, da sie die Möglichkeit einer hocheffizienten Strom- und Wasserstofferzeugung bieten. Im Hinblick auf eine breitere Kommerzialisierung von SOFCs und SOECs ist die Reduzierung der Betriebstemperatur von hohen (750°C-1000°C) auf mittlere Temperaturen (450°C-600°C) eines der wichtigsten Ziele. Für SOFCs stellt die Sauerstoffreduktion an der Kathode immer noch einen der größten kinetischen Engpässe dar, da dieser Prozess stark temperaturaktiviert ist und daher eine niedrigere Betriebstemperatur deutlich höhere Widerstandsverluste verursachen würde. Diese Arbeit konzentriert sich darauf, Faktoren zu erforschen, die die Kinetik der Sauerstoffaustauschreaktion (OER) beeinflussen, und darüber hinaus das mechanistische Verständnis der OER auf SOFC Kathodenmaterialien zu verbessern. Diese Erkenntnisse sind von großer Bedeutung, um die weitere Entwicklung von Elektrodenmaterialien zu unterstützen. Während für reale SOFCs poröse Elektroden verwendet werden, wurden in unseren Modellstudien Impedanzmessungen an Dünnfilmelektroden durchgeführt, die durch gepulste Laserabscheidung auf einkristallinen Elektrolytsubstraten abgeschieden wurden. Die meisten elektrochemischen Messungen wurden mit *in-situ*-PLD-Impedanzspektroskopie (*i*-PLD) durchgeführt, einer speziellen Technik, die in unserer Forschungsgruppe entwickelt wurde und die es ermöglicht, Elektroden direkt nach dem Wachstum in der Kammer der PLD zu charakterisieren. Als großer Vorteil wird bei *i*-PLD-Messungen üblicherweise eine hohe Stabilität des Polarisationswiderstands beobachtet, was es erlaubte, weitreichende mechanistische Schlussfolgerungen zu ziehen. Darüber hinaus ermöglicht die *i*-PLD-Technik die Elektrodenoberfläche zu modifizieren (z. B. mit sub-Monolagen-Mengen von Dotierungen) und gleichzeitig den Widerstand der Elektrode zu verfolgen. Als Modellelektroden wurden Materialen in Perowskitstruktur ($La_{0.6}Sr_{0.4}FeO_{3-\delta}$ (LSF), $La_{0.6}Co_{0.4}FeO_{3-\delta}$) (LSC), $SrTi_{0.3}Fe_{0.7}O_{3-\delta}$ (STF)) und Materialien in CaF_2 Struktur, wie $Pr_{0.1}Ce_{0.9}O_{2-\delta}$ (PCO) verwendet.

Die ersten beiden Studien befassen sich mit der Wirkung von Platin auf die Sauerstoffaustauschkinetik von LSF. Platin-Nanopartikel wurden sowohl auf die Elektrodenoberfläche aufgesputtert als auch als Pt^{4+} in die LSF Elektrode dotiert (Dotierungsniveau ~1%). Interessanterweise war die Wirkung von Platin in diesen beiden Anwendungsformen sehr unterschiedlich. Auf mit Platin-Nanopartikeln dekorierten LSF-Elektroden ergaben Messungen einen beträchtlichen Abfall des Polarisationswiderstandes (z.B. bei 0.25 mbar O_2 wurde

Die approbierte gedruckte Originalversion dieser Dissertation ist an der TU Wien Bibliothek verfügbar.
The approved original version of this doctoral thesis is available in print at TU Wien Bibliothek.
TU Bibliothek Your knowledge hub WIEN

ein Abfall des Widerstandes von 125 Ωcm^2 auf ~2 Ωcm^2 beobachtet) und interessanterweise wurde auch eine drastische Änderung der Sauerstoffpartialdruckabhängigkeit des Polarisationswiderstandes beobachtet, was auf eine Änderung des geschwindigkeitsbestimmenden Schrittes hinweist. Im Gegensatz dazu zeigte Platin (als Pt^{4+}) dotiert in LSF-Elektroden, eine Leistungssteigerung von etwa einem Faktor 2-3. In dieser Studie wurde der Polarisationswiderstand unter Verwendung einer innovativen Mehrschichttechnik verfolgt. Diese ermöglicht es, unterschiedlich zusammengesetzte Elektroden auf demselben Substrat abzuscheiden, wodurch fast alle Gründe für Probenstreuung ausgeschlossen werden. Bei Pt dotiertem LSF zeigen die Ergebnisse, dass der OER-Mechanismus unverändert bleibt, was darauf hindeutet, dass eine leichte Erhöhung der Sauerstoffleerstellenkonzentration für den niedrigeren Polarisationwiderstand verantwortlich ist. In einer anderen Studie zeigten Impedanzmessungen bei Elektroden einen starken Unterschied in der Elektrodeneigenschaft, wenn sie mit herkömmlichen *ex-situ*-Techniken oder mit der *i*-PLD Technik gemessen wurden. Hier ergaben Röntgenphotoelektronenspektroskopie Messungen, dass geringe Mengen von Schwefelverunreinigungen, die während *ex-situ*-Messungen im Messgas vorhanden sind, zu dem beobachteten starken Leistungsverlust führen. Darüber hinaus ermöglichten *i*-PLD-Messungen, den Elektrodenwiderstand epitaktischer LSF Elektroden während des Wachstums zu verfolgen. Solche Messungen zeigten einen ungewöhnlichen Anstieg des Polarisationswiderstands während des Wachstums. Unter Verwendung von HRTEM Messungen wurde eine Abnahme des Einheitszellvolumens über der Elektrodendicke festgestellt, was die Zunahme des Elektrodenwiderstands aufgrund einer Abnahme der Sauerstoffleerstellen erklärt. In der letzten Studie wurden die Auswirkungen der Oberflächendekoration mit binären Oxiden auf den Polarisationswiderstand von PCO10-Elektroden untersucht. Während saure Oxide (TiO_2, SnO_2) zu einer Erhöhung des Polarisationswiderstandes führten, führten basische Oxide (SrO, CaO) zu einer starken Abnahme des Polarisationswiderstandes. Mögliche Gründe wurden durch Messung des Oberflächenpotentials und der Oberflächenelektronenkonzentration während AP-XPS-Messungen diskutiert.

Zusammenfassend konnte in dieser Arbeit das mechanistische Verständnis der Sauerstoffaustauschreaktion an gemischt leitenden Elektroden stark vertieft werden. Insbesondere wurde das Zusammenspiel zwischen Elektrodendefektchemie und Sauerstoffaustauschkinetik besser geklärt.

Die approbierte gedruckte Originalversion dieser Dissertation ist an der TU Wien Bibliothek verfügbar.
The approved original version of this doctoral thesis is available in print at TU Wien Bibliothek.
TU Bibliothek Your knowledge hub WIEN

Contents

1 Motivation and Introduction **1**

1.1 Motivation 1

1.2 Working principle fuel cells 2

1.3 State of the art 3

2 Outstanding oxygen reduction kinetics of $La_{0.6}Sr_{0.4}FeO_{3-\delta}$ surfaces decorated with platinum nanoparticles **7**

2.1 Introduction 7

2.2 Experimental section 8

2.3 Results 10

2.3.1 Morphological, structural and chemical characterization 10

2.3.2 The effect of platinum nanoparticles on the oxygen exchange reaction at the LSF64 surface - impedance spectra 12

2.3.3 pO_2 dependency of the polarization resistance of platinum decorated electrodes 14

2.3.4 Effect of the deposited platinum amount on the polarization resistance 15

2.3.5 Effect of sample prehistory and degradation on the resistance of platinum decorated electrodes 17

2.4 Mechanistic discussion 18

2.5 Conclusion 21

2.6 Supporting Information 22

2.6.1 Characterization of LSF64 target and LSF64 thin film by means of X-ray diffraction 22

2.6.2 Effect of the deposited platinum amount on the resistance: SEM images 23

2.6.3 Effect of the deposited platinum amount on the resistance: XPS results 24

2.6.4 Effect of platinum nanoparticles on other MIEC materials and in humidified H_2 25

3 Performance modulation through selective, homogeneous surface doping of lanthanum strontium ferrite electrodes revealed by *in-situ* PLD impedance measurements **27**

3.1 Introduction 27

Die approbierte gedruckte Originalversion dieser Dissertation ist an der TU Wien Bibliothek verfügbar.
The approved original version of this doctoral thesis is available in print at TU Wien Bibliothek.
TU WIEN Bibliothek Your knowledge hub

3.2 Experimental section . . . 29
3.2.1 Sample preparation . . . 29
3.2.2 Electrochemical measurements . . . 29
3.2.3 Characterisation of thin film surface and bulk composition, structure, and morphology . . . 30
3.3 Results . . . 31
3.3.1 Stoichiometric composition of the electrodes . . . 32
3.3.2 Structural and morphological characterization of the electrodes . . . 32
3.3.3 Ambient pressure XPS measurements . . . 35
3.3.4 *In-situ* electrochemical characterisation during growth of multi-layers 36
3.3.5 $p(O_2)$ and temperature dependence of LSF and LSF-Pt2 polarisation resistance . . . 41
3.4 Discussion . . . 43
3.5 Conclusions . . . 46
3.6 Supporting Information . . . 47
3.6.1 Degradation behaviour . . . 47
3.6.2 Spectra and results of *ex-situ* XPS measurements . . . 49
3.6.3 SEM and AFM images of pristine and degraded LSF-Pt1 electrodes . 51
3.6.4 Platinum current collector grid . . . 51
3.6.5 Results of AP-XPS measurements . . . 52

4 *In-situ* techniques reveal the true capabilities of SOFC cathode materials and their sudden degradation due to omnipresent sulfur trace impurities 53
4.1 Introduction . . . 53
4.2 Experimental section . . . 54
4.3 Results . . . 57
4.3.1 Surface-related polarization resistance of pristine electrodes compared by *i*-PLD impedance measurements . . . 57
4.3.2 Comparison of *i*-PLD surface resistances with literature data . . . 59
4.3.3 Monitoring electrode degradation by simultaneous AP-XPS and *in-situ* impedance measurements . . . 60
4.3.4 Ex-situ investigation of pristine surfaces and comparison with *i*-PLD results . . . 62
4.4 Discussion . . . 66
4.5 Conclusion . . . 69
4.6 Supporting Information . . . 70
4.6.1 XPS spectra of LSC electrode during AP-XPS measurements: . . . 70
4.6.2 LSC and PCO electrodes directly after *i*-PLD measurements: . . . 71
4.6.3 X-ray fluorescence spectroscopy (XRF): . . . 72

Die approbierte gedruckte Originalversion dieser Dissertation ist an der TU Wien Bibliothek verfügbar.
The approved original version of this doctoral thesis is available in print at TU Wien Bibliothek.
TU WIEN Bibliothek Your knowledge hub

5 *In-situ* electrochemical observation of anisotropic lattice contraction of $La_{0.6}Sr_{0.4}O_{3-\delta}$ electrodes during pulsed laser deposition 73
5.1 Introduction . . . 73
5.2 Experimental section . . . 74
5.3 Results . . . 75
5.3.1 Structural characterization and surface morphology . . . 75
5.3.2 *i*-PLD growth of epitaxial and polycrystalline LSF thin films . . . 76
5.3.3 High resolution transmission electron microscopy (HRTEM) . . . 82
5.3.4 Comparison of lattice parameters and volume on polycrystalline and epitaxial LSF . . . 84
5.4 Discussion . . . 85
5.5 Conclusion . . . 89
5.6 Supporting Information . . . 90
5.6.1 *i*-PLD measurements of a 100 nm LSF thin film on YSZ-GDC . . . 90
5.6.2 Brownmillerite type LSF . . . 91
5.6.3 Rietveld analysis . . . 92

6 Modifying the surface potential on praseodymium doped ceria electrodes: An *in-situ* PLD and ambient pressure XPS study 93
6.1 Introduction . . . 93
6.2 Experimental section . . . 94
6.3 Results . . . 95
6.3.1 Oxygen exchange activity of PCO10 electrodes during stepwise decoration with binary oxides . . . 95
6.3.2 pO_2 and temperature dependence of the polarization resistance on pure and decorated PCO10 electrodes . . . 99
6.3.3 AP-XPS measurements of pure and decorated PCO10 electrodes . . . 100
6.4 Mechanistic discussion . . . 103
6.5 Conclusion . . . 107

7 Conclusion 108

List of publications 111

List of conference contributions 113

List of abbreviation 115

Bibliography 116

List of Figures 138

Die approbierte gedruckte Originalversion dieser Dissertation ist an der TU Wien Bibliothek verfügbar.
The approved original version of this doctoral thesis is available in print at TU Wien Bibliothek.
TU WIEN Bibliothek Your knowledge hub

Acknowledgements 145

Die approbierte gedruckte Originalversion dieser Dissertation ist an der TU Wien Bibliothek verfügbar.
The approved original version of this doctoral thesis is available in print at TU Wien Bibliothek.
TU WIEN Bibliothek Your knowledge hub

1 Motivation and Introduction

1.1 Motivation

Developing emission-free and green ways of power generation is one of the major challenges of the 21st century. Following the goal of the European Union reducing the emission of greenhouse gases (CO_2, CH_4, HCFC, N_2O) is of high importance. According to the European Environment Agency in 2019 77.01 % of the greenhouse gas emission was attributed to energy, 9.1 % to industry, 10.55 % to agriculture and 3.32 % to waste management. By the year 2030 the EU demands its member states to reduce the emission by -55 % compared to the year 1990. This goal is not easy to achieve, nevertheless it must given priority to slow down global climate change. As energy posses the biggest emitter of greenhouse gases, a focus on renewable energy technologies including water, wind, biomass and solar energy is necessary together with minimizing the energy consumption. Following plans of the EU by 2030 40 % of the energy production shall be renewable.

In recent years, especially the introduction of electric cars mark a new era of mobility. However, currently available lithium batteries still require several improvements, as capacity, durability and the high inflammability limit the applicability. [1] Besides batteries, fuel cells pose a second important technology, which still lacks behind in development, but has great potential in the next decades. Fuel cells offer the main advantage to convert the chemical energy of a fuel together with an oxidizing agent into electric energy at an efficiency higher than in conventional caloric power stations. The possible area of operation for fuel cells range from auxiliary power units (APUs) for automotives with combustion engines, to electric power supply for electric cars or remote heat and power supply. Currently, several different fuel cell types are under investigations, which will be introduced in the next chapter. In addition, also solid electrolyzer fuel cells (SOECs) are gaining more importance recently. SOECs are SOFCs operated in reverse mode to achieve the electrolysis of water to hydrogen and oxygen. Due to the high efficiency of conversion, production of "green hydrogen" or syngas from SOECs is a very promising technology. [2]

Die approbierte gedruckte Originalversion dieser Dissertation ist an der TU Wien Bibliothek verfügbar.
The approved original version of this doctoral thesis is available in print at TU Wien Bibliothek.
TU WIEN Bibliothek Your knowledge hub

1.2 Working principle fuel cells

In the following, different types of fuel cells will be introduced. One of the major advantages of fuel cells is the high efficiency of power conversion. Currently, fuel cells operate at an electrical efficiency between 40 % - 60 % depending on the type of the fuel cell and the operation mode (electric mode or heat and power mode). [3] In Figure 1.1 different types of fuel cells are shown: Direct methanol fuel cell (DMFC), proton-exchange membrane fuel cells (PEMFC), alkaline fuel cells (AFC), phosphoric acid fuel cells (PAFC), molten-carbonate fuel cells (MCFC) and solid oxide fuel cell (SOFC). As can be seen, different fuel cell types operate at varying temperatures, which also requires different electrode materials.

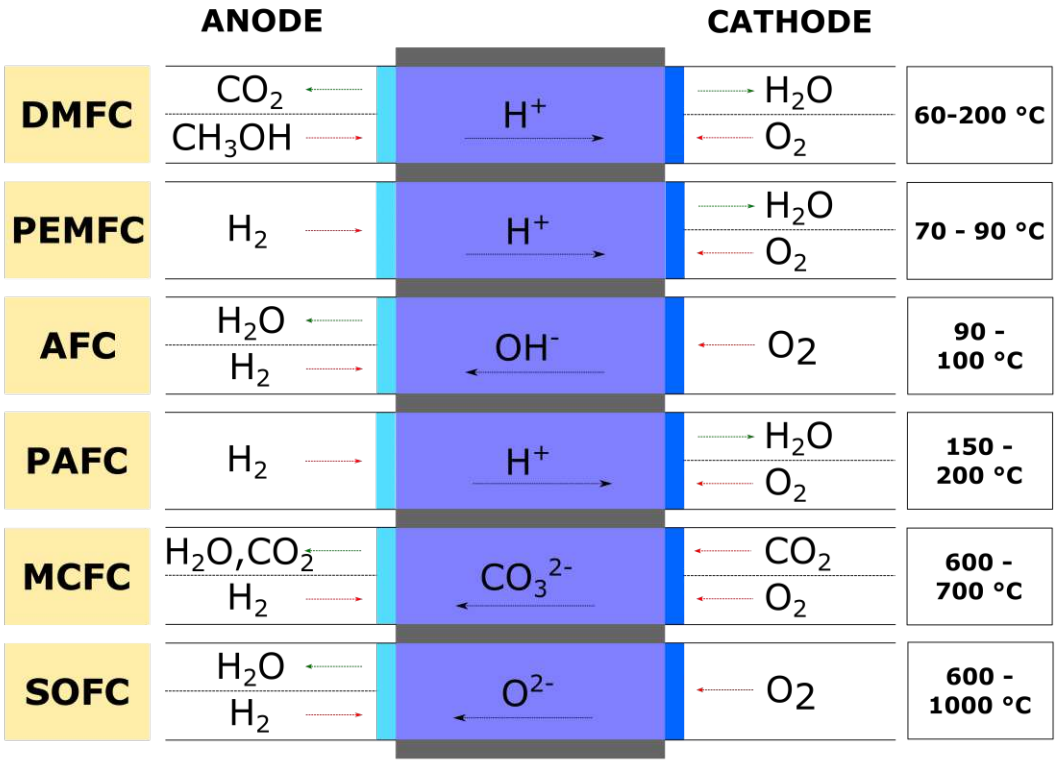

Figure 1.1: Sketch explaining the chemical reation taking place on different types of fuel cells. Operation temperatures are taken from literature [3].

Die approbierte gedruckte Originalversion dieser Dissertation ist an der TU Wien Bibliothek verfügbar.
The approved original version of this doctoral thesis is available in print at TU Wien Bibliothek.
TU Bibliothek Your knowledge hub WIEN

The work of this study is focused on solid oxide fuel cells (SOFCs), which still operate at relatively high temperatures of 800 °C. At the cathode side of the SOFC oxygen is reduced and incorporated into the cathode.

$$\frac{1}{2}O_2 + 2e' \rightarrow O^{2-} \tag{1.1}$$

Oxide ions are transported through the electrolyte to the anode, where it reacts with hydrogen to form water.

$$O^{2-} + H_2 \rightarrow H_2O + 2e' \tag{1.2}$$

1.3 State of the art

Lowering the operation temperature of solid oxide fuel cells (SOFCs) to intermediate temperatures (450 °C - 600 °C) is one of the main goals of current research activities on this topic and requires electrode materials with sufficiently fast surface reaction kinetics even at those relatively low temperatures. [4–9] In general, currently available high temperature (HT)-SOFCs posses several challenges, as the high temperatures (800 °C - 1000 °C) cause thermal stress, requires costy materials for interconnects, suffer from long start-up times and high heat inputs. In addition, the high operation temperature may reduces the life time of the cell. [5] Nevertheless, these high operations are currently necessary as the conductivity and the oxygen exchange activity of the applied materials is strongly temperature dependent and thus a lower operation temperature would lead to significant resisitive losses. New materials, which allow operation at intermediate temperatures would thus lead to several improvements, like a wider material selection, reduction of system costs, corrosion rates and materials costs. In addition, a decrease of material degradation is expected.[10]

While currently $La_{1-x}Sr_xMnO_{3-\delta}$ (LSM) or $La_{1-x}Sr_xCo_{1-y}Fe_yO_{3-\delta}$ (LSCF) based composites are mostly used as cathode materials in SOFCs [11], a recent study reported exceptionally high power density for SOFCs with $La_{1-x}Sr_xCoO_{3-\delta}$ air electrodes [12], which enables a performance increase up to a factor of 10. In the past years, several studies dealt with either finding new cathode materials or improving the existing ones. Here, mostly perovskite-type mixed ion and electron conducting (MIECs) cathode materials, such as $La_{1-x}Sr_xCoO_{3-\delta}$ (LSC),[13–20] $La_{1-x}Sr_xFeO_{3-\delta}$ (LSF), [21–25] $La_{1-x}Ba_xCoO_{3-\delta}$ (LBC), [26, 27] $Sm_{1-x}Sr_xCoO_{3-\delta}$ (SSC) [28–30], $La_{1-x}Sr_xCo_{1-y}Fe_yO_{3-\delta}$ (LSCF) [31–36], $SrTi_{1-x}Fe_xO_{3-\delta}$, (STF)[37–40] or $Ba_{1-x}Sr_xCo_{1-y}Fe_yO_{3-\delta}$ (BSCF) [41–43] were investigated. In addition, studies were conducted on $Pr_{1-x}Ce_xO_{2-\delta}$ (PCO) [44, 45], $NdNi_2O_{4+\delta}$ (NNO) [46, 47] or $La_2NiO_{4+\delta}$ (LNO)[48, 49].

Die approbierte gedruckte Originalversion dieser Dissertation ist an der TU Wien Bibliothek verfügbar.
The approved original version of this doctoral thesis is available in print at TU Wien Bibliothek.
TU Bibliothek Your knowledge hub WIEN

While for "real-life" SOFCs porous electrodes are applied due to their large surface area, for mechanistic studies often model electrodes deposited by pulsed laser deposition (PLD) on single crystalline electrolyte substrates are used due to their well-defined surface structure and geometry.[50] Such studies on thin film electrodes often aim at a deepening of the understanding of the exact reaction mechanism taking place on the solid oxide fuel cell cathodes. An improved understanding of the oxygen exchange reaction (OER) could greatly support knowledge-driven materials improvement for future SOFC cathodes. [51] In general, the oxygen exchange reaction (in incorporation direction) involves the following steps: Oxygen diffusion to the cathode surface, adsorption of oxygen on the surface, (partial) ionization and/or splitting of oxygen, incorporation of the oxygen species into an oxygen vacancy. [50] In the past years, several studies were conducted which significantly improved the mechanistic understanding of the OER reaction. [44, 45, 52–57] Nevertheless, numerous questions regarding the OER reaction still remain unanswered.

In order to reveal the OER kinetics of an electrode, different experimental techniques can be applied, such as *ex-situ* impedance spectroscopy at OCV conditions [21, 26, 46, 58] or under bias polarization [25, 59–61], tracer diffusion [62–66] or conductivity relaxation experiments [24, 67–70], which all can be performed at different oxygen partial pressures and temperatures to gain mechanistic insights. It should be mentioned that all these measurement techniques yield information on different modes of the surface reaction, which are often not straightforward to compare between each other.[71]

In the past years several studies on MIEC electrodes focused on improving the understanding of electrode defect chemistry on different electrode materials like LSF,[59] PCO[72], STF [37] or LSM [73], or in the next step, understanding the interplay between defect chemistry and oxygen exchange kinetics. [37, 44, 50, 74] In addition, many investigations were conducted regarding the stability of SOFC cathode materials, as many promising electrode materials show low resistance at the beginning of the measurements, which unfortunately strongly increase after several hours at measurement temperature. [75–81] Studies have identified several reasons for sample degradation, including strontium segregation [75, 77, 78, 82] or the presence of contamination like sulphur [83–88], chromium [47, 89–91] or silicon [89, 90, 92] on the electrode surface. However, results are often conflicting as, for example, measurements both found SrO to both increase or decrease [93] oxygen exchange activity. Moreover, studies showed that surface treatment with H_2O[94], DC voltage pulses [28] or microstructural optimization [94–96] increase surface activity of the electrode. In other studies, the effect of strain on the OER kinetics was investigated.[46, 97–100] Tensile lattice strain was found to increase the OER activity, while compressive strain led to an increase of the polarization resistance. In order to assess influences on the oxygen exchange properties, the surface was modified with numerous surface decorations, such as Pd, Pt, Ag, Ca, Sr, Ba, Co, Ni, Mn, Fe, Zr, Ca, Sr, Pr, La.[23, 101–103] However, results are often ambiguous, as partly op-

Die approbierte gedruckte Originalversion dieser Dissertation ist an der TU Wien Bibliothek verfügbar.
The approved original version of this doctoral thesis is available in print at TU Wien Bibliothek.
TU WIEN Bibliothek Your knowledge hub

posing results were reported. Regarding surface decoration with binary oxides, an advanced study by Nicollet et. al has recently discovered that the Smith acidity[104] is suitable as a sensitive descriptor of the PCO10 OER kinetics. [45] Moreover, X-ray photoelectron spectroscopy (XPS) studies were conducted to characterize the surface of electrodes. [60, 105–107] Finally, also several theoretical studies using DFT calculations were performed, which tried to understand OER kinetics from a more theoretical perspective. [108, 109]

A further step forward to improve knowledge of OER was possible by combining preparation (of thin films) and electrochemical characterization in so-called: *in-situ* PLD impedance spectroscopy measurements [52, 76, 93, 95, 99, 110]. *Ex-situ* measurements on thin films, which for several years posed the backbone of several pioneering studies [21, 25, 37, 74, 94, 111], suffer from several disadvantages as the polarization resistance observed during such *ex-situ* measurements is often not very stable and increases strongly with time, which makes it difficult to draw mechanistic conclusions, as a change of the polarization resistance can be driven by a change of measurements conditions or simply by degradation. The application of *in-situ* measurements allows to avoid this problem, as the stability of the polarization resistance observed is usually significantly higher due to the absence of contamination. Moreover, *i*-PLD measurements allow to modify the electrode surface (e.g. with surface decorations) and to simultaneously track changes of the polarization resistance. In addition, also the fabrication of multilayer electrodes is possible, which allow the comparison of the different electrode materials on the same sample. These advantages allow new insights into the electrode reduction kinetics and enable precise measurements on pristine electrodes, which were not accessible before.

In this work, five different studies were conducted, several of them using *i*-PLD measurements. All dealt with improving the understanding of the oxygen reduction kinetics on MIEC electrodes. In the first study, the effect of platinum nanoparticles on the LSF polarization resistance was investigated. Results reveal that, especially at low oxygen partial pressures (0.25 mbar O_2), platinum nanoparticles decrease the polarization resistance by a factor of 100. Moreover, comparison of the pO_2 dependence on pure and Pt decorated LSF electrodes revealed different dependencies of the polarization resistance, which indicates a change of the rate limiting step.
In the second study, the performance of pure LSF and LSF doped with minor amounts of platinum (Pt^{4+}, 1-1.5 % of the total cation amount) was compared by innovative *i*-PLD multilayer technique, which allowed us to measure the polarization resistance of differently composed electrodes on one sample, avoiding almost all reasons for sample scattering. Pt doping increased the oxygen exchange activity by a factor of 2-3, which was mainly driven by an increase of the oxygen vacancy concentration on the electrode surface. In contrast to the first study, a change of the oxygen exchange mechanism was not observed.
A third series of investigations revealed that MIEC electrodes show very low polarization

Die approbierte gedruckte Originalversion dieser Dissertation ist an der TU Wien Bibliothek verfügbar.
The approved original version of this doctoral thesis is available in print at TU Wien Bibliothek.
TU WIEN Bibliothek Your knowledge hub

resistance during *i*-PLD measurements, while, after sample transfer to a standard *ex-situ* measurement setup a strong performance decrease was observed. By ambient pressure XPS (AP-XPS) measurements we observed that minor amounts of SO_2 contaminations, present in high-purity measurement gas in the range of ppb, adsorb on the electrode surface and are responsible for the strong performance loss.

In the fourth study, *i*-PLD measurements were used to electrochemically observe the polarization resistance of LSF electrodes grown either polycrystalline or epitaxial on different electrolyte substrates. For epitaxial LSF electrodes a continuous increase of the polarization resistance was measured and related to a decrease of the unit cell volume. A change of the unit cell volume leads to changes of the defect chemistry, which influences the oxygen exchange kinetics.

In the last set of experiments, sub-monolayer amounts of binary oxides (SrO, TiO_2, SnO_2, CaO) were deposited on PCO10 electrodes and the performance change was simultaneously measured by *i*-PLD measurements. Combining *i*-PLD and AP-XPS measurements revealed a correlation between the surface potential and the oxygen exchange kinetics, which allowed us to better describe how surface decorations affect the oxygen exchange kinetics.

Die approbierte gedruckte Originalversion dieser Dissertation ist an der TU Wien Bibliothek verfügbar.
The approved original version of this doctoral thesis is available in print at TU Wien Bibliothek.
TU WIEN Bibliothek Your knowledge hub

2 Outstanding oxygen reduction kinetics of $La_{0.6}Sr_{0.4}FeO_{3-\delta}$ surfaces decorated with platinum nanoparticles

Large parts of the study presented in this chapter are also published in Christoph Riedl et al 2020 J. Electrochem. Soc. 167 104514. [112] The experimental work of this study was partly conducted during the time of my diploma thesis.

2.1 Introduction

Platinum is known for its catalytic properties especially in aqueous systems and in polymer electrolyte membrane fuel cells (PEM-FC), which operate below 100 °C. In these cells, platinum nanoparticles (pure or alloyed) are used to accelaterate the oxygen reduction reaction (ORR) at the cathode [113] and much research has been done to understand the ORR, to improve its performance [114], to understand the size effect of platinum particles on the ORR [115] or to develop non-platinum catalysts [116]. However, the exakt intermediate steps of the ORR mechanism are still debated, also because of difficulties in detecting the intermediate species of the ORR [117]. In the field of ceramic oxide ion conductors, porous Pt electrodes are commonly used in oxygen sensors [118] and also many fundamental studies have been performed to understand oxygen reduction, for example at Pt|YSZ interfaces [111, 119–132].

Interestingly, Pt electrodes are very rarely used in SOFCs, not only because of costs but also because Pt electrodes generally lead to higher polarization resistances than cathodes made of mixed conducting oxides. This may be surprising since Pt is known to catalyze dissociation of oxygen molecules [133, 134]. However, in SOFC-related YSZ|Pt cathodes the oxygen reduction reaction is limited to the so-called triple phase boundary (TPB) [111], in contrast to the entire surface being potentially active in case of a MIEC cathode [135]. Accordingly, the number of electrochemically active sites is rather small, compared to mixed conducting electrode materials. This raises the question whether changes in the electrode design may help still exploiting the oxygen splitting capability of platinum.

Die approbierte gedruckte Originalversion dieser Dissertation ist an der TU Wien Bibliothek verfügbar.
The approved original version of this doctoral thesis is available in print at TU Wien Bibliothek.
TU WIEN Bibliothek Your knowledge hub

In this study, we used platinum nanoparticles to accelerate the oxygen reduction on $La_{0.6}Sr_{0.4}FeO_{3-\delta}$ (LSF64) thin films and measured the performance improvement of the electrode by electrochemical impedance spectroscopy. Symmetrical thin film electrodes were prepared by pulsed laser deposition of LSF64 on yttria stabilized zirconia single crystals (YSZ) and investigated before and after sputter deposition of tiny amounts of Pt (nominally a few monolayers) onto the LSF64 surface. We show that a huge performance improvement is possible, especially in reduced oxygen partial pressure (only *ca.* 2 Ωcm^2 polarisation resistance at 600 °C in 0.25 mbar pO_2). Moreover, from the partial pressure dependence, degradation behaviour and reproducibility studies we can draw far-reaching conclusions on the oxygen reduction mechanism of these surface decorated MIEC electrodes.

2.2 Experimental section

Platinum current collector grids with either 25/10 µm mesh/strip width or 10/10 µm mesh/strip width were prepared on both sides of YSZ(100) single crystals (0.5*0.5*0.05 cm^3) (CrysTec, Germany) by lift-off lithography and subsequent magnetron sputter deposition of 5 nm titanum and 100 nm platinum. Dense $La_{0.6}Sr_{0.4}FeO_{3-\delta}$ (LSF64) thin films were prepared on top of those current collectors by pulsed laser deposition (PLD). LSF64 powder was synthesized via the Pechini route from Fe, La_2O_3 and $SrCO_3$ and the PLD target was then prepared by isostatic pressing (150 MPa) and sintering at 1200 °C for 12 h. Laser ablation was performed at 600 °C substrate temperature and 0.04 mbar oxygen partial pressure (Alphagaz^{TM}, 99.995 %) with a KrF excimer laser (Complex Pro 210F, wavelength 248 nm) at a frequency of 5 Hz, a laser energy of 2 J/cm^2 and a target to substrate distance of 6 cm. The deposition time was 30 minutes (9000 pulses) leading to a LSF64 thickness of 200 nm. The resulting samples are sketched in Figure 2.2 a).

For impedance measurements, samples were contacted with platinum meshes (75/500 µm strip/width) and heated to 600 °C in a measurement station made of Al_2O_3 (corundum). Electrochemical Impedance Spectroscopy (EIS) measurements were done with a Novocontrol Alpha Frequency Analyzer (Novocontrol Technologies, Germany) from 10^6 to 10^{-2} Hz and an AC amplitude of 10 mV. The integration time was either 1 sec or 1 period. Oxygen partial pressures between 210 mbar and 0.25 mbar were investigated.

After initial electrochemical characterization of the pristine samples and some defined degradation upon measurement conditions, the surface of the thin films was decorated with platinum particles. This was done by magnetron sputter deposition (BAL-TEC MED 020, Liechtenstein) for a very short time at a pressure of $2*10^{-2}$ mbar Ar and a sputter current of 100 mA. The typical deposition time was 2 seconds. However, to vary the Pt amount, the sputter cur-

Die approbierte gedruckte Originalversion dieser Dissertation ist an der TU Wien Bibliothek verfügbar.
The approved original version of this doctoral thesis is available in print at TU Wien Bibliothek.
TU WIEN Bibliothek Your knowledge hub

rent (between 25 and 100 mA) and the sputter duration (between 2 and 5 sec) was also varied. For the standard conditions (2 sec., 100 mA) a Pt layer with a nominal thickness of 1.6 nm results. However, at measurement temperatures this layer agglomerates to small Pt nanoparticles, see sketch at 2.2 a) and section Results. The obtained symmetrical samples with Pt decorated LSF64 electrodes were then again electrochemically characterized by means of impedance spectrocopy.

In order to investigate the deposited amount of platinum, additional YSZ(100) single crystals were positioned in the sputter chamber next to the YSZ samples with LSF64. Afterwards the platinum was dissolved from the YSZ with concentrated aqua regia ($HCl:HNO_3$ = 3:1) and the solution was diluted with distilled water. Chemical analysis was performed with an inductively coupled plasma mass spectrometry (ICP-MS) iCAP Q (Thermo Scientific, United States of America). Scanning electron microscopy (SEM) measurements were carried out with a FEI Quanta 250 FEGSEM. The morphology was determined by analysing secondary electrons images (SE) and backscattered electrons images (BSE). Samples for transmission electron microscopy (TEM) were prepared with a Quanta 200 3D DualBeam-FIB and measured with a FEI TECNAI F20. Gracing incidence measurements were performed with a Empyrean X-ray diffractometer (Malvern Panalytical) equipped with a parallel beam mirror on the incident beam side and a parallel plate collimator and a scintillation detector on the diffracted beam side. Measurements in Bregg-Bretano geometry were performed with an Malvern Panalytical, MPD Pro.

Die approbierte gedruckte Originalversion dieser Dissertation ist an der TU Wien Bibliothek verfügbar.
The approved original version of this doctoral thesis is available in print at TU Wien Bibliothek.
TU WIEN Bibliothek Your knowledge hub

2.3 Results

2.3.1 Morphological, structural and chemical characterization

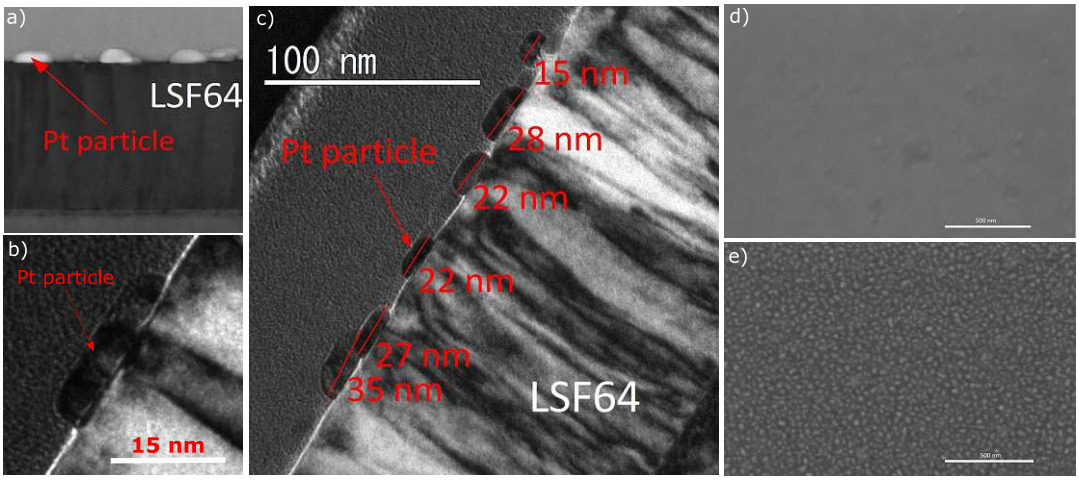

Figure 2.1: a) STEM image of a platinum decorated LSF64 electrode. b) magnified TEM image of a single platinum nanoparticle on LSF64. c) FIB-TEM image of a platinum decorated LSF64 electrode. d) SEM image of pristine LSF64 electrode. e) SEM image of a platinum decorated LSF64 electrode after 16 h in 0.25 mbar O_2 at 600 °C.

To characterize the surface composition and morphology of the Pt decorated LSF64 thin film electrodes, several analytical techniques were applied. The amount of platinum on the electrodes was quantified by Inductively Coupled Plasma - Mass Spectrometry (ICP-MS) measurements. The applied standard procedure of Pt deposition corresponds to a film thickness of 1.6 nm assuming a continuous layer. However, after heating to 600 °C in the measurement setup, surface morphology characterization revealed agglomerated Pt particles in accordance with literature [130]. Scanning electron microscopy (SEM) in backscattered electrons (BSE) mode clearly shows the difference between a pristine LSF64 (Figure 2.1 d)) and a platinum decorated LSF64 electrode Figure 2.1 e)). According to SEM images, the size of the platinum particles was between 20 nm and 40 nm. This was also confirmed by transmission electron microscopy (TEM) measurements, see (Figure 2.1 a) b) c)). The platinum particles had an average height of about 6 nm in the TEM images. Comparision with the nominal thickness of 1.6 nm this indicates a surface coverage in the range of 30 %.

This is also in good accordance with X-ray photoelectron spectroscopy (XPS) measurements. Those revealed a surface composition with about 36 % of the surface atoms being platinum see Figure 2.2 b)). Moreover, XPS measurements showed that the oxidation state of platinum was Pt(0) and no evidence was found that platinum had oxidized to PtO or PtO_2 during elec-

Die approbierte gedruckte Originalversion dieser Dissertation ist an der TU Wien Bibliothek verfügbar.
The approved original version of this doctoral thesis is available in print at TU Wien Bibliothek.
TU WIEN Bibliothek Your knowledge hub

trochemical measurements (Figure 2.2 c)). The binding energy found for the Pt-4f$_{(5/2)}$ [136] and the Pt-4f$_{(7/2)}$ [137] line corresponds to metallic Pt. The crystallinity of the LSF64 films is clearly shown in the diffractograms (see Supporting Information Figure 2.7). The polycrystalline columnar nature of the LSF64 film growth is also visible in the TEM images. Owing to their small amount and size, it was not possible to detect any signal from the platinum particles on the surface of LSF64 by means of the lab-based diffractometer.

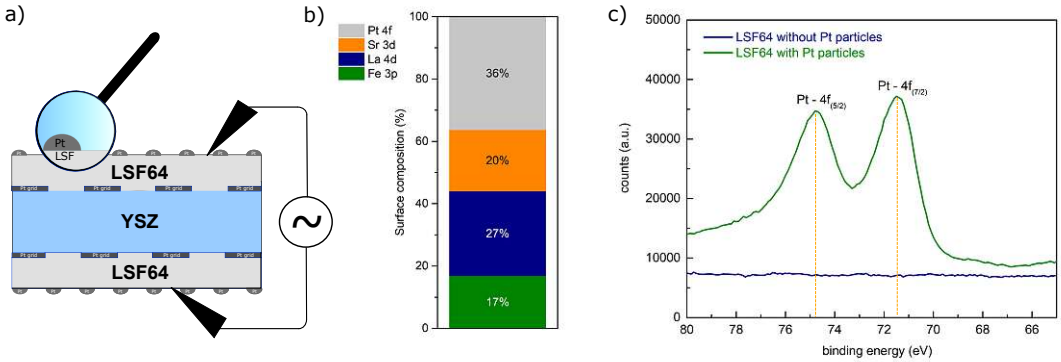

Figure 2.2: a) Sample sketch with embedded current collecting Pt grid at the LSF64|YSZ interface and catalytically active Pt nanoparticles on top of LSF64. b) Surface composition of a platinum decorated LSF64 electrode analyzed from XPS spectra measured after heating to 600 °C for 14 hours. c) Section of the XPS spectra showing a pristine LSF64 electrode and a LSF64 electrode decorated with platinum nanoparticles.

Die approbierte gedruckte Originalversion dieser Dissertation ist an der TU Wien Bibliothek verfügbar.
The approved original version of this doctoral thesis is available in print at TU Wien Bibliothek.
TU WIEN Bibliothek Your knowledge hub

2.3.2 The effect of platinum nanoparticles on the oxygen exchange reaction at the LSF64 surface - impedance spectra

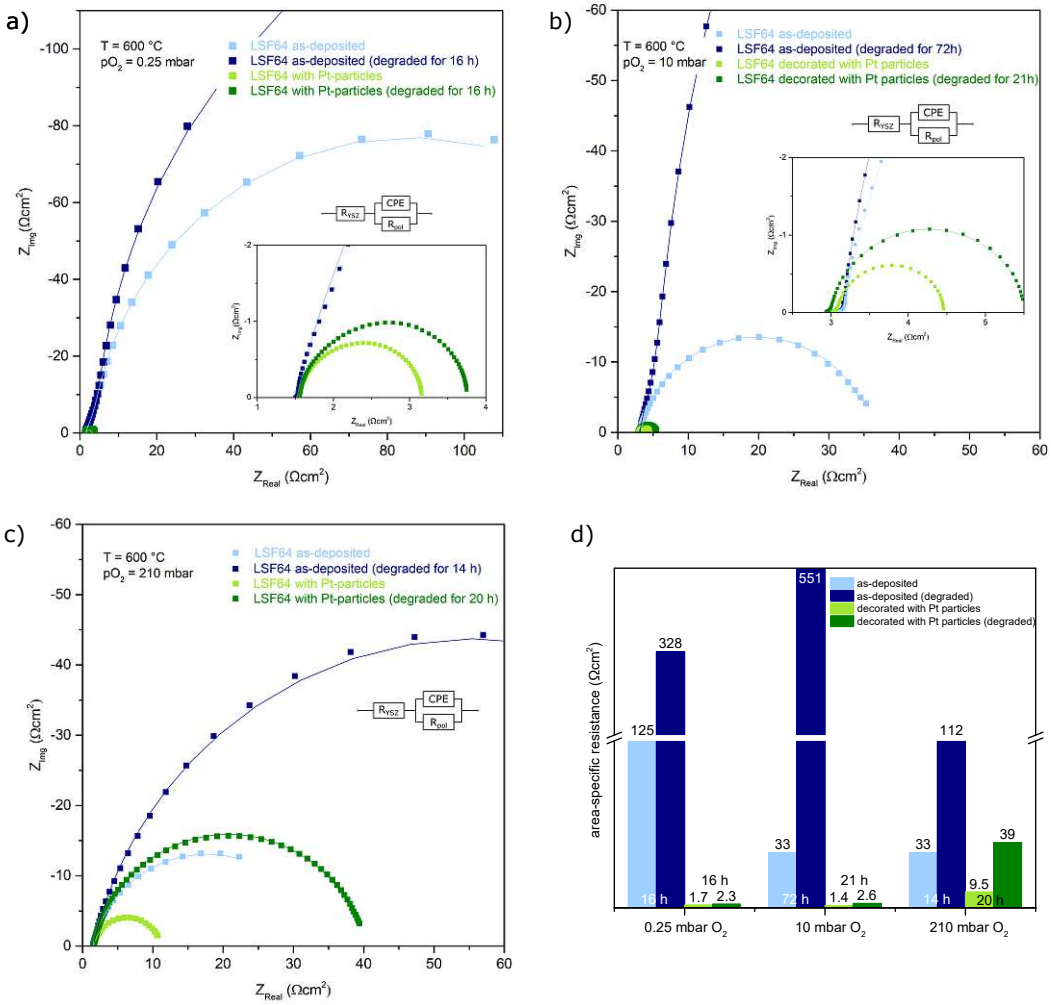

Figure 2.3: (a) - (c) Impedance spectra of symmetrical samples with LSF64 electrodes measured at 600 °C in 0.25 mbar O_2 (a), 10 mbar O_2 (b) and 210 mbar O_2 (c) before and after platinum decoration. The impedance data are normalized to the active electrode area and divided by two (to reveal ASR values of one electrode). Symbols are measured data, lines are fits to the equivalent circuits shown in the insets. (d) Bar chart showing the area specific resistance of LSF64 electrodes at 600 °C before and after platinum decoration. Times written on the bars indicate degradation times.

The electrochemical properties of the LSF64 electrode was investigated on samples with symmetrical LSF64 electrodes, as sketched in Figure 2.2 a). The strong electrochemical effect of platinum nanoparticles on the surface of LSF64 is displayed in the impedance spectra of Figure 2.3 a) - c), measured on three different samples in different gas atmospheres (0.25 mbar, 10 mbar, 210 mbar O_2). The plots show the spectra obtained on pristine LSF64, spectra mea-

Die approbierte gedruckte Originalversion dieser Dissertation ist an der TU Wien Bibliothek verfügbar.
The approved original version of this doctoral thesis is available in print at TU Wien Bibliothek.
TU Bibliothek Your knowledge hub WIEN

sured after some time at elevated temperature under measurement conditions (degradation) and spectra obtained on the same samples after Pt particle deposition. The degradation of the electrochemical performance for free LSF surfaces is a well-known phenomenon and mostly attributed to Sr segregation [81, 94, 138, 139]. Also the XPS measurements in this study show a significant surface enrichment of A-site cations (see below).

The impedance spectra were fitted using the equivalent circuits shown as insets in Figure 2.3. All spectra exhibit a high-frequency offset, which did not show any oxygen partial pressure dependency and can be assigned to transport of O^{2-} ions through the YSZ single crystal [58]. Small differences of the high-frequency intercept can be explained by slightly different temperatures of the samples. The dominating semicircle in the low frequency range displays a strong dependency on the oxygen partial pressure and can be assigned to the oxygen exchange reaction on the electrode surface [58]. This semicircle was fitted to an R|CPE element (CPE = constant phase element). In the medium frequency range often a slight shoulder of the main arc is found, which can most likely be attributed to the LSF64|YSZ interface. However, this rather small part was neglected in most fits. In the following, we label the surface related resistance of the main arc R_{pol}. The electrode capacitance, modeled by the constant phase element (CPE) is attributed to the chemical capacitance and thus to oxygen stoichiometry changes in the bulk of the electrode [140].

Area specific resistances (ASR) of the individual electrodes were calculated from the polarization resistances R_{pol} and the active area and are plotted in Figure 2.3 d). Earlier measurements showed that only the area of LSF64 films directly above YSZ contributes to the oxygen exchange reaction, while the LSF64 above the current collecting Pt grid is inactive due to the relatively large in-plane ionic resistance in the films [21]. Hence, the active surface area used in this analysis was only 25 % or 50 % of the total area depending on the platinum current collector used. However, the area covered by the Pt nanoparticles was not included in this normalisation. As can be seen from Figure 2.3, the deposition of platinum nanoparticles always led to a drastic decrease of the area-specific resistance. The effect of the platinum nanoparticles was especially prounounced at low oxygen partial pressures (0.25 mbar), where the pristine sample exhibited rather slow kinetics. The improvement of Pt with respect to the initial value (LSF64 as deposited) was a factor of 70 and compared to the degraded state of the free LSF64 surface the Pt particles lead to > 200 times better kinetics. Interestingly, also the degradation of the electrode was much less pronounced with the Pt particles. In synthetic air (210 mbar O_2) Pt improved the reaction rate less (still a factor > 3) and degradation with Pt particles was also faster.

The chemical capacitance (C_{chem}) of the electrodes was calculated from the obtained fitting parameters of the CPE element according to $C_{chem} = (Q * R_{pol}{}^{1-n})^{\frac{1}{n}}$, with Q and n being the fit parameters of the CPE element [141]. The values measured without Pt are in reasonable

Die approbierte gedruckte Originalversion dieser Dissertation ist an der TU Wien Bibliothek verfügbar.
The approved original version of this doctoral thesis is available in print at TU Wien Bibliothek.
TU Bibliothek Your knowledge hub WIEN

agreement with literature [74]. However, a partly strong decrease of the capacitance is found after the platinum deposition, as can be seen from Table 2.1. The change of the capacitance is most pronounced for measurements at 0.25 mbar O_2, with a decrease by a factor of about 2. According to literature the chemical capacitance of a mixed conducting thin film can be attributed to oxygen stochiometry changes in the bulk of the electrode [142]. Then, however, the Pt surface decoration is not expected to change the corresponding bulk related values, which should be proportional to the sampled volume [74]. The active MIEC electrode volume should not change due to decoration. So far, we do not have a simple explaination for the process behind the decrease of the chemical capacitance after platinum decoration. Since the focus of the present work is laid on the effect of Pt decoration on the surface exchange reaction, a detailed discussion of this effect on C_{chem} is beyond the scope of this paper and will be the topic of future studies.

Table 2.1: Chemical capacitance at 600 °C measured in different gases with and without Pt decoration.

gas	before Pt decoration	after Pt decoration	literature value [74]
0.25 mbar pO_2	3700 Fcm^{-3}	1500 Fcm^{-3}	3300 Fcm^{-3}
10 mbar pO_2	1470 Fcm^{-3}	860 Fcm^{-3}	1600 Fcm^{-3}
210 mbar pO_2	1300 Fcm^{-3}	1000 Fcm^{-3}	750 Fcm^{-3}

2.3.3 pO_2 dependency of the polarization resistance of platinum decorated electrodes

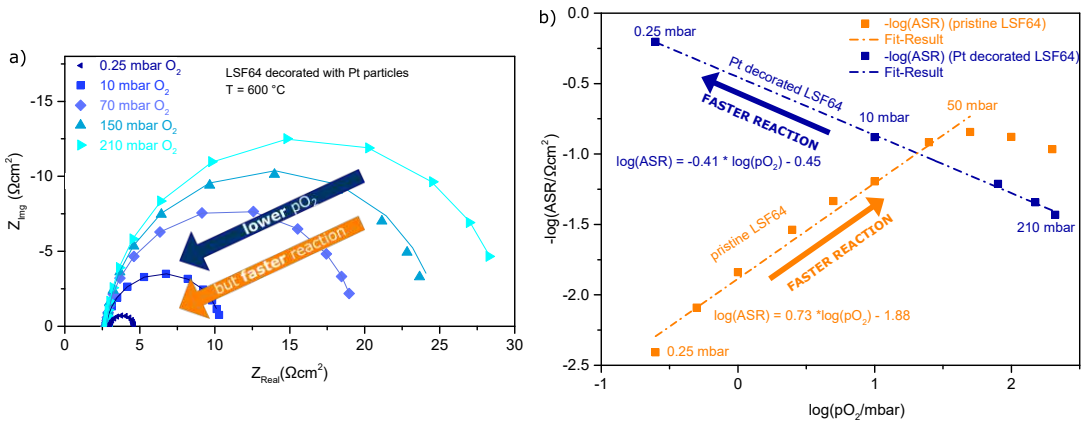

Figure 2.4: a) Impedance spectra of a sample with LSF64 electrodes decorated with Pt particles, measured at different pO_2, revealing faster oxygen incorporation at lower pO_2. b) ASR vs. pO_2 on a -log/log-scale for a pristine sample with LSF64 electrodes (orange data points) from reference[25] and a sample with platinum decorated LSF64 electrodes (blue data points), all measured at 600 °C.

Die approbierte gedruckte Originalversion dieser Dissertation ist an der TU Wien Bibliothek verfügbar.
The approved original version of this doctoral thesis is available in print at TU Wien Bibliothek.
TU Bibliothek Your knowledge hub WIEN

Platinum decorated LSF64 electrodes were measured in different oxygen partial pressures (210 mbar to 0.25 mbar) at 600 °C. As can be seen from Figure 2.4 a), a rather unusual strong increase of the reaction rate - i.e decrease of the polarization resistance- is found for lower oxygen partial pressures. Kinetic studies on mixed conducting oxides usually show faster oxygen incorporation at higher oxygen partial pressure [26, 74, 143–148], in accordance with standard expectations of kinetic models of oxygen reduction (more oxygen molecules enhance the reaction rate). The surprising pO_2 dependence of the ASR was analyzed in terms of a power law with an exponent n according to $ASR^{-1} = \alpha * p_{O_2}{}^{n}$, *i.e.* $-\log(ASR) = \log(\alpha) + n*\log(p_{O_2})$. In Figure 2.4 the negative logarithm of the ASR is plotted against the logarithm of the pO_2 and a reaction order n of -0.41 is found.

The negative reaction order is completely opposite of what is found for LSF64 surfaces without Pt, where a reaction order of + 0.73 was measured between 0.25 and 50 mbar as reported in literature [25] for nominally identical LSF64 electrodes (see also Figure 2.4 b)). Obviously, deposition of Pt particles leads to a situation, where an increase of the oxygen concentration in the gas phase does not enhance the reaction rate of oxygen reduction, but rather decreases it. Interestingly the obtained reaction order is rather close to the slope (-0.5) of the concentration of oxygen vacancies $V_O^{\bullet\bullet}$ in the high pressure range of the Brouwer diagram [59, 74] of LSF64, suggesting a correlation of kinetics and defect concentration. The proposed reaction mechanism is further discussed below. Please note that in Figure 2.4 two different samples were considered, one with Pt and one without Pt. In Figure 2.3, on the other hand, one and the same sample was used for investigating the effect of Pt decoration in a given amtosphere, while different samples were used in different gases. Owing to the scatter of values from sample to sample, see also below, absolute values may thus differ despite nominally identical conditions. Most relevant in Figure 2.4 are the very different reaction orders with and without Pt.

2.3.4 Effect of the deposited platinum amount on the polarization resistance

In an additional experiment the deposited amount of platinum was varied. The LSF64 films were prepared in one single batch in the PLD and measured at 600 °C and 10 mbar O_2 partial pressure before and after platinum decoration. In Figure 2.5 the impedance spectra after Pt deposition are displayed and the area specific resistances of all samples are summarized. As can be seen from the impedance spectra, the deposited platinum amount has a clear effect on the area specific resistance of the LSF64 electrodes and the lowest polarization resistance is found for 0.383 µg Pt on 0.25 cm^2. Similar to earlier studies [21, 142] the polarisation resistance of pristine LSF scatters strongly, but the initial value does not show any correlation with the value found after Pt decoration.

Die approbierte gedruckte Originalversion dieser Dissertation ist an der TU Wien Bibliothek verfügbar.
The approved original version of this doctoral thesis is available in print at TU Wien Bibliothek.
TU WIEN Bibliothek Your knowledge hub

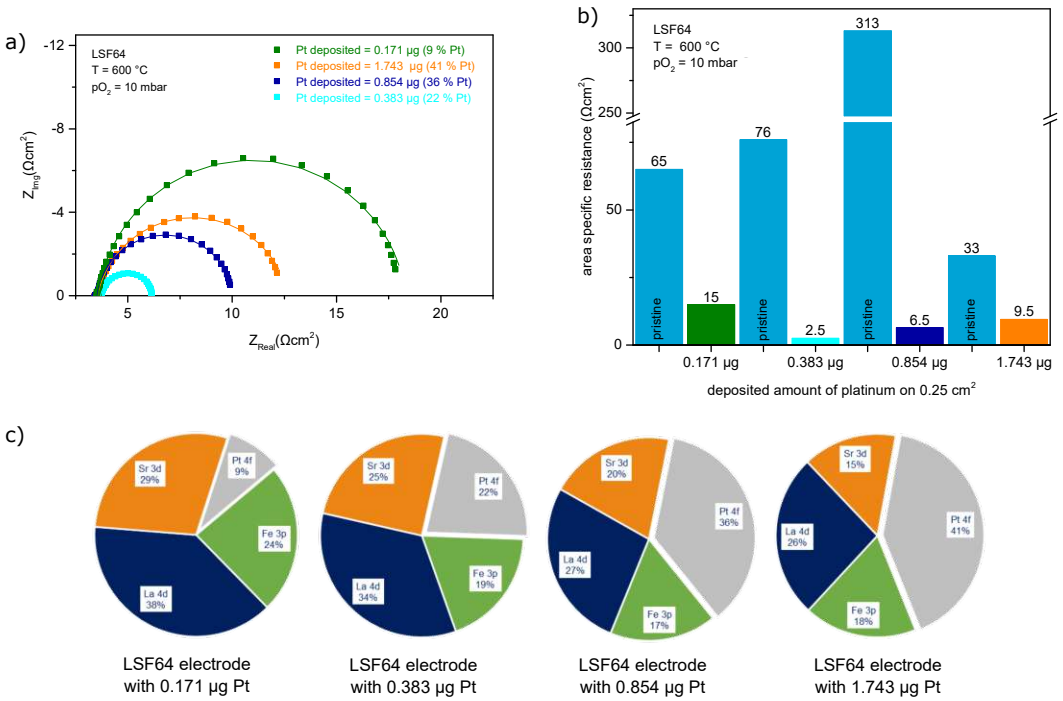

Figure 2.5: a) Impedance spectra of four different LSF64 electrodes decorated with different amounts of platinum and measured at 600 °C in 10 mbar pO_2. b) Bar chart summarizing the effect of different amounts of platinum on the polarisation resistance of LSF64 electrodes. c) Surface composition of all investigated samples from a) measured by XPS.

XPS was carried out to investigate the surface composition of each sample and thus the surface coverage with Pt. The deposited Pt amount was obtained by ICP-MS. As can be seen from the results in Figure 2.5, the surface coverage with platinum does not increase linearly with the deposited platinum amount. This is most probably due to a change of the Pt particle height. Assuming cylindrically shaped particles, the average height of the platinum particles was calculated from the results in Figure 2.5 and the resulting values (between about 3 and 8 nm) are summarized in Table 2.2. BSE images of every sample surface can be found in the Supporting Information (Figure 2.8).

The EIS results suggests that there is an optimum amount of platinum on the surface of LSF64. An increase of the deposited platinum amount beyond this value leads to increased area specific resistances. Not surprisingly, also too little Pt is disadvantageous. However, it is though remarkable that already the deposition of 0.171 µg platinum on 0.25 cm^2 (surface coverage 9 % Pt) led to an improvement of the area specific resistance from 65 Ωcm^2 to 15 Ωcm^2.

Die approbierte gedruckte Originalversion dieser Dissertation ist an der TU Wien Bibliothek verfügbar.
The approved original version of this doctoral thesis is available in print at TU Wien Bibliothek.
TU WIEN Bibliothek Your knowledge hub

Table 2.2: Height of the platinum particles calculated from the deposited amount of Pt on 0.25 cm^2 (from ICP-MS) and the estimated surface coverage (from XPS).

	deposited Pt (µg)	**surface Pt** (%)	**particle height** (nm)
Sample 1	0.171 ± 0.008	9	3
Sample 2	0.383 ± 0.004	22	3
Sample 3	0.854± 0.034	36	4
Sample 4	1.743± 0.069	41	8

2.3.5 Effect of sample prehistory and degradation on the resistance of platinum decorated electrodes

Also the effect of sample prehistory and sample degradation on the area specific resistance of platinum decorated electrodes was further investigated. Four samples with symmetrical LSF64 electrodes (A-D) were prepared in one batch in the PLD chamber and were also sputter-coated with Pt in one batch to exclude effects of varying platinum amounts. EIS measurements were carried out at 600 °C and 10 mbar O_2 partial pressure. While sample A and sample B were measured for 17 h and 72 h, sample C and sample D were not exposed to measurement conditions before platinum deposition. In Table 2.3 the measured polarization resistances are summarized and reveal that the sample prehistory or degradation does not have a significant influence on the observed resistance values of the platinum decorated electrodes.

All four platinum decorated samples showed very similar area specific resistances between 1.1 Ωcm^2 - 1.4 Ωcm^2 and fairly comparable and moderate degradation behaviour. Pt free samples A,B, on the other hand had very different polarization resistances and degradation behaviour, in agreement with the results and data scattering presented above and mentioned in literature for perovskite type thin film electrodes [21]. While sample A showed very fast oxygen reduction kinetics with an area specific resistance of 9.5 Ωcm^2 and degraded very slowly to 14.5 Ωcm^2 in 19 h, sample B exhibited much worse oxygen reduction kinetics already in the pristine state with an area specific resistance of 33 Ωcm^2, which degraded quickly to about 551 Ωcm^2 after 72 h of measurement. The very similar ASR values found after Pt deposition shows that the Pt particles obviously affect the oxygen exchange reaction in a manner neither depending on the intial state of the LSF64 surface nor on its degraded state. This is another very strong indication that a severe change of the reaction mechanism or the rate limiting step takes place with Pt on the surface. As a result of this mechanistic modification, the polarisation resistance becomes much less prone to changes of the MIEC surface. In the Supporting Information (Figure 2.11) it is shown that such an effect of Pt nanoparticles is not restricted to LSF64, but can also be found for $SrTi_{0.7}Fe_{0.3}O_{3-\delta}$ (STF73). Moreover, the Pt nanoparticles also improve the polarization resistance of LSF64 in humidified hydrogen.

Die approbierte gedruckte Originalversion dieser Dissertation ist an der TU Wien Bibliothek verfügbar.
The approved original version of this doctoral thesis is available in print at TU Wien Bibliothek.
TU WIEN Bibliothek Your knowledge hub

Table 2.3: Effect of degradation and sample prehistory of four identically prepared samples with LSF64 electrodes (A-D) (one batch) with and without platinum decoration. "Time" indicates degradation time.

	pristine LSF64 samples			platinum decorated LSF64 samples		
	as-deposited	degraded	time	as-deposited	degraded	time
A	9.5 Ωcm^2	14.5 Ωcm^2	19 h	1.2 Ωcm^2	2.6 Ωcm^2	21 h
B	33 Ωcm^2	551 Ωcm^2	72 h	1.4 Ωcm^2	2.6 Ωcm^2	21 h
C	not measured			1.1 Ωcm^2	1.8 Ωcm^2	23 h
D	not measured			1.2 Ωcm^2	2.1 Ωcm^2	23 h

2.4 Mechanistic discussion

The results shown so far have strong implications for the mechanistic interpretation of oxygen exchange on mixed conducting oxides, here LSF64. Essentially six experimental facts have to be interpreted:

- the surprising negative reaction order, *i.e.* the much faster reaction upon lower pO_2.
- the fact that a reduced Pt amount may still cause an improved reaction rate.
- the increase of the polarization resistance for very small amounts of platinum.
- the high reproducibility of the polarization resistance with Pt decoration, irrespective of the LSF64 degradation state.
- the reduced degradation rate with Pt.

In the following we suggest a simple mechanistic model that can explain all these effects. We base our discussion on the reaction mechanism for oxygen incorporation on single phase MIEC cathodes proposed in reference[50]: On dense thin film samples oxygen reduction and incorporation happens via the so-called bulk path. In this path oxygen gas diffuses to the electrode, adsorbs on the surface of the oxide, dissociates and is incorporated into an oxygen vacancy. The ionization steps may take place during dissociation and/or during incorporation. The oxygen ions are then transfered through the electrode to the electrolyte. Electrons needed for the oxygen reduction are transported from the current collector to the active reduction site on the surface of the MIEC oxide. This is sketched in Figure 2.6, together with the modification that comes along with the Pt particles.

Die approbierte gedruckte Originalversion dieser Dissertation ist an der TU Wien Bibliothek verfügbar.
The approved original version of this doctoral thesis is available in print at TU Wien Bibliothek.
TU WIEN Bibliothek Your knowledge hub

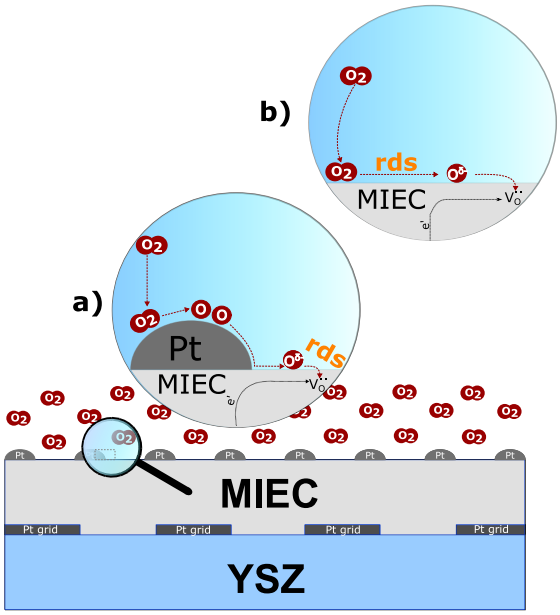

Figure 2.6: Sketch explaining the suggested reaction mechanism for oxygen incorporation on a platinum decorated MIEC (a) and a pristine MIEC (b).

With Pt on the MIEC surface, oxygen (O_2) from the gas phase, adsorbs on the Pt surface and dissociates. The resulting oxygen (O_{ad}) atom (possibly partly charged) then diffuses from the platinum particle onto the free, uncovered MIEC electrode surface (= spill-over) and gets incorporated into the oxide. The final ionisation step may take place either before or during incorporation into the oxide lattice. In contrast to classical triple-phase active electrodes, the oxygen vacancy and also the electrons required for oxygen incorporation are provided from the mixed conductor. For a steady state reaction, the electrons flow from the current collector into the MIEC, while oxygen vacancies are replaced from the electrolyte.

The decreased polarization resistance of platinum decorated MIEC samples (observation i)), can then easily be explained by a complete change of the rate limiting step, induced by the presence of Pt. Since Pt can only accelerate the oxygen dissociation, but not the incorporation into the MIEC vacancy, we conclude that oxygen reduction on pure MIEC surfaces is most probably limited by oxygen dissociation (possibly including partial ionization). This rate limiting dissociation step is now bypassed by the platinum particles. Hence, we have a kind of job sharing between platinum particles and MIEC, performing oxygen dissociation and incorporation, respectively. This is a true two phase process and not an effect of the MIEC|Pt interface.

Since less platinum surface area and thus more free MIEC surface can still lower the resistance (observation iii)), we conclude that also with platinum particles on top, the rate limiting step still takes place on the MIEC surface. However, no longer dissociation on the MIEC is

Die approbierte gedruckte Originalversion dieser Dissertation ist an der TU Wien Bibliothek verfügbar.
The approved original version of this doctoral thesis is available in print at TU Wien Bibliothek.
TU Bibliothek Your knowledge hub WIEN

decisive, but oxygen incorporation into the MIEC (*i.e.* into a vacancy) and/or ionization. This can also explain the surprising $p(O_2)$ dependence (observation ii)): At higher oxygen partial pressures the concentration of O_2 in the gas atmosphere is higher and this accelerates the rate limiting dissocation on free LSF64. However, adsorption and oxygen dissociation on the platinum particles is fast and the oxygen surface coverage on Pt is significant, even for very low pO_2 [149–151]. Thus incorporation into an oxygen vacancy on the MIEC becomes the decisive step. According to the Brouwer diagram of LSF64 [25] the concentration of oxygen vacancies, which are needed for incorporation inside the material, is higher at lower pO_2 and therefore the incorporation of oxygen is faster at lower oxygen partial pressures. Since both, empirical reaction order of ASR^{-1} vs. pO_2 (-0.41) and slope in the Brouwer diagram (-0.5) are very similar, the true reaction order with respect to the oxygen vacancies seems to be close to 1. [25, 59, 74]

According to this reaction scheme the rate limiting dissocation step on pure MIEC materials (here LSF64) depends very strongly on active sites for dissociation. Those may severely depend on prehistory and degradation. Moreover, the number of very active dissociation sites appears to be strongly limited anyway: A study on LSC showed that already a few percent of a SrO monolayer double the polarization resistance and can deactivate most of the highly active sites on LSC [93]. The rate limiting step for platinum decorated MIECs, however, is related to the oxygen vacancy concentration, which seems to be less prone to changes or deactivation. This would explain observations v) and vi) *i.e.* the high reproducibility and the reasonable stability of the polarization resistance for the Pt decorated LSF64.

Finally, lowering the platinum amount to 9 % surface coverage (observation iv)) led to an increase of the area-specific resistance. The observation can be explained if one assumes that the spill-over of atomic oxygen onto LSF64 surfaces is limited to a distinct zone close to the TPB. This would imply that the area supplied with dissociated oxygen species and thus being more active for oxygen incorporation (*i.e.* rings around the Pt particles) becomes smaller than the entire free MIEC surface for the case of very few and largely spaced Pt particles. Then a co-limitation of oxygen surface diffusion on the MIEC and oxygen incorporation (into a vacancy) is effective. Future experiments may reveal the width of the active region and thus the spill-over width of oxygen on MIECs.

Die approbierte gedruckte Originalversion dieser Dissertation ist an der TU Wien Bibliothek verfügbar.
The approved original version of this doctoral thesis is available in print at TU Wien Bibliothek.
TU WIEN Bibliothek Your knowledge hub

2.5 Conclusion

In this study we showed that decoration of $La_{0.6}Sr_{0.4}FeO_{3-\delta}$ (LSF64) thin film electrode surfaces with platinum nanoparticles (*ca.* 20 nm-40 nm diameter and *ca.* 4 nm-6 nm height, *ca.* 30 % surface coverage) strongly lowers the polarization resistance of the electrode. At lower oxygen partial pressure (0.25 mbar) almost two orders of magnitude faster oxygen reduction kinetics was measured for Pt decorated films. Moreover, the Pt decorated surfaces exhibit an uncommon pO_2 dependence of the polarization resistance, where less oxygen concentration leads to lower polarization resistance (= faster reaction kinetics). Also the reproducibility of electrochemical properties and degradation behaviour were improved. All this can be explained by assuming a job sharing mechanism with Pt dissociating oxygen, spill-over of dissociated oxygen from Pt onto LSF64 and final ionization and incorporation into oxygen vacancies on the LSF64 surface. While without Pt oxygen dissociation on LSF64 is rate-limiting, Pt by-passes this slow step and rate-limiting oxygen ionization and incorporation on LSF64 remains.

Die approbierte gedruckte Originalversion dieser Dissertation ist an der TU Wien Bibliothek verfügbar.
The approved original version of this doctoral thesis is available in print at TU Wien Bibliothek.
TU WIEN Bibliothek Your knowledge hub

2.6 Supporting Information

2.6.1 Characterization of LSF64 target and LSF64 thin film by means of X-ray diffraction

Figure 2.7 shows a diffractogram of a LSF64 thin film decorated with platinum particles, measured in gracing incidence geometry, and the LSF64 target used for the deposition of the thin films measured in Bragg-Bretano geometry. Owing to their small amount and size, it was not possible to detect any signal from the platinum particles on the surface of LSF64 by means of the lab-based diffractometer.

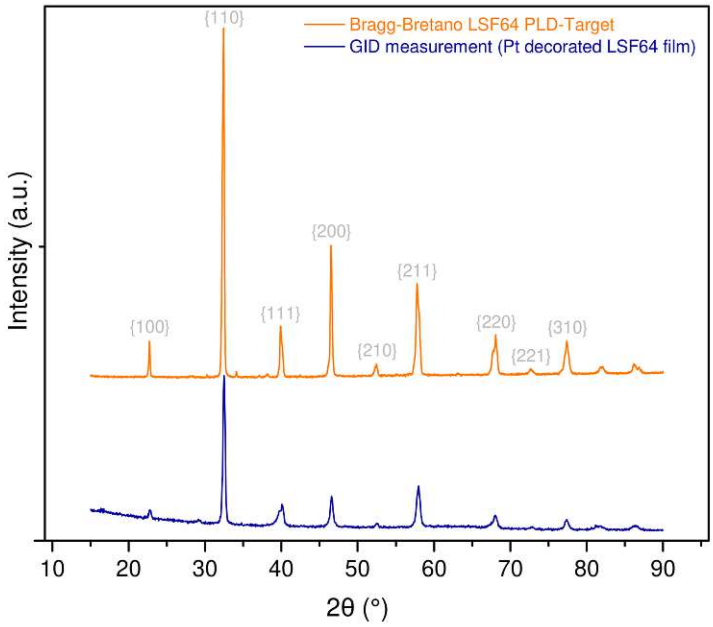

Figure 2.7: Diffraction pattern of LSF64 thin film decorated with Pt particles, measured in gracing incidence geometry (GID); LSF64 target measured in Bragg-Bretano geometry.

Die approbierte gedruckte Originalversion dieser Dissertation ist an der TU Wien Bibliothek verfügbar.
The approved original version of this doctoral thesis is available in print at TU Wien Bibliothek.
TU WIEN Bibliothek Your knowledge hub

2.6.2 Effect of the deposited platinum amount on the resistance: SEM images

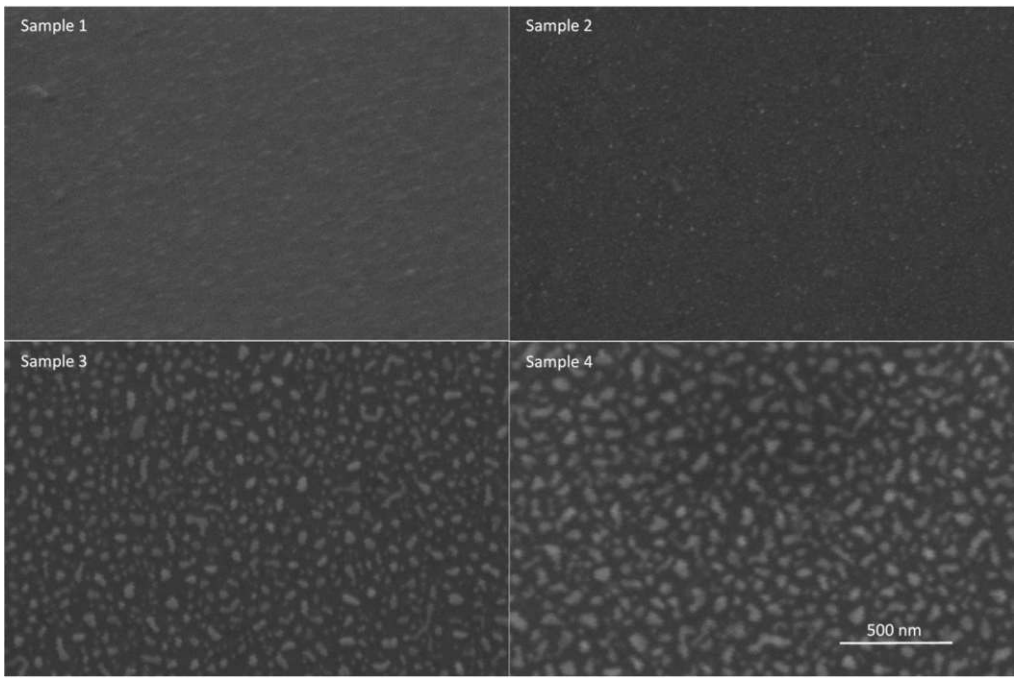

Figure 2.8: BSE images of all samples decorated with different amounts of platinum.

Die approbierte gedruckte Originalversion dieser Dissertation ist an der TU Wien Bibliothek verfügbar.
The approved original version of this doctoral thesis is available in print at TU Wien Bibliothek.
TU WIEN Bibliothek Your knowledge hub

2.6.3 Effect of the deposited platinum amount on the resistance: XPS results

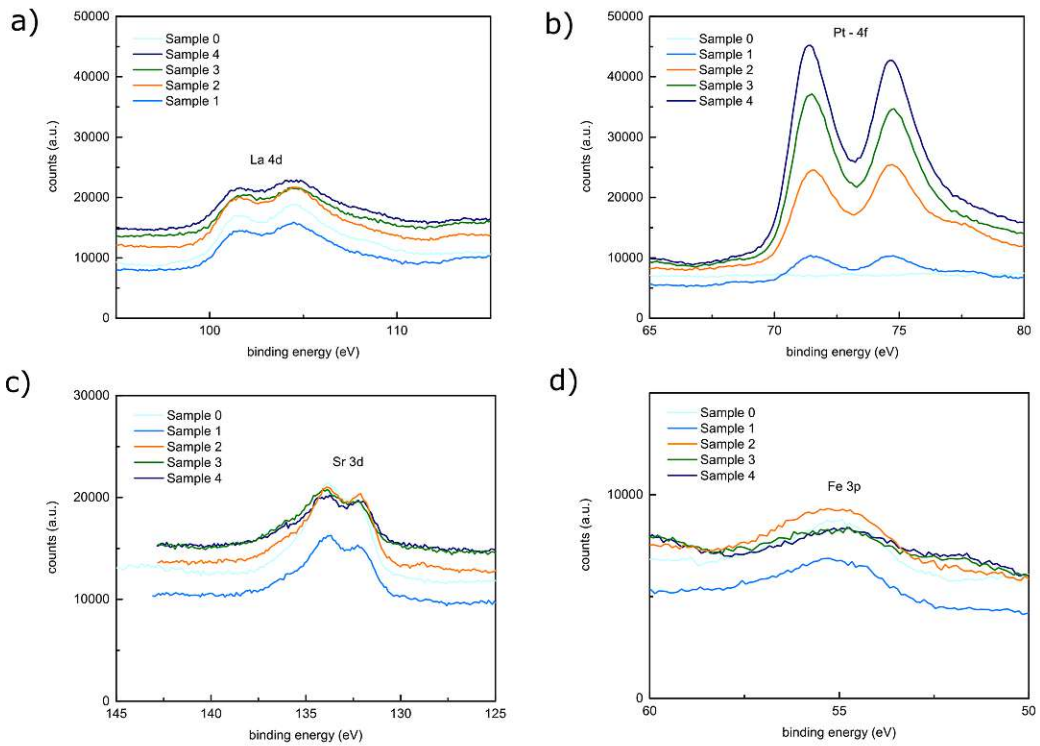

Figure 2.9: Results of XPS measurements on LSF64 electrodes decorated with different amounts of Pt. a) XPS spectra of La, b) XPS spectra of Pt, c) XPS spectra of Sr, d) XPS spectra of Fe.

Die approbierte gedruckte Originalversion dieser Dissertation ist an der TU Wien Bibliothek verfügbar.
The approved original version of this doctoral thesis is available in print at TU Wien Bibliothek.
TU WIEN Bibliothek Your knowledge hub

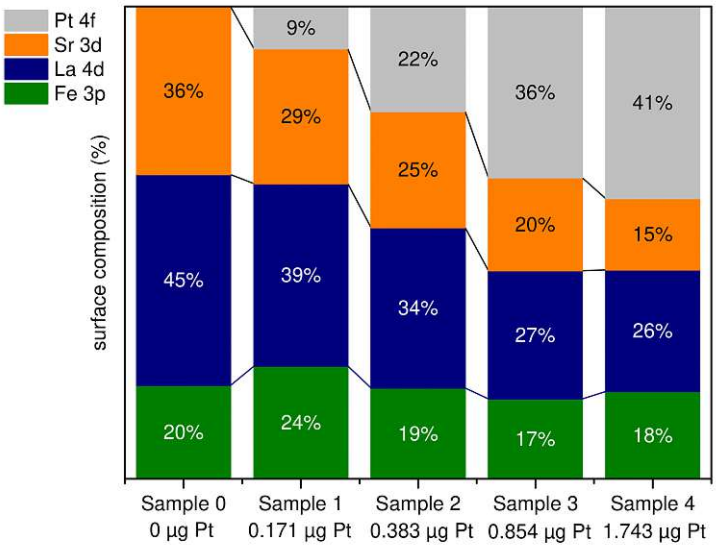

Figure 2.10: Surface composition of samples with LSF64 electrodes decorated with different amounts of platinum determined by XPS measurements.

2.6.4 Effect of platinum nanoparticles on other MIEC materials and in humidified H_2

The accelerating effect of Pt nanoparticles is not restricted to LSF64 in oxidizing conditions. Figure 2.11 a) displays the same type of measurements for $SrTi_{0.7}Fe_{0.3}O_{3-\delta}$ thin film electrodes with and without Pt, before and after degradation. A symmetrical sample with STF73 electrodes was prepared according to reference [152] and measured in 0.25 mbar O_2 at 600 °C. The area specific resistance of the pristine STF73 electrode was 86 Ωcm^2 and reached 150 Ωcm^2 after 16 h of measurement. The freshly Pt decorated sample exhibited an ASR of 6.5 Ωcm^2, which increased to 15 Ωcm^2 after 20 h at 600 °C. Owing to an additional impedance feature, the spectra of both the undecorated and the decorated sample were fitted with a resistance in series with two R-CPEs. It was observed that due to platinum decoration the low frequency resistance (R2) and capacitance (C2) changed, while the intermediate frequency resistance (R1) and capacitance (C1) stayed constant. The latter was therefore assigned to the STF73-YSZ interface. Considering only the surface-related resistance, we find a change by Pt decoration from 85 Ωcm^2 to 5 Ωcm^2, clearly showing that again much faster oxygen exchange is found with Pt (though the effect is not as pronounced as for LSF64 with Pt).

In addition to measurements under oxidizing conditions, a symmetrical sample with LSF64 electrodes was investigated under reducing conditions (2.4% humidified H_2 in Argon, pO_2 = 10^{-21} mbar at 600 °C). The obtained spectra (figure 2.11 b)) were fitted to two R-CPE element,

Die approbierte gedruckte Originalversion dieser Dissertation ist an der TU Wien Bibliothek verfügbar.
The approved original version of this doctoral thesis is available in print at TU Wien Bibliothek.
TU Bibliothek Your knowledge hub WIEN

one to describe the rather pronounced shoulder in the mid frequency range and another R-CPE to describe the semicircle in the low frequency range. Under these conditions, where already pristine LSF64 thin films exhibit fast kinetics, the effect of platinum decoration was smaller, but still observable, with about a factor of 2 faster surface reaction. This result is similar to the promoting effect of metallic Fe particles exsolved from LSF64 electrodes under reducing conditions [153] thus indicating that the deposited particles may act via a similar mechanism as the exsolved ones. The obtained spectra were fitted to two R-CPE element, one to describe the rather pronounced shoulder in the mid frequency range and another R-CPE to describe the semicircle in the low frequency range. The degradation process of the sample was not investigated, but earlier studies had shown that LSF64 exhibits very little degradation in humidified H_2.[21] Accordingly we conclude that the beneficial effect of Pt nanoparticles is not restricted to the oxygen reduction reaction.

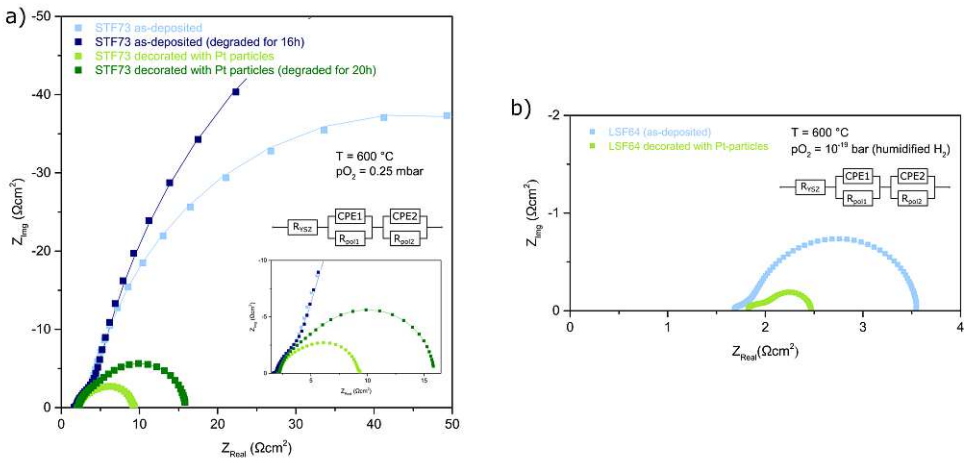

Figure 2.11: EIS spectra of a) a sample with STF73 electrodes in 0.25 mbar and b) with LSF64 electrodes in humidified H2 measured in 600 °C before and after Pt decoration..

Die approbierte gedruckte Originalversion dieser Dissertation ist an der TU Wien Bibliothek verfügbar.
The approved original version of this doctoral thesis is available in print at TU Wien Bibliothek.
TU WIEN Bibliothek Your knowledge hub

3 Performance modulation through selective, homogeneous surface doping of lanthanum strontium ferrite electrodes revealed by *in-situ* PLD impedance measurements

Large parts of the study presented in this chapter are also published in Christoph Riedl et al, J. Mater. Chem. A, 2022,10, 2973-2986. [154]

3.1 Introduction

Platinum is well known for its favourable redox catalytic properties, which are widely used in a broad range of applications (e.g.: oxygen sensors [155–157], electrode in aqueous electrolyte solutions [158, 159]). In the context of our study, the usage of platinum or platinum-based catalysts in polymer electrode membrane fuel cells (PEMFC) cathodes to accelerate the oxygen reduction reaction might be most relevant.[160, 161] Lots of efforts have been made to reduce the Pt loading in PEMFC to about 0.1 mg/cm^2. [162, 163] Nevertheless, in the field of solid oxide fuel cells, the usage of platinum electrodes is very rare, not only because of costs, but also because Pt electrodes generally lead to higher polarisation resistances than mixed conduction oxide electrodes. That might be surprising at first glance, but is related to the fact that in case of Pt electrodes residing on an oxide ion conducting ceramics only the region very close to the triple phase boundary (i.e. where YSZ electrolyte, Pt and O_2 meet) is electrochemically active for oxygen reduction, which has been shown in several mechanistic studies. [111, 119, 124–127, 132]

The OER activity of MIEC electrodes can be increased by depositing catalytically active Pt species, which show a high affinity for oxygen splitting and ionization. [164] In a recent study [112], platinum nanoparticles were deposited on the surface of LSF thin film electrodes and, especially at very low oxygen partial pressures (0.25 mbar O_2) a severe decrease of the

Die approbierte gedruckte Originalversion dieser Dissertation ist an der TU Wien Bibliothek verfügbar.
The approved original version of this doctoral thesis is available in print at TU Wien Bibliothek.
TU WIEN Bibliothek Your knowledge hub

polarisation resistance was observed. In addition, a change of the oxygen reduction mechanism was found and the improved oxygen exchange kinetics was explained by a job-splitting with oxygen dissociation taking place on the platinum nanoparticles and oxygen incorporation occurring at the free surface of LSF. While metallic nanoparticles sputter deposited on a MIEC surface are usually relatively large, with diameters of more than ten nanometers[112], incorporation of the catalytically active platinum group elements into the lattice of the pervoskite-type MIEC (i.e. doping) may offer the advantage to achieving exsolved nanoclusters or even single atoms of the catalyst dopants in the electrode material. With a high dispersion of the metal, the catalytically advantageous properties of platinum may then be most efficiently utilised.

Several studies have already shown that the performance of established SOFC electrodes can be improved by doping with additional catalytically active elements. For example, studies on $SrTi_xFe_{1-x}O_{3-\delta}$ revealed positive effects of Co [165], Ni[166, 167] or Ru[168] doping on the polarisation resistance of the electrode and showed increased long term stability. Similar effects were found on $La_{1-x}Sr_xCrO_{3-\delta}$ after doping with Ru or Ni. [169]. In addition, "self-regenerating" automotive catalysts were developed by doping Pt, Rd or Pd metal into the perovskite host lattice. While highly active exsolved nanoparticles were found under reducing conditions on the catalyst surface, studies showed that these nanoparticles were reincorporated into the host lattice under oxidizing conditions. [170–172]

In this study, we reveal how minor amounts of platinum doping (of the order of only 1 % of the overall cation amount) can strongly decrease the polarization resistance of lanthanum strontium ferrite (LSF) thin film electrodes grown by pulsed laser deposition (PLD). Moreover, the fabrication of multilayer electrodes allowed us to directly compare the electro-catalytic activity of electrodes with different surface composition (in this study, pure LSF electrodes and Pt doped LSF electrodes). For electrochemical characterization, impedance measurements were conducted *in-situ* on thin film electrodes directly inside the setup of the PLD immediately after growth (*i*-PLD). This technique was already employed successfully in several studies [76, 93, 95, 99, 110] and enables characterizing electrodes unaltered by externally triggered degradation effects. The unusually high stability of the polarisation resistance in *i*-PLD studies enables its observation over a longer period of time and allowed us studying the electrode kinetics at different $p(O_2)$ and temperatures, thus leading to additional mechanistic insights into the OER on the surface of LSF with and without Pt. In order to establish correlations between the surface composition and the electrocatalytic activity of the electrode, in-situ ambient pressure X-ray photoelectron spectroscopy (AP-XPS) was performed under operation conditions. In addition, inductively coupled plasma mass spectroscopy (ICP-MS) was used to determine the total platinum amount in the thin films. Atomic force microscopy (AFM) and transmission electron microscopy (TEM) were used to reveal the surface and bulk morphology of the electrodes and the obtained results support our mechanistic interpretations.

Die approbierte gedruckte Originalversion dieser Dissertation ist an der TU Wien Bibliothek verfügbar.
The approved original version of this doctoral thesis is available in print at TU Wien Bibliothek.
TU Bibliothek Your knowledge hub WIEN

3.2 Experimental section

3.2.1 Sample preparation

LSF and Pt-doped LSF powders were prepared via the Pechini route [173] from Fe, La_2O_3, $SrCO_3$ and $Pt(NO_3)_2(NH_3)_4$ (all bought from Sigma Aldrich, at least 99.99,% purity). For the doped material, two different Pt concentrations - nominally 0.9 at% and 1.5 at% of cations- were chosen, which are denoted LSF-Pt1 and LSF-Pt2, respectively. The obtained powders were calcined at 800 °C in air, pressed into PLD targets by cold-isostatic pressing at 150 MPa and sintered at 1200 °C in air for 12 h. As electrolyte substrates (100)-oriented yttria stabilized zirconia single crystals (YSZ) (0.5×0.5×0.05 cm^3) (CrysTec, Germany) for polycrystalline film growth and (100)-oriented
$La_{0.95}Sr_{0.05}Ga_{0.95}Mg_{0.05}O_{3-\delta}$ (LSGM) single crystals for epitaxial film growth were used [174]. Before deposition of oxide thin films, current collecting platinum grids (with 15|5 µm or 25|10 µm mesh|strip width) were prepared on the single crystals by lift-off lithography and subsequent magnetron sputtering of 5 nm titanium (as an adhesion promoter) and 100 nm platinum (BAL-TEC MED 020, Liechtenstein). As counter electrode nano-porous $La_{0.6}Sr_{0.4}CoO_{3-\delta}$ was deposited by PLD at 450 °C and 0.4 mbar O_2 with a target to substrate distance of 5 cm. This leads to kinetically very fast electrodes with almost negligible polarisation resistance compared to the dense working electrode. The working electrodes (i.e. LSF, LSF-Pt1, LSF-Pt2) were grown on the single crystal substrates with current collector grids by ablating the respective targets with a KrF excimer laser (Compex Pro 201F, wavelength 248 nm). Multilayers of LSF, LSF-Pt1 and LSF-Pt2 were grown during the *i*-PLD characterisation. The substrate temperature (measured by pyrometer) and oxygen background pressure were 600 °C and 0.04 mbar O_2, respectively. A film thickness of 10 nm was obtained after applying 1000 pulses with a laser frequency of 2 Hz, a laser fluence of 1.1 Jcm^{-2} (measured inside the PLD chamber), and a target to substrate distance of 6 cm. The growth rate was determined by measurements with a profilometer (DekTakXT, Bruker, USA) after the deposition of a known number of pulses.

3.2.2 Electrochemical measurements

In-situ electrochemical measurements during PLD deposition (*i*-PLD) were conducted with an Alpha-A High Performance Frequency Analyzer equipped with an Electrochemical Test Station POT/GAL 30V/2A setup (both Novocontrol Technologies, Germany). For *i*-PLD measurements, a sample was placed on the PLD heater and covered with a corundum mask (cutout 0.45×0.45 cm^2) to prevent short circuiting of working electrode and counter electrode via the edges of the sample during the subsequent film deposition. The working electrode

Die approbierte gedruckte Originalversion dieser Dissertation ist an der TU Wien Bibliothek verfügbar.
The approved original version of this doctoral thesis is available in print at TU Wien Bibliothek.
TU WIEN Bibliothek Your knowledge hub

was contacted with a PtIr-needle and the counter electrode via platinum paste brushed onto the heater. A sketch of the measurement setup can be found in Figure 3.1.
Impedance measurements were typically conducted in a frequency range from 10^6 to 10^{-1} Hz (if needed for resolving the electrode feature, the frequency range was extended to 10^{-2} Hz), with an amplitude of 10 mV root-mean-square, and a resolution of 5 or 10 points per frequency decade. In many cases oxygen partial pressure and temperature were kept at 600 °C and 0.04 mbar O_2 as for deposition; in some cases pressure and temperature were varied for a more detailed impedance characterisation.

3.2.3 Characterisation of thin film surface and bulk composition, structure, and morphology

X-ray photoelectron spectroscopy (XPS) spectra were acquired using a lab-based AP-XPS machine [175] with monochromated Al k-alpha radiation. For better comparability of the different Pt oxidation states, the spectra were corrected for the Fermi level shift of the grounded working electrode that is introduced by electrochemical polarization, or atmospheric variations. [106, 176] Due to the absence of carbon, the binding energy was calibrated to the main O1s component at 529.8 eV. Quantification was performed using Scofield cross-sections [177] and S-type “Shirley” backgrounds with the software "Casa XPS". In order to achieve equal probing depth for all elements we compared peaks with similar photoelectron energy (and effective attenuation length of ca. 1.8 nm), Sr3d (BE 130 eV), La4d (BE 110 eV), Pt4f (BE 75 eV) and Fe3p (BE 58 eV) .
Two modes were used for analysing the surface chemistry of LSF-Pt2 electrodes: The XPS machine was operated either in UHV or the sample was exposed to 1 mbar O_2 (AP-XPS mode). In the latter case the sample was heated to typical operation temperature (600 °C) and partly even a bias voltage was applied (leaving an overpotentials of ± 300 mV) in order to drive the electrode into oxygen reduction or oxygen evolution mode.

Atomic force microscopy (AFM) was performed in tapping mode with a Nanoscope V multimode setup (Bruker, United States of America) over a scan area of 1×1 μm^2. Data were plotted with python™.

For measuring the bulk composition of the deposited films, 100 nm thin layers were prepared on YSZ substrates (without Pt grid and counter electrode). The samples were then digested in triplicates with 0.5 mL aqua regia (HCl: HNO_3 =3:1) by heating to 60°C for half an hour in falcon tubes and then diluted to a volume of 10 mL with millipure water. All chemicals were purchased from Merck in the highest available purity, single element ICP standards were also purchased from Merck. For the analytical experiments samples were diluted 1:100 with 1 v% HNO_3 with 1 ng/g indium as internal standard. The internal standard was used

Die approbierte gedruckte Originalversion dieser Dissertation ist an der TU Wien Bibliothek verfügbar.
The approved original version of this doctoral thesis is available in print at TU Wien Bibliothek.
TU WIEN Bibliothek Your knowledge hub

to correct instrumental drift during the course of the measurement. Measurements were conducted on a iCAP-Q ICP-MS instrument (Thermo Scientific, United States of America) with a ESI SC-2-DX autosampler (ESI, USA) and a Fast valve (ESI, USA), see [178] for detailed instrument parameters. The following ions were monitored during the measurement: $^{57}Fe^{+}$, $^{139}La^{+}$, $^{86}Sr^{+}$,$^{88}Sr^{+}$, $^{194}Pt^{+}$, $^{196}Pt^{+}$ and $^{115}In^{+}$. Matrix matched external standards were used for quantification of background corrected signals.

Scanning electron microscopy (SEM) measurements were carried out with a FEI Quanta 250 FEGSEM. A thin electron transparent lamella was produced using a ThermoFisher Scios 2 Dual Beam FIB. In order to protect the surface to the lamella a thin C-layer (about 35 nm) was deposited first by electron beam deposition followed by a W-protection layer. For transmission electron microscopy (TEM) a TECNAI F20 field emission TEM was used equipped with a high angle annular dark field detector (HAADF) in scanning transmission (STEM) mode and a Rio 16 CMOS Camera in TEM mode, respectivley.

Grazing incidence X-ray diffraction (XRD) measurements were performed with an Empyrean X-ray diffractometer (Malvern Panalytical, GB) equipped with a parallel beam mirror on the incident beam side and a parallel plate collimator and a scintillation detector on the diffracted beam side.

3.3 Results

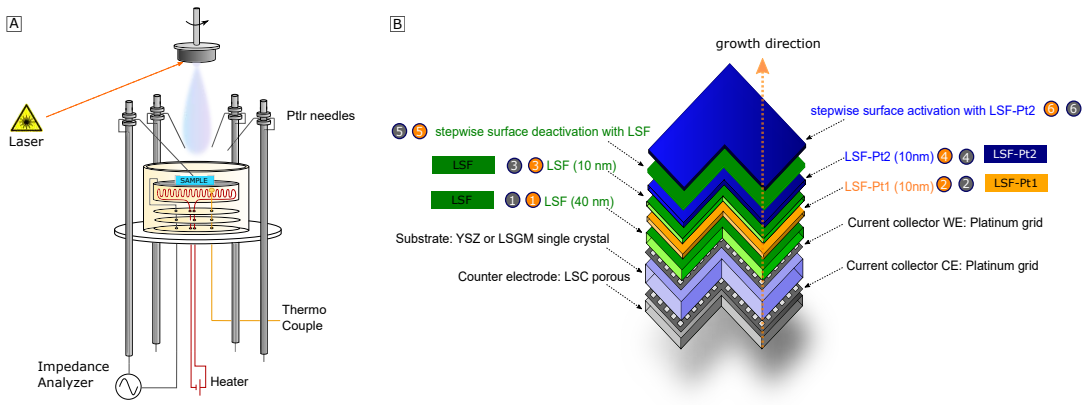

Figure 3.1: A) Sketch of the *i*-PLD heater. B) Sketch of the multi-layer structure of the *i*-PLD sample grown on YSZ or LSGM single electrodes. This nomenclature is identical in figures 3.1, 3.6, 3.7 and the numbers are also mentioned in the text.

Die approbierte gedruckte Originalversion dieser Dissertation ist an der TU Wien Bibliothek verfügbar.
The approved original version of this doctoral thesis is available in print at TU Wien Bibliothek.
TU WIEN Bibliothek Your knowledge hub

3.3.1 Stoichiometric composition of the electrodes

The compositions of the PLD-grown LSF and LSF-Pt thin films were determined by acidic digestion of the entire films and quantification of the cations in the resulting solution using ICP-MS. A thin film stoichiometry of $La_{0.5207\pm0.008}Sr_{0.4793\pm0.008}Fe_{1.0}O_{3-\delta}$ for LSF, $La_{0.5285\pm0.004}Sr_{0.4715\pm0.004}Fe_{0.9817\pm0.001}Pt_{0.0183\pm0.001}O_{3-\delta}$ for LSF-Pt1 and $La_{0.5207\pm0.008}Sr_{0.4747\pm0.004}Fe_{0.9728\pm0.001}Pt_{0.0272\pm0.001}O_{3-\delta}$ for LSF-Pt2 was found. Thus from ICP-MS measurements we assumed about 0.9 at% of all cations of LSF-Pt1 and 1.4 at% of LSF-Pt2 to be platinum.

In order to verify these results, X-ray photoelectron spectroscopy (XPS) measurements were carried out in UHV on pristine thin films directly after PLD deposition. From the XPS spectra 0.9 at% and 1.5 at% of the total cation amount of LSF-Pt1 and LSF-Pt2 were identified to be platinum, respectively. This very good agreement of surface sensitive XPS results with bulk composition suggests absence of any noteworthy surface accumulation or depletion of Pt. The binding energies (77.5 eV and 74.0 eV) found for Pt-$4f_{5/2}$ and Pt-$4f_{7/2}$ were in good accordance with literature data [179] for Pt^{4+} Accordingly, we conclude that platinum was successfully incorporated into the perovskite lattice of LSF. This is also in accordance with the results of several other characterisation techniques, which did not yield an indication for a possible phase separation (details see below). Assuming B-site occupation of Pt^{4+} we thus have about 2 % and 3 % of Pt on this site in the two sample types (LSF-Pt1 and LSF-Pt2).

3.3.2 Structural and morphological characterization of the electrodes

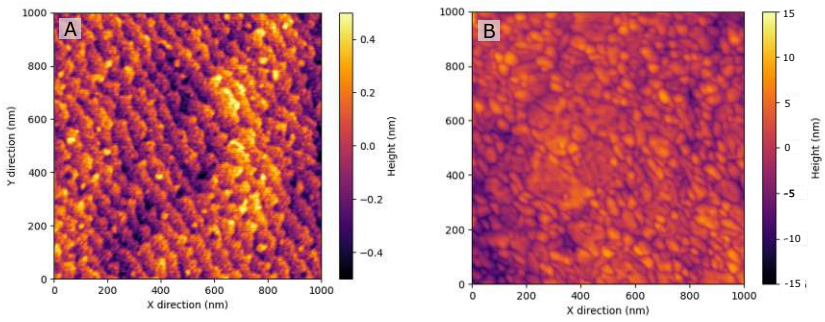

Figure 3.2: AFM image of the measured multilayer electrodes grown on LSGM (A) and YSZ (B) with a top layer made of LSF-Pt2 (10 nm). Please note the different scale bars.

For surface morphology characterization, atomic force microscopy (AFM) measurements were conducted on multi-layer electrodes grown on $La_{0.95}Sr_{0.05}Ga_{0.95}Mg_{0.05}O_{3-\delta}$ (LSGM) and yttria stabilized zirconia (YSZ) substrates. As depicted in Figure 3.2, epitaxial film growth

Die approbierte gedruckte Originalversion dieser Dissertation ist an der TU Wien Bibliothek verfügbar.
The approved original version of this doctoral thesis is available in print at TU Wien Bibliothek.
TU Bibliothek Your knowledge hub WIEN

with clearly visible atomic steps (height: ~0.4 nm = 1 lattice constant) was observed on LSGM, while polycrystalline film growth was found on YSZ. On neither substrate the deposited thin films show any indication for phase separation such as occurrence of surface particles, pinholes or cracks. (Please see Supporting Information for SEM and additional AFM images of the pristine and degraded electrodes (Figure 2.7).)

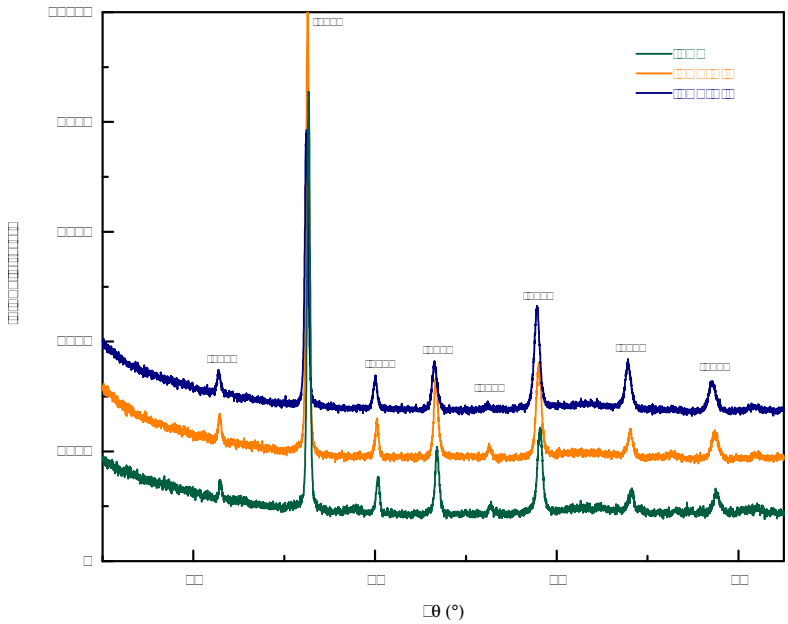

Figure 3.3: Diffractogram of pristine LSF (green), LSF-Pt1 (orange) and LSF-Pt2 (blue) thin films deposited on YSZ single crystals. The inset shows a magnification of the 211 reflex.

The polycrystalline growth of the thin films on YSZ was also revealed by XRD measurements in gracing incidence mode. As visible in Figure 3.3, especially at higher 2θ values a small shift of the reflexes to lower 2θ was observed. This reveals that incorporation of platinum leads to a slight enlargement of the LSF unit cell. Transmission electron microscopy (TEM) was conducted to study the bulk and surface morphology of the electrode. In Figure 3.4 an HAADF-STEM image (A) and a TEM image (B) of a multilayer electrode grown on LSGM consisting of several layers of LSF, LSF-Pt1 and LSF-Pt2 with a top layer made from LSF-Pt2 can be found. The structure of the electrode is sketched in Figure 3.1 and the electrochemical performance of the different layers is shown in Figure 3.7. In accordance with AFM and SEM measurements, also HAADF-STEM and TEM measurements confirmed that platinum is well incorporated into the perovskite host lattice and significant formation of platinum exsolution on the electrode surface can be excluded. The contrast in HAADF-STEM is related

Die approbierte gedruckte Originalversion dieser Dissertation ist an der TU Wien Bibliothek verfügbar.
The approved original version of this doctoral thesis is available in print at TU Wien Bibliothek.
TU Bibliothek Your knowledge hub WIEN

to the thickness, (average) atomic number and density of the sample position. In Figure 3.4 (A) the individual layers in the multi-layer electrode appear uniform. No formation of Pt nanoparticles is visible, which would be seen as brighter regions.

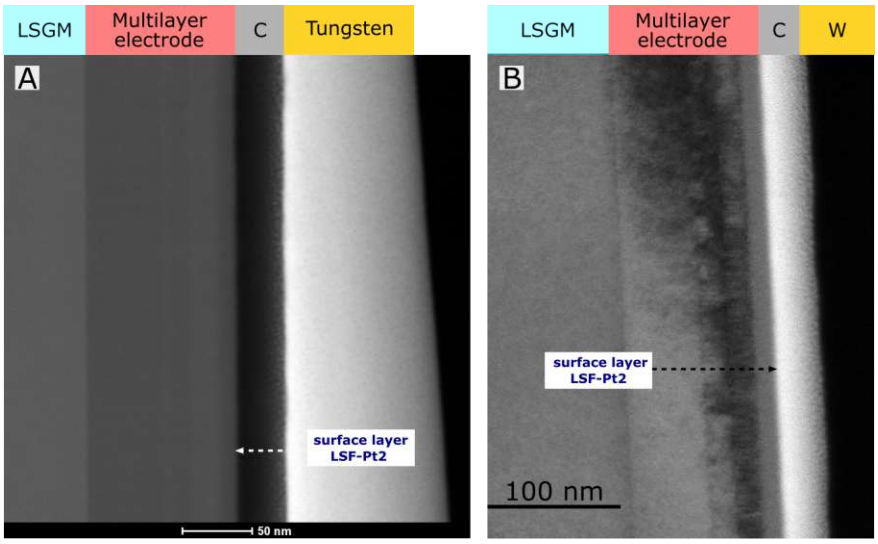

Figure 3.4: A) HAADF-STEM and B) TEM image of a multilayer electrode (top layer: LSF-Pt2). No exsolutions of platinum nanoparticles are visible on the electrode surface.

Die approbierte gedruckte Originalversion dieser Dissertation ist an der TU Wien Bibliothek verfügbar.
The approved original version of this doctoral thesis is available in print at TU Wien Bibliothek.
TU WIEN Bibliothek Your knowledge hub

3.3.3 Ambient pressure XPS measurements

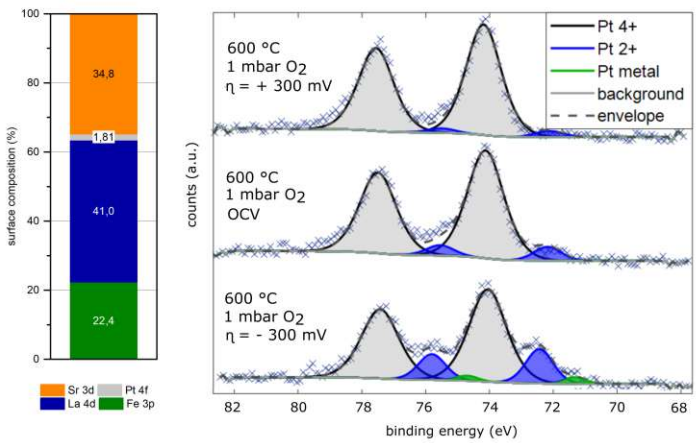

Figure 3.5: Results of ambient pressure XPS (AP-XPS) measurements on a LSF-Pt2 electrode under open circuit voltage and with polarization. Observed binding energies of platinum and distribution of the platinum oxidation states under different working electrode overpotentials η.

In addition to XPS characterization in UHV, ambient pressure XPS (AP-XPS) measurements were conducted at 600 °C in 1 mbar O_2 to study the surface composition of the LSF-Pt2 electrode at conditions very similar to the *i*-PLD impedance measurements. In good accordance with *ex-situ* XPS measurements conducted on LSF-Pt2 in UHV, where 1.5 at% of the surface composition was found to be platinum, AP-XPS detected 1.8 at% of the cations in the near surface region to be platinum. AP-XPS was further used to study the oxidation states of platinum at operation conditions. As shown in Figure 3.5, also AP-XPS confirmed that under oxidizing conditions platinum is present in oxidized form as Pt^{4+} (97 %) and Pt^{2+} (3 %), thus further supporting the interpretation the noble metal being incorporated into the perovskite-type oxide and, most probably, occupying the B site. Since device limitations do not allow oxygen partial pressures higher than 1 mbar O_2 for AP-XPS measurements, an electrochemical overpotential was applied to systematically modify the point defect concentration of the thin film working electrodes and thus to achieve higher as well as lower effective oxygen partial pressures in the electrodes. For a surface limited working electrode (WE) and a reversible counter electrodes (CE) the effective oxygen partial pressure in the WE ($p_{O2}{}^{WE}$) depends on the WE overpotential η as given in Eq. (5.1). This requires absence of significant transport limitations and of charge transfer polarisation at the electrolyte interface, which is fulfilled in our films. For a detailed explanation, please see reference[25, 106, 180]

$$p_{O_2}^{WE} = p_{O_2}^{At} * exp(\frac{4 * F * \eta}{R * T}) \tag{3.1}$$

Die approbierte gedruckte Originalversion dieser Dissertation ist an der TU Wien Bibliothek verfügbar.
The approved original version of this doctoral thesis is available in print at TU Wien Bibliothek.
TU Bibliothek Your knowledge hub WIEN

Therein pO_2^{At} is the oxygen partial pressure of the surrounding atmosphere in the single chamber setup, F is Faraday's constant, R the gas constant, and T the absolute temperature. The working electrode's overpotential was obtained by subtracting the ohmic voltage drop (electrolyte) from the applied voltage.

$$\eta = U_{set} - I * R_{ohm} \tag{3.2}$$

An anodic overpotential of 300 mV at 1 mbar O_2, which is equivalent to about 8 orders of magnitude higher effective $p(O_2)$, did not lead to any significant changes of the oxidation states of platinum. On the other hand, the application of -300 mV cathodic overpotential (about 8 orders of magnitude lower effective $p(O_2)$) clearly revealed changes of platinum oxidation states. As visible in Figure 3.5, platinum metal (3 %) and Pt^{2+} (20 %) together with Pt^{4+} (77 %) were found on the cathodically polarized surface of the electrode. This may be an indication for the onset of an exsolution process of metallic Pt under these reducing conditions.

It is further worth mentioning that our surface chemistry and surface morphology results obtained by AFM, SEM, TEM and AP-XPS measurements on Pt containing LSF are in excellent accordance with literature [170–172, 181]. Different studies on noble metal doped pervoskites also showed the noble metal to be incorporated into the pervoskite lattice under oxidizing conditons. Only under reducing conditions, which are not topic of this study, metallic nanoparticles were found on the surface of the material.

3.3.4 *In-situ* electrochemical characterisation during growth of multi-layers

Multi-layer structures of LSF, LSF-Pt1 and LSF-Pt2 were sequentially deposited on single crystals of YSZ (for polycrystalline film growth) and LSGM (for epitaxial film growth). The polarization resistance of the obtained electrodes was continuously characterized by impedance spectroscopy in the PLD chamber, i.e. instantly after each film growth at deposition pressure and temperature. The required *i*-PLD setup, which was used for sample heating and electronic contacting of the working electrode with a PtIr needle, is shown in Figure 3.1A). Our measurements show excellent reproducibility, as for each substrate all the thin films were deposited at the exactly same temperature (600 °C), same oxygen partial pressure (0.04 mbar O_2) and without any external influences (such as humidity, CO_2, or impurities from ambient air), many reasons for a scattering of polarization resistance are excluded.

In this section, *i*-PLD experiments on LSF/Pt-LSF multi-layers are shown, which demonstrate that extremely small amounts of Pt surface doping can already strongly improve the oxygen exchange kinetics.The main reason for preparing multi-layer structures in combination with

Die approbierte gedruckte Originalversion dieser Dissertation ist an der TU Wien Bibliothek verfügbar.
The approved original version of this doctoral thesis is available in print at TU Wien Bibliothek.
TU WIEN Bibliothek Your knowledge hub

i-PLD measurements is the direct comparison of the polarization resistances of different LSF electrodes surfaces (pure and Pt doped) on the very same substrate. The structure of a deposited multi-layer electrode is sketched in figure 3.1B. The impedance spectra measured

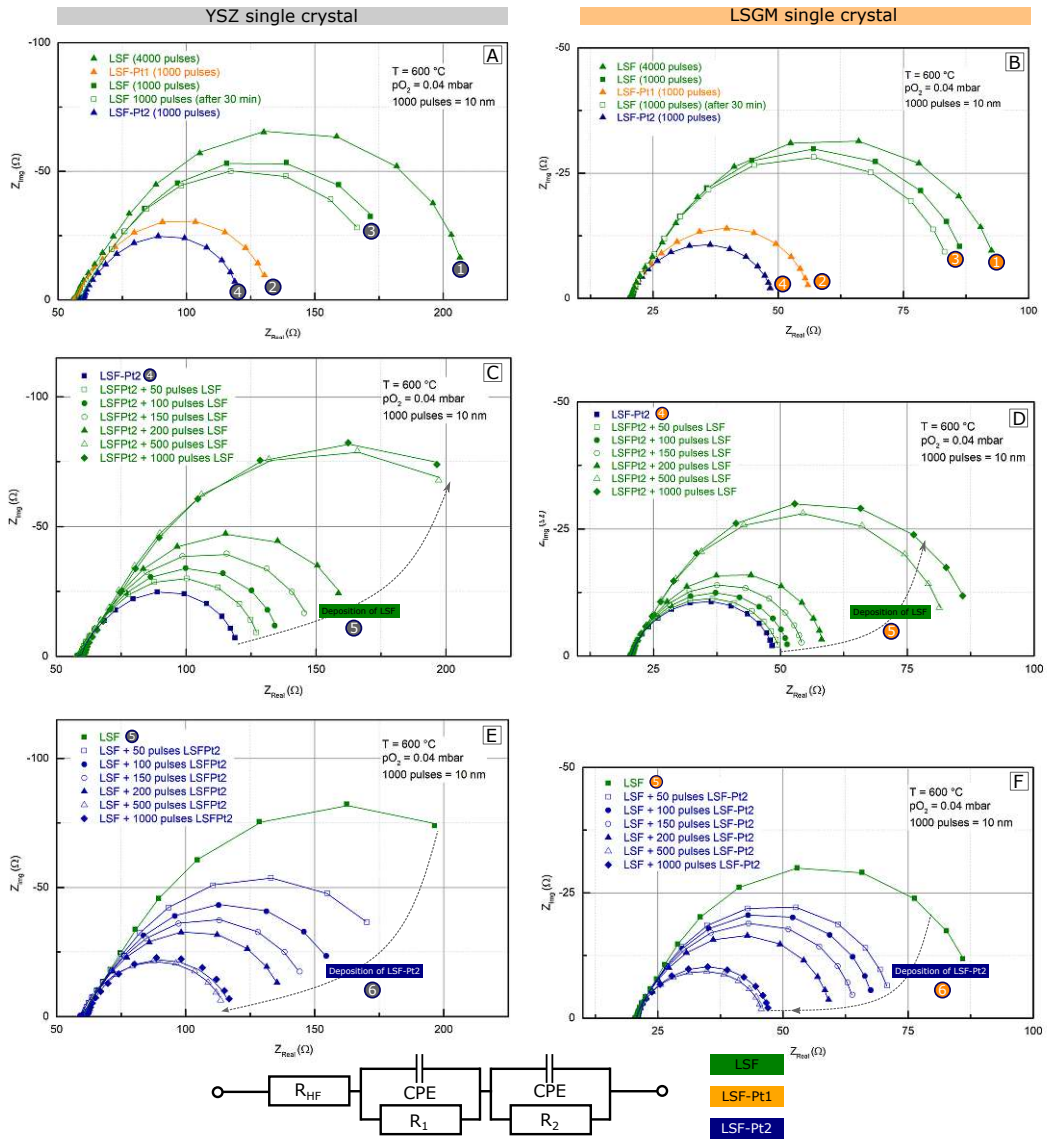

Figure 3.6: Measured impedance spectra from a *i*-PLD multi-layer experiment grown on YSZ (A,C,E) and LSGM (B,D,F) single crystals. Symbols are measured data, lines are fits to the equivalent circuit shown. (A) and (B) Initial deposition of the LSF, LSF-Pt1, LSF-Pt2 electrodes (10 nm each). (C) and (D) Stepwise deactivation of a LSF-Pt2 electrode by depositing LSF on its surface. (E) and (F) Stepwise surface activation of a LSF electrode by growing LSF-Pt2 on top. The obtained area specific resistances of the electrode surface are summarized in figure 3.7. The encircled numbers refer to certain steps in the course of the *i*-PLD experiment and details of the individual steps are explained in the text.

Die approbierte gedruckte Originalversion dieser Dissertation ist an der TU Wien Bibliothek verfügbar.
The approved original version of this doctoral thesis is available in print at TU Wien Bibliothek.
TU WIEN Bibliothek Your knowledge hub

upon growth of such a multilayered electrode are displayed in figure 3.6. The impedance spectra measured upon growth of such a multilayered electrode are displayed in Figure 6. In order to improve the readability of impedance results, all data in Figure 6 and 7 dealing with LSF are plotted in green, while data of LSF-Pt1 and LSF-Pt2 are plotted in orange and blue, respectively. All spectra exhibit a high-frequency intercept, which can be assigned to the transport of O^{2-} ions through the single crystalline YSZ or LSGM electrolyte substrate. [174, 182] Due to different oxygen ion conductivity of the two substrates, different high frequency resistance values were found on YSZ (53 Ω) and LSGM (23 Ω). These values are in excellent accordance with the conductivity of YSZ[182] and LSGM [174] at 600 °C reported in literature.

According to many literature studies on similar materials (LSF, LSC, LSCF) the main arc in the impedance spectra is related to the oxygen exchange kinetics on the electrode surface, [21, 28, 37, 44] as long as electronic in-plane conductivity and ionic across-plane conductivity are sufficiently high, which is the case for our films. In the medium frequency range sometimes a shoulder was observed, which is most likely associated with the ion transfer across the electrode/electrolyte interface. [28] The formation of detrimental amounts of $SrZrO_3$ between the electrode and the YSZ single crystal was excluded in accordance with earlier studies at 600 °C [21, 95, 112] and measurements indicating the formation of $SrZrO_3$ at temperatures above 800 °C. [183]. The impedance spectra were fitted to the equivalent circuit shown in figure 3.6, where one of the R|CPE elements (CPE = constant phase element [141]) represents the low frequency surface feature of the electrode impedance, and the other one the medium frequency interface shoulder.

Although this circuit only approximates the mechanistic model, [28] we chose this more robust circuit for the sake of obtaining a stable fit, since the interface feature was not well established for all the measurements and especially the more interesting low frequency arc can thus be fitted with high accuracy. The most interesting fit parameter extracted from the low frequency feature is the surface polarization resistance, which characterizes the activity of the electrode surface for oxygen exchange. For better comparability, it was referred to the active electrode area (thus yielding an area specific surface resistance, "surface ASR"), as prior studies have shown that only the area above the YSZ is active for the oxygen exchange reaction, while the area above the platinum grid is inactive due to a relative large in-plane ionic resistance in the LSF film. [21] (Images of the platinum grid structure can be found in the Supporting Information Figure 3.13.) The resulting surface ASR values for the entire course of the *i*-PLD experiment are summarized in Figure 3.7 for both electrolytes and for all terminating surface layers achieved by *in-situ* deposition of pure LSF and Pt doped LSF.

Die approbierte gedruckte Originalversion dieser Dissertation ist an der TU Wien Bibliothek verfügbar.
The approved original version of this doctoral thesis is available in print at TU Wien Bibliothek.
TU Bibliothek Your knowledge hub WIEN

Let us first focus on the results obtained on YSZ substrates (see left column of Figure 3.6). In the beginning of the shown *i*-PLD experiment 4000 pulses (= 40 nm) LSF were deposited on YSZ and the impedance of the electrode was measured immediately at 600 °C and 0.04 mbar O_2 - see number ① in figure 3.6A and B. Please note that encircled numbers are used in the figures 3.1, 3.6, 3.7 and throughout the text to identify each subsection of the *i*-PLD experiment. The subsequent deposition of 1000 pulses (= 10 nm) LSF-Pt1 on the LSF electrode caused a decrease of the surface-ASR from 10.8 to 5.7 Ωcm^2; see ②. The electrode was then "deactivated" to 9.2 Ωcm^2 by depositing 1000 pulses of LSF; see ③. As visible in Figure 3.6, the polarisation resistance slightly decreased after an annealing time of 30 min and saturated at 9 Ωcm^2. This might be explained by Pt diffusing through the thin LSF top layer (10 nm) to the surface of the electrode. However, this effect is small compared to the performance boost achieved by the general effect of Pt doping and was thus not further investigated.

In the next step, the electrode was reactivated again by 1000 pulses of LSF-Pt2 to 4.5 Ωcm^2; see ④.

LSF was stepwise deposited in small amounts (50, 50, 50, 50, 300, 500 pulses) on the terminating LSF-Pt2 layer of the already existing heterostructure and accordingly a stepwise increase of the polarization resistance was observed - see number ⑤ in figure 3.6C. After a total of 500 pulses a polarisation resistance of 14.1 Ωcm^2 was found, which just slightly increased to 14.3 Ωcm^2 after depositing another 500 pulses of LSF. This shows that a 5 nm thick surface layer is sufficient to imprint the thin film electrode with the surface kinetics of LSF.

Vice-versa the electrode performance was subsequently again improved by another stepwise deposition of LSF-Pt2 until a polarization resistance of 4.2 Ωcm^2 was reached; see ⑥ in figure 3.6E. Remarkably, already the deposition of the first 50-100 pulses LSF-Pt2, which corresponds to only 0.5 nm - 1 nm of deposited material, led to a significant drop of the polarization resistance. This result points out the outstanding effectiveness of surface doping, which may point to future pathways of highly efficient precious metal utilization also in solid oxide cells. Again, after a total of 500 pulses of LSF-Pt2 deposition the polarization resistance of the electrode reached a virtually constant value and no further significant changes could be observed after deposition of another 500 pulses of LSF-Pt2. This is highly remarkable because it indicates that already ca. 1.5 at% Pt cations (=3 %Pt on B site) within 5 nm can more than double the reaction rate compared to pure LSF. The Pt amount corresponds to 80 ng/cm^2, which is drastically lower compared to typical Pt loading in PEM fuel cells, with is often in the range of 0.1 mg/cm^2. [163]

The entire *i*-PLD multilayer experiment was repeated in exactly the same way with LSGM as electrolyte. The measurements revealed that LSF with epitaxial structure shows superior oxygen reduction kinetics (5.7 Ωcm^2 compared to 10.8 Ωcm^2 for LSF in polycrystalline

Die approbierte gedruckte Originalversion dieser Dissertation ist an der TU Wien Bibliothek verfügbar.
The approved original version of this doctoral thesis is available in print at TU Wien Bibliothek.
TU WIEN Bibliothek Your knowledge hub

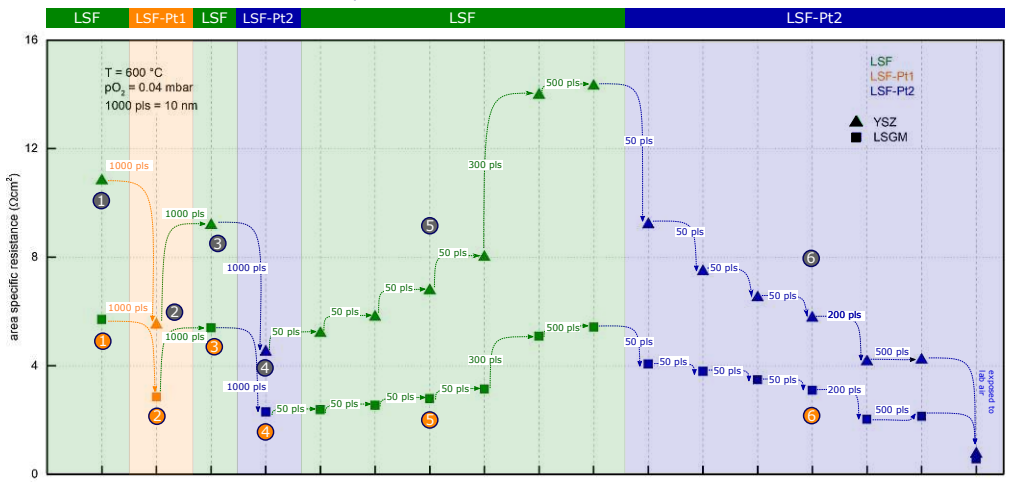

Figure 3.7: Area specific resistance of *i*-PLD multi-layer electrodes grown on YSZ (triangles, top row) and LSGM (squares, bottom row) calculated from the spectra shown in figure 3.6. Green symbols and lines display deposition of LSF, blue symbols and lines display deposition of LSF-Pt2, orange symbols and lines display deposition of LSF-Pt1.

structure). However, as evident from the impedance spectra in Figures 3.6B, D, and F the qualitative behavior of the electrodes is identical. Roughly speaking the surface modification with LSF-Pt again improves the performance by about a factor of 2-2.5 (2.8 Ωcm^2 for LSF-Pt1 and 2.3 Ωcm^2 for LSF-Pt2). The difference between films on YSZ and on LSGM are attributed to the fact that LSF on YSZ grows polycrystalline, while LSGM supports epitaxial film growth. The observed surface ASR difference is also in accordance with literature, where epitaxially strained thin films showed different oxygen exchange kinetics than unstrained, polycrystalline thin films. While tensile strain is known to promote oxygen reduction, compressive strain was found to decrease oxygen exchange activities. [46, 99, 184]

Moreover, the long-term stability of LSF-Pt2 in the setup of the *i*-PLD electrodes was investigated and compared to LSF. After annealing LSF-Pt2 electrodes for 16 h in synthetic air at 600 °C the formation of particles on the electrode surface was observed. In addition, XPS measurements revealed a strong increase of the platinum surface composition after annealing together with a shift of the binding energy, which indicates the observed particles to be metallic Pt. Additional *i*-PLD measurements show that as Pt diffuses to the surface, also the beneficial effect of Pt doping is lost and over the time an increase of the surface-ASR is found. However, since our in this study *i*-PLD measurements allowed us to characterize pristine electrodes directly after PLD deposition, the observed low long term stability does not affect the mechanistic conclusions made in this study. For a more detailed description of this Pt related degradation, please refer to the Supporting Information Figure 3.9.

Die approbierte gedruckte Originalversion dieser Dissertation ist an der TU Wien Bibliothek verfügbar.
The approved original version of this doctoral thesis is available in print at TU Wien Bibliothek.
TU WIEN Bibliothek Your knowledge hub

3.3.5 $p(O_2)$ and temperature dependence of LSF and LSF-Pt2 polarisation resistance

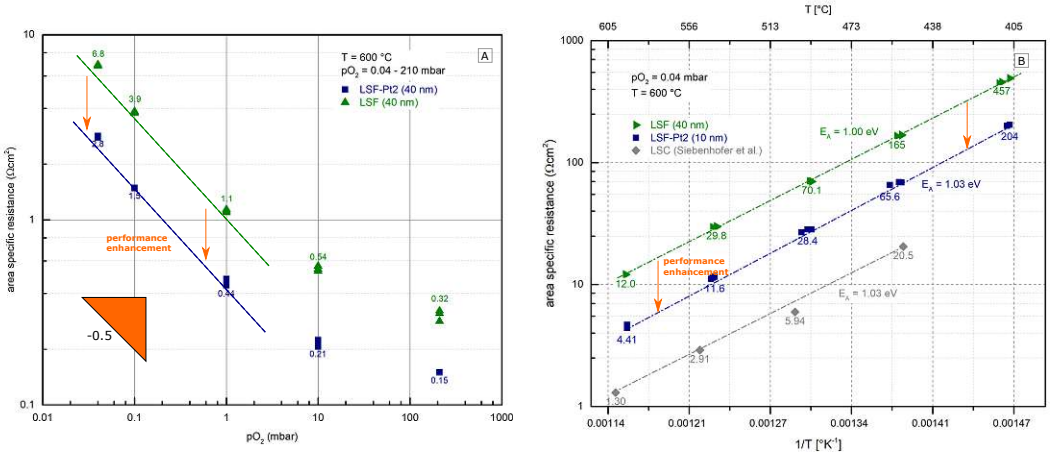

Figure 3.8: (A) Surface-ASR of LSF (green) and LSF-Pt2 (blue) (two different samples) versus the oxygen partial pressure plotted as log/log diagram. The numbers next to the symbols are the mean ASR values in Ωcm^2. Lines are a guide for the eye. (B) Area specific resistance plotted versus inverse temperature for LSF (green), LSF-Pt2 deposited on top of LSF (blue) and LSC (grey). Data for LSC are taken from reference[95] for comparison.

Owing to the high reproducibility and sufficient stability of the electrode kinetics in the *i*-PLD experiments (see Supporting Information Figure 3.9), very reliable $p(O_2)$ and T dependencies of the oxygen exchange reaction can also be obtained. Those are highly interesting, since they offer the possibility of improving the mechanistic understanding of the oxygen reduction kinetics on pervoskite-type electrodes. Hence, the dependence of the surface ASR on the oxygen partial pressure was studied in the *i*-PLD setup on 40 nm thick LSF and LSF-Pt2 electrodes freshly deposited on two different YSZ substrates. YSZ substrates were chosen for the reason of better comparability with literature data, which are primarily available for this type of electrolyte. Impedance measurements were carried out at 0.04 mbar, 0.1 mbar, 1 mbar, 10 mbar and 210 mbar O_2 by adjusting the oxygen flow in the PLD chamber at 600 °C. The obtained surface-ASR values are plotted on a log/log scale versus the $p(O_2)$ in figure 3.8A. In accordance with measurements from the multi-layer experiment (see figure 3.7), LSF-Pt2 showed around a factor of 2.5 faster oxygen reduction kinetics than pure LSF. Surprisingly, LSF and LSF-Pt2 exhibit the very same oxygen partial pressure dependence, as visible in figure 3.8A. However, the pO_2 dependence cannot be described by a single slope in this pO_2 range. Rather, the line strongly flattens towards higher pO_2, with a slope > 0.5 at low pressures and little dependence at high pO_2.

Die approbierte gedruckte Originalversion dieser Dissertation ist an der TU Wien Bibliothek verfügbar.
The approved original version of this doctoral thesis is available in print at TU Wien Bibliothek.
TU WIEN Bibliothek Your knowledge hub

In addition, the temperature dependence of the surface ASR was investigated on both LSF and LSF-Pt2. To do so, temperature dependent impedance measurements were first conducted on a 40 nm LSF electrode. Subsequently, 10 nm of LSF-Pt2 were deposited onto the electrode and the temperature dependent measurements were repeated. As shown above, the deposition of 10 nm is way sufficient to entirely switch the electrode behavior to the kinetics determined by the surface layer. The accurate temperature of the sample was calculated from the YSZ offset resistance according to reference [182]. Comparing LSF and LSF-Pt2 reaction kinetics again reveals a factor of 2.5 faster reaction kinetics of the Pt surface doped material. For data analysis the logarithm of the surface ASR was plotted versus the inverse temperature (see Arrhenius diagram in figure 3.8 B). The obtained plot reveals excellent linear behaviour over the whole investigated temperature range indicating an Arrhenius-type temperature dependence. The activation energy was calculated from the slope of the linear fit. For LSF an activation energy of 1.00 eV was found and LSF-Pt2 showed virtually the same activation energy of (1.03 eV). In an earlier study, the activation energy of $La_{0.6}Sr_{0.4}CoO_{3-\delta}$ was also measured in the *i*-PLD setup under the same conditions. While LSC electrodes showed even better oxygen reduction kinetics than LSF-Pt2, also an identical activation energy of 1.03 eV was found. [95] This almost identical activation energy for all three materials, in addition to the identical $p(O_2)$ dependence mentioned above, indicates that the reaction mechanism is the same on all these perovskite-type oxygen reduction electro-catalysts is the same. Moreover, studies on STF and LSC revealed activation energies to strongly depend on oxygen partial pressure. While usually, in accordance with this study, activation energies of 1 eV are reported at lower oxygen partial pressure (0.04 mbar), activation energy of 1.6 eV for LSC[95] and values between 1.6 eV and 2.5 eV (depending on the Fe:Ti ratio) for STF [37] are found at ambient air. According to literature [37, 95] a change of the oxygen exchange reaction mechanism on the electrode surface at higher pO_2 may explains the change of the activation energies. This might also be in accordance with Figure 8A), where a change of the pO_2 dependence of the ASR was found at higher pO_2. Possible mechanisms and rate determining steps on LSF, LSF-Pt2 and LSC are discussed below.

Die approbierte gedruckte Originalversion dieser Dissertation ist an der TU Wien Bibliothek verfügbar.
The approved original version of this doctoral thesis is available in print at TU Wien Bibliothek.
TU WIEN Bibliothek Your knowledge hub

3.4 Discussion

In the following we conclude our findings regarding the superior properties of Pt doped LSF in comparison to pure LSF, suggest mechanistic explanations and connect them with recent findings in literature. Overall, the following experimental facts have to be considered by a mechanistic explanation:

- Pt is incorporated into the LSF lattice in an oxidized state and no evidence for metallic Pt on the electrode surface was found (please see Figure 3.4 and 3.5). The preferred Pt^{4+} oxidation state indicates occupation on the B-site.
- The polarisation resistance of Pt surface doped LSF electrodes is about a factor of 2.5 lower than of LSF, despite the small concentration of platinum used (please see, for instance, figure 3.7).
- A few nanometers of Pt doped LSF deposited on top of undoped LSF are sufficient to achieve this excellent oxygen exchange kinetics (please see figure 3.7 & 3.6).
- On LSF, LSF-Pt2 (and LSC in an earlier study [95]) the same activation energy of 1.00-1.03 eV of the oxygen exchange reaction was found (please see figure 3.8 B).
- LSF and Pt doped LSF exhibit the same partial pressure dependence of the polarisation resistance (please see figure 3.8 A).

Based on the above mentioned experimental observations, we need to find an explanation considering the significantly improved surface kinetics upon presence of platinum, while the reaction mechanism and rate limiting step remain the same, as suggested by the identical $p(O_2)$ dependence and activation energy. Especially the latter is a clear indication that in the present case platinum does not act as a classical catalyst, which would be evident by establishing a novel reaction pathway with a different activation energy and probably a different $p(O_2)$ dependence. This is in strong contrast to an earlier study where we deposited Pt nanoparticles on LSF[112]. This caused not only a dramatic drop of the polarisation resistance, but also a complete change of the $p(O_2)$ dependence (even including a change of the sign).

In literature[59] the reaction rate of oxygen exchange was defolded into its different contribution and the following equation was suggested to describe the kinetics:

$$r = r_0 * p(O_2)^{v_p} * \prod_i [i]^{v_i} * e^{\frac{\beta e \chi_0}{kT}} * e^{\frac{\beta e \Delta\chi}{kT}} \tag{3.3}$$

Die approbierte gedruckte Originalversion dieser Dissertation ist an der TU Wien Bibliothek verfügbar.
The approved original version of this doctoral thesis is available in print at TU Wien Bibliothek.
TU Bibliothek Your knowledge hub WIEN

This equation includes the oxygen partial pressure $p(O_2)$, the concentrations [i] of the reacting species i (i.e. Fe^{3+} and oxygen vacancies for oxygen reduction), the effect of any surface potential χ_0 or its change upon voltage $\Delta\chi$ (which can become relevant if charge is transferred across the surface) and a prefactor r_0 which includes kinetic contributions (chemical activation barriers) but also thermodynamic contributions due to mass action equilibria before the rate limiting step, k and T denote Boltzmann's constant and temperature. The relevant species of oxygen reduction are oxygen gas molecules or oxygen adsorbates coupled to the gas via a fast adsorption step, and defects at the LSF surface. The oxygen partial pressure thus enters the equation with a reaction order $n(\nu_p)$, which considers the fast adsorption kinetics (if relevant), e.g. without site restriction we get $\nu_p = 1$ for molecular adsorption. Relevant defects for oxygen reduction are particularly oxygen vacancies and Fe^{3+} ions, the latter providing the electron for reduction (thus forming Fe^{4+} = holes, which then enter the rate equation of the oxygen reduction reaction). Symbol ν_i is the reaction order of the defect i, which depends on the specific mechanism and rate limiting step.

This general approach is very helpful for deducing any mechanistic conclusion from the given experimental data. It is far beyond the scope of this paper to discuss details of the specific mechanism and to identify the rate limiting step for these materials. However, the virtually identical activation energy for LSF with and without Pt as well as the same $p(O_2)$ dependence still enable important conclusions about the oxygen exchange mechanism.

Eq. (3.3) shows that the oxygen partial pressure enters the reaction rate twice: First it enters directly via the gas or adsorbate species ($p(O_2)^{\nu_p}$ term) and second it enters the rate indirectly via the partial pressure dependent defect concentrations. The latter are often rather well-known in the bulk (Brouwer diagrams, e.g. reference[76] for LSF thin films), but one should keep in mind that absolute concentrations at the surface may differ from the bulk (surfaces are often more reduced). Moreover, surface segregates and additional reactions with gas contaminants may change the surface drastically and bulk defect chemistry is no longer an optimal tool for estimating the surface defect concentrations. (Effects of the oxygen partial pressure on the surface potential are also possible but neglected here, in accordance with reference [25, 106]). With this in mind we can now suggest that the identical $p(O_2)$ dependence of the two sample types, together with the same activation energy, indicates that Pt is not directly involved as a classical catalyst but changes a relevant defect concentrations. Electron-delivering Fe^{3+} ions are most probably still available in high concentrations at these partial pressures and can hardly be increased substantially by Pt doping. We thus believe that the Pt doping rather increases the surface oxygen vacancy concentration. Depending on the reaction order with respect to vacancies this might be an increase by a factor of 2.5 for $n(\nu_V) = 1$ or 1.6 for $n(\nu_V) = 2$. However, also some small effects of Pt^{4+} on mass action equilibria of reaction steps before the rate limiting step may be present, which would induce changes of the prefactor r_0. The exact mechanism how Pt increases the surface vacancy concentration

Die approbierte gedruckte Originalversion dieser Dissertation ist an der TU Wien Bibliothek verfügbar.
The approved original version of this doctoral thesis is available in print at TU Wien Bibliothek.
TU Bibliothek Your knowledge hub WIEN

is still unknown, but it seems plausible that the incorporation of larger Pt^{4+} ions on the Fe^{3+} lattice site leads to a slight enlargement of the unit cell, which decreases the formation enthalpy of oxygen vacancies. [46, 97, 185] This is also in accordance with XRD measurement, where an increase of the unit cell of Pt doped LSF compared to pure LSF was observed.

The slope in the partial pressure dependence is then largely an interplay between increasing oxygen gas concentration and decreasing vacancy concentration for increasing $p(O_2)$. The higher the $p(O_2)$, the stronger decreases the vacancy concentration until it reaches a -1/2 slope in the Brouwer diagram, thus explaining the weakened slope of the reaction rate at higher oxygen partial pressures. A more detailed quantitative analysis in terms of mechanisms needs much further data (including bias dependent measurements) and is beyond the scope of this study.

However, our results reveal that Pt shows the tendency to leave the perovskite lattice of Pt doped LSF forming Pt particles on the surface, see also to the Supporting Information Figure 3.9. Thus the beneficial effect of platinum (formation of oxygen vacancies) is lost and an increase of the polarisation resistance is found, which is in good accordance with our mechanistic model. In our study, Pt was chosen as dopant as prior studies on this material combination were available[170–172, 181], nevertheless the effect should not be limited to platinum as also other - cheaper and more stable - dopants might lead to a slight similar enlargement of the LSF unit cell.

Die approbierte gedruckte Originalversion dieser Dissertation ist an der TU Wien Bibliothek verfügbar.
The approved original version of this doctoral thesis is available in print at TU Wien Bibliothek.
TU WIEN Bibliothek Your knowledge hub

3.5 Conclusions

In this study, we show how small amounts of platinum doping (0.9 at% and 1.5 at%) can significantly improve the oxygen reduction kinetics of LSF electrodes. Interestingly, Pt was not present in its otherwise typical catalytically active form as a metal, but rather it was found to be incorporated into the LSF perovskite in oxidized form (Pt^{4+}). For characterization of the electro-catalytic activity of pure and Pt doped LSF electrodes, impedance measurements were conducted *in-situ* inside the chamber of the PLD, which guarantees electrodes with very clean surfaces unaltered by external degradation. Moreover, multilayer growth of different electrode materials on the same substrate under the very measurement conditions allows excellent comparability of resistance values. Despite the small amount of platinum doping in a very thin layer (5 nm of LSF-Pt2) (80 ng/cm^2 Pt loading) about a factor of 2.5 lower polarisation resistance was measured. This significant increase in electrochemical performance was especially interesting as both pure LSF and Pt doped LSF showed the same oxygen partial pressure dependence and activation energy, which indicates that still the same mechanism and rate limiting step is active on both materials. Consequently, the addition of Pt is interpreted to increase the number of defects relevant in the reaction, more specific the concentration of oxygen vacancies at the surface.

Die approbierte gedruckte Originalversion dieser Dissertation ist an der TU Wien Bibliothek verfügbar.
The approved original version of this doctoral thesis is available in print at TU Wien Bibliothek.
TU WIEN Bibliothek Your knowledge hub

3.6 Supporting Information

3.6.1 Degradation behaviour

While numerous MIEC electrodes have already shown sufficiently fast oxygen reduction kinetics at pristine state, many of them suffer from poor stability of the polarisation resistance with degradation rates above an order of magnitude resistance increase within 10 hours being absolutely possible. [94, 98] In this experiment, the degradation behaviour of LSF and LSF-Pt2 electrodes were compared *in-situ* directly in the setup of the *i*-PLD at 600 °C in synthetic air. As shown in Figure 3.9A, different degradation behaviour was found for LSF and LSF-Pt2 upon annealing. While, on the one hand, for LSF moderate oxygen reduction kinetics were observed at pristine state, the polarisation resistance increased only little over time (0.75 Ωcm^2 to 1.25 Ωcm^2 in 16 h). LSF- Pt2, on the other hand, showed superior oxygen reduction kinetics at pristine state (< 0.2 Ωcm^2), which increased to about 1.25 Ωcm^2 after 11 h of annealing at 600 °C. This degradation is still slow enough to warrant the $p(O_2)$ and temperature dependent measurements shown in the main text. AFM and XPS was carried out on pristine and degraded LSF-Pt1 electrodes to reveal changes of the electrode surface composition and morphology. AFM images shown in Figure 3.9B (pristine LSF-Pt1 electrode) and 3.9C (LSF-Pt1 electrode annealed for 16 h in synthetic air) expose very different surface morphologies. On pristine LSF-Pt1 electrodes flat surfaces (surface roughness < ±1 nm) with clearly visible grains were observed. XPS measurements revealed 0.9 % of the surface to be platinum, which excellently matches the bulk Pt concentration measured by ICP. On degraded LSF-Pt1 electrodes, however, numerous nanoparticles in the range of 50 nm were found by means of AFM on the surface of the electrode. In addition, XPS measurements showed a strong increase of the platinum fraction on the surface to 5.5 % together with a clear shift of the binding energy of the Pt signal to significantly lower values. (Complete electrode surface composition and XPS spectra can be found in the Supporting Information section 3.11, 3.15). Thus, we expected the observed particles to be mainly metallic platinum. In literature, several recent studies have claimed Sr segregation to be one of the main reasons behind electrode degradation. [31, 80, 81, 88, 186–188]. Moreover, sulphur contamination [76, 86, 189, 190] or silicon poising [90, 92] may deactivate the catalytically active sides on the surface of the MIEC. In the case of LSF-Pt2 electrodes, we expect that degradation is mainly triggered by agglomeration of platinum on the surface of the electrode, especially because XPS did not show a significant increase of the Sr concentration on degraded LSF-Pt1 samples and the degradation is much more pronounced than on LSF. Moreover, in an earlier study on Pd doped perovskite catalysts noble metal particles were found on the surface of the electrode after annealing for several hours at high temperatures in air. [191] Hence, essentially the oxygen vacancy concentration increase triggered by Pt^{4+} in the oxide seems to be largely lost when Pt agglomerates at the surface. The degradation of LSF was much less pronounced

Die approbierte gedruckte Originalversion dieser Dissertation ist an der TU Wien Bibliothek verfügbar.
The approved original version of this doctoral thesis is available in print at TU Wien Bibliothek.
TU WIEN Bibliothek Your knowledge hub

and was most probably driven by Sr segregation or poising of the electrode surface, but was not further investigated in this study.

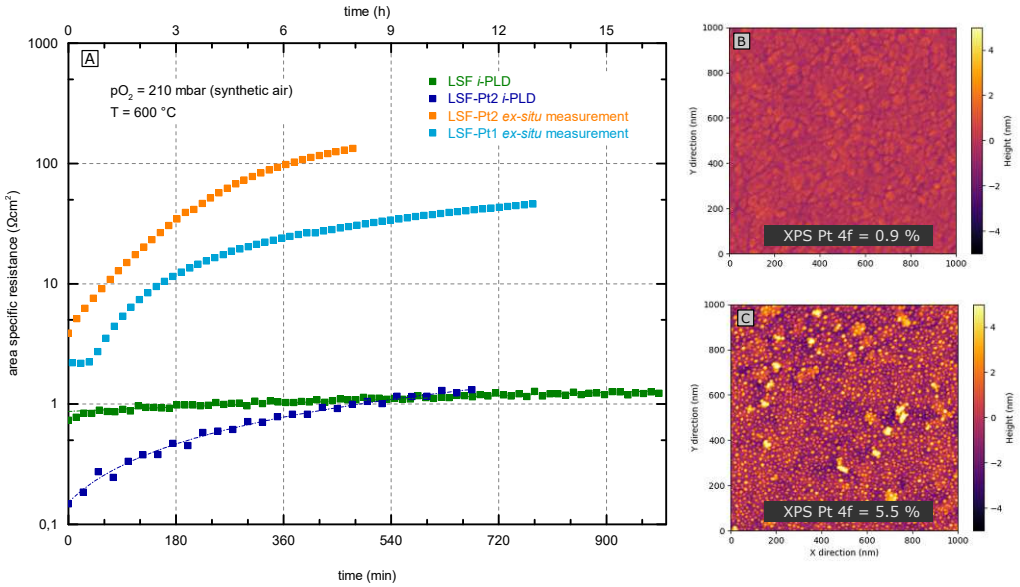

Figure 3.9: A) Degradation behaviour of LSF and LSF-Pt2 during *i*-PLD measurements at 600 °C in synthetic air. B) AFM image of a pristine LSF-Pt1 electrode directly after PLD deposition C) AFM image of a LSF-Pt1 electrode annealed for 16 h in synthetic air at 600 °C. The inset in figure B), C) shows the observed surface composition with platinum measured with XPS.

Die approbierte gedruckte Originalversion dieser Dissertation ist an der TU Wien Bibliothek verfügbar.
The approved original version of this doctoral thesis is available in print at TU Wien Bibliothek.
TU Bibliothek Your knowledge hub WIEN

3.6.2 Spectra and results of *ex-situ* XPS measurements

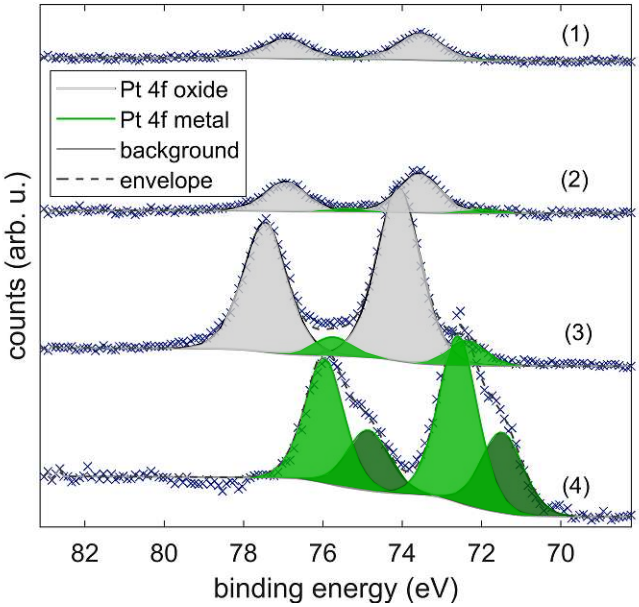

Figure 3.10: *ex-situ* XPS measurements (1) pristine LSF-Pt1 (2) pristine LSF-Pt1 heated up to 450 °C in UHV chamber directly before XPS measurements (3) LSF-Pt1 annealed for 16 h in synthetic air, (4) LSF-Pt1 annealed for 16 h in synthetic air, heated up to 450 °C in UHV directly before XPS measurements.

XPS was measured on pristine LSF-Pt1 electrodes (1) and on LSF-Pt1 electrodes annealed in synthetic air for 16 h (3). In addition, the same electrodes were heated up to 450 °C (heater thermocouple located close the sample) in UHV before the XPS measurements to reduce the oxidation state of platinum particles on the surface of the electrode (2) & (4). Platinum incorporated into the pervoskite host lattice is not reduced upon this conditions.

Die approbierte gedruckte Originalversion dieser Dissertation ist an der TU Wien Bibliothek verfügbar.
The approved original version of this doctoral thesis is available in print at TU Wien Bibliothek.
TU WIEN Bibliothek Your knowledge hub

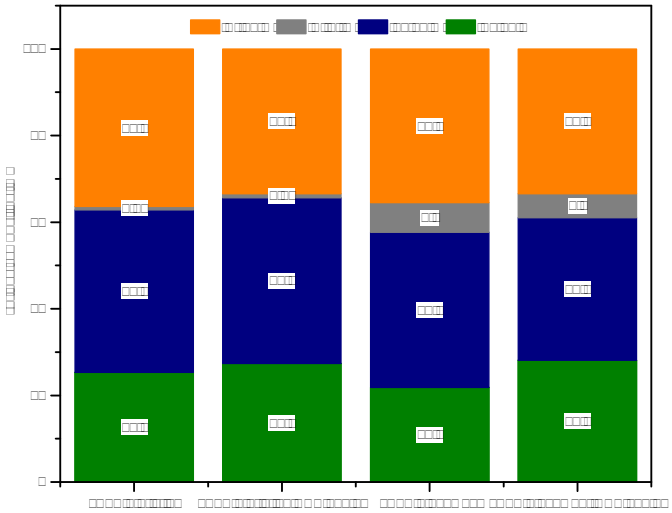

Figure 3.11: Calculated surface composition from *Ex-situ* XPS measurements on (1) pristine LSF-Pt1 (2) pristine LSF-Pt1 heated up to 450 °C in UHV chamber directly before XPS measurements (3) LSF-Pt1 annealed for 16 h in synthetic air, (4) LSF-Pt1 annealed for 16 h in synthetic air, heated up to 450 °C in UHV directly before XPS measurements.

Die approbierte gedruckte Originalversion dieser Dissertation ist an der TU Wien Bibliothek verfügbar.
The approved original version of this doctoral thesis is available in print at TU Wien Bibliothek.
TU WIEN Bibliothek Your knowledge hub

3.6.3 SEM and AFM images of pristine and degraded LSF-Pt1 electrodes

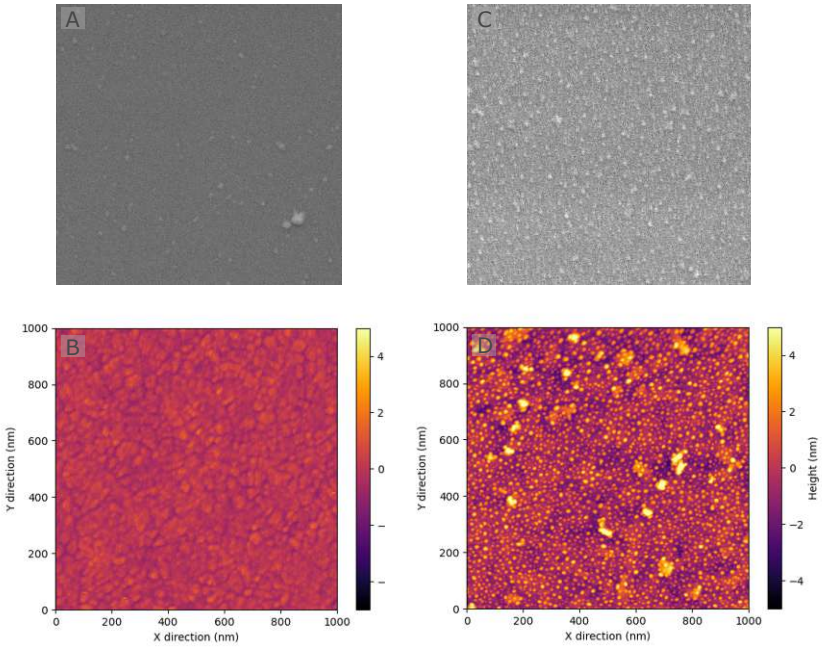

Figure 3.12: A) SEM image of a pristine LSF-Pt1 electrode directly after deposition B) SEM image of a LSF-Pt1 electrode, which was annealed for 16 h at 600 °C in synthetic air. C) AFM image of a pristine LSF-Pt1 electode directly after deposition D) AFM image of a LSF-Pt1 electrode,which was annealed for 16 h in synthetic air.

3.6.4 Platinum current collector grid

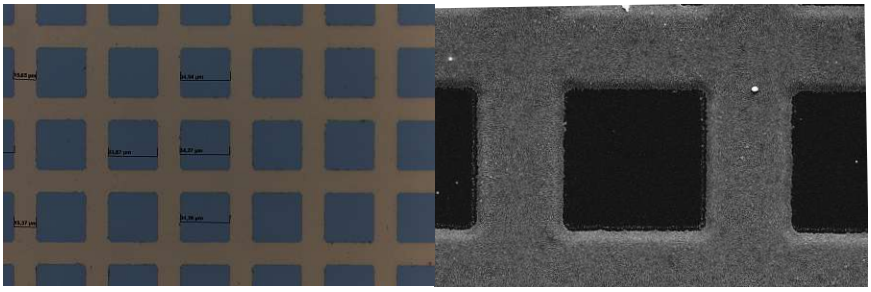

Figure 3.13: Platinum grid used for electrode contacting. Images from reflected light and secondary electron microscope.

Die approbierte gedruckte Originalversion dieser Dissertation ist an der TU Wien Bibliothek verfügbar.
The approved original version of this doctoral thesis is available in print at TU Wien Bibliothek.
TU WIEN Bibliothek Your knowledge hub

3.6.5 Results of AP-XPS measurements

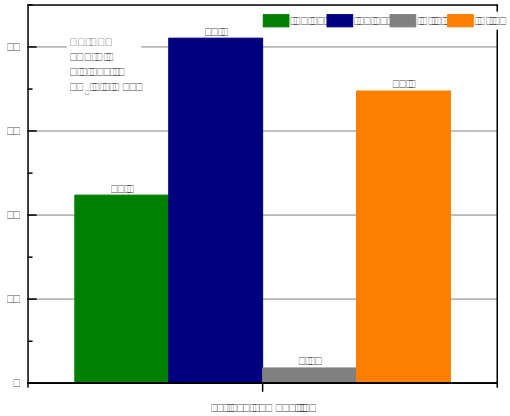

Figure 3.14: Surface composition of a LSF-Pt2 electrode measured at 600 °C and 1 mbar O_2

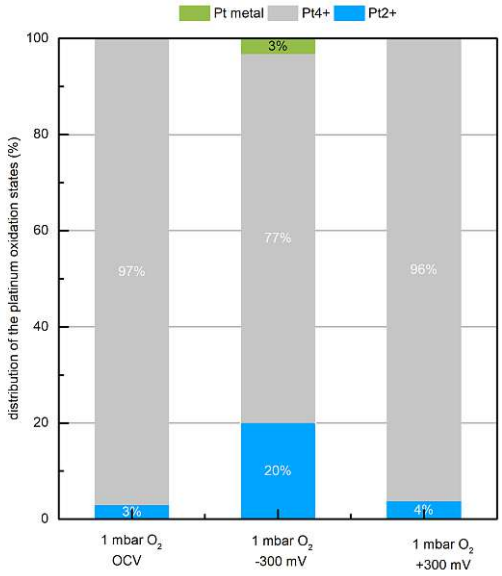

Figure 3.15: Distribution of the platinum oxidation states at OCV and upon application of -300 mV and +300 mV of overpotential.

Die approbierte gedruckte Originalversion dieser Dissertation ist an der TU Wien Bibliothek verfügbar.
The approved original version of this doctoral thesis is available in print at TU Wien Bibliothek.
TU Bibliothek Your knowledge hub WIEN

4 *In-situ* techniques reveal the true capabilities of SOFC cathode materials and their sudden degradation due to omnipresent sulfur trace impurities

Large parts of the study in this chapter are also published in C. Riedl, M. Siebenhofer* et al, J. Mater. Chem. A, 2022, Advance Article [192].*

4.1 Introduction

Several studies have shown that LSC and STF can exhibit enormously fast oxygen reduction kinetics shortly after fabrication of thin film electrodes[37] (e.g.: about 1 Ωcm^2 for dense LSC thin films at 600 °C in air [75]). Moreover, *in-situ* impedance measurements inside of the PLD chamber revealed even lower resistances (1 Ωcm^2 at 600 °C and 0.04 mbar O_2) [52] However, such low resistances could never be reproduced in *ex-situ* setups. Additionally a strong increase of their polarization resistance is observed over time, which is usually called "degradation". [75, 76, 86, 88] Manifold reasons for degradation have been proposed, for example, studies have suggested Sr segregation to the surface and the concomitant formation of parasitic SrO phases to be a main reason for degradation. [77, 81, 82, 88, 143, 186, 193]. Moreover, it is well established that secondary phase formation due to sulfur species such as SO_2 [31, 76, 79, 84, 86, 87, 103, 123, 189, 194–201] as well as silicon [89, 202] and chromium contaminations [91, 203] can strongly decrease the performance of SOFC cathodes.

In most of the studies mentioned above, either thin film electrodes are deposited on single crystalline substrates by PLD, or porous samples are prepared by sintering and are then transferred to *ex-situ* measurement setups. This approach suffers from several limitations as electrodes might already be exposed to contaminations during sample transfer or heating and equilibration in the *ex-situ* measurement setup, which may strongly alter the oxygen exchange kinetics and may even change oxygen reduction pathways. Different preparation conditions, but importantly, also different degradation states are almost certainly a main rea-

Die approbierte gedruckte Originalversion dieser Dissertation ist an der TU Wien Bibliothek verfügbar.
The approved original version of this doctoral thesis is available in print at TU Wien Bibliothek.
TU WIEN Bibliothek Your knowledge hub

son why polarization resistances obtained from different studies in various research groups are often afflicted by substantial scatter. This severely complicates a comparison of properties of different materials.

To avoid the above-mentioned obstacles, this study applies *in-situ* impedance spectroscopy during pulsed laser deposition (*i*-PLD), [76, 93, 95]a technique where thin film electrodes are characterized during or directly after growth in the chamber of the PLD.[76, 93, 95, 110] In contrast to *ex-situ* experiments, this ensures pristine and thus extremely clean surfaces and enables an otherwise impossible observation of the inherent polarization resistance of electrode materials. LSC, LSF, Pt doped LSF, STF and PCO electrodes were studied under exactly the same conditions inside the PLD chamber and all materials exhibit by far faster oxygen reduction kinetics (i.e. lower electrode polarization resistances) than previously reported in *ex-situ* studies. Moreover, LSC electrodes were investigated by combined electrochemical and ambient pressure X-ray photoelectron spectroscopy (AP-XPS) measurements, which allow to simultaneously study the surface chemistry of the electrodes by XPS and the polarization resistance of the electrodes by impedance measurements. This novel combination of methods unveils sulfur adsorbates due to omnipresent gas phase impurities as the reason for the strong initial degradation of pristine surfaces and advances the general understanding of the oxygen exchange kinetics and their degradation on SOFC cathode materials.

4.2 Experimental section

Powders were prepared following a synthesis method already described in literature. LSF, LSC, Pt doped LSF and PCO were synthesized via a (modified) Pechini route [21, 202], STF via solid state synthesis [152]. All chemicals were purchased from Sigma Aldrich with 99.995 % purity or higher. The obtained powders were calcined at 800 °C in air, pressed into PLD targets by isostatic pressing (150 MPa) and sintered at 1200 °C in air for 12 h. The crystallinity of the deposited thin films was examined by X-ray diffraction analysis. As electrolytes, yttria stabilized zirconia single crystals (YSZ (100), 0.5×0.5×0.05 cm^3, 9.5 mol% Y_2O_3) (CrysTec, Germany) were used. Before PLD thin film growth, platinum grids (15|5 µm or 25|10 µm mesh|strip width) were prepared on the single crystals by lift-off photo lithography and magnetron sputtering of 5 nm titanium and 100 nm platinum (BAL-TEC MED 020, Liechtenstein). As counter electrode, nano-porous $La_{0.6}Sr_{0.4}CoO_{3-\delta}$ (LSC) was deposited on the bottom side of the crystals by PLD with a KrF excimer laser (Complex Pro 201F, wavelength 248 nm) at 450 °C (substrate temperature measured with a pyrometer) and 0.4 mbar O_2 with a target to substrate distance of 5 cm [93]. At the beginning of every experiment, a 40 nm thick LSC layer was deposited onto the substrate (mixed ionic/electronic conductor with >1000 S/cm electronic conductivity) to ensure sufficient in-plane conduction for the subsequent working

Die approbierte gedruckte Originalversion dieser Dissertation ist an der TU Wien Bibliothek verfügbar.
The approved original version of this doctoral thesis is available in print at TU Wien Bibliothek.
TU WIEN Bibliothek Your knowledge hub

electrode layer. The working electrodes (i.e. ($La_{0.6}Sr_{0.4}CoO_{3-\delta}$ (LSC), $La_{0.6}Sr_{0.4}FeO_{3-\delta}$ (LSF), Pt doped LSF ($La_{0.6}Sr_{0.4}Fe_{0.985}Pt_{0.015}O_{3-\delta}$), $SrTi_{0.3}Fe_{0.7}O_{3-\delta}$ (STF) and $Pr_{0.1}Ce_{0.9}O_{2-\delta}$ (PCO)) were then deposited on top of the LSC layer by laser ablation (2 Hz) at 600 °C substrate temperature, a target to substrate distance of 6 cm and 0.04 mbar O_2. During working electrode growth, the substrate temperature was monitored via the high frequency intercept of the measured impedance spectra using the known temperature dependence of the ionic conductivity of YSZ [93, 182]. The growth rate was determined *ex-situ* on samples specially prepared for this purpose by measurements with a profilometer (DekTakXT, Bruker, USA) after a deposition of a certain number of pulses: LSF 1 nm/ 71 pulses; LSC 1 nm/33 pulses; STF 1 nm/60 pulses; Pt doped LSF 1 nm/77 pulses and PCO 1 nm/ 18 pulses. Impedance measurements were conducted with an Alpha-A High Performance Frequency Analyser in combination with an Electrochemical Test Station POT/GAL 30V/2A (both: Novocontrol Technologies, Germany). For *i*-PLD measurements (*in-situ* impedance spectroscopy during PLD) a sample was placed on the PLD heater and covered with an alumina mask (cut-out 0.45×0.45 cm^2) to prevent short circuiting around the edges of the sample during film deposition.[110] The working electrode was contacted with a PtIr-needle and the counter electrode was placed on the heating stage, which was brushed with platinum paste. Impedance spectra were recorded in a frequency range from 10^6 to 10^{-1} Hz (10^{-2} Hz, if needed) with an AC amplitude of 10 mV root mean square, and a resolution of 5 or 10 points per frequency decade. For *ex-situ* measurements, electrodes fabricated with the same parameters as the *i*-PLD electrodes were clamped between platinum meshes in a measurement setup made of quartz. The temperature was determined from the high frequency intercept in impedance spectra representing mainly the YSZ single crystal resistance [93, 182] and double checked with a type S thermocouple mounted in < 1 cm distance to the sample.

Gas cylinders (50 L; 200 bar) filled with synthetic air (5.0) and oxygen (5.0) (Messer Austria GmbH) and equipped with standard pressure regulators were used as feed gas supply in all experiments. For further purification of the feed gas, a self-made gas cleaning equipment was constructed. The gas was first bubbled through three gas washing bottles containing saturated calcium hydroxide solution, saturated copper sulfate solution and bi-distilled water, respectively. The gas was then piped through a cooling trap filled with frozen ethanol (-120 °C) to freeze out water vapour. The gas was further cleaned with a solid-state adsorption column containing milled calcined LSF powder and subsequently dried in an High-Capacity Moisture Trap (Restek^{TM}). To measure the sulphur compounds content of the used gases, the feed gas was bubbled (54 sccm) through two gas washing bottles equipped with a frit (porosity 3) containing 150 mL of distilled water with 3 % H_2O_2, which allowed to getter sulfur compounds from the feed gas as SO_4^{2-}. The concentration of SO_4^{2-} in the gas washing bottles was then measured via inductively coupled plasma mass spectrometry (ICP-MS). These measurements were carried out on a iCAP Q quadrupole ICP-MS (Thermo Fischer Scientific, Germany), coupled with a autosampler (SC-2-DX, ESI, USA) combined with an ESI Fast valve

Die approbierte gedruckte Originalversion dieser Dissertation ist an der TU Wien Bibliothek verfügbar.
The approved original version of this doctoral thesis is available in print at TU Wien Bibliothek.
TU WIEN Bibliothek Your knowledge hub

(ESI, USA) and data were collected using the instrument software, Qtegra Version 2.8. Samples were diluted with 1 %(v/v) HNO_3 and 1 ng/g indium was added as internal standard. For sulfur, the $^{32}S^{16}O^+$ and $^{34}S^{16}O^+$ ions were measured in reaction mode by introducing using a mixture of 10 % oxygen in helium into the collision/reaction cell of the instrument. The sulfur concentration was quantified using standard addition. The detected amount of sulfur in the first gas washing bottle was 20 times higher than in the second gas washing bottle, thus we could safely assume that indeed virtually the entire amount of SO_2 in the gas stream was captured in both washing bottles.

In-situ XPS spectra were acquired in a lab-based AP-XPS setup with a PHOIBOS NAP photoelectron analyser (SPECS, Germany) and a monochromated Al K-alpha XR 50 MF (microfocus) X-ray source. Therein, the solid oxide cell was mounted on a special sample holder with a centred 4.9×4.9 mm^2 sized hole for heating with a near-infrared diode laser. [175] Electrical contacts for working and counter electrodes were established by Pt-Ir and sintered platinum paste tips, respectively. The temperature of the sample was controlled via the conductivity of the YSZ electrolyte. Although in principle the setup can handle up to 20 mbar gas phase pressure, XPS spectra were measured at 5×10^{-6}-5×10^{-3} mbar O_2, in order to minimize the concentrations of any contaminant species (especially SO_2). XPS spectra were collected at an analyzer pass energy of 30 eV, which provided a reasonable balance of count rate and energy resolution.

Die approbierte gedruckte Originalversion dieser Dissertation ist an der TU Wien Bibliothek verfügbar.
The approved original version of this doctoral thesis is available in print at TU Wien Bibliothek.
TU WIEN Bibliothek Your knowledge hub

4.3 Results

4.3.1 Surface-related polarization resistance of pristine electrodes compared by *i*-PLD impedance measurements

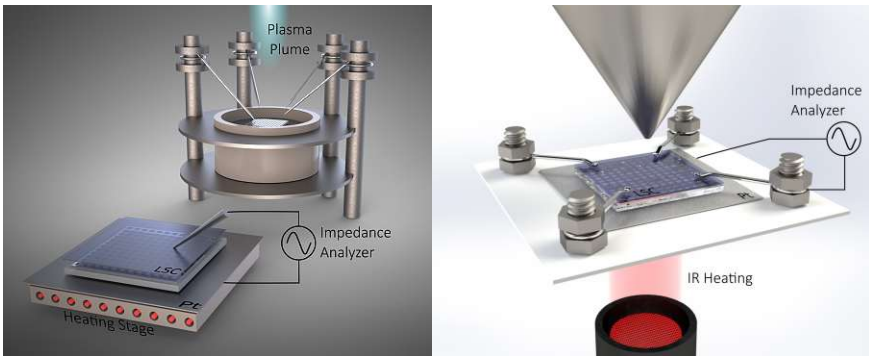

Figure 4.1: Sketch of the *i*-PLD setup (l.h.s) and the AP-XPS setup (r.h.s) with simultaneous electrochemical characterization.

The polarization resistances of different electrodes ($La_{0.6}Sr_{0.4}CoO_{3-\delta}$ (LSC), $La_{0.6}Sr_{0.4}FeO_{3-\delta}$ (LSF), Pt doped LSF ($La_{0.6}Sr_{0.4}Fe_{0.985}Pt_{0.015}O_{3-\delta}$), $SrTi_{0.3}Fe_{0.7}O_{3-\delta}$ (STF) and $Pr_{0.1}Ce_{0.9}O_{2-\delta}$ (PCO) were measured directly inside the vacuum chamber of the PLD setup at 600 °C and 0.04 mbar O_2 or 1000 mbar O_2. The corresponding *i*-PLD setup is depicted in Figure 1 (l.h.s), details on mounting and contacting the samples are described elsewhere [95, 175]. *i*-PLD measurements allow us to compare different thin film electrodes in their truly pristine state, which means unaltered by degradation and virtually free of any surface contaminations. For all samples, first a 40 nm thick LSC base layer was deposited to guarantee sufficient electronic in-plane conductivity and comparable surface morphologies. Subsequently, the electrode material of interest was deposited on top of this thin layer. Figure 4.2 displays the surface-related polarization resistance resulting from the impedance measurements accompanying the deposition of the LSC base layer and the material of interest. A rather constant resistance is found for base layer after ca 20 nm, but significant changes of the surface properties were observed right after changing the material. The corresponding polarization resistance values scattered in the first few nanometers and equilibrated after a material-specific critical thickness was reached.

The surface-related polarization resistances were determined from the recorded impedance spectra. Those show very similar features for all materials that could be described with the same equivalent circuit, see inset of Figure 4.2 (A). Details on the interpretation of the impedance of *i*-PLD studies can be found elsewhere. Essentially, all spectra exhibit a high frequency intercept of about 50 Ω assigned to the ionic conductivity of the YSZ single crystal used as substrate plus the ohmic resistance of the electronic current collection. The dominant

Die approbierte gedruckte Originalversion dieser Dissertation ist an der TU Wien Bibliothek verfügbar.
The approved original version of this doctoral thesis is available in print at TU Wien Bibliothek.
TU WIEN Bibliothek Your knowledge hub

pronounced low frequency semicircle was fitted to a single R|CPE element (CPE = constant phase element). As it has been shown in several studies, [28, 37, 204] this resistance is inversely proportional to the oxygen exchange reaction rate on the surface of the electrode. In the following, only this resistance is considered and termed surface resistance or surface-related polarization resistance.

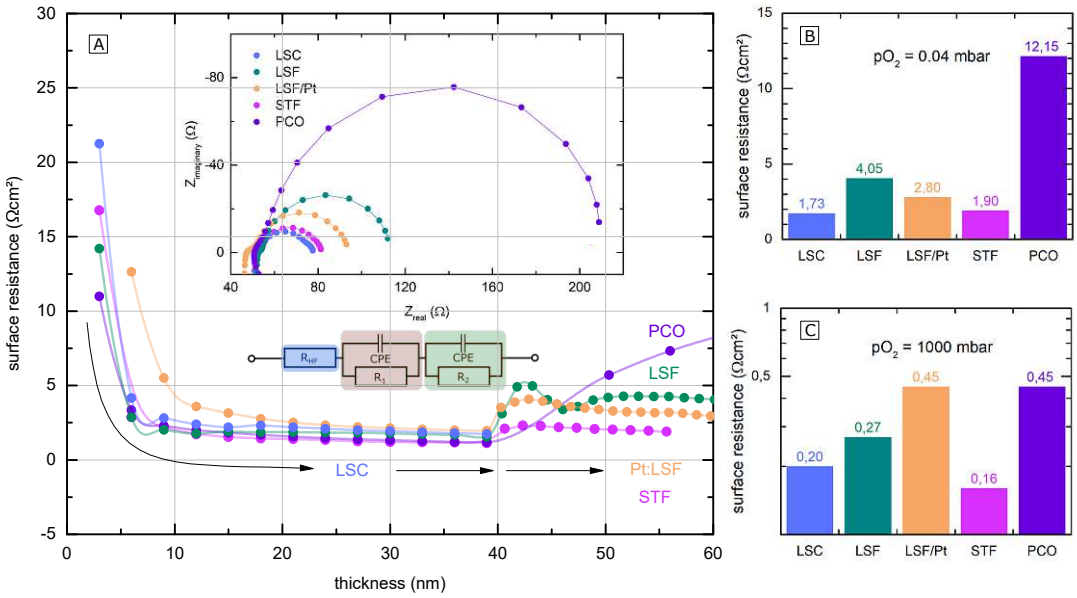

Figure 4.2: A) Surface-related polarization resistance of the investigated electrodes, determined by *i*-PLD measurements, plotted over the electrode thickness. At first, 40 nm of LSC were deposited, followed by different other electrode materials (LSF (green), Pt doped LSF (orange), STF (pink) and PCO (purple)). B), C) Bar charts of calculated area specific surface resistances of the electrodes at 0.04 mbar and 1000 mbar O_2.

The parallel chemical capacitance describes the capability of the MIEC material to alter its oxygen stoichiometry upon changes of the oxygen chemical potential (e.g. by the AC signal during impedance spectroscopy)[25]. In the medium frequency range, a more or less pronounced shoulder was observed, which is most likely associated with the ion transfer across the electrode/electrolyte interface and which was described by an additional R|CPE element. For calculation of the area-specific resistance, the measured surface resistance was normalized to the area of the thin film, which was deposited directly on the YSZ (25 - 50 % of the total electrode area). This way of normalization has already been proven meaningful in previous studies, where it was demonstrated that only the area above the YSZ is electrochemically active for oxygen reduction, while the regions above the current collector grid are inactive due to relatively low ionic in-plane conduction. [21]

Die approbierte gedruckte Originalversion dieser Dissertation ist an der TU Wien Bibliothek verfügbar.
The approved original version of this doctoral thesis is available in print at TU Wien Bibliothek.
TU Bibliothek Your knowledge hub WIEN

The surface-related polarization resistances of all materials at 0.04 mbar O_2 (i.e. at deposition pressure) and at 1000 mbar O_2 (measured after deposition but in the PLD chamber) are plotted in the bar charts in figures 4.2B) and C) for a temperature of 600 °C. While at 0.04 mbar O_2, the perovskite electrodes (LSF, LSC, STF and Pt doped LSF) show significantly lower surface-related polarization resistances than PCO, at 1000 mbar the differences in the surface resistance mostly vanish. The different $p(O_2)$ dependence of this resistance for PCO can be attributed to the very different defect chemistry of PCO [72] compared to the perovskite-type electrodes [25]. An in-depth mechanistic discussion of the relation between polarization resistance and defect chemistry is beyond the scope of the present work but can be found in a separate study [52].

4.3.2 Comparison of *i*-PLD surface resistances with literature data

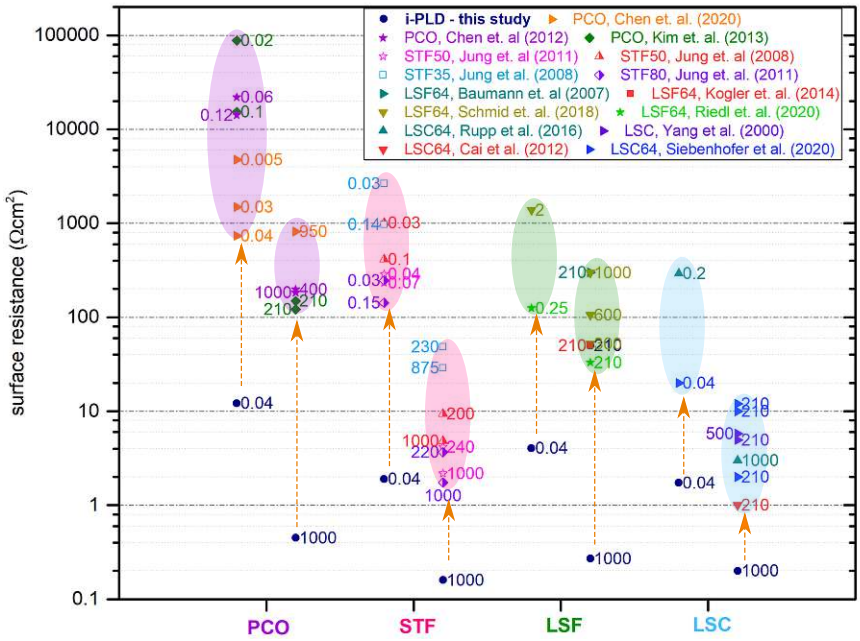

Figure 4.3: Electrode surface resistances from the present study at 0.04 mbar and 1000 mbar O_2 compared with values from figures published in literature: PCO [44, 205, 206] STF [37, 40] LSF [21, 28, 112] LSC [26, 75, 95, 207]. Numbers next to the resistance values in the plot indicate the oxygen partial pressure in mbar, at which the respective electrodes were measured.

Electrode surface resistances measured by the *i*-PLD technique in this study were compared with resistance values from other thin film studies in literature (including earlier data from our group). As shown in Figure 4.3, resistance values found in literature are usually orders of magnitude higher for all materials. Please note that the data are grouped into low and high pO_2 (values given in the table). All surface resistance values taken from literature were

Die approbierte gedruckte Originalversion dieser Dissertation ist an der TU Wien Bibliothek verfügbar.
The approved original version of this doctoral thesis is available in print at TU Wien Bibliothek.
TU Bibliothek Your knowledge hub WIEN

conducted in conventional *ex-situ* measurement setups. From this we must conclude that standard *ex-situ* experiments cannot access the full catalytic capabilities of the studied electrodes. Rather, already degraded states are measured. More specific, for LSC at both 0.04 mbar and 1000 mbar O_2, literature data usually report at least 10 times higher surface-related polarization resistances than the values obtained by *i*-PLD in this study. For LSF the observed resistance difference is even more pronounced, where different studies report more than two orders of magnitude higher polarization resistances. The same behavior was also observed on STF and PCO electrodes: compared to literature, up to two orders of magnitude lower surface resistances were found during *i*-PLD measurements. The occurrence of this trend for a wide range of different materials underlines the general validity of this effect for a broad range of SOFC cathode materials.

4.3.3 Monitoring electrode degradation by simultaneous AP-XPS and *in-situ* impedance measurements

In general, the oxygen reduction is known to take place on the surface of the mixed conducting electrodes. [28] Hence, changes of the electrode surface chemistry can be expected to increase or decrease the activity of the surface towards oxygen reduction. The very low surface-related electrode polarization resistances observed by *i*-PLD measurements might thus be explained by a virtually uncontaminated and consequently highly active surface of the investigated electrode material. To test this hypothesis, ambient pressure X-ray photoelectron spectroscopy (AP-XPS) measurements were conducted in combination with simultaneous *in-situ* electrochemical impedance measurements at different temperatures and oxygen partial pressures. Thus, changes in the surface composition can be correlated with changes of the surface resistance.

For this experiment, an LSC electrode was first prepared and measured by *i*-PLD, where an area specific resistance of 18 Ωcm^2 at 600 °C and 0.005 mbar O_2 was measured. Subsequently, the sample was transferred to the AP-XPS chamber, where XPS measurements at room temperature and UHV conditions found a clean electrode surface with no other contaminations than adventitious carbon (which is a well-known contaminant on surfaces stored in lab-air and is removed upon heating to 400°C in AP-XPS conditions) - in particular, no silicon or sulfur was observed.

Besides determination of the overall electrode surface composition, special focus was laid on the detection of sulfur traces on the electrode surface, as sulfur contaminations (typically from SO_2 and H_2S in the gas phase) are well known for the poisoning of SOFC cathodes.[31, 76, 79, 84, 86, 87, 103, 123, 189, 194–201] To determine the sulfur concentration on the surface of the LSC electrodes, XPS spectra of the S2p core levels and O1s core levels were recorded. Upon heating the electrode to 400 °C in 0.005 mbar O_2, XPS measurements found significant

Die approbierte gedruckte Originalversion dieser Dissertation ist an der TU Wien Bibliothek verfügbar.
The approved original version of this doctoral thesis is available in print at TU Wien Bibliothek.
TU WIEN Bibliothek Your knowledge hub

amounts of oxidized sulfur on the surface of the sample. This can only be explained by trace impurities of sulfur compounds in the 99.999 % high purity oxygen feed gas. Subsequently, the sample was heated to 600 °C, where simultaneous impedance and XPS measurements were carried out. The observed surface resistance (168 Ωcm^2) was already much higher than the value found in the *i*-PLD (18 Ωcm^2) and it further degraded for longer annealing times, saturating at 195 Ωcm^2. The evolution of the surface-related resistance and of the sulfur adsorbate concentration is shown in Figure 4.4.

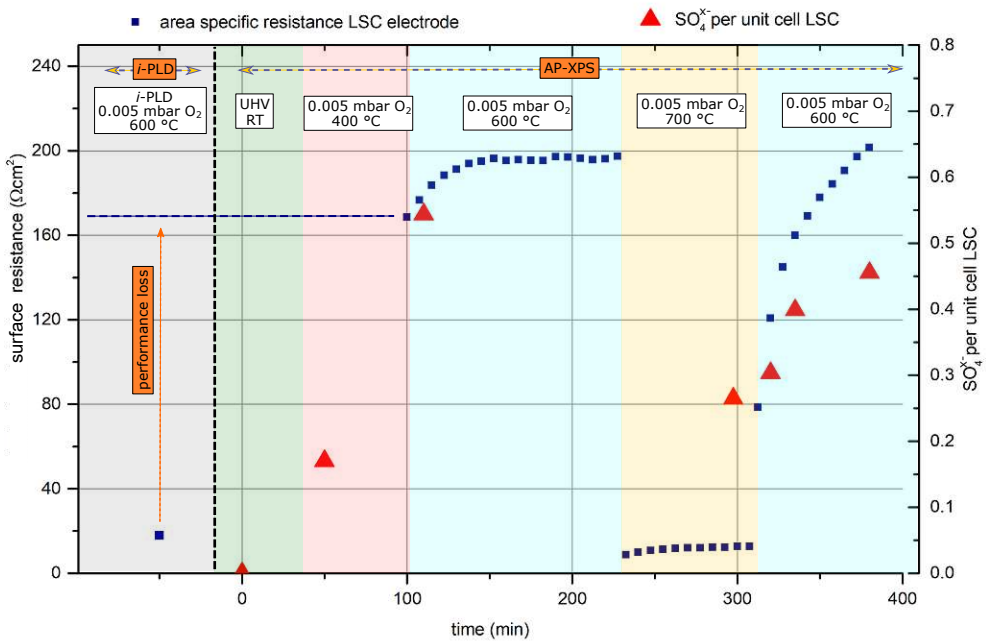

Figure 4.4: Surface related polarization resistance of an LSC electrode (blue rectangles) measured first by *i*-PLD and subsequently during AP-XPS. Red triangles represent sulfur oxide species detected on the surface of the electrode (in SO_4^{x-} per (surface) unit cell of the perovskite.)

Simultaneous to the electrochemical degradation process, the S2p species at a binding energy of 169-170 eV increased together with an O1s species at ca. 532 eV (see Figure 4.5). After correction for photoemission cross-sections and analyzer transmission, a linear relationship of S2p and 532 eV O1s atomic fractions with a slope of 0.23 was found (see Supporting Information, Figure 4.8), being in excellent agreement with the stoichiometry of a SO_4^{x-} surface species. The calculated SO_4^{x-} amount per unit cell is plotted in Figure 4.4 (0.55 SO_4^{x-} of unit cell LSC after heating to 600 °C) and already indicates a relationship to the degradation of the surface resistance. Noticeably, various authors of previous studies (including some of the co-authors of this paper) [106, 208–210] already observed the 532 eV O1s component on the surface of LSC and related materials and struggled with the assignment due to the unusually high binding energy, compared to perovskite bulk oxygen or typical hydroxide species. Only

Die approbierte gedruckte Originalversion dieser Dissertation ist an der TU Wien Bibliothek verfügbar.
The approved original version of this doctoral thesis is available in print at TU Wien Bibliothek.
TU Bibliothek Your knowledge hub WIEN

recently, a correlation of sulfur impurities and the 532 eV O1s component was found. [210] It is therefore likely, that sulfur contamination of the electrode surfaces was unnoticed in many studies, due to the very small photoemission cross-section of the S2p orbitals, and the 1:4 molar S:O ratio in SO_4^{x-}.

Thereafter, the electrode was heated to 700 °C, where a much lower surface resistance was found (10 Ωcm^2), which is partly caused by the acceleration of the OER kinetics due to temperature activation. Also, a significant decrease of the SO_4^{x-} surface coverage to 0.25 SO_4^{x-} per unit cell LSC was measured. Accordingly, the SO_4^{x-} species are probably not present as a separate phase (e.g.: as $SrSO_4$), but rather as adsorbed ions with charge compensation taking place in LSC (more oxidized Co in a near-surface (space charge) layer). After cooling the sample down to 600 °C, a lower surface-related polarization resistance (80 Ωcm^2) resulted. Within 100 minutes again a strong increase of the surface resistance to around 200 Ωcm^2 was observed, and simultaneously also the surface coverage with SO_4^{x-} increased again to 0.45 SO_4^{x-} per unit cell LSC. Because of this very clear correlation between SO_4^{x-} coverage and electrochemical electrode activity it appears very reasonable to directly relate the adsorption and subsequent oxidation of sulfur species like SO_2 with the increase of the polarization resistance and hence with electrode deactivation. As already mentioned above, the detrimental effect of SO_2 on SOFC cathode performance was also observed in previous work. [85, 86, 189, 211] However, in most studies SO_2 was intentionally added to the feed gas in concentration of a few ppm and long term degradation effects were investigated. Moreover, mostly formation of a $SrSO_4$ second phase was either observed or supposed and degradation was attributed to this second phase. At a first glance, it might look surprising that even trace amounts of sulfur contained in high purity measurement gases can poison the surface reaction so quickly. However, assuming a sticking coefficient of 1 and sulfur being present in form of SO_2, a dose of 1 Langmuir (= 1.33×10^{-6} mbar*1 s) is sufficient to cover the surface. Directly after cooling from 700 °C to 600 °C, the SO_4^{x-} coverage increases by ca. 1 mono-layer/10 000 sec as can be roughly estimated from Figure 4.4. Therefore, the SO_2 partial pressure in the AP-XPS atmosphere seems to be of the order of 10^{-10} mbar. At a total gas pressure of 0.005 mbar, this corresponds to an SO_2 concentration of at least 0.2 ppm_{vol} in the feed gas, which is in good agreement to impurity analysis of the bottled gas cylinders (see below).

4.3.4 Ex-situ investigation of pristine surfaces and comparison with *i*-PLD results

The AP-XPS measurements showed that already at very low gas phase pressures, trace impurities of sulfur species in high purity gases are sufficient to cause a significant surface coverage with SO_4^{x-} anions. Consequently, further purification of gases is crucial to eliminate all sulfur sources. To address this issue, a gas purification setup was developed to reduce

Die approbierte gedruckte Originalversion dieser Dissertation ist an der TU Wien Bibliothek verfügbar.
The approved original version of this doctoral thesis is available in print at TU Wien Bibliothek.
TU WIEN Bibliothek Your knowledge hub

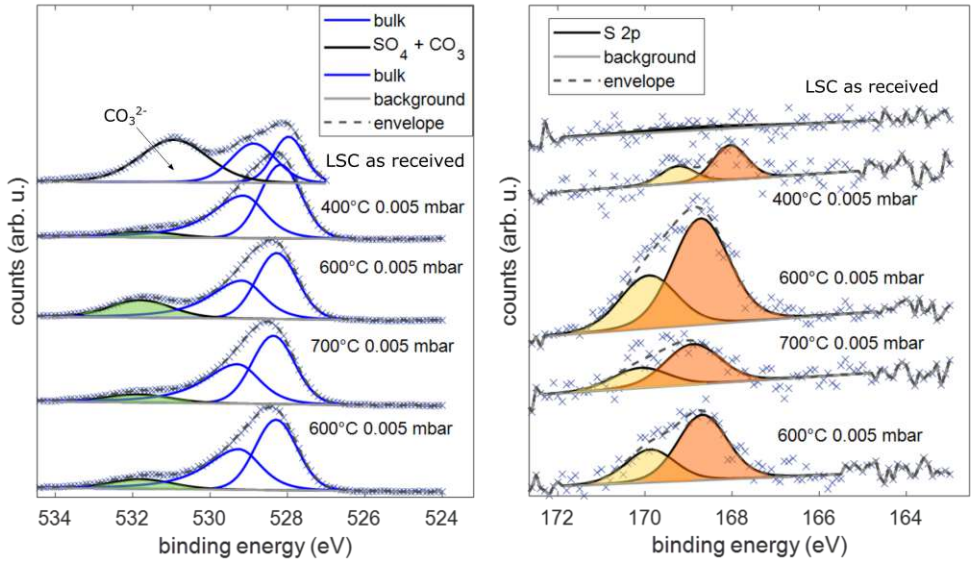

Figure 4.5: Spectra of the binding energy area of O1s and S2p at different conditions during AP-XPS measurements.

the sulfur contamination in the already high purity (99.999 %) measurement gas. A detailed explanation of the setup can be found in the Experimental Part.

In this experiment, the surface-related polarization resistance of LSC and PCO electrodes were measured in three different ways at 600 °C: *in-situ* in the *i*-PLD chamber, *ex-situ* in synthetic air (99.999 %) in a conventional tubular measurement setup and *ex-situ* in the same measurement setup, but with purified synthetic air. The surface resistances of electrodes in a pristine state (directly after heating to 600 °C) and degraded electrodes (annealed for 10 h in synthetic air at 600 °C) was compared and is plotted in Figure 4.6. In addition, the feed gas (unpurified, purified with the described setup and after being fed through the PLD) was subjected to ICP-MS measurements to determine the amount of sulfur compounds in the gas.

While 0.477 ppm_{vol} (1.250 $\mu g/m^3$) of sulfur compounds were found by ICP-MS in the feed gas taken from synthetic air gas bottle provided by the producer (99.999 % pure), after gas purification with the described setup just 0.096 ppm_{vol} (0.251 $\mu g/m^3$) of sulfur compounds remained. (We expect the sulfur compounds to be mainly SO_2 and H_2S, but with the conducted measurements we cannot distinguish between different sulfur species. Most interestingly, the sulfur content decreased to an even lower 0.036 ppm_{vol} (0.094 $\mu g/m^3$) after letting the gas flow through the setup of the cold PLD. While this may be surprising at first, note that the inner walls of the PLD chamber (about 0.5 m^2) are coated with amorphous and highly porous layers of residues from PLD depositions during the 15 years of operation. This "coating", built up over the years, seems to act as a very efficient getter for sulfur compounds and most probably also for other contaminations, thus explaining why electrodes during *i*-PLD mea-

Die approbierte gedruckte Originalversion dieser Dissertation ist an der TU Wien Bibliothek verfügbar.
The approved original version of this doctoral thesis is available in print at TU Wien Bibliothek.
TU WIEN Bibliothek Your knowledge hub

surements experience such low degradation rates. For an in-depth characterization of the "coating", X-ray fluorescence spectroscopy (XRF) measurements were conducted, which revealed the PLD walls to be mainly composed of La (20.4 %), Mn (18.6 %), Co (13.2 %) and Sr (11.8 %)) oxides, please see Figure 4.11 in the Supporting Information for precise composition. A high sticking coefficient is expected for sulfur on these oxides. [212] Moreover, also considering the area difference between the PLD wall (0.5 m^2) and the area of the investigated thin film electrode (0.5 cm^2), absorption of SO_2 is far more likely on the PLD walls.

As can be seen in Figure 4.6, a clear correlation can be found between the concentration of

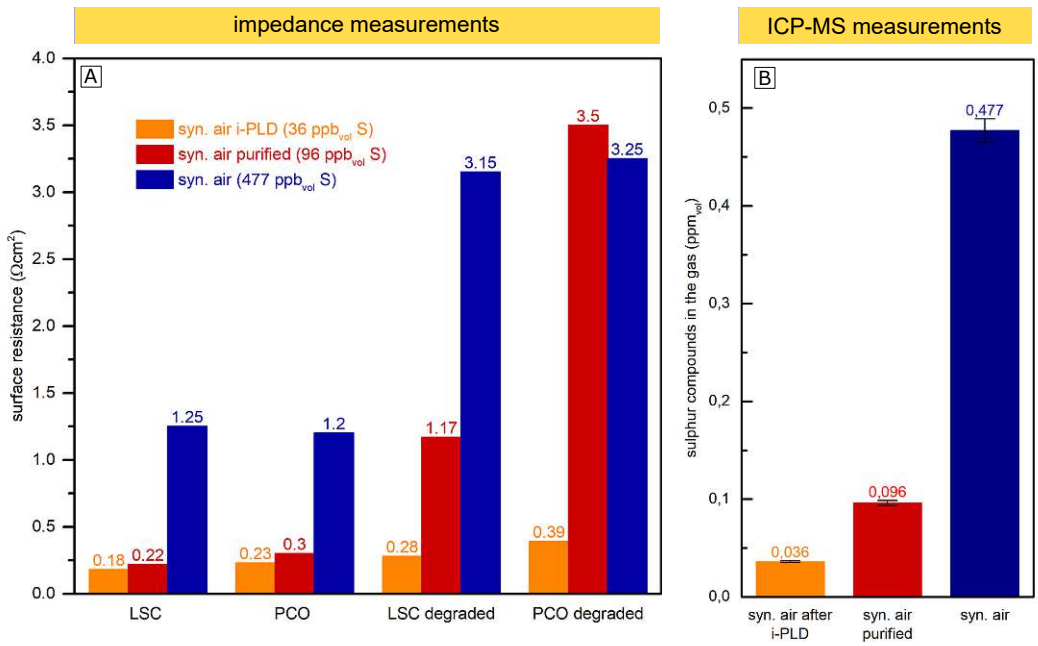

Figure 4.6: A) Surface related polarization resistance of LSC and PCO electrodes measured in the *i*-PLD in synthetic air, in an *ex-situ* measurement setup in synthetic air, and *ex-situ* with purified synthetic air. Values are shown for pristine electrodes and the same electrodes annealed for 10 h at 600 °C in the corresponding gas ("degraded"). B) Sulfur compounds found in the measurement feed gas by ICP-MS measurements without purification, after purification with the described setup, and after being passed through the PLD chamber.

sulfur compounds detected in the feed gas and the measured pristine electrode surface resistance. In the *i*-PLD, electrodes showed very low resistances and also upon annealing only a slight increase of the surface resistance was observed. The surface composition of LSC and PCO electrodes was investigated by XPS measurements after annealing for 12 h in synthetic air in the setup of the *i*-PLD and, as expected, no sulfur contaminations were found on the electrode surface, (see Supporting Information Figure 4.9).

Ex-situ measurements with feed gas from unpurified synthetic air (99.999 %) yielded significantly higher surface-related polarization resistances with electrodes having around an order

Die approbierte gedruckte Originalversion dieser Dissertation ist an der TU Wien Bibliothek verfügbar.
The approved original version of this doctoral thesis is available in print at TU Wien Bibliothek.
TU WIEN Bibliothek Your knowledge hub

of magnitude larger resistances compared to the values found during *i*-PLD measurements, being in good agreement with the usual difference between *in-situ* and *ex-situ* measurements performed in our group. Measurements with synthetic air purified by the described setup, where a large extent of sulfur was removed from the feed gas, showed very low surface resistances compared to unpurified synthetic air, almost reaching the extremely low values found during *i*-PLD measurements. The slightly higher surface resistance found during impedance measurements with purified synthetic air compared to measurements in the *i*-PLD may already reflect the sulfur concentration of both atmospheres, thus highlighting the high sensitivity of the electrode surfaces towards sulfur poisoning. It is further worth mentioning that the sudden strong performance decrease during *ex-situ* measurements was observed with different gas composition/mixtures (premixed synthetic air (5.0) as well as synthetic air mixed in our laboratory with MFCs from Oxygen 5.0 and Nitrogen 5.0) and was also independent from the gas bottle provider (Messer™ or Airliquide™). With regard to the long-term stability of the surface-related polarization resistance, the measurements revealed very little degradation inside the PLD chamber, while during *ex-situ* measurements a much stronger increase of the resistance values was observed, despite additional purification. This might be caused by residual contaminations from the measurement setup (e.g. steel or quartz parts of the setup). This assumption is supported by the fact that gas purification only showed a significant effect if the *ex-situ* measurement setup was baked out at 800 °C before the measurement, thus removing residual contaminations. Moreover, the coated *i*-PLD heater may also act as a sulfur getter and further decrease the amount of sulfur on the sample surface.

Die approbierte gedruckte Originalversion dieser Dissertation ist an der TU Wien Bibliothek verfügbar.
The approved original version of this doctoral thesis is available in print at TU Wien Bibliothek.
TU WIEN Bibliothek Your knowledge hub

4.4 Discussion

In this chapter, we summarize our findings regarding the high activity of pristine, contamination-free MIEC cathodes and its degradation, suggest mechanistic explanations and discuss them in the context of recent findings in literature. Overall, the following experimental facts have to be considered:

- All investigated SOFC cathode materials (LSF, LSC, STF, PCO and Pt doped LSF) measured in the *i*-PLD setup exhibit very low surface resistances both at 0.04 mbar and 1000 mbar O_2.
- Surface-related polarization resistances reported in literature are usually one or even two orders of magnitude higher than the resistances found during *i*-PLD measurements.
- *In-situ* AP-XPS measurements revealed a clear correlation between the presence of an SO_4^{x-} species on the electrode surface and a strong performance loss of the investigated LSC electrode.
- The surface coverage of those species and ease of desorption at 700 °C strongly suggest that a separate $SrSO_4$ phase has not formed yet.
- Sulfur contaminations were detected in high purity measurement gas (99.999 %) and their removal by a gas purification setup allowed to achieve significantly lower surface-related polarization resistances.

Based on these results, we have strong reason to believe that large parts of the performance degradation of SOFC electrodes are directly correlated to minor sulfur contaminations. As we have shown, trace amounts of sulfur in the feed gas from high purity (99.999 %) gas bottles - even when they are used in an AP-XPS setup with SO_2 partial pressures $<10^{-9}$ bar - already cause a saturation of the surface with SO_4^{x-} species and a significant increase of the surface polarization resistance. Thus, we suggest that in virtually all studies conducted on thin film electrodes reported in literature, sulfur contaminations are also present, albeit mostly unperceived.

In general, the effect of sulfur poisoning of SOFC cathodes has already been intensely studied in literature on cathode materials like LSM, [31, 194–196] LSC, [86, 87, 197, 198] BSCF, [84] or LSCF [79, 123, 199–201] and the fact that sulfur contaminations are detrimental for the surface exchange kinetics is not surprising. In addition, the formation of a $SrSO_4$ secondary phase was frequently observed. [31, 84, 86, 87, 189, 195, 196, 198, 213] However, most studies were conducted with higher $p(SO_2)$, which was intentionally added and/or at higher temper-

Die approbierte gedruckte Originalversion dieser Dissertation ist an der TU Wien Bibliothek verfügbar.
The approved original version of this doctoral thesis is available in print at TU Wien Bibliothek.
TU WIEN Bibliothek Your knowledge hub

atures and/or for longer degradation times. For example, Bucher et al. reported that trace impurities of a few ppb SO_2 present in nominally pure measurement gases are responsible for a performance loss of LSC electrodes [86] by a factor of 10, but this degradation took place over a time period of 1000 h. In contrast, we found a nearly instantaneous dramatic performance loss, which is presumably omnipresent, but went unnoticed in most experiments so far. Accordingly, we are confident that the sulfur poisoning considered here (i.e. the formation of a charged adsorbate layer) is fundamentally different from sulfur poisoning due to a second phase formation as discussed in Refs. [31, 84, 86, 87, 189, 195, 196, 198, 213], see also above.

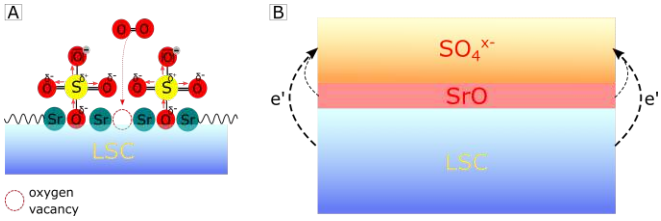

Figure 4.7: Sketch showing how adsorption of SO_4^{x-} on a LSC electrode surface hamper oxygen adsorption by a) steric effects and b) by a charge transfer from the electrode to sulfate adsorbates (b) thus forming a space charge beneath.

With regard to the detailed mechanism of how SO_2 reversibly deactivates the electrode surface, it is important to note that the oxygen reduction mechanism itself is not fully understood yet. However, we will suggest a realistic hypothesis for the deactivation process, which explains our (and a variety of other) experimental results. We assume that SO_2 adsorbs on the electrode surface by forming a bond at an O lattice site and that it is subsequently oxidized to SO_4^{x-} by directly or indirectly involving gaseous oxygen. At this point it is noteworthy, that the final equilibrium is independent of whether SO_2 adsorbs directly on an O lattice site or in a surface vacancy, as previously proposed by Wang et al. on LSCF [201]. In accordance with an increase of the work function [214] and differences in electronegativity [215], we propose that the SO_4^{x-} adsorbate layer extracts charge electrode material below which consequently leads to a negatively charged surface and to the formation of a subsurface space charge (see Fig. 4.7B). A similar phenomenon can also be observed on Taguchi sensors [216], where charge is transferred from an SnO_2 surface to adsorbed O_2 molecules.

The consequences of this altered sulfate-rich surface on the oxygen exchange kinetics are manifold. First, already due to steric reasons, i.e. by blocking adsorption sites (see Figure 4.7A), the oxygen exchange rate is decreased. Second, electronic charge carriers enter the rate equation of the oxygen reduction reaction and a reduced electron concentration (or an increased electron hole concentration) is expected to lower the ORR rate and thus increases the electrode polarization resistance. Third, the sulfate adsorbates accumulate negative charge and reduce the probability of charge transfer to adsorbed oxygen molecules, which is an es-

Die approbierte gedruckte Originalversion dieser Dissertation ist an der TU Wien Bibliothek verfügbar.
The approved original version of this doctoral thesis is available in print at TU Wien Bibliothek.
TU WIEN Bibliothek Your knowledge hub

sential step in the path of the oxygen reduction reaction. It is worth mentioning that even without any additional charge, the bulky adsorbates on top of the electrode may cause a substantial surface potential (χ) increase due to a dipole-like charge redistribution.

In addition to explaining our experimental results, this hypothesis is also in accordance with a recent study by Nicollet et al. on PCO [45], where a strong correlation between the oxygen exchange kinetics and the relative acidity [104] (which is the ionic equivalent of the here proposed work function / electronegativity difference) of decorated surface oxides was found (acidic oxides are e.g. SiO_2, CrO_3 or SO_2 and SO_3 while basic oxides are e.g. CaO, Li_2O or SrO). Moreover, we may link the model presented here (degradation by SO_4^{x-} adsorbates) to reports on Sr segregation as the main reason for the degradation of Sr-containing electrodes. [77, 81, 82, 88, 143, 186, 193]. In all those studies, no specific removal of trace amounts of sulfur compounds from the feed gases was performed and, presumably, electrode surfaces were therefore a priori poisoned by SO_4^{x-} species. Several studies by us and by other groups likely report signs of sulfur contaminations on the electrode surface in the O1s binding energy region (532 eV) of XPS spectra, which were not discussed or possibly wrongly assigned to other chemical compounds. For all these studies, additional XPS measurements in the binding energy region of sulfur were not conducted. Therefore, we suggest that a major part of the performance degradation of SOFC cathodes, which was previously ascribed to Sr segregation, is in fact caused by trace amounts of sulfur, omnipresent in all measurement gases. However, the surface dipole layer may accelerate Sr segregation to the electrode surface and the here suggested SO_4^{x-} adsorption is simply the first step of a subsequent $SrSO_4$ formation with ongoing Sr segregation, which causes a further long-term degradation. Thus it would be interesting to study Sr segregation in highly pure, sulfur-free measurement feed gases and compare those with the current results.

Die approbierte gedruckte Originalversion dieser Dissertation ist an der TU Wien Bibliothek verfügbar.
The approved original version of this doctoral thesis is available in print at TU Wien Bibliothek.
TU WIEN Bibliothek Your knowledge hub

4.5 Conclusion

Impedance measurements on thin film electrodes within the PLD chamber (*i*-PLD) revealed that the pristine surface of several promising cathode materials for intermediate temperature solid oxide fuel cells (LSC, LSF, PCO, STF) possess by far better oxygen reduction kinetics than determined in previous studies using common electrochemical *ex-situ* characterization. The surface related polarization resistances measured during *i*-PLD were often one to two orders of magnitude lower than values previously determined in literature. In order to clarify the origin of this huge difference, ambient pressure XPS measurements with simultaneous impedance measurements were carried out after *i*-PLD impedance measurements. These experiments revealed the formation of SO_4^{x-} species on the electrode surface, even when using high purity gases at very low pressures. It could be shown, that those SO_4^{x-} adsorbates clearly correlate with a severe degradation of the oxygen reduction kinetics. A gas purification setup was used to further clean the high purity feed gases and the corresponding removal of sulfur compounds from the feed gas led to very low surface polarization resistances in conventional *ex-situ* measurement setups which were close to *i*-PLD values. While sulfur is well known for its detrimental effect on the oxygen exchange kinetics of fuel cell cathodes during long-time degradation experiments, this study shows that the very high inherent activity of these materials is already substantially reduced by trace amounts of sulfur in nominally pure feed gases. The corresponding initial very quick but still reversible degradation step has to be separated from any subsequent degradation by $SrSO_4$ second phase formation, even though it might be an important driving force for the latter or for the well-known Sr segregation. This virtually omnipresent (but significant) degradation often goes unnoticed, but is crucial for the development of novel SOFC materials, as it further emphasizes the importance of the sulfur resilience of cathode surfaces.

Die approbierte gedruckte Originalversion dieser Dissertation ist an der TU Wien Bibliothek verfügbar.
The approved original version of this doctoral thesis is available in print at TU Wien Bibliothek.
TU WIEN Bibliothek Your knowledge hub

4.6 Supporting Information

4.6.1 XPS spectra of LSC electrode during AP-XPS measurements:

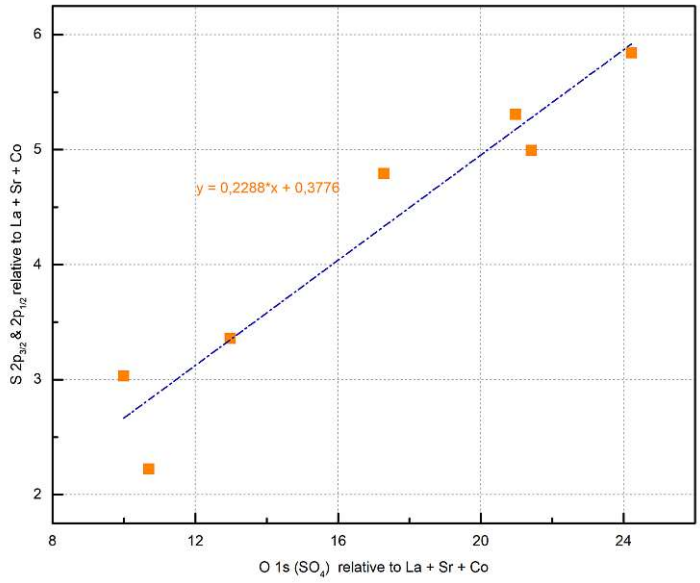

Figure 4.8: Linear correlation between the S 2p peak area (relative to La + Sr + Co) plotted versus the O 1s (SO_4) area (relative to La + Sr + Co). The observed slope corresponds well with the stoichiometric ratio of SO_4

.

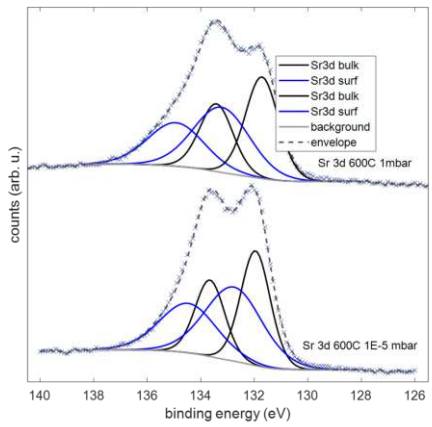

Figure 4.9: Spectra in the Sr 3d binding energy region of the LSC electrode.

In Figure 4.8 the S 2p peak area is plotted versus the O 1s area. Linear fitting of the data points yields a slope of 0.228, which corresponds well to the stoichiometric ratio observed in SO_4. Moreover, in Figure 4.9 the Sr 3d binding energy region is plotted. The measurements revealed that no significant change in the Sr 3d binding energy region occurred over

Die approbierte gedruckte Originalversion dieser Dissertation ist an der TU Wien Bibliothek verfügbar.
The approved original version of this doctoral thesis is available in print at TU Wien Bibliothek.
TU Bibliothek Your knowledge hub WIEN

time, which allows us to exclude Sr segregation as reason for the strong performance loss observed in our measurements. The Sr-3d spectra recorded at 10^{-5} mbar were measured on a pristine SO_4 free surface, whereas a significant SO_4 coverage was detected when conducting the measurements at 1 mbar. Mostly likely the counter ion for SO_4 is a surface strontium ion. Therefore the surface strontium ions undergo a chemical transition from SrO-like to $SrSO_4$-like surface terminations, which is reflected by a change in the binding energy of the Sr-3d component.

4.6.2 LSC and PCO electrodes directly after *i*-PLD measurements:

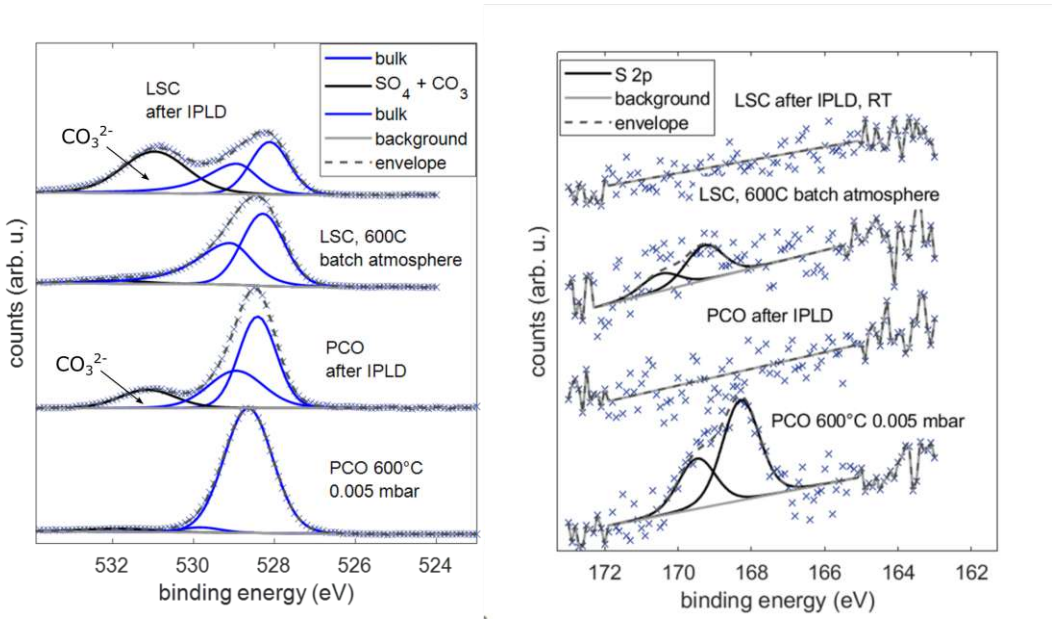

Figure 4.10: Spectra of O 1s and S 2p binding energy of an LSC and PCO electrode directly after *i*-PLD measurements.

The investigated LSC and PCO electrodes were annealed at 600 °C in synthetic air in the *i*-PLD for 12 h. As visible in figure 4.10, conducted XPS measurements revealed sulfur free surfaces directly after the *i*-PLD. After heat up of the eletrodes to 600 °C in the setup of the AP-XPS, sulfur contaminations were detected on the electrode surface. This is in excellent accordance to the superior oxygen exchange kinetics observed during *i*-PLD measurements.

Die approbierte gedruckte Originalversion dieser Dissertation ist an der TU Wien Bibliothek verfügbar.
The approved original version of this doctoral thesis is available in print at TU Wien Bibliothek.
TU Bibliothek Your knowledge hub WIEN

4.6.3 X-ray fluorescence spectroscopy (XRF):

In Figure 4.11 the powder obtained from the PLD walls was analyzed by X-ray fluorescence spectroscopy (XRF). XRF found that the powder was mostly composed of La (20,4 %), Mn (18,6 %), Co (13,2 %) and Sr (18,6 %). It was not possible to detect residual amounts of sulfur as the emission lines of sulfur overlap with emission lines of Co.

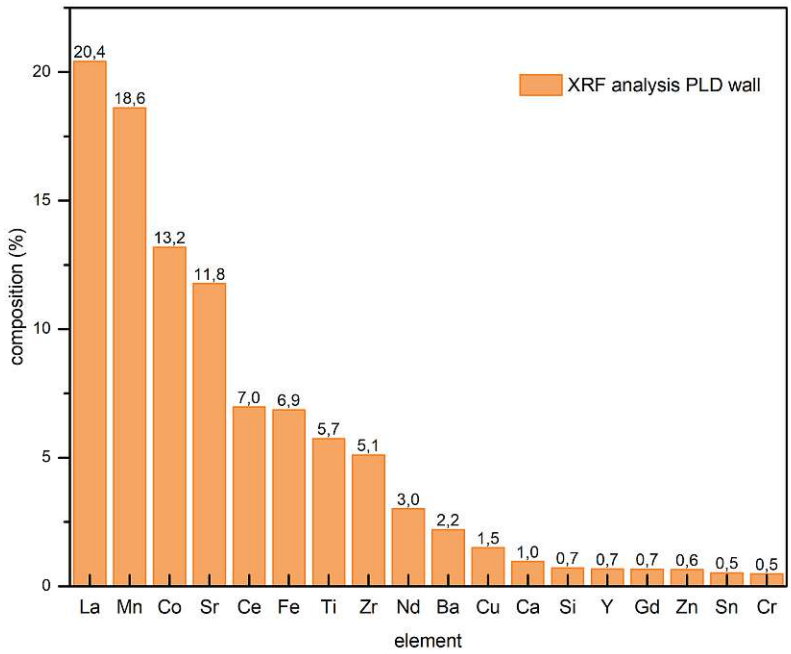

Figure 4.11: Analysis of powder scraped from the PLD wall.

Die approbierte gedruckte Originalversion dieser Dissertation ist an der TU Wien Bibliothek verfügbar.
The approved original version of this doctoral thesis is available in print at TU Wien Bibliothek.
TU WIEN Bibliothek Your knowledge hub

5 *In-situ* electrochemical observation of anisotropic lattice contraction of $La_{0.6}Sr_{0.4}O_{3-\delta}$ electrodes during pulsed laser deposition

Large parts of this study have been submitted to the journal "Chemistry of Materials" for peer review.

5.1 Introduction

Another approach to affect the oxygen exchange kinetics on oxide surfaces makes use of lattice strain. Impedance measurements on NNO [46] and LSC [99] electrodes showed that tensile strain accelerates the oxygen exchange activity, while for compressively strained electrodes decreased oxygen exchange kinetics were observed. In several thin film studies under tensile strain not only faster oxygen exchange kinetics, but also higher concentrations of oxygen vacancies in the bulk of the electrode were found.[99, 217, 218] Similarly, ^{18}O isotope exchange measurements revealed an enhanced surface exchange rate and a higher oxygen vacancy diffusion coefficient of tensile-strained LSC thin films compared to compressively strained LSC films [97, 219]. Moreover, HRTEM studies showed oxygen vacancy ordering in LSC films with tensile strain [97] and DFT studies suggested that tensile biaxial strain reduces the oxygen vacancy migration barrier across the systems [220], which can be explained by a decrease of the oxygen vacancy formation enthalpy.[217] The results from experiments on strained thin films are in good accordance with recent mechanistic studies, which quantified how the oxygen vacancy concentration enters the rate law of the oxygen exchange reaction. [44, 110] However, there is a lack of systematic investigations on strain variation within SOC thin film electrodes and their impact on oxygen exchange kinetics.

In this study, epitaxial and polycrystalline LSF thin film electrodes were stepwise grown by pulsed laser deposition (PLD) and their OER resistance was measured *in-situ* by impedance spectroscopy during deposition, i.e. after each deposition step, in the PLD chamber (*i*-PLD).

Die approbierte gedruckte Originalversion dieser Dissertation ist an der TU Wien Bibliothek verfügbar.
The approved original version of this doctoral thesis is available in print at TU Wien Bibliothek.
TU WIEN Bibliothek Your knowledge hub

This approach allows to grow an electrode material and simultaneously monitor its OER resistance. Thus, thickness dependent changes of the electrode properties can be tracked during growth, unveiling essential information which is usually inaccessible by standard *ex-situ* measurements. In addition, *i*-PLD measurements enable impedance measurements on pristine electrodes free from any external contaminations or electrode degradation, which gives further novel insights into the electrode oxygen reduction kinetics. Employing this technique, the electrochemical properties of growing LSF thin films are examined with special emphasis on the relations between anisotropic *out-of-plane* lattice parameter contraction during PLD growth and oxygen surface exchange kinetics. Additional high resolution transmission electron microscopy measurements (HRTEM) and X-ray diffraction (XRD) measurements help explaining the electrochemical impedance results.

5.2 Experimental section

In the course of the experiments, three different substrates were used: (i) (100)-oriented yttria stabilized zirconia (YSZ, 9.5 mol% Y_2O_3, Crystec GmbH, Germany) single crystals (5x5x0.5 mm^3), (ii) (100)-oriented $La_{0.95}Sr_{0.05}Ga_{0.95}Mg_{0.05}O_{3-\delta}$ (LSGM) single crystals (5x5x0.5 mm^3) grown by the Czochralski technique [174] and (iii) YSZ single crystals from (i) with a 5 nm $Gd_{0.1}Ce_{0.9}O_{2-\delta}$ (GDC) buffer layer. The GDC buffer layer was deposited via pulsed laser deposition (PLD) at a substrate temperature of 600 °C in 0.01 mbar O_2 at a substrate-target distance of 6.0 cm and a laser frequency of 1 Hz. For all *i*-PLD measurements, Ti/Pt grids (15/5 μm holes/mesh) were prepared on both sides of the substrates by lift-off photolithography and magnetron sputtering. As a counter electrode, nanoporous $La_{0.6}Sr_{0.4}CoO_{3-\delta}$ was deposited on top of one the Ti/Pt grids (bottom grid) via PLD at 450 °C in 0.4 mbar O_2 at a substrate-target distance of 5.0 cm and a laser frequency of 5 Hz [94, 221]. During the actual *i*-PLD measurements, $La_{0.6}Sr_{0.4}FeO_{3-\delta}$ (LSF) was deposited onto the top Ti/Pt grid via PLD at a temperature of 600 °C, a pressure of 0.04 mbar O_2, a substrate-target distance of 6.0 cm and a laser frequency of 2 Hz. For all depositions, a KrF Excimer Laser (λ=248 nm, Lambda Physics, COMPex Pro 201) with a laser fluence of ~1 J/cm^2 was used.

Impedance spectroscopic measurements inside the PLD chamber were performed on a specially built heating stage [110] with an Alpha-A High Performance Frequency Analyzer and Electrochemical Test Station POT/GAL 30V/2A setup (Novocontrol Technologies) in a frequency range from 10^6 to 10^{-1} Hz. For a more detailed description of *i*-PLD measurements, the reader is referred to earlier studies employing this technique [93, 95, 99, 110, 154]. The sample temperature was measured via the high frequency intercept of the recorded

Die approbierte gedruckte Originalversion dieser Dissertation ist an der TU Wien Bibliothek verfügbar.
The approved original version of this doctoral thesis is available in print at TU Wien Bibliothek.
TU Bibliothek Your knowledge hub WIEN

impedance spectra, consisting of the only very slightly temperature dependent and known wiring resistances of the setup and the Ti/Pt grid and the strongly temperature dependent electrolyte resistance [111, 174].

X-ray diffraction (XRD) measurements were performed with an Empyrean X-ray diffractometer (Malvern Panalytical). For all measurements, a hybrid monochromator was used on the incident beam side and a GaliPIX3D area detector was used in the diffracted beam path (both Malvern Panalytical). Diffractograms were analyzed with Panalytical Highscore [222], reciprocal space maps data were calculated with Microsoft Excel.

Atomic force microscopy (AFM) measurements were performed in tapping mode with a Nanoscope V multimode setup (Bruker) on a scan range of 1 x 1 μm^2. The AFM results were evaluated with Gwyddion [223] to gain information about the surface morphology and crystallinity of the deposited thin films.

The lamella for TEM was prepared by conventional lift-out technique [224] on a Thermo Fisher Scios 2 DualBeam FIB/SEM with a Ga-ion beam operating at 30 kV accelerating voltage. For final thinning and polishing, the voltage was successively reduced to 5 kV and 2 kV. HRTEM images were acquired using an image-side Cs-corrected JEOL 2100F field-emission transmission electron microscope operating at 200 kV. In order to evaluate lattice parameters, geometrical phase analysis (GPA) technique was used. Each measurement is an average of the area profile spanning in width of about 28 atomic distances.

5.3 Results

5.3.1 Structural characterization and surface morphology

An important goal of this study is the correlation between crystallographic and electrochemical properties of LSF thin films. Hence, information on the film structure is required. Numerous studies have already shown polycrystalline film growth of perovskite-based electrode materials, like LSC[94, 95], LSM [135, 225] or LSF [21, 154] on YSZ single crystals. Polycrystalline LSF without preferential crystal orientation on YSZ is also found in our study. In order to realize epitaxial film growth, we used LSGM and YSZ-GDC (YSZ single crystals with a 5 nm PLD grown buffer layer of $Gd_{0.1}Ce_{0.9}O_{2-\delta}$; cube-on-cube alignment) substrates, see sketch in Figure 5.1. While for the perovskite based substrate LSGM (orthorombic, *Imma*), epitaxial growth of LSF is not surprising and was already shown in a previous study,[154] it might be unexpected that LSF can grow epitaxially on GDC. However, studies in literature

Die approbierte gedruckte Originalversion dieser Dissertation ist an der TU Wien Bibliothek verfügbar.
The approved original version of this doctoral thesis is available in print at TU Wien Bibliothek.
TU Bibliothek Your knowledge hub WIEN

have already shown the epitaxial growth of similar LSC on the GDC buffer layer [105, 226, 227] with a 45 ° in-plane rotation. In our study, also LSF turned out to grow epitaxially on YSZ-GDC.

This is demonstrated by X-ray diffraction in θ-2θ geometry and reciprocal space mapping. From the θ-2θ scans in Figure 5.2a) it is apparent, that LSF on both LSGM and YSZ-GDC grows highly oriented along the (100) direction. Moreover, on LSGM the quasi-cubic c-axis lattice parameter is larger (3.947 Å) than for LSF grown on YSZ-GDC (3.883 Å). Also, both peaks are broadened, indicating a relatively small crystallite size or a varying lattice parameter. In addition, a reciprocal space map was recorded on LSF thin films grown on LSGM as substrate. The results show that the LSGM single crystal exhibits multiple domains with slightly varying lattice parameters. (Please note that single crystals of LSGM are very rare.) Furthermore, the LSF film peak is clearly visible below the single crystal reflex, indicating laterally compressive strain of the film. As can be seen in Figure 5.2b), the film peak is not distinctly separated, but is smeared out over a relatively wide range of c-axis parameters, which indicates a change of the lattice parameter over the film thickness.

The surface of dense LSF thin films grown on LSGM, YSZ-GDC and YSZ was investigated by atomic force microscopy, see images in Figure 5.3. While LSF thin films on both LSGM and YSZ-GDC exhibited very flat surfaces - 0.24 nm root-mean-square (RMS) roughness on LSGM and 0.25 nm RMS roughness on YSZ-GDC - , the surface of LSF grown directly on YSZ showed a strongly granular structure and a comparatively rough surface (5.78 nm RMS roughness). From the XRD results and the AFM scans we thus conclude that LSF grows epitaxially on LSGM and YSZ-GDC, oriented in the (100) direction, and in a polycrystalline structure without preferential orientation on YSZ single crystals.

5.3.2 *i*-PLD growth of epitaxial and polycrystalline LSF thin films

In order to understand how the different crystallographic structures of LSF influence the oxygen exchange kinetics, the electrochemical properties of all three types of LSF (on LSGM, YSZ-GDC and YSZ) were tracked by impedance spectroscopic measurements during growth (*i*-PLD). In Figure 5.4, exemplary impedance spectra are shown. All spectra exhibit a real-axis offset at high frequencies corresponding to ohmic resistances of the setup, the Ti/Pt grid and the electrolyte. The spectra in Figure 5.4 correspond to a substrate temperature of 600 °C [174, 182]; different off-sets are due to different ionic conductivities of LSGM and YSZ single crystals. Furthermore, one dominant impedance feature was observed in all measurements, which corresponds to the oxygen exchange resistance at the surface of the growing working electrode in parallel to the chemical capacitance of the thin film. [25, 37, 46, 110] Upon growth of the film, significant changes of this low frequency feature were found (see Figure 5.5),

Die approbierte gedruckte Originalversion dieser Dissertation ist an der TU Wien Bibliothek verfügbar.
The approved original version of this doctoral thesis is available in print at TU Wien Bibliothek.
TU WIEN Bibliothek Your knowledge hub

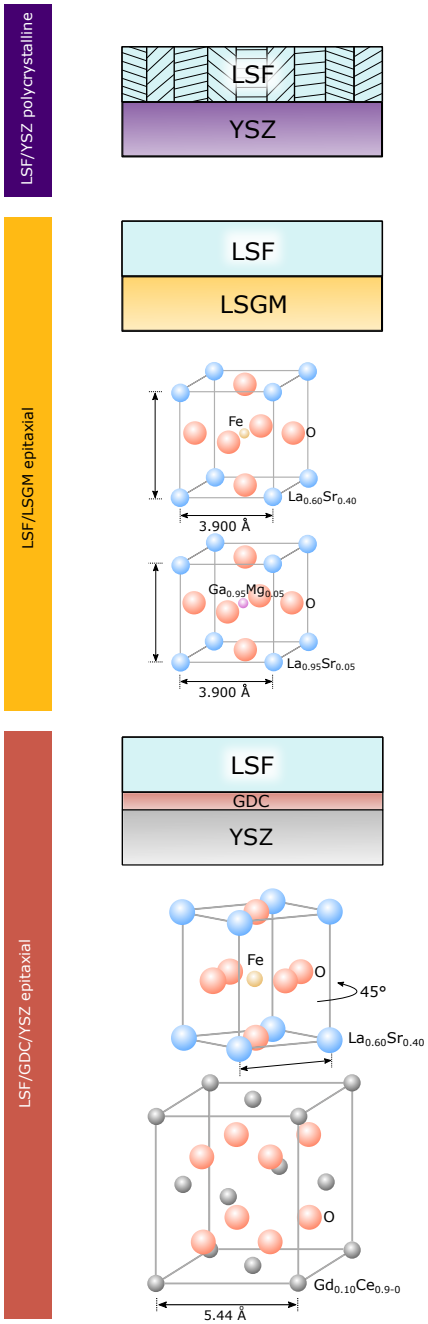

Figure 5.1: Sample sketch showing the morphology of LSF electrodes grown on YSZ, LSGM and YSZ-GDC. Lattice parameters of substrates are taken from literature. [174, 227, 228]

Die approbierte gedruckte Originalversion dieser Dissertation ist an der TU Wien Bibliothek verfügbar.
The approved original version of this doctoral thesis is available in print at TU Wien Bibliothek.
TU WIEN Bibliothek Your knowledge hub

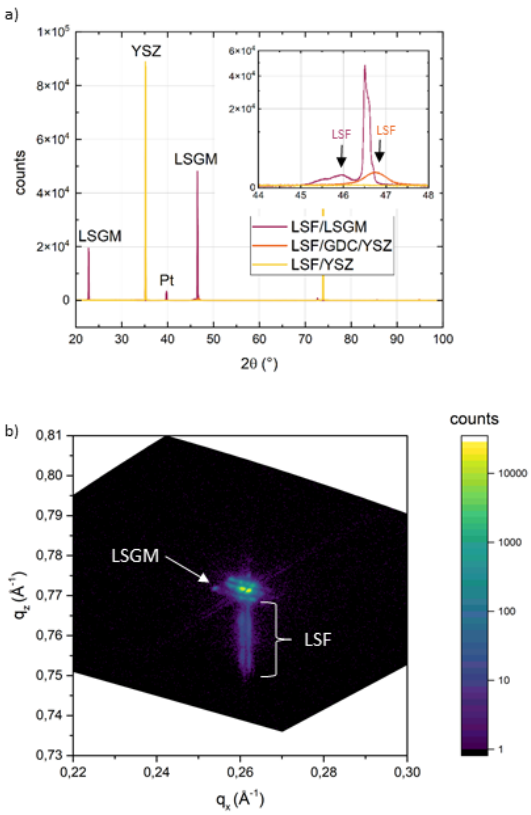

Figure 5.2: a) θ-2θ scans of LSF on LSGM, YSZ-GDC and YSZ showing oriented growth on LSGM and GDC/YSZ and polycrystalline growth on YSZ b)Reciprocal space map of an LSF thin film (50 nm) grown on LSGM.

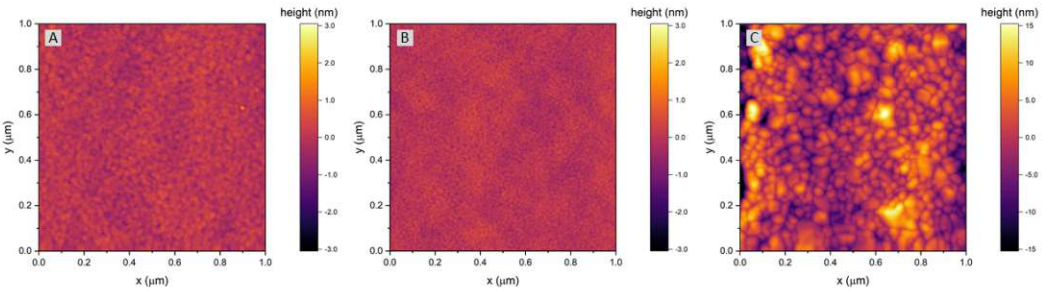

Figure 5.3: AFM images of LSF thin films grown on LSGM, YSZ-GDC and YSZ. Please note the different height scale bars for LSF thin films grown on LSGM and YSZ-GDC vs. LSF thin films grown on YSZ.

Die approbierte gedruckte Originalversion dieser Dissertation ist an der TU Wien Bibliothek verfügbar.
The approved original version of this doctoral thesis is available in print at TU Wien Bibliothek.
TU Bibliothek Your knowledge hub WIEN

which will be discussed in detail below. It should also be mentioned that at the high frequency end of the main semicircle a slight shoulder was observed in some measurements. However, extended investigations of this phenomenon were beyond the scope of these experiments. In literature, similar shoulder-like features were attributed to interfacial resistances between the thin film and the substrate. This interpretation is also supported by the fact that the interfacial resistance was most prominent for LSF grown on YSZ i.e. an interface which is prone to reaction. [21]

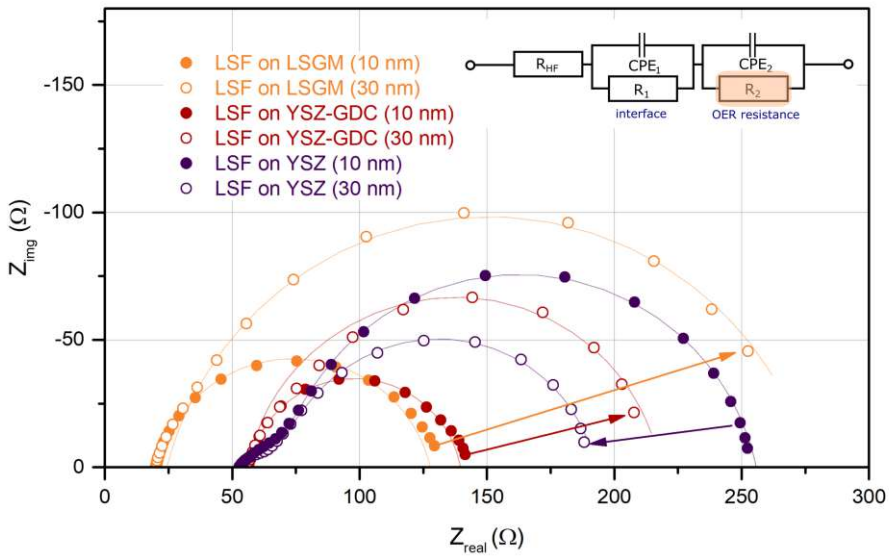

Figure 5.4: Impedance spectra (Nyquist plot) of LSF thin films after 2000 and 6000 pulses of LSF deposited on the different substrates LSGM, YSZ-GDC and YSZ, measured at 600 °C in 0.04 mbar O_2. The inset displays the equivalent circuit used for fitting; CPE = constant phase element. $R_1||CPE_1$ was only required for some of the spectra. The oxygen exchange reaction (OER) resistance R_2 was analyzed in more detail.

Impedance spectra were repeatedly recorded after 1000 laser pulses, corresponding to ~5 nm of deposited material. The area specific resistance of the oxygen exchange reaction (OER) was extracted from the main arc (R_2) of the impedance spectra by using the equivalent circuit sketch in Figure 5.4. We would like to emphasize that the resistance values found in this study by *i*-PLD measurements on polycrystalline LSF thin films are about an order of magnitude lower than values usually reported in literature during standard *ex-situ* measurements, which is owed to the very clean measurement conditions inside the setup of the *i*-PLD. Supposedly, trace amounts of sulfur contamination in the range of ppb may cause a significant increase of the OER resistance in standard *ex-situ* setups.

Die approbierte gedruckte Originalversion dieser Dissertation ist an der TU Wien Bibliothek verfügbar.
The approved original version of this doctoral thesis is available in print at TU Wien Bibliothek.
TU WIEN Bibliothek Your knowledge hub

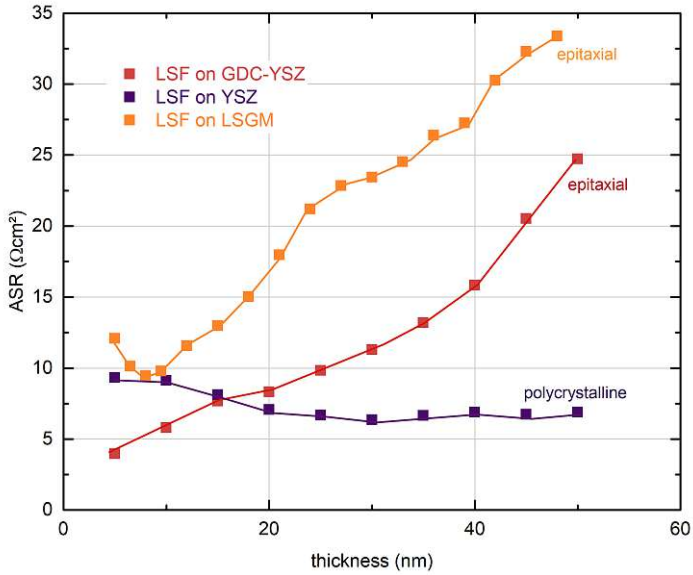

Figure 5.5: Thickness dependent area-specific oxygen exchange resistance (ASR) of dense LSF thin films on LSGM, YSZ/GDC and YSZ substrates measured by *i*-PLD, at 600 °C and 0.04 mbar oxygen partial pressure. Lines are a guide to the eye.

In Figure 5.5, the thickness dependent area-specific oxygen exchange resistance (ASR(from R_2)) can be seen for LSF grown on different substrates. It is apparent that the oxygen exchange resistance develops rather differently for polycrystalline and epitaxial LSF thin films. On polycrystalline LSF a slight variation in the beginning is followed by an almost constant OER resistance after around 20 nm. The OER resistances of the two epitaxial thin films grown on LSGM and YSZ-GDC, on the other hand, exhibit a strong increase over film thickness by a factor of about 3-6. This is surprising as the overall composition of the thin film should not change with its thickness nor should degradation phenomena play a role, since every 5 nm the surface is completely renewed by PLD. It is also different from LSC grown on both LSGM and YSZ; there, an earlier study showed a constant ASR after a film thickness of about 30 nm was reached. [95, 99] In addition, one LSF thin film electrode was grown on YSZ-GDC to reveal whether a saturation of the ASR can be observed. As can be seen in the Supporting Information (Figure 5.12) the polarization resistances increases up to a film thickness of about 60 nm and then decreases. Although the reasons for this trend reversal are of course also interesting, in the present study we would like to focus on the processes causing the unusual ASR increase in the first 50 nm of film growth.

In further experiments, the oxygen partial pressure dependence of the OER resistance (R_2) of LSF (on YSZ-GDC) at 600 °C was compared with LSF grown on YSZ. To do so, the oxygen partial pressure in the PLD chamber was changed by adjusting the oxygen flow through the chamber. Please note that the *i*-PLD technique allows very precise characterization of

Die approbierte gedruckte Originalversion dieser Dissertation ist an der TU Wien Bibliothek verfügbar.
The approved original version of this doctoral thesis is available in print at TU Wien Bibliothek.
TU Bibliothek Your knowledge hub WIEN

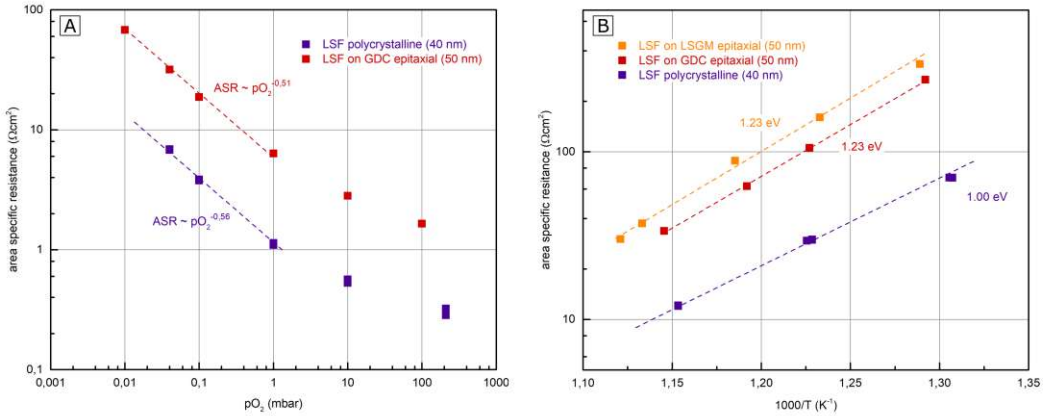

Figure 5.6: A) pO_2 dependence of the area specific oxygen exchange resistance of polycrystalline LSF (purple) compared with LSF grown in epitaxial structure on GDC (red) at 600 °C. B) Determination of the activation energy at an oxygen partial pressure of 0.04 mbar of epitaxial LSF (grown on LSGM (orange) and GDC (red)) and polycrystalline LSF (purple).

such properties due to the excellent stability of the OER resistance on long time scales. This is attributed to the lack of external degradation factors in contrast to *ex-situ* measurement setups. Measurement data for polycrystalline LSF were taken from an earlier study. [154] The comparison of results can be found in Figure 5.6A) and reveal that, in general, polycrystalline and epitaxially grown LSF show a very similar pO_2 dependence of the OER resistance. This suggests that the same oxygen exchange mechanism is active on both electrodes while the concentration of a decisive reacting species or active site seems to differ. The observed shape, including the flattening above 1 mbar O_2, as well as the slopes are also in good agreement with a recent study on similar LSF films. [110]

Moreover, the activation energy of epitaxial LSF grown on YSZ-GDC and LSGM at an oxygen partial pressure of 0.04 mbar O_2 was compared with polycrystalline LSF grown on YSZ. Measurement data for polycrystalline LSF were again taken from reference [154], see Figure 5.6B). While an activation energy of 1.00 eV was found on polycrystalline LSF, a much higher activation energy of 1.23 eV resulted on LSF grown epitaxially on LSGM and YSZ-GDC. As shown in Ref[110], the activation energy includes temperature dependences of defect concentrations as well as kinetic barriers. Different activation energies thus do not necessarily indicate different reaction mechanism. Rather, they can act as a sensitive descriptor of changes in the electrode defect chemistry. The different values found here may thus indicate a shift of the defect thermodynamics. A detailed discussion of the relationship between film thickness, growth mode, point defect chemistry and ASR will be given in the Discussion section below.

Die approbierte gedruckte Originalversion dieser Dissertation ist an der TU Wien Bibliothek verfügbar.
The approved original version of this doctoral thesis is available in print at TU Wien Bibliothek.
TU Bibliothek Your knowledge hub WIEN

5.3.3 High resolution transmission electron microscopy (HRTEM)

As *i*-PLD measurements revealed a substantial increase of the OER resistance with film thickness on electrodes grown in epitaxial structure, HRTEM measurements were conducted to further investigate the structure of the electrode on an atomic level. In Figure 5.7, high resolution transmission electron microscopy (HRTEM) images of an LSF thin film grown on LSGM are shown. The interface between LSGM and LSF is clearly visible and HRTEM images reveal that the LSF thin film grows epitaxially on the single crystalline LSGM substrate. Moreover, no dislocations were observed in the LSF thin film. However, local fast Fourier transform (FFT) analysis found minor amounts of brownmillerite phase to be present in the thin film, which was equally distributed throughout the thin film and no correlation with film thickness was found. Thus, we assume that brownmillerite type phases are a kind of growth defect of our films and do not play a decisive role in explaining our measurement results. (FFT patterns can be found in the Supporting Information, Figure 5.13).

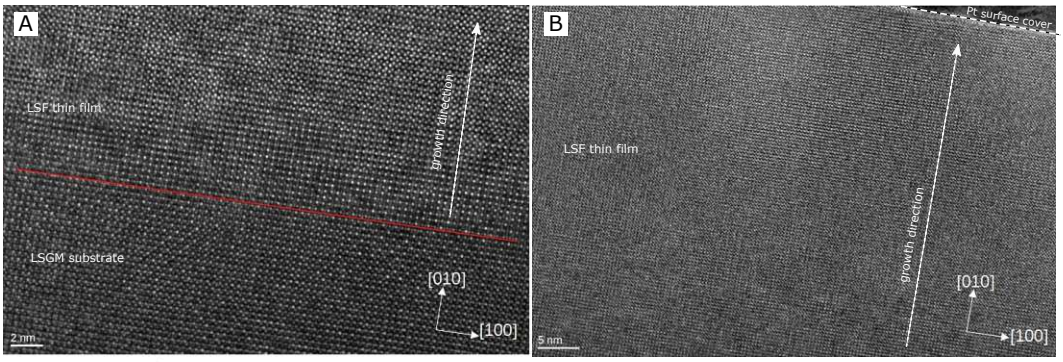

Figure 5.7: A) HRTEM image of the interface region between LSGM and LSF B) HRTEM image of the LSF thin film (surface near region visible).

In addition, HRTEM measurements also enable investigation of the lattice parameters at different positions of the LSF thin film. In order to gain statistically meaningful data, the lattice parameters were measured at 15 different measurement positions on the TEM lamella in close proximity to the LSGM interface (5 nm) and 35 nm away from the interface. As can be seen in Figure 5.8, these measurements reveal that the *in-plane* and *out-of-plane* lattice parameter exhibit a very different behavior with electrode film thickness. First of all, the *out-of-plane* lattice parameter is significantly larger than the *in-plane* lattice parameter. Second, for the *in-plane* lattice parameter HRTEM measurements found a value of 3.871±0.006 Å close to the LSGM interface, which hardly changed with film thickness (3.873±0.008 Å at 35 nm). For the *out-of-plane* lattice parameter, however, a strong change with film thickness was observed. The lattice parameter decreased from 3.973±0.007 Å close to the interface to 3.946±0.005 Å 35 nm away from the substrate, which corresponds to a decrease of the *out-of-plane* lattice parameter by about -0.68 %. An in-depth explanation of how the *out-of-plane* lattice parameter

Die approbierte gedruckte Originalversion dieser Dissertation ist an der TU Wien Bibliothek verfügbar.
The approved original version of this doctoral thesis is available in print at TU Wien Bibliothek.
TU WIEN Bibliothek Your knowledge hub

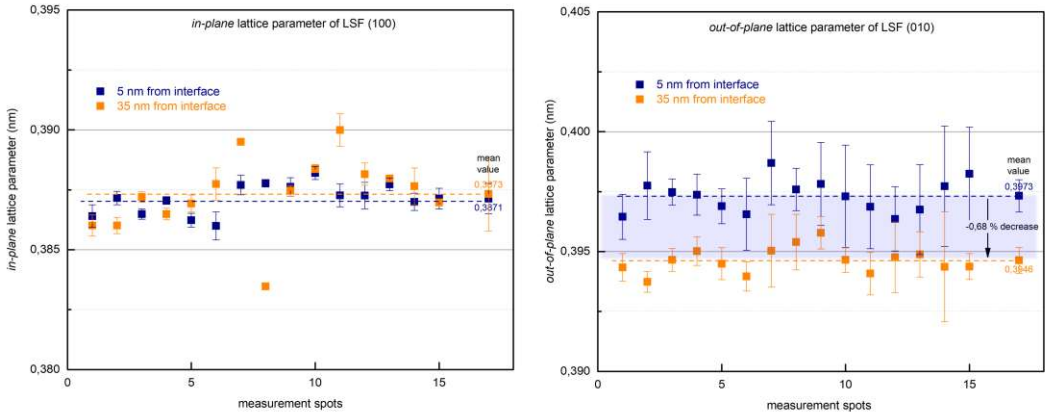

Figure 5.8: A) Lattice parameter in the *in-plane* (100) direction 5 nm from the LSGM interface (blue) and 35 nm from the LSGM interface (orange). B) Lattice parameter in the *out-of-plane* (010) direction 5 nm from the LSGM interface (blue) and 35 nm from the LSGM interface (orange).

contraction and thus the decrease of the LSF unit cell volume influence the defect chemistry of LSF and the oxygen exchange kinetics of LSF thin films will be given in the Discussion section. Moreover, an energy dispersive X-Ray (EDX) line profile was acquired to exclude

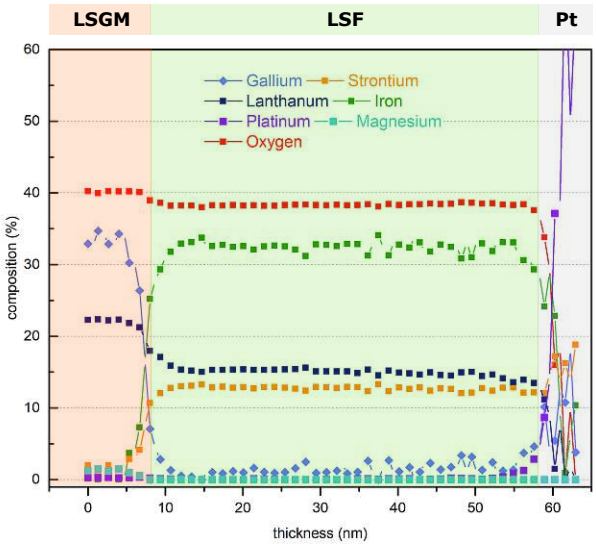

Figure 5.9: EDX line scan of a LSF thin film grown on a LSGM substrate with a Pt protection layer.

that severe changes of the electrode composition over film thickness influence the electrode OER resistance. The EDX composition analysis agrees reasonably well with the overall composition determined by ICP-MS measurements. Especially the ratio between Fe:La:Sr is in good accordance with the expected stoichiometry of LSF. The interfaces between LSGM|LSF

Die approbierte gedruckte Originalversion dieser Dissertation ist an der TU Wien Bibliothek verfügbar.
The approved original version of this doctoral thesis is available in print at TU Wien Bibliothek.
TU WIEN Bibliothek Your knowledge hub

and LSF|Pt protection layer are clearly visible in the EDX line profile images. (The platinum protection layer was applied on the electrode surface after electrochemical measurements to prevent damages during the FIB-cut.) Even more important than the absolute composition values, the EDX analysis reveals that no compositional change is observed across the film, see plot of EDX results as a function of thickness in Figure 5.9. Thus, the observed changes of the OER resistance cannot be attributed to compositional changes of the electrode.

5.3.4 Comparison of lattice parameters and volume on polycrystalline and epitaxial LSF

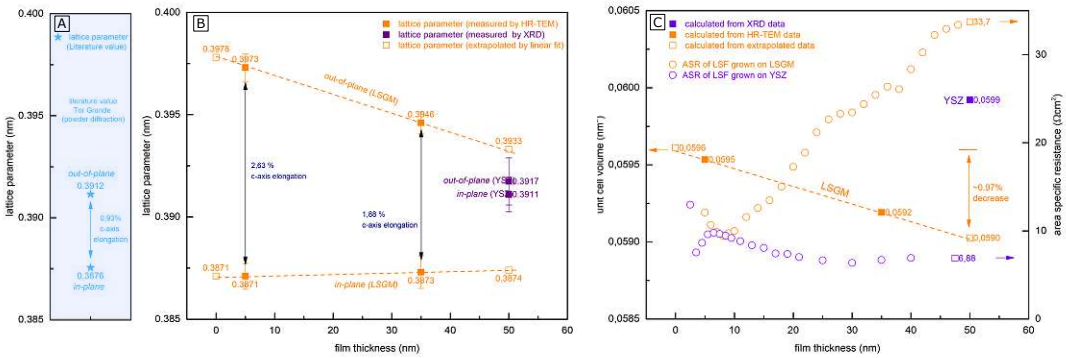

Figure 5.10: a) Lattice parameters of LSF obtained from literature [229] (powder diffraction) B) Comparison of the *in-plane* and *out-of-plane* lattice parameters of LSF grown on LSGM measured by HRTEM with the lattice parameter of LSF grown on YSZ measured by XRD are shown. C) Comparison of the lattice volume of polycrystalline vs. epitaxial grown LSF and the measured ASR.

In Figure 5.10B) the lattice parameters of epitaxial LSF (derived by HRTEM measurements, see Figure 5.8) are compared with the lattice parameters of polycrystalline LSF (obtained by XRD measurements and subsequent Rietveld analysis); literature data of polycrystalline powders are shown in Figure 5.10B). The diffraction data of LSF grown on YSZ was refined with the space group $R\bar{3}c$ (goodness of fit R_{wp}:6.1) according to literature [229], obtaining lattice parameters of 5.5400 ± 0.0017 Å for a_h and b_h (= in-plane) and 13.5489 ± 0.0059 Å for c_h (= out-of-plane). For comparison with TEM results, the normalized pseudocubic lattice parameters $a_{pc}=a_h/\sqrt{2}$ and $c_{pc}=c_h/\sqrt{12}$ were calculated and are also plotted in Figure 5.10. While an almost cubic structure was found for polycrystalline LSF grown on YSZ, a tetragonal structure resulted for epitaxial LSF. Moreover, based on our HRTEM measurement results, the lattice parameters of epitaxial LSF were approximated assuming a linear relationship to extrapolate the lattice parameter decrease for the entire LSF thin film thickness (i.e. 0-50 nm; see dashed orange lines in Figure 5.10B)). For polycrystalline LSF grown on YSZ the lattice parameter is presumed to be constant over the entire electrode thickness.

Die approbierte gedruckte Originalversion dieser Dissertation ist an der TU Wien Bibliothek verfügbar.
The approved original version of this doctoral thesis is available in print at TU Wien Bibliothek.
TU Bibliothek Your knowledge hub WIEN

In addition, the volume of the unit cell was calculated and is displayed in Figure 5.10 C). From our approximation of the *out-of-plane* lattice parameter made in Figure 5.10B), the volume of the tetragonal LSF unit cell was calculated and a decrease of the unit cell volume from 0 to 50 nm film thickness by about 1 % was found. The decrease of the unit cell volume comes along with a significant increase of the OER resistance. For polycrystalline LSF on YSZ, the unit cell is constant and larger than for epitaxial growth, which correlates well with the lower and thickness independent OER resistance.
As the *out-of-plane* lattice parameter and thus the LSF unit cell volume is the only property, for which a significant dependence on the film thickness was measured, we assume that the variation of this parameter is responsible for the increase of the OER resistance on epitaxial LSF thin films during *i*-PLD measurements. In the following Discussion, an in-depth explanation will be given on how the decrease of the unit cell volume may influence the oxygen exchange reaction rates in LSF via point defect concentrations.

5.4 Discussion

First, we summarize our findings regarding the thickness dependent electrochemical properties of epitaxial LSF thin film electrodes upon *i*-PLD growth and then suggest mechanistic explanations and connect them with recent findings in literature. Overall, the following experimental facts have to be considered in a mechanistic model:

- A continuous increase of the OER resistance is observed for epitaxial LSF thin films grown on LSGM or YSZ-GDC substrates up to a thin film thickness of at least 50 nm, while little variation of the OER resistance is found for polycrystalline LSF electrodes grown on YSZ. At a film thickness of 50 nm the OER resistance of epitaxial LSF (grown on LSGM) is about a factor of 6 higher than that of polycrystalline LSF, (see Figure 5.5).

- An increased activation energy (measured at 0.04 mbar O_2) is deduced on 50 nm epitaxial LSF thin films (1.23 eV) compared to a polycrystalline LSF thin film (1.00 eV), (see Figure 5.6 B).

- No major change of the pO_2 dependence of the OER resistance is found, which indicates that the same oxygen exchange reaction mechanism is active on all LSF electrodes, (see Figure 5.6 A).

- For epitaxial LSF thin films grown on LSGM, HRTEM measurements found a decrease of the *out-of-plane* lattice parameter with increasing LSF film thickness, while the *in-plane* lattice parameter stayed almost constant. We can estimate that over the entire LSF thin film thickness the unit cell volume decreases by about 1 %.

Die approbierte gedruckte Originalversion dieser Dissertation ist an der TU Wien Bibliothek verfügbar.
The approved original version of this doctoral thesis is available in print at TU Wien Bibliothek.
TU WIEN Bibliothek Your knowledge hub

As the oxygen exchange reaction rate on the LSF surface is heavily influenced by point defect concentrations [59, 110], it stands to reason that the observed changes of the OER resistance are caused by changing defect concentrations. Based on literature, we first discuss the defect chemical changes expected from the measured decrease of the LSF unit cell volume over film thickness, i.e. how thermodynamic equilibrium constants are affected by lattice strain. Subsequently, we correlate the expected defect chemical changes with the observed OER resistances and activation energies.

Chemical expansion has been intensely studied in literature both on CaF_2-type and perovskite-type electrodes. [230–239] For perovskite-type oxides, numerous studies in literature have found that the radius of an oxygen vacancy is larger than that of an oxygen ion. [229, 234, 236, 239, 240] Thus, a decrease of the unit cell volume is suggested to be accompanied by a decrease of the oxygen vacancy concentration in the material. However, as charge neutrality has to be maintained in LSF electrodes with constant cation stoichiometry, a change of the $V_O^{\bullet\bullet}$ concentration has to be counterbalanced by a change of other point defect concentrations. In general, the concentrations [] of positively charged point defects ($h^\bullet$ and $V_O^{\bullet\bullet}$) and negatively charged point defects (e' and Sr'_{La}) balance each other in LSF according to

$$[V_O^{\bullet\bullet}] + [h^\bullet] = [e'] + [Sr'_{La}] \tag{5.1}$$

, with e' being negligible in oxidizing conditions. [59] An equilibrium of the oxygen exchange reaction.

$$V_O^{\bullet\bullet} + \frac{1}{2}O_2 + 2Fe_{Fe}^{\times} \rightleftharpoons O_O^{\times} + 2Fe_{Fe}^{\bullet} \tag{5.2}$$

$$K_{ox} = \frac{[Fe_{Fe}^{\bullet}]^2 * [O_O^{\times}]}{\sqrt{pO_2} * [V_O^{\bullet\bullet}] * [Fe_{Fe}^{\times}]^2} \tag{5.3}$$

Electron holes are often considered as being localized at Fe ions or the surrounding oxygen atoms, indicated by $Fe_{Fe}^{\bullet}$. Moreover, the Gibbs free energy, enthalpy and entropy of oxygen incorporation (ΔG_{ox}, ΔH_{ox}, ΔS_{ox}) are related to the mass action constant K_{ox} by:

$$K_{ox} = K_{ox}^{\circ} * \exp^{-\frac{\Delta G_{ox}}{k*T}} \tag{5.4}$$

$$\Delta G_{ox} = \Delta H_{ox} - T * \Delta S_{ox} \tag{5.5}$$

The prefactor K_{ox}° includes the concentration of reference states. In a recent study, Lee et al. [217] demonstrated the dependence of the vacancy formation enthalpy and thus of ΔH_{ox} on the strain state of the electrode. As stated in the equation above, an increase of K_{ox} (= decrease of ΔH_{ox}) triggered by a decrease of the LSF unit cell volume leads to a lowered oxygen vacancy concentration. From equation (5.1) and (5.3), it is further evident that a change of the oxygen vacancy concentration is accompanied by a change of the electron hole concentration.

Die approbierte gedruckte Originalversion dieser Dissertation ist an der TU Wien Bibliothek verfügbar.
The approved original version of this doctoral thesis is available in print at TU Wien Bibliothek.
TU WIEN Bibliothek Your knowledge hub

These alterations unavoidably influence the oxygen exchange kinetics. In literature [25, 59, 241], the following equation was suggested to quantify the different contributions influencing the rates of the OER in forward or backwards reaction:

$$r = r_0 * pO_2{}^{v_p} * \prod_i [i]^{v_i} * e^{\frac{\beta e \chi_0}{kT}} * e^{\frac{\beta e \Delta\chi}{kT}} \tag{5.6}$$

The reaction rate r includes the concentrations [i] of the reacting defect species i (i.e. for oxygen reduction: $V_O^{\bullet\bullet}$ and $Fe_{Fe}^{\times}$), the effect of oxygen partial pressure via adsorbates ($pO_2{}^{v_p}$) , the effect of any surface potential χ_0 or its change upon voltage $\Delta\chi$ (which can become relevant if charge is transferred across the surface in this mechanism) and a prefactor r_0, which includes kinetic contributions (chemical activation barriers), but also thermodynamic contributions due to mass action equilibria before the rate limiting step.

In our specific case, we consider the oxygen reduction reaction direction. We assume that the surface potential χ_0 does not vary with pO_2 and lattice volume and its term can be included into r_0 (now $r_0^{'}$). Since no bias voltage was applied we have $\Delta\chi = 0$. Hence, we obtain $\vec{r} = r_0^{'} * pO_2{}^{v_p} * \prod_i [i]^{v_i}$. Based on a detailed study on pO_2 and voltage dependent OER resistances, a reaction mechanism was recently proposed for oxygen incorporation into LSF thin films. [110] This includes fast molecular oxygen adsorption and first ionization of the adsorbed molecule, followed by a second ionization and dissociation as the rate limiting step. In this case, the rate law for the rate of oxygen reduction in Equation (6.1) can be specified as:

$$\vec{r} = K_i K_{ii} \vec{k}_{iii} * pO_2 * [V_O^{\bullet\bullet}][Fe_{Fe}^{\times}]^2 [Fe_{Fe}^{\bullet}]^{-1} \tag{5.7}$$

K_i and K_{ii} are mass action constants of preceding reaction steps and $\vec{k}_{iii}$ the rate prefactor of the rate limiting step (β=0 due to absence of electronic charge transfer across the surface). From equation (5.7) it is evident that a decrease of the oxygen vacancy concentration, together with an increase of electron holes, leads to a decrease in $\vec{r}$, which is equivalent to an increase of the OER resistance.

In Figure 5.11A), the equilibrium concentrations of $V_O^{\bullet\bullet}$, $Fe_{Fe}^{\times}$ and $Fe_{Fe}^{\bullet}$ in LSF64 electrodes are simulated for different values of ΔH_{Ox} with ΔS_{Ox} taken from literature[25]. According to literature, polycrystalline LSF exhibits a ΔH_{ox} value of -94 kJ/mol. [25] The predicted concentrations for other ΔH_{ox} values from Figure 5.11 can now be used in Eq. (5.7) in order to estimate, how much the reaction rate changes when modifying ΔH_{ox}. The sketch Figure 5.11B) illustrates the changes which we consider or neglect in the simulations. For the sake of simplicity, we neglect the unknown effect of ΔH_{Ox} on the mass action constants K_i, K_{ii} and on $\vec{k}_{iii}$. Then we can determine the change of the inverse reaction rate, i.e. the relative change of the OER resistance in dependence of ΔH_{ox}. The corresponding ASR trend of the OER is also shown in Figure 5.11 (in arbitrary units, indicating changes but not absolute values). An

Die approbierte gedruckte Originalversion dieser Dissertation ist an der TU Wien Bibliothek verfügbar.
The approved original version of this doctoral thesis is available in print at TU Wien Bibliothek.
TU Bibliothek Your knowledge hub WIEN

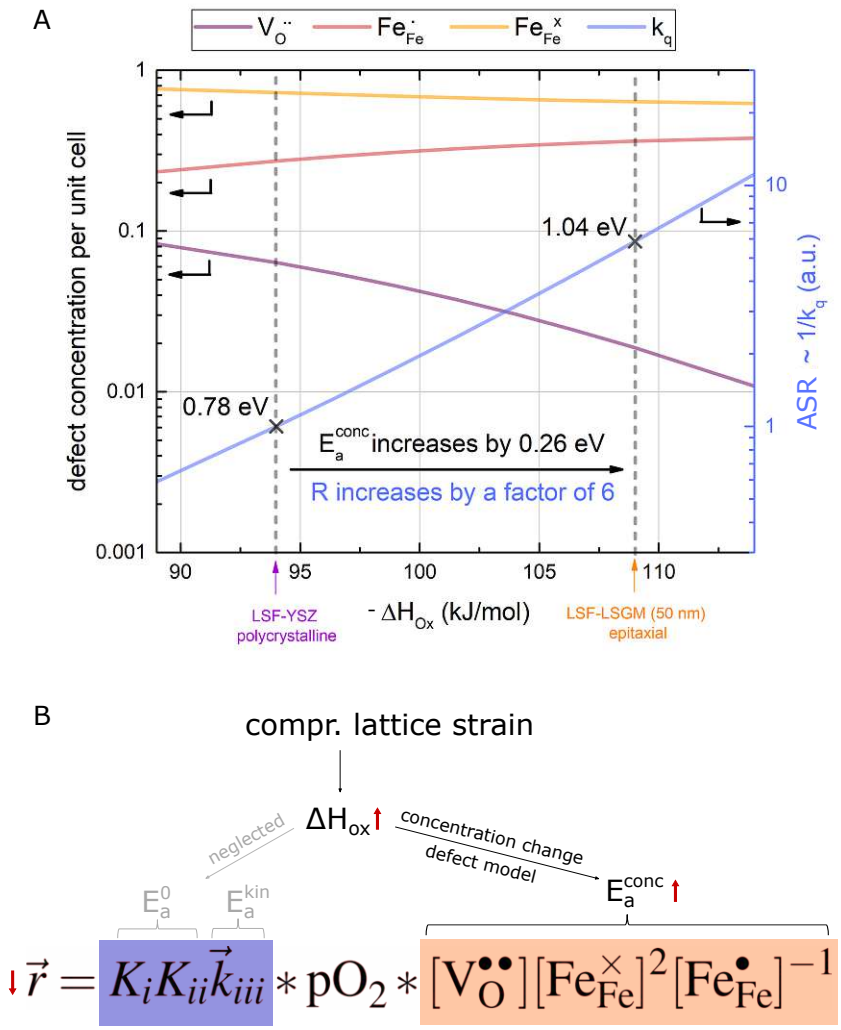

Figure 5.11: A) Calculation of defect concentrations and inverse reaction rates of LSF for different values of ΔH_{ox}; calculation of the concentration amended activation energy ($E_a^{conc.}$) and simulation of the increase of the concentration contribution to the reaction rate (ASR ~ $1/k_q$), B) Sketch explaining the conducted calculations

almost linear dependence of log(ASR) on ΔH_{ox} is found within this approximation. In our experiments we find a OER resistance increase in the range of 3-6 (see Fig. 5.5). According to the plot in Figure 5.11 an increase of ΔH_{ox} by 15 kJ/mol decreases the concentration term in Eq. (5.7) ($[V_O^{\bullet\bullet}] * [Fe_{Fe}^{\times}]^2 * [Fe_{Fe}^{\bullet}]^{-1}$) by a factor of 6 and thus increases the ASR by a factor of six. In other words: a change of the oxygen incorporation enthalpy by 15 kJ/mol can explain the measured resistance change.

The same type of calculations can also be made for a given ΔH_{ox} but with different temperatures. This gives us information on the expected changes of the ASR activation energy. The

Die approbierte gedruckte Originalversion dieser Dissertation ist an der TU Wien Bibliothek verfügbar.
The approved original version of this doctoral thesis is available in print at TU Wien Bibliothek.
TU Bibliothek Your knowledge hub WIEN

effective activation energy of the ASR itself is a highly non-trivial convolution of temperature dependencies of all concentrations and of the thermodynamic and kinetic prefactors in the rate equation. A more detailed discussion is beyond the scope of the this paper and can be found in literature [110]. However, we can again estimate how the activation energy of the ASR changes when changing ΔH_{ox}. We only have to assume that a change of ΔH_{ox} primarily changes the equilibrium defect concentrations, while changes in the exponential terms of K_i, K_{ii} and $\vec{k}_{iii}$ are small. Then we can calculate an effective activation energy change. The activation energy contribution of the concentrations in Eq. (5.7) increases from 0.78 eV to 1.04 eV, i.e. by 0.26 eV when increasing ΔH_{ox} by 15 kJ/mol. This activation energy change is rather close to our measured change of 0.23 eV and also supports our assumption that reaction rates change primarily via defect concentration changes. Defect simulations are thus able to explain our *i*-PLD measurement results and also agree well with the observations from HRTEM measurements, where a decrease of the LSF unit cell volume was found over film thickness. It only remains unanswered why the epitaxial LSF electrodes show such a growth behavior.

Alltogether, we have thus a very reasonable and well-supported model to explain the effect to lattice strain on the electrode defect chemistry and the resulting changes of the oxygen exchange kinetics. *i*-PLD measurements allowed us to precisely elucidate the effect of lattice strain on the oxygen exchange kinetics. It clearly shows that controlling the strain state is a valuable for tuning the electrochemical material properties. This improved understanding of the effect of lattice strain in solid oxide cells thus opens novel paths regarding further material improvements for optimized cell performance.

5.5 Conclusion

The OER resistances of epitaxial LSF thin films on LSGM or YSZ-GDC and of polycrystalline LSF thin film electrodes on YSZ were measured during growth by *in-situ* PLD impedance measurements. Results reveal that the OER resistance of epitaxial thin film electrodes strongly increases with film thickness, up to a factor of six between 5 nm and 50 nm. The OER resistance of polycrystalline LSF electrodes, on the other hand, is hardly film thickness dependent. HRTEM measurements show a decrease of the *out-of-plane* lattice parameter with film thickness in the epitaxial films, which leads to a volume contraction of about 1 % in 50 nm. Defect thermodynamic calculations suggest that the volume contraction of the unit cell leads to a decrease of the oxygen vacancy concentration with increasing film thickness, which subsequently causes an increased OER resistance. This study thus explains and quantifies the severe effect of lattice strain on the electrode defect chemistry and oxygen exchange kinetics. This opens additional paths for the development of highly optimized electrode and electrolyte materials in solid oxide cells.

Die approbierte gedruckte Originalversion dieser Dissertation ist an der TU Wien Bibliothek verfügbar.
The approved original version of this doctoral thesis is available in print at TU Wien Bibliothek.
TU WIEN Bibliothek Your knowledge hub

5.6 Supporting Information

5.6.1 *i*-PLD measurements of a 100 nm LSF thin film on YSZ-GDC

In the Figure 5.12 the OER resistance of a LSF electrode grown on YSZ-GDC is shown. It can be seen that the OER resistance decreases after reaching an electrode thickness of about 60 nm.

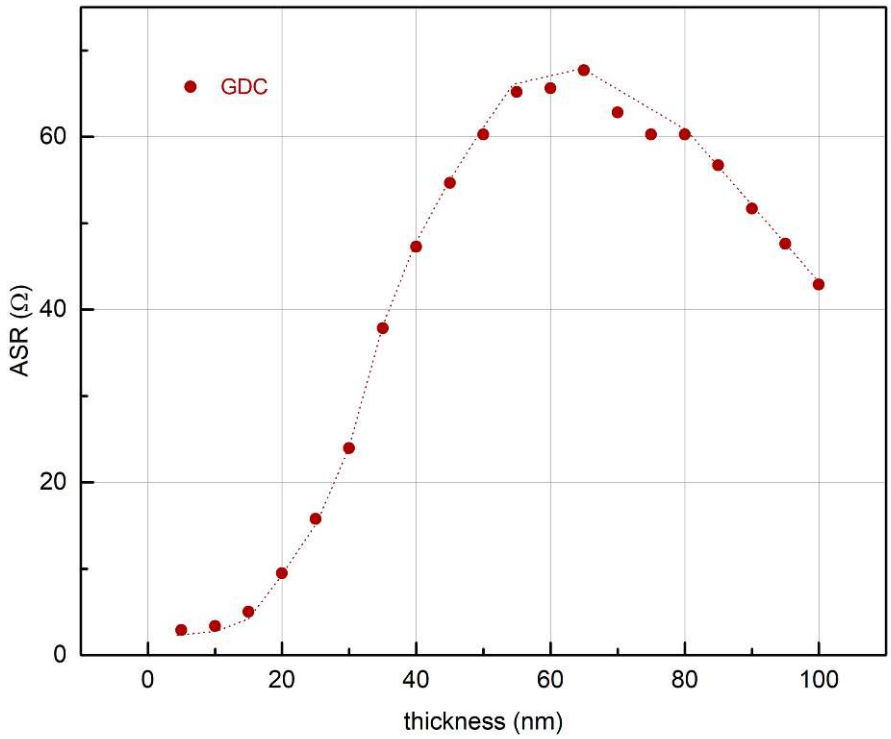

Figure 5.12: Area-specific resistance of a dense LSF thin film electrode grown on YSZ/GDC. Straight lines are a guide to the eye.

Die approbierte gedruckte Originalversion dieser Dissertation ist an der TU Wien Bibliothek verfügbar.
The approved original version of this doctoral thesis is available in print at TU Wien Bibliothek.
TU WIEN Bibliothek Your knowledge hub

5.6.2 Brownmillerite type LSF

In Figure 5.13, a FFT analysis of the LSF thin film is shown. Minor amounts of the brownmillerite phase were found in the entire thin film.

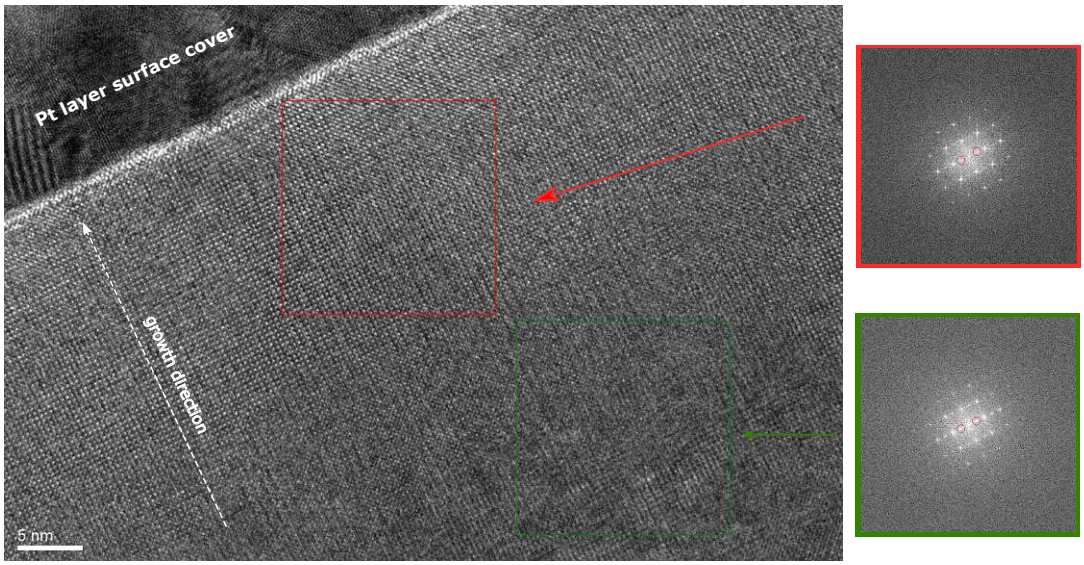

Figure 5.13: FFT analysis of LSF thin film. Red circles in the FFT patterns highlights the half-integer reflections indicating the presence of the brownmillerite phase.

Die approbierte gedruckte Originalversion dieser Dissertation ist an der TU Wien Bibliothek verfügbar.
The approved original version of this doctoral thesis is available in print at TU Wien Bibliothek.
TU WIEN Bibliothek Your knowledge hub

5.6.3 Rietveld analysis

In Figure 5.14 a XRD diffractogram of a 50 nm thick LSF thin film grown on YSZ is shown. A Rietveld analysis was conducted to extract the lattice parameter of the polycrystalline LSF thin film.

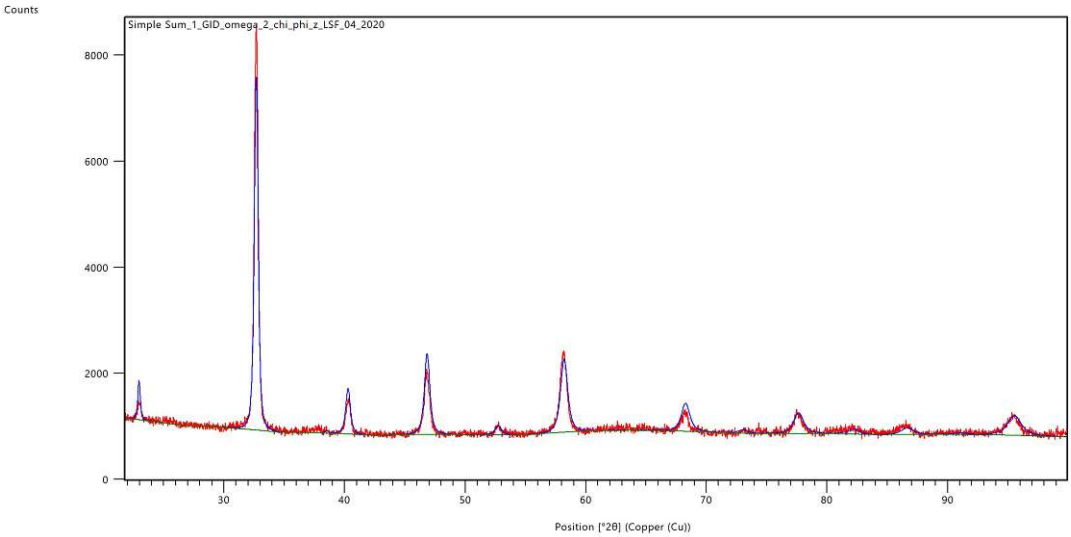

Figure 5.14: Rietveld analysis of LSF thin film grown on YSZ. Red line: XRD recorded in GID geometry, Blue line: Rietveld refinement Green line: background

Die approbierte gedruckte Originalversion dieser Dissertation ist an der TU Wien Bibliothek verfügbar.
The approved original version of this doctoral thesis is available in print at TU Wien Bibliothek.
TU WIEN Bibliothek Your knowledge hub

6 Modifying the surface potential on praseodymium doped ceria electrodes: An *in-situ* PLD and ambient pressure XPS study

This chapter contains in large parts material in preparation for publication.

6.1 Introduction

Recently, several studies investigated the oxygen exchange reaction (OER) kinetics on cathode materials in great detail. They revealed that the oxygen exchange kinetics strongly depends on defect concentrations (e.g. holes, electrons, oxygen vacancies), which are affected by the doping concentration, pO_2 and temperature of the respective electrode material. [37, 44, 50, 52] Moreover, studies in literature revealed factors increasing the oxygen exchange activity of electrodes, for example, by decoration with platinum nanoparticles [112], surface treatment with H_2O [143] or micro-structural optimization [184]. In addition, several studies in literature were conducted to address methods to improve the stability of SOFC electrodes and investigate the degradation behaviour [76, 242, 243]. In a recent pioneering work of Nicollet et al. a change of the oxygen exchange activity of porous PCO10 electrodes after infiltration with binary oxides was reported. [45] The acidity scale for binary oxides as proposed by Smith [104] was found to be a sensitive descriptor to predict changes of the OER activity. While basic oxides (e.g. LiO, CaO, Gd_2O_3) led to an increase of the oxygen exchange activity (= decrease of the electrode polarization resistance), acidic oxides (e.g. SiO_2, Al_2O_3) decreased the oxygen exchange activity.

Building on these promising results, we present here a study on the underlying mechanism by employing *in-situ* PLD impedance spectroscopy (*i*-PLD) and ambient pressure X-Ray photo spectroscopy (AP-XPS). A special focus is laid on characterizing the surface chem-

Die approbierte gedruckte Originalversion dieser Dissertation ist an der TU Wien Bibliothek verfügbar.
The approved original version of this doctoral thesis is available in print at TU Wien Bibliothek.
TU WIEN Bibliothek Your knowledge hub

istry of PCO10 by AP-XPS measurements after decoration with the respective binary oxides. Thereby, effects like oxidation state or surface potential changes can be correlated with oxygen exchange kinetics. Especially the latter was rarely investigated in previous studies. [244]

In this study, epitaxial PCO10 thin films electrodes were decorated by acidic (TiO_2, SnO_2) and basic (SrO, CaO) binary oxides and their performance during stepwise decoration was characterized by *i*-PLD measurements. The applied *i*-PLD measurements are based on a novel technique developed over the last years, which allows to directly measure the electrode polarization resistance while still growing the electrode in the chamber of the *i*-PLD set up. [52, 76, 93, 95, 99, 154] Measurements conducted with the *i*-PLD technique benefit from an excellent stability and high reproducibility of the electrode polarization resistance, which facilitates meaningful mechanistic conclusions. Moreover, *i*-PLD measurements allow to stepwise modify the electrode surface (in the case of this study with binary oxides) and monitor changes of the electrode performance after each deposited pulse, information which is usually inaccessible by standard *ex-situ* measurement methods. Beside characterizing changes of the polarization resistance, also variations of the PCO10 surface potential after decoration with binary oxides were investigated by AP-XPS, significantly advancing the mechanistic understanding of oxygen exchange kinetics and the effect of surface decorations.

6.2 Experimental section

For all *i*-PLD measurements, Ti/Pt grids (25/5 μm holes/mesh, 5/300 nm Ti/Pt thickness) were prepared on the substrates by lift-off photolithography and magnetron sputtering. (100)-oriented yttria stabilized zirconia (YSZ, 9.5 mol% Y_2O_3, Crystec GmbH, Germany) single crystals (5x5x0.5 mm^3) were used as substrates. As a counter electrode, nanoporous LSC was deposited on top of one the Ti/Pt grids via PLD at 450 °C, in 0.4 mbar O_2, at a substrate-target distance of 5,0 cm and a laser frequency of 5 Hz [143, 221] before the *i*-PLD measurements. Before starting the *i*-PLD measurements, a mulitlayer structure of GDC (5 nm), LSC (50 nm) and GDC (5 nm) was deposited on the platinum grid structure of the working electrode side at a temperature of 600 °C and 0.04 mbar O_2. The multilayer structure was applied to ensure sufficient in-plane conductivity for the PCO10 thin film grown on top of it, while still enabling subsequent epitaxial growth of the fluorite PCO on the perovskite LSC.

During *i*-PLD measurements, $Pr_{0.1}Ce_{0.9}O_{2-\delta}$ (PCO10) was deposited on the top of the GDC|LSC|GDC multilayer structure via PLD at a temperature of 600 °C, a pressure of 0.04 mbar O_2, a substrate-target distance of 6,0 cm and a laser frequency of 2 Hz. For all depositions, a KrF excimer laser (λ=248 nm, Lambda Physics, COMPex Pro 201) with a laser fluence of ~1 J/cm^2 was used. For the decoration of the PCO10 thin film electrodes, targets of the

Die approbierte gedruckte Originalversion dieser Dissertation ist an der TU Wien Bibliothek verfügbar.
The approved original version of this doctoral thesis is available in print at TU Wien Bibliothek.
TU Bibliothek Your knowledge hub WIEN

respective binary oxides (SrO, CaO, TiO_2, SnO_2) were prepared from the respective calcined powders (Sigma Aldrich, > 99.995 %) by isostatic pressing and sintering. During the period of the measurements, targets were stored in a desiccator under vacuum and with a drying agent (silica gel) to avoid hydrolysis of the oxidic targets. Before every *i*-PLD measurement, the deposition rate of each decoration target was determined with a quartz balance installed inside the PLD chamber at 0.04 mbar O_2 and room temperature. Usually up to 2 monolayers (= 1 unit cell) of the respective binary oxide were deposited on the PCO10 electrode.

Impedance spectroscopic measurements inside the PLD chamber were performed on a specially built heating stage [110] with an Alpha-A High Performance Frequency Analyzer and Electrochemical Test Station POT/GAL 30V/2A setup (Novocontrol Technologies™, Germany) in a frequency range from 10^6 to 10^{-1} Hz. For a more detailed description of *i*-PLD measurements, the reader is referred to earlier studies employing this technique [52, 76, 93, 95, 99, 154]. The sample temperature was measured via the high frequency intercept of the recorded impedance spectra, consisting of the only very slightly temperature dependent resistances of the setup and the Ti/Pt grid and the strongly temperature dependent electrolyte resistance [26, 182].

In-situ XPS spectra were acquired in a lab-based AP-XPS setup with a PHOIBOS NAP photoelectron analyser (SPECS, Germany) and a monochromated Al K-alpha XR 50 MF (microfocus) X-ray source. Therein, the solid oxide cell was mounted on a special sample holder with a centred 4.9×4.9 mm^2 sized hole for heating with a near-infrared diode laser. [175] Electrical contacts for working and counter electrodes were established by Pt-Ir and sintered platinum paste tips, respectively. The temperature of the sample was controlled via the conductivity of the YSZ electrolyte. AP-XPS measurements were conducted at 1 mbar O_2 and an electrode temperature of 550 °C. The temperature of the electrode was controlled via the high frequency offset of the electrode. XPS spectra were collected at an analyzer pass energy of 30 eV, which provided a reasonable balance of count rate and energy resolution.

6.3 Results

6.3.1 Oxygen exchange activity of PCO10 electrodes during stepwise decoration with binary oxides

The effect of surface decoration with binary oxides on the OER resistance was measured via *i*-PLD. The sample and the procedure is sketched in Figure 6.1. First, a 50 nm PCO10 thin film was deposited on top of the well-conducting GDC|LSC|GDC multi layer. This PCO10 electrode was decorated step-wise with 2 monolayers of the respective binary oxide and the

Die approbierte gedruckte Originalversion dieser Dissertation ist an der TU Wien Bibliothek verfügbar.
The approved original version of this doctoral thesis is available in print at TU Wien Bibliothek.
TU WIEN Bibliothek Your knowledge hub

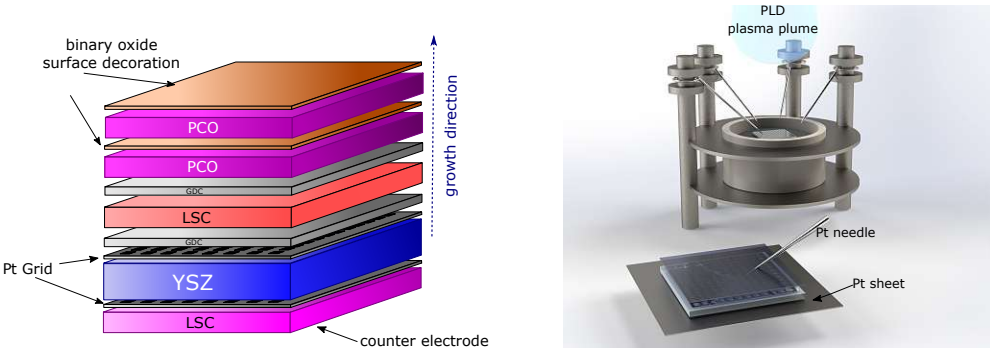

Figure 6.1: Sketch of the multilayer sample applied for *i*-PLD measurements. Sketch of the *i*-PLD measurement setup.

change of the impedance was simultaneously tracked by *i*-PLD measurements. After depositing 2 monolayer, measurements of the pO_2 dependence of the polarization resistance and determination of the activation energy were conducted to gain mechanistic insights into the oxygen exchange kinetics. Afterwards, 10 nm-20 nm of PCO10 were deposited on top of the electrode to "reset" the polarization resistance to its initial value before the next decoration cycle was carried out. The applied multilayer technique guarantees excellent comparability of impedance results as all measurements of the four different decoration materials were conducted on the same electrolyte substrate under the very same parameters (temperature, pO_2, laser fluence, active electrode surface), which allows us to reduce reasons for sample scattering. In addition, *i*-PLD measurements exhibit a higher stability of the polarization resistance, compared to standard *ex-situ* measurements and allow to draw more reliable mechanistic conclusions.

In Figure 6.2 the change of the PCO10 polarization resistance upon decoration with the respective binary oxides is shown. Our results reveal that the decoration with acidic binary oxides (TiO_2, SnO_2) yields a substantial increase of the polarization resistance already with minor amounts of the binary oxide. While with SnO_2 the polarization resistance increased by 400 % after the deposition of 2 monolayers of surface decoration, the effect of the surface decoration with TiO_2 was even more pronounced with an increase of polarization resistance by a factor of 600 %. Impedance spectra of PCO10 decorated with different amounts of TiO_2 can be found in Figure 6.3. For fitting of the well-defined spectra the equivalent circuit shown in the inset of Figure 6.2 was applied. The high frequency intercept was assigned to the grid resistivity and the oxygen ion conductivity of the YSZ substrate and the value (50 Ω) is in good accordance with literature for 600 °C [182]. The main semicircle of the impedance spectra was fitted with an R|CPE element, where the resistance, as several studies in literature have shown, can be assigned to the oxygen exchange on the surface of the electrode. [21, 50, 245] The electrode polarization resistance was further related to the active electrode surface area (PCO directly grown on YSZ), as past studies have shown the area above the Pt grid to be

Die approbierte gedruckte Originalversion dieser Dissertation ist an der TU Wien Bibliothek verfügbar.
The approved original version of this doctoral thesis is available in print at TU Wien Bibliothek.
TU Bibliothek Your knowledge hub WIEN

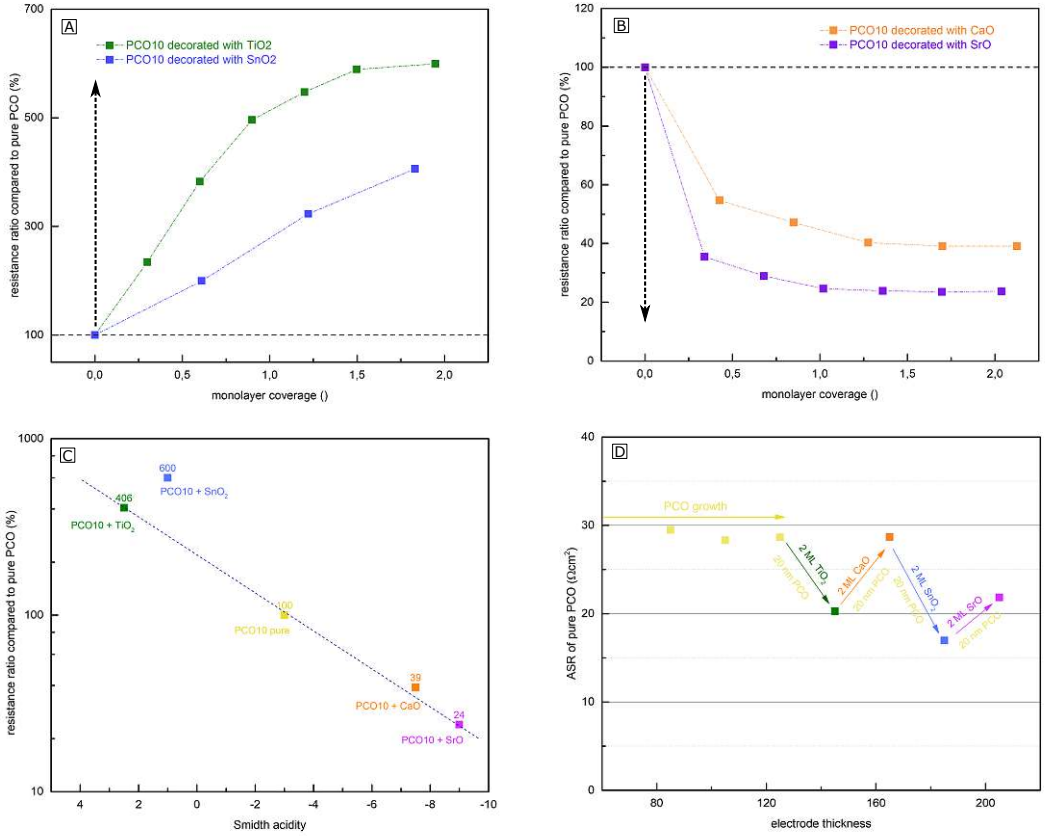

Figure 6.2: A) Resistance ratio compared to pure PCO10 after decoration with acidic oxides (TiO_2, SnO_2); B) Resistance ratio compared to pure PCO10 after decoration with basic oxides (SrO, CaO); All measurements were conducted at 600 °C and 0.04 mbar O_2. C) Resistance ratio compared to pure PCO10 after decoration with the respective binary oxides plotted versus the Smith acidity[104] D) Graphic displaying that a "reset" of the polarization resistance to initial values is possible after decorating the electrode surface with 2 ML of the respective binary oxides by depositing 20 nm of PCO10.

inactive for oxygen exchange due to the high in-plane conductivity of PCO. [21] The shoulder in the mid frequency range was fitted with an additonal R|CPE element and is mostly attributed to interfacial effects at the electrode electrolyte junction, as well as double layer capacitances at interfaces [99].

As can be seen in Figure 6.2 B) also the effect of CaO and SrO on the polarization resistance of PCO10 was investigated and, in accordance with the Smith acidity [104], the surface decoration had the opposite effect on the polarization resistance. While 2 monolayers of CaO reduced the polarization resistance to 40 % of its original value, the improvement effect was even stronger with SrO, which reduced the polarization resistance of PCO10 to 25 % of its

Die approbierte gedruckte Originalversion dieser Dissertation ist an der TU Wien Bibliothek verfügbar.
The approved original version of this doctoral thesis is available in print at TU Wien Bibliothek.
TU Bibliothek Your knowledge hub WIEN

orginal value. The beneficial effect of SrO is of major interest as most studies in literature reported SrO segregation to be responsible for a strong performance decrease of the SOFC electrodes. [75, 77] In addition, in Figure 6.2 the change of the electrode performance after the deposition of 2 monolayers of the respective binary oxides is summarized. A clear correlation between the electrode performance change and the Smidth acidity is found. Just the measured performance increase of PCO10 decorated with SnO_2 deviates from the linear correlation. Thus, our measurement results are in excellent accordance with the study of Nicollett et. al, which conducted similar experiments and reported equal trends between Smidth acidity and oxygen exchange kinetics. [45] Moreover, in Figure 6.2 D) the "reset" of the PCO10 polarization resistance is shown. After decorating the electrode surface with 2 ML of the respective binary oxides, the polarization resistance was restored by depositing 20 nm of PCO10. As can be seen in Figure 6.2 D) the polarization resistance almost reaches its initial value after depositing (especially when considering the strong changes observed before upon surface decoration), which reveals the excellent applicability of the multi layer technique.

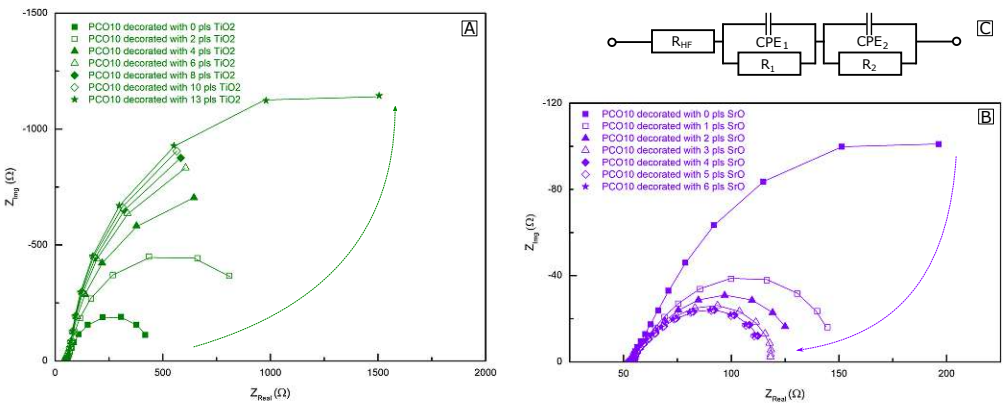

Figure 6.3: A) Impedance spectra of a PCO10 electrode decorated with increasing amounts of TiO_2. B) Impedance spectra of a PCO10 electrode decorated with increasing amounts of SrO. C) Equivalent circuit used for fitting the spectra shown in A) and B). Lines shown are fits conducted with the equivalent circuits shown.

Die approbierte gedruckte Originalversion dieser Dissertation ist an der TU Wien Bibliothek verfügbar.
The approved original version of this doctoral thesis is available in print at TU Wien Bibliothek.
TU Bibliothek Your knowledge hub WIEN

6.3.2 pO_2 and temperature dependence of the polarization resistance on pure and decorated PCO10 electrodes

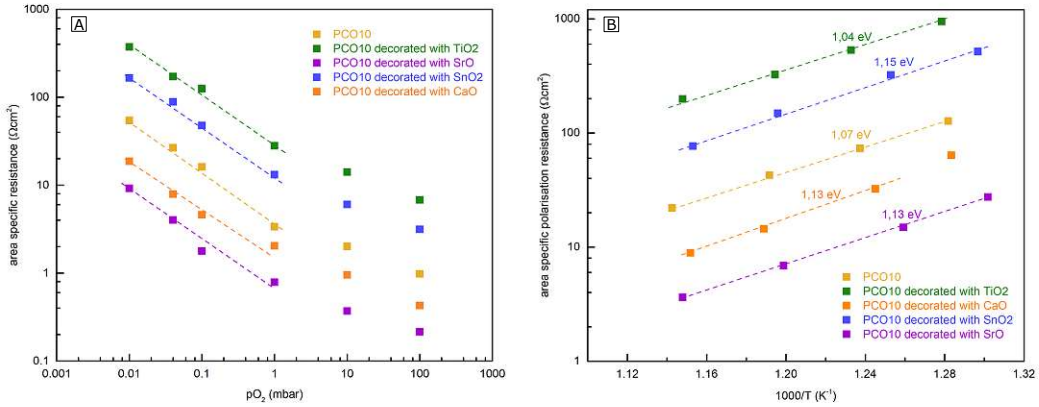

Figure 6.4: A) pO_2 dependence of the polarization resistance on pure and decorated PCO10 electrodes at 600 °C B) Determination of the activation energy on pure and decorated PCO10 electrodes at 0.04 mbar O_2

In addition, also the pO_2 dependence of the polarization resistance was investigated on pure and decorated PCO10 electrodes. In Figure 6.4 A) the area specific resistance is plotted versus pO_2 and, as can be seen in the plot, all electrodes (pure and decorated) show the same dependence. While a steeper curve is found below 1 mbar O_2, a flattening of the curve is observed at higher pO_2. The dependence observed here agrees very well with a recent *i*-PLD study of our group, where the oxygen exchange mechanism on different MIEC materials was investigated. [52] As both pure and decorated PCO10 electrodes exhibit the same pO_2 dependence, it is likely that the same oxygen exchange mechanism is active. This is also supported by measurements of the activation energy on the respective electrodes. For determination of the activation energy, the polarization resistance was measured at different temperatures between 500 °C and 600 °C at 0.04 mbar O_2 and plotted in an Arrhenius diagram (see Figure 6.4B). The activation energy was then calculate from the slope of a linear fit. Results reveal that no systematic alteration of the activation energy was observed after surface decoration with binary oxides. While on pure PCO10 electrodes an activation energy of 1.07 eV was obtained, after decoration with acidic oxides an activation energy of 1.04 eV (TiO_2) and 1.15 eV (SnO_2) and with basic oxides of 1.13 eV (SrO) and 1.13 eV (CaO) was found. Thus, changes of the activation energy on decorated PCO10 electrodes were in the range of ± 10 % compared to the value measured on pure PCO10. Moreover, no clear correlation between the Smith acidity and the change of the activation energy was found, supporting the conclusion that the decorations do not affect the mechanism of the oxygen exchange reaction. Minor activation energy changes in the order of 0.1 eV (e.g. due to surface potential changes) might however go unnoticed due to experimental inaccuracies.

Die approbierte gedruckte Originalversion dieser Dissertation ist an der TU Wien Bibliothek verfügbar.
The approved original version of this doctoral thesis is available in print at TU Wien Bibliothek.
TU Bibliothek Your knowledge hub WIEN

6.3.3 AP-XPS measurements of pure and decorated PCO10 electrodes

In order to reveal how surface decoration with binary oxides affect the surface chemistry of PCO10 electrodes, ambient pressure XPS (AP-XPS) measurements were conducted. The main objectives of the AP-XPS measurements were to measure if surface decorations change the ratio of Pr^{3+} to Pr^{4+} in the upmost region of the PCO10 electrode and to investigate how surface decorations influence the surface potential of the PCO10 electrodes. For the AP-XPS measurements, undecorated ("pure") PCO10 electrodes were compared with PCO10 electrodes decorated with 2 monolayers ("ML") of either SnO_2 or SrO. Samples were prepared in the *i*-PLD setup and were than transferred to the AP-XPS chamber. AP-XPS measurements were carried out at 600 °C, 1 mbar O_2 and with a special gas purification column, which reduces sulfur contaminations in the measurement gas. Moreover, bias polarization was applied to simulate higher and lower oxygen partial pressures. The effects of bias polarization on the electrode surface defect chemistry can be found in literature. [25]

First of all, XPS measurements were conducted to assess the effect of surface decoration on the Pr oxidation state in the surface near region. It is important to note that in the pioneering study of Nicollet et al., the authors have proposed that surface decorations lead to a band bending at the surface and thus increase (basic) or decrease (acidic) the electron concentration in the electrode subsurface and consequently the oxygen exchange activity of the decorated electrodes. Thus, our XPS measurement were targeted towards investigating changes in the electron concentration in the subsurface of the electrode. To do so, the Pr^{4+}/Pr^{3+} ratio was determined, as Pr3+ represent the majority electronic charge carrier at such conditions in PCO10 [145]. In good accordance with literature [107], the Pr^{3+} 3d and Pr^{4+} 3d peaks were found at a binding energy of 931 eV and 927 eV. Measurements were conducted at 1 mbar O_2 and 550 °C. The temperature of the PCO10 electrode was determined by measurements of the high frequency intercept, which displays the ionic conductivity of the YSZ substrate and was compared with literature values [182].

In Figure 6.5 A) the ratio of Pr^{4+}/Pr^{3+} on pure and decorated PCO10 electrodes under different bias polarization is shown. The ratios found do not agree well with our expectations from the model of Nicollet et al. The results show that under cathodic bias for all PCO10 electrodes (pure and decorated) the ratio is significantly < 1, which agrees with the model that at strongly reducing conditions Pr is mostly present in its reduced state, which is the 3+ state. At OCV conditions on SrO the ratio is > 1, while for pure and PCO10 decorated with SnO_2 a ratio of around 0.8 was found. The results obtained at OCV conditions are surprising and reveal that surface decorations do not influence the electron concentration as expected. Decoration with a basic oxid (SrO) led to an increase of the Pr^{4+} concentration, while at OCV conditions PCO10 decorated with an acidic oxide (SnO_2) and pure PCO10 showed the same ratio, which was not expected. Also under anodic bias a similar picture was obtained, PCO10

Die approbierte gedruckte Originalversion dieser Dissertation ist an der TU Wien Bibliothek verfügbar.
The approved original version of this doctoral thesis is available in print at TU Wien Bibliothek.
TU WIEN Bibliothek Your knowledge hub

decorated with SrO showed a higher concentration of Pr^{4+}. The opposite effect was found on PCO10 decorated with SnO_2, where a higher concentration of Pr^{3+} was found. In conclusion, the XPS measurements yielded fundamentally different results as expected from the model of Nicollet et al. as decoration with a basic oxide seems to decrease the Pr^{3+} concentration in the upmost region of the thin film and vice versa for acidic decoration.

Moreover, the Pr polaron concentration was estimated by investigating the fermi edge region. The results are shown in Figure 6.5 B) and, in accordance with the results from the Pr^{4+}/ Pr^{3+} ratio, measurements show that the Pr^{3+} concentration in the subsurface region is higher on electrodes decorated with SnO_2 than on electrodes decorated with SrO. The changes of the Pr polaron area upon cathodic bias polarization are in line with expectations as bias led to an increase of the polaron area and anodic bias leds to a decrease of the Pr^{3+} concentration compared to OCV conditions.

Thirdly, the surface potential was investigated on pure and decorated PCO10 electrodes. For this purpose, the position of the oxygen gas phase peak with regard to the bulk O 1s binding energy was compared for pristine and decorated thin films, as this difference is a measure for the potential step at the electrode surfaceAs can be seen in Figure 6.5 C) the value of the surface potential strongly varies with the decoration. On pure PCO10 electrodes at 550 °C and 1 mbar pO_2 a difference between oxygen gas phase and bulk O 1s binding energy of 9.45 eV was found, while on a PCO10 electrode decorated with 2 ML of SnO_2 (acidic decoration) a much lower value of 9.11 eV was measured. Interestingly, on PCO10 decorated with 2 ML of SrO (basic decoration) an increase to 10,14 eV was found. In addition, sample contamination with SO_2 (a strongly acidic oxide) lowered the value to 8.91 eV. In conclusion, surface decorations were found to alter the surface potential of PCO10 electrodes according to their relativ acidity, however, a corresponding change of the Pr^{3+} concentration was not observed. In Figure 6.5 D) also the surface potential found on the pure and decorated PCO10 electrodes is correlated with the Smidth acidity. As can be seen in the Figure, an almost linear dependence is found.

Die approbierte gedruckte Originalversion dieser Dissertation ist an der TU Wien Bibliothek verfügbar.
The approved original version of this doctoral thesis is available in print at TU Wien Bibliothek.
TU WIEN Bibliothek Your knowledge hub

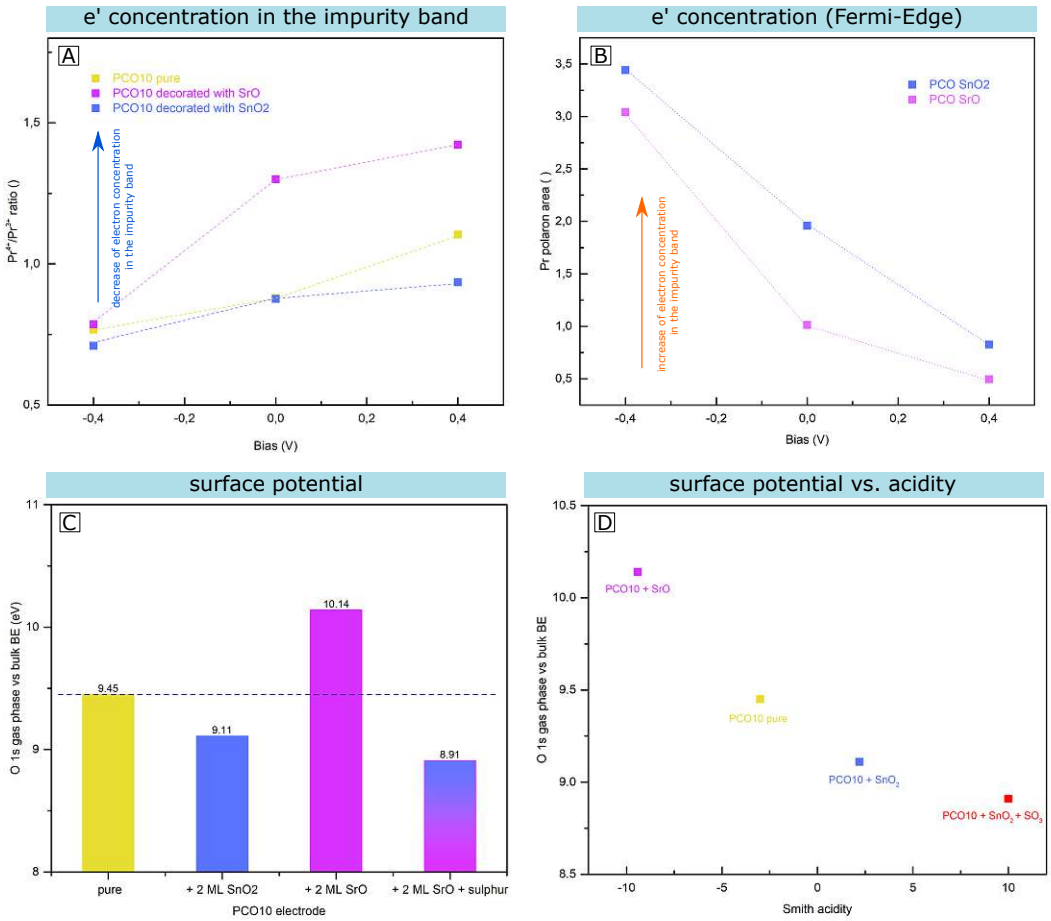

Figure 6.5: A) Pr^{4+}/Pr^{3+} ratio on PCO10 pure, PCO10 decorated with 2 ML SrO, PCO10 decorated wit 2 ML SnO_2 at OCV, under cathodic bias (-0.4 V) and under anodic bias (0.4 V) B) Polaron area on PCO10 decorated with 2 ML SnO2 or 2 ML SrO under OCV and cathodic (-0.4 V) and anodic polarisation (0.4 V) C) Difference between oxygen gas phase and O 1s bulk binding energy of pure PCO10, PCO10 decorated with 2 ML SnO_2, PCO10 decorated with 2 ML SrO and PCO10 decorated with 2 ML SrO and contaminated with sulphur D) Surface potential measured correlated with the Smith acidity.

Die approbierte gedruckte Originalversion dieser Dissertation ist an der TU Wien Bibliothek verfügbar.
The approved original version of this doctoral thesis is available in print at TU Wien Bibliothek.
TU WIEN Bibliothek Your knowledge hub

6.4 Mechanistic discussion

In the following, we discuss in more detail how surface decorations influence the oxygen exchange kinetics of PCO10 electrodes. Overall, the following experimental facts have to be considered by a mechanistic explanation:

- *i*-PLD measurements revealed that already sub-monolayer amounts of binary oxides show strong impacts on the area specific resistance of PCO10. While basic oxides (SrO, CaO) accelerate the oxygen exchange kinetics (a decrease partly down to 25 % of the initial resistance), acidic oxides (SnO_2, TiO_2) lead to a strong increase of the electrode polarization resistance (up to 600 % of the inital resistance).
- Although a significant change of the electrode impedance was observed after surface decoration, the same oxygen exchange mechanism is most probably active on both pure and decorated PCO10 electrodes, as the same activation energy and pO_2 dependence of the polarization resistance was measured.
- AP-XPS revealed a change of the surface potential after decoration with binary oxides. While a higher surface potential was observed on electrodes decorated with SnO_2, decoration with SrO led to a lower surface potential.
- Unexpectedly, XPS measurements did not detect corresponding changes of the electron concentration (Pr^{3+}) in the impurity band of PCO10 after decoration with binary oxides.

First of all, we can confidently confirm the results of Nicollet et al. [45] that the Smith acidity [104] can be used as a sensitive descriptor to estimate changes of the oxygen exchange kinetics of PCO10 electrodes. Oxides, which are acidic relative to PCO10, like TiO_2 and SnO_2, decrease the oxygen exchange activity, while binary oxides, which are basic relative to PCO10, accelerate the oxygen exchange kinetics. For a more detailed discussion, it is essential to consider various different effects that can alter the oxygen exchange kinetics without changing the oxygen exchange mechanism itself. In literature [25, 59, 241], the following equation was suggested to describe contributions influencing the kinetics of the OER reaction.

$$r = r_0 * p(O_2)^{v_p} * \prod_i [i]^{v_i} * e^{\frac{\beta e \chi_0}{kT}} * e^{\frac{\beta e \Delta\chi}{kT}} \tag{6.1}$$

This equation includes the concentrations [i] of the reacting species i (i.e. for oxygen reduction: $V_O^{\bullet\bullet}$ and Pr'_{Ce}), the oxygen partial pressure (pO_2), mechanism dependent reaction orders v_i and v_p the effect of any surface potential χ_0 or its change upon voltage $\Delta\chi$ (which can become relevant if charge is transferred across the surface) and a prefactor r_0, which includes kinetic contributions (chemical activation barriers) but also thermodynamic contribu-

Die approbierte gedruckte Originalversion dieser Dissertation ist an der TU Wien Bibliothek verfügbar.
The approved original version of this doctoral thesis is available in print at TU Wien Bibliothek.
TU WIEN Bibliothek Your knowledge hub

tions due to mass action equilibria before the rate limiting step, k and T denote Boltzmann's constant and temperature. The factor β depends on the specific mechanism, without any charged surface species it may even be zero. The reaction order ν_p refers to the effects of pO_2 on adsorbates only, since defects are separately considered. From our conducted AP-XPS measurements we have concluded that decoration with binary oxides significantly modifies the surface potential. In addition, we should consider that changes in the surface potential will most probably also lead to changes of the defect chemistry at the surface of the electrode, as we will discuss below. As the oxygen partial pressure was kept constant and no bias polarization was applied during *i*-PLD measurements, we do not further consider the ${pO_2}^{\nu_p}$ and the $\Delta\chi$ term in equation (6.1). Thus the equation can be simplified to:

$$r \sim r_0 \prod_i [i]^{v_i} * e^{\frac{\beta e \chi_0}{kT}} \tag{6.2}$$

In the following, we would like to discuss how surface decoration can tune the OER kinetics of PCO10 electrodes. Nicollet et al. suggested changing electron concentrations [45] as well as altered adsorption kinetics as reasons for the observed effects on the oxygen exchange kinetics. However, based on our results we suspect that the fundamental cause is an interplay of several different effects, which are strongly correlated with each other. Moreover, the situation is further complicated by the fact that already sub-monolayers of decorations are active and then unavoidably two different kinds of surfaces are present, the decorated surface and the free surface, see sketch in Figure 6.6. In principle, oxygen can now be incorporated across the decoration or still at the free surface. The latter seems more probable since we do not have indications of a severe mechanism change due to small amounts of decorations. In accordance with equation (6.2), (at least) three possibilities can be identified of how surface decoration with binary oxides may affect the oxygen exchange kinetics without changing the reaction mechanism. As can be seen in Figure 6.6, a surface decoration i) may change the surface potential on the PCO electrode surface and thus modifies the OER kinetics, ii) can lead to a change of the defect concentration in the electrode subsurface due to the imposed surface potential change and the modified standard chemical potentials of ions and electrons ($\mu^o_{O^{2-}}$, $\mu^o_{e^-}$) in the PCO electrode, beneath the decoration, and the surface decoration iii) may affect the thermodynamics of reaction steps taking place before the rate limiting step, which leads to a change in the prefactor r_0, at least for the oxygen exchange across the decoration.

Regarding (i), several authors have so far discussed the role of a surface potential χ on the OER kinetics and remarked that the adsorption of charged oxygen species, such as $O^-_{2,ad}$, $O^{2-}_{2,ad}$ or O^-_{ad} leads to an electrostatic surface potential χ. [57, 246, 247] Moreover, model calculation were conducted, which revealed how the electronic repulsion of charged adsorbates influences the surface coverage. While the actual surface potential on pure PCO10 electrodes is unknown and hard to determine, we expect the free surface to be slightly negatively charged

Die approbierte gedruckte Originalversion dieser Dissertation ist an der TU Wien Bibliothek verfügbar.
The approved original version of this doctoral thesis is available in print at TU Wien Bibliothek.
TU WIEN Bibliothek Your knowledge hub

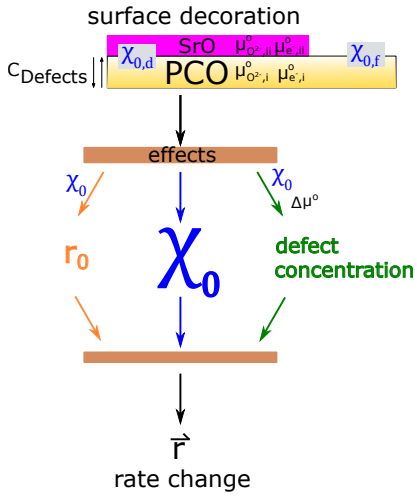

Figure 6.6: Sketch explaining the possible different effects of surface decoration on the PCO10 electrode. It affects directly the surface potential at the site of the decorations χ_0, d, but also slightly extends its effect electrostatically along the free surface χ_0, f.

due to the adsorption of negatively charged oxygen species. In this study, the deposition of binary oxides allowed us to tune the surface potential. For simplification, we assume that the deposited binary oxides form a dipole layer on top of the PCO10 electrode with the charge of the topmost decoration layer being positive for basic decorations and negative for acidic oxides, thus inducing an inversely charged space charge layer in the PCO10 surface and consequently altering the surface potential step (see Figure 7). This dipole also affects the surface potential of the free surface in close vicinity of the decoration. As the rate determining reaction step or a preceding step is often discussed to include a charge transfer, a change of the surface potential will most certainly influence the OER kinetics.

Moreover, based on our model, the changed surface potential and the difference of the oxygen chemical potential between the PCO electrode and surface decoration layer also trigger changes of the defect concentrations in the (sub)-surface of the PCO10 electrode (effect ii). These changes thus also influence the oxygen exchange kinetics. During our conducted measurements, so far only the Pr^{3+} concentration after decoration was monitored by AP-XPS measurements, however, also measurements/simulations of other defect concentrations are needed to fully understand the complete contribution to the reaction rate.

Regarding (iii), we suppose that the very similar pO_2 dependencies and activation energies indicate the same surface being active for oxygen exchange , i.e. the free surface. For oxygen exchange across the decorations we would expect more severe changes. Thus effect (iii) most probably plays a minor role.

Die approbierte gedruckte Originalversion dieser Dissertation ist an der TU Wien Bibliothek verfügbar.
The approved original version of this doctoral thesis is available in print at TU Wien Bibliothek.
TU WIEN Bibliothek Your knowledge hub

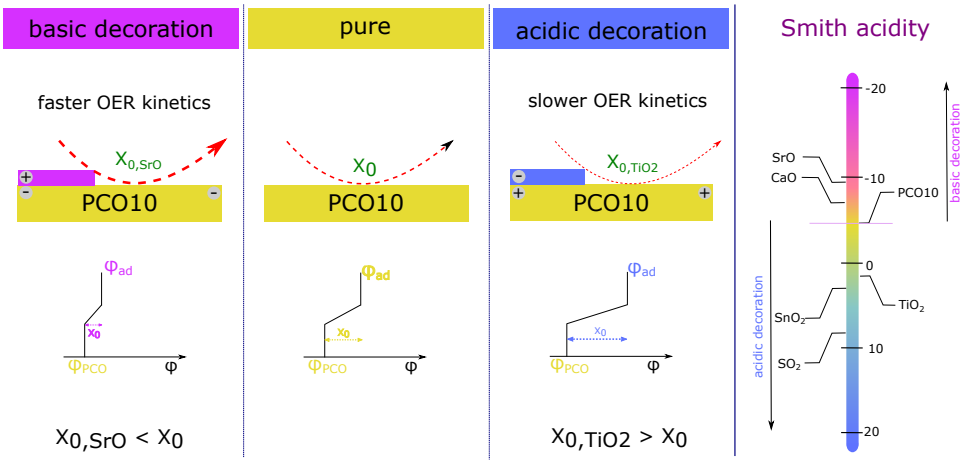

Figure 6.7: Sketch explaining the effect of surface decoration on the surface potential. Smith acidity of the binary oxides deposited compared to the PCO10 electrode. Data taken from [45].

We believe that a convolution of the described effects (i) and (ii) is responsible for the observed change of the OER kinetics on decorated PCO electrodes. Most probably they partly counterbalance each other, since only a change of χ_0 by 1 eV would cause very severe rate changes for β factors in the range of 0.5-1. However, at the current state of research it is not possible to disentangle the contribution of each effect. To gain conclusive insight into the defect chemistry of decorated surfaces, detailed computational studies of energetics and charge redistribution at decorated surfaces are necessary. Nevertheless, as has been shown in this study, surface decorations represent a promising possibility to enhance the catalytic activity of MIEC surfaces towards oxygen exchange and this study lays foundations for a more comprehensive investigation of the fundamental processes responsible for the effect of surface decorations on the oxygen exchange activity.

Die approbierte gedruckte Originalversion dieser Dissertation ist an der TU Wien Bibliothek verfügbar.
The approved original version of this doctoral thesis is available in print at TU Wien Bibliothek.
TU WIEN Bibliothek Your knowledge hub

6.5 Conclusion

PCO10 thin film electrodes were decorated with 0.3 to 2 (nominal) monolayers of binary oxides with different Smith acidity (SrO, CaO, TiO_2 and SnO_2 from basic to acidic). The effect of surface decorations on the OER resistance was tracked by *i*-PLD impedance spectroscopy which enabled very precise measurements of the OER activity. These experiments confirmed previous results that the Smith acidity of MIEC surfaces is a sensitive descriptor of the oxygen exchange activity, i.e. basic oxides increase the OER kinetics and acidic oxides have the opposite effect. Changes of the surface chemistry and the surface potential were investigated by AP-XPS and the measurements revealed that surface decorations substantially alter the surface potential according to their acidity (acidic decorations increase the surface potential step and vice versa). Defect concentration in the near surface region, however, are hardly affected. Despite substantial changes of the surface exchange resistance, the pO_2 and temperature dependence remained unaffected by the surface decoration. Based on these results, we propose a mechanistic model, which can explain the effects a surface decoration might have on a PCO electrode and its oxygen exchange kinetics.

Die approbierte gedruckte Originalversion dieser Dissertation ist an der TU Wien Bibliothek verfügbar.
The approved original version of this doctoral thesis is available in print at TU Wien Bibliothek.
TU WIEN Bibliothek Your knowledge hub

7 Conclusion

To conclude, in this work the interplay between oxygen exchange kinetics and the defect chemistry of different SOFC materials was investigated with several approaches. Among others, two *in-situ* techniques were employed for gaining novel insights. *In-situ* PLD impedance spectroscopy was used as a powerful tool for characterizing pristine electrodes without any contamination of the electrode surface directly after deposition. The innovative *i*-PLD technique allowed new insights into oxygen exchange kinetics, as most of the conducted measurements could not be conducted in standard *ex-situ* measurement setups. In addition, ambient pressure XPS in combination with simultaneous, i.e. *in-situ* impedance characterization was a valuable tool to improve the understanding of processes taking place on the electrode surface.

In the first study, the deposition of Pt nanoparticles (20 nm-40 nm) on the surface of $La_{0.6}Sr_{0.4}FeO_{3-\delta}$ (LSF) led to a strong drop of the electrode surface polarization resistance. Most interestingly, the effect was much more pronounced at lower pO_2 (0.25 mbar O_2), where a drop by a factor 100 was observed, while at higher pO_2 (synthetic air) only about a factor of 3 better polarization resistance was detected. Measurements of the pO_2 dependence of LSF electrodes decorated with platinum nanoparticles revealed a very uncommon pO_2 relationship, where less oxygen concentration leads to lower polarization resistance. We thus conclude that Pt nanoparticles accelerate the oxygen splitting on the electrode surface and the incorporation of (partially splitted) oxygen into a oxygen vacancy gets rate limiting.

The effect of platinum on the OER kinetics was further investigated by doping Pt ions into LSF electrodes (1-1.5 % of the total cation amount). AP-XPS measurements found platinum to be well incorporated into the perovskite structure of LSF as Pt^{4+}, Pt exsolutions were not observed under oxidizing conditions. An innovative *i*-PLD multilayer technique was applied to precisely compare the polarization resistance of differently composed LSF electrodes (pure, LSF with 2 different doping levels of Pt). This approach prevents almost any reason for sample scattering. While LSF doped with Pt lead to a decrease of the polarisation resistance by a factor of 3, still the same dependence of the polarization resistance on the pO_2 and the same activation energy of Pt doped LSF and LSF was measured. Thus, the same rate limiting step has to be active on both materials. The improved oxygen exchange kinetics on Pt doped LSF was explained by an increase of oxygen vacancies concentration at the surface of Pt doped

Die approbierte gedruckte Originalversion dieser Dissertation ist an der TU Wien Bibliothek verfügbar.
The approved original version of this doctoral thesis is available in print at TU Wien Bibliothek.
TU WIEN Bibliothek Your knowledge hub

LSF, as the incorporation of Pt leads to a slightly larger unit cell, which reduces the vacancy formation enthalpy (ΔH_{ox}). It should be emphasized that decoration with Pt nanoparticles and Pt doping into the LSF electrodes had very different effects on the oxygen exchange reaction, especially from a mechanistic point of view.

In the third study, it is shown that surfaces with very fast oxygen exchange kinetics in *i*-PLD measurements exhibit a strong performance loss after transferring them from the *i*-PLD setup to a conventional *ex-situ* measurement setup. This performance loss of about one or even two orders of magnitude was omnipresent on all investigated SOFC electrode materials. Here, the combination of AP-XPS surface characterization together with simultaneous impedance measurements allowed us to reveal minor amounts of sulfur contamination in the range of ppb to be responsible for a major performance loss of the electrodes. In addition, a gas purification setup was developed, which allowed to remove these sulfur contamination from the measurement feed gas and to measure very low polarization resistances also in standard *ex-situ* measurement setups. Accordingly, we suppose that sulfur contaminations are unperceived present on most MIEC electrodes investigated in literature.

In the fourth study, the effect of lattice strain on the LSF oxygen exchange kinetics was investigated. While during the growth of epitaxial LSF electrodes on LSGM a continuous increase of the polarisation resistance was observed until a film thickness of 50 nm was reached, polycrystalline LSF grown on YSZ showed a constant value for a broad thickness range. After reaching a film thickness of 50 nm the polarisation resistance of epitaxial LSF was a factor of 3-6 times higher than for polycrystalline LSF. In addition, also an increase of the activation energy on epitaxially grown LSF was observed. HR-TEM measurements revealed a contraction of the *out-of-plane* lattice parameter of LSF, which led to a decrease of the LSF unit cell volume over film thickness. This suggests an increase of ΔH_{ox} triggered by the volume contraction. Defect thermodynamic calculations revealed that the corresponding decrease of the oxygen vacancy concentration explains our observed decreased oxygen exchange activity and increase of activation energy.

In the last study, the surface of $Pr_{0.1}Ce_{0.9}O_{2-\delta}$ (PCO10) electrodes was modified with submonolayer amounts of binary oxides (SrO, CaO, TiO_2, SnO_2) and the change of the electrode performance was directly tracked by *i*-PLD measurements. While basic oxides (SrO, CaO) were found to accelerate the oxygen exchange kinetics, acidic oxides (TiO_2, SnO_2) drastically increased the polarization resistance. A change of the pO_2 dependence of the polarization resistance or activation energy was not observed. Additional AP-XPS measurements revealed a change of the surface potential on the electrode which can be correlated with changed oxygen exchange kinetics. Pr^{3+} concentrations, on the other hand, did not exhibit a simple

Die approbierte gedruckte Originalversion dieser Dissertation ist an der TU Wien Bibliothek verfügbar.
The approved original version of this doctoral thesis is available in print at TU Wien Bibliothek.
TU Bibliothek Your knowledge hub WIEN

correlation with the electrochemical performance. This indicates that additional ab-initio calculations are highly desirable to further clarify mechanistic details of the decoration effects.

Die approbierte gedruckte Originalversion dieser Dissertation ist an der TU Wien Bibliothek verfügbar.
The approved original version of this doctoral thesis is available in print at TU Wien Bibliothek.
TU WIEN Bibliothek Your knowledge hub

List of publications

1. Riedl, C.; Schmid, A.; Nenning, A.; Summerer, H.; Smetaczek, S.; Schwarz, S.; Bernardi, J.; Optiz, A.; Limbeck, A. and Fleig, J.; Outstanding Oxygen Reduction Kinetics of $La_{0.6}Sr_{0.4}FeO_{3-\delta}$ Surfaces Decorated with Platinum Nanoparticles, Journal of The Electrochemical Society, 2020, 167, 104514. [112]

2. Weiss, M.; Riedl, C.; Frank, J.; Fleig, J. and Limbeck, A.; Quantitative analysis of the platinum surface decoration on lanthanum strontium iron oxide thin films via online-LASIL-ICP-MS; Microchemical Journal, Elsevier BV, 2021, 166, 106236. [178]

3. Siebenhofer, M.*; Riedl, C.*; Schmid, A.; Limbeck, A.; Opitz, A. K.; Fleig, J. and Kubicek, M.; Investigating oxygen reduction pathways on pristine SOFC cathode surfaces by in situ PLD impedance spectroscopy, Journal of Materials Chemistry A, Royal Society of Chemistry (RSC), 2022, 10, 2305-2319. [52]

4. Riedl, C.*; Siebenhofer, M.*; Nenning, A.; Friedbacher, G.; Weiss, M.; Rameshan, C.; Bernardi, J.; Limbeck, A.; Kubicek, M.; Opitz, A. K. and Fleig, J.; Performance modulation through selective, homogenous surface doping of lanthanum strontium ferrite electrodes revealed by in situ PLD impedance measurements Journal of Materials Chemistry A, Royal Society of Chemistry (RSC), 2022, 10, 2973-2986. [154]

5. Riedl, C.*; Siebenhofer, M.*; Nenning, A.; Schmid, A.; Weiss, M.; Rameshan, C.; Limbeck, A.; Kubicek, M.; Opitz, A. K. and Fleig, J.; Insitu techniques reveal the true capabilities of SOFC cathode materials and their sudden degradation due to omnipresent sulfur trace impurities, Journal of Materials Chemistry A, Royal Society of Chemistry (RSC), 2022, 10, 14838-14848. [192]

6. Riedl, C.*; Siebenhofer, M.*; Ražnjević, S.; Bumberger, A.; Friedbacher, G.; Z. Zhang,; Limbeck, A.; Opitz, A.K.; Fleig, J.; Kubicek, M.; In-situ electrochemical observation of anisotropic lattice contraction of LSF electrodes during pulsed laser deposition, *submitted*

7. Riedl, C.*; Siebenhofer, M.*; Nenning, A.; Rameshan, C.; Limbeck, A.; Opitz, A.K.; Kubicek, M.; Fleig, J.; Modifying the surface potential on praseodymium doped ceria electrodes: An *in-situ* PLD and ambient pressure XPS study, *in preperation*

Die approbierte gedruckte Originalversion dieser Dissertation ist an der TU Wien Bibliothek verfügbar.
The approved original version of this doctoral thesis is available in print at TU Wien Bibliothek.
TU WIEN Bibliothek Your knowledge hub

8. Siebenhofer, M.*; Riedl, C.*, Nenning, A.; Limbeck, A.; Opitz, A.K.; Fleig, J.; Kubicek, M.; Improving and degrading the oxygen exchange kinetics of LSC by in-situ Sr decoration, *in preperation*

Die approbierte gedruckte Originalversion dieser Dissertation ist an der TU Wien Bibliothek verfügbar.
The approved original version of this doctoral thesis is available in print at TU Wien Bibliothek.
TU WIEN Bibliothek Your knowledge hub

List of conference contributions

1. C. Riedl, A. Schmid, A.K. Opitz, J. Fleig; Studying the Effects of Surface Modification on the Oxygen Reduction Kinetics of Mixed Conducting Oxide Surfaces by In-Situ Impedance Spectroscopy (Poster presentation); Current Trends in SOFC Research, Vienna; 11.02.2019 - 12.02.2019.

2. C. Riedl, A. Schmid, H. Summerer, A. Limbeck, J. Fleig; Electrochemical properties of platinum nanoparticle decorated MIEC electrodes (Poster presentation), 18. Österreichische Chemietage, Linz; 24.09.2019 - 27.09.2019.

3. C. Riedl, A. Schmid, A. Nenning, A. Limbeck, A.K. Opitz, J. Fleig; Outstanding Oxygen Reduction Kinetics of $La_{0.6}Sr_{0.4}FeO_{3-\delta}$ Surfaces Decorated with Platinum Nanoparticles (Oral presentation); Electronic Materials and Applications 2021, Orlando (*online*); 19.01.2021 - 21.01.2021.

4. C. Riedl, M. Siebenhofer, A. Nenning, A. Limbeck, C. Rameshan, M. Kubicek, A.K. Opitz, J. Fleig; In-situ PLD studies on pristine lanthanum based pervoskite electrodes (Poster presentation); EMRS Spring Meeting 2021, (*online*); 31.05.2021 - 03.06.2021.

5. C. Riedl, M. Siebenhofer, A. Nenning, A. Limbeck, C. Rameshan, M. Kubicek, A.K. Opitz, J. Fleig; Performance boost of LSF electrodes by platinum doping revealed by super sensitive in-situ PLD impedance measurements (Oral presentation); EMRS Spring Meeting 2021, (*online*); 31.05.2021 - 03.06.2021.

6. C. Riedl, M. Siebenhofer; A. Limbeck; A. K. Opitz; M. Kubicek; J. Fleig; Surface decoration of PCOx electrodes with binary oxides measured by in-situ PLD technique (Poster presentation); Electronic Materials and Applications 2022, Orlando (*online*); 19.01.2022 - 21.01.2022.

7. C. Riedl, M. Siebenhofer, A. Nenning, M. Kubicek, C. Rameshan, A. Limbeck, A. K. Opitz, J. Fleig; Performance loss of promising SOFC cathode materials by sub-ppm sulfur poisoning revealed by in-situ PLD and AP-XPS studies (Oral presentation); Electronic Materials and Applications 2022, Orlando (*online*); 19.01.2022 - 21.01.2022.

Die approbierte gedruckte Originalversion dieser Dissertation ist an der TU Wien Bibliothek verfügbar.
The approved original version of this doctoral thesis is available in print at TU Wien Bibliothek.
TU WIEN Bibliothek Your knowledge hub

8. C. Riedl, M. Siebenhofer, A. Schmid, A. Limbeck, A.K. Opitz, J. Fleig, M. Kubicek; Investigating oxygen reduction pathways on pristine SOFC cathode surfaces by in situ PLD impedance spectroscopy (Oral presentation); 23rd International Conference on Solid State Ionics (SSI-23); 17.07.2022 - 22.07.2022, Boston, MA.

9. C. Riedl, M. Siebenhofer, S. Raznjevic, Z. Zhang, M. Kubicek, A.K. Opitz, J. Fleig; Electrochemical Observation of Compressive Strain Built-Up During Pulsed Laser Deposition (Poster presentation); 23rd International Conference on Solid State Ionics (SSI-23); 17.07.2022 - 22.07.2022, Boston, MA.

Die approbierte gedruckte Originalversion dieser Dissertation ist an der TU Wien Bibliothek verfügbar.
The approved original version of this doctoral thesis is available in print at TU Wien Bibliothek.
TU WIEN Bibliothek Your knowledge hub

List of abbreviation

AFM: atomic force microscopy
ASR: area specific resistance
AP: ambient pressure
CE: counter electrode
CPE: constant phase element
EDX: energy dispersive X-ray spectroscopy
EIS: electrochemical impedance spectroscopy
GID: grazing incidence diffraction
ICP-MS: inductively coupled plasma - mass spectrometry
ICP-OES: inductively coupled plasma- optical emission spectrometry
LSF: lanthanum strontium iron oxide
LSC: lanthanum cobalt iron oxide
SEM: scanning electron microscopy
STEM: scanning transmission electron microscopy
SOFC: solid oxide fuel cell
SOEC: solid oxide electrolyzer cell
TEM: transmission electron microscopy
MIEC: mixed ionic electronic conducting
OER: oxygen exchange kinetics
PCO: praseodymium doped ceria
PLD: pulsed laser deposition
RDS: rate determining step
RMS: root mean square
RSM: reciprocal space mapping
WE: working electrode
XPS: X-ray spectroscopy
XRD: X-ray diffraction
YSZ: yttria-stabilized zirconia

Die approbierte gedruckte Originalversion dieser Dissertation ist an der TU Wien Bibliothek verfügbar.
The approved original version of this doctoral thesis is available in print at TU Wien Bibliothek.
TU WIEN Bibliothek Your knowledge hub

Bibliography

[1] M. M. Thackeray, C. Wolverton, and E. D. Isaacs. "Electrical energy storage for transportation approaching the limits of, and going beyond, lithium-ion batteries". In: *Energy Environmental Science* 5.7 (2012), p. 7854.

[2] A. Nechache and S. Hody. "Alternative and innovative solid oxide electrolysis cell materials: A short review". In: *Renewable and Sustainable Energy Reviews* 149 (Oct. 2021), p. 111322.

[3] S. Mekhilef, R. Saidur, and A. Safari. "Comparative study of different fuel cell technologies". In: *Renewable and Sustainable Energy Reviews* 16.1 (2012), pp. 981–989.

[4] J. A. Kilner and M. Burriel. "Materials for Intermediate Temperature Solid Oxide Fuel Cells". In: *Annual Review of Materials Research* 44.1 (2014), pp. 365–393.

[5] D. J. L. Brett, A. Atkinson, N. P. Brandon, and S. J. Skinner. "Intermediate temperature solid oxide fuel cells". In: *Chemical Society Reviews* 37.8 (2008), p. 1568.

[6] A. Tarancon, S. J. Skinner, R. J. Chater, F. Hernandez-Ramirez, and J. A. Kilner. "Layered perovskites as promising cathodes for intermediate temperature solid oxide fuel cells". In: *Journal of Materials Chemistry* 17.30 (2007), p. 3175.

[7] Z. Gao, L. V. Mogni, E. C. Miller, J. G. Railsback, and S. A. Barnett. "A perspective on low temperature solid oxide fuel cells". In: *Energy Environmental Science* 9.5 (2016), pp. 1602–1644.

[8] R. M. Ormerod. "Solid oxide fuel cells". In: *Chemical Society Reviews* 32.1 (2002), pp. 17–28.

[9] E. Ivers-Tiffee, A. Weber, and D. Herbstritt. "Materials and technologies for SOFC components". In: *Journal of the European Ceramic Society* 21.10-11 (2001), pp. 1805–1811.

[10] A. Stambouli and E. Traversa. "Solid oxide fuel cells SOFCs: a review of an environmentally clean and efficient source of energy". In: *Renewable and Sustainable Energy Reviews* 6.5 (2002), pp. 433–455.

[11] M. Liu, M. E. Lynch, K. Blinn, F. M. Alamgir, and Y. Choi. "Rational SOFC material design: new advances and tools". In: 14.11 (2011), pp. 534–546.

Die approbierte gedruckte Originalversion dieser Dissertation ist an der TU Wien Bibliothek verfügbar.
The approved original version of this doctoral thesis is available in print at TU Wien Bibliothek.
TU Bibliothek Your knowledge hub WIEN

[12] D. Udomsilp, J. Rechberger, R. Neubauer, C. Bischof, F. Thaler, W. Schafbauer, N. H. Menzler, L. G. de Haart, A. Nenning, A. K. Opitz, O. Guillon, and M. Bram. "Metal Supported Solid Oxide Fuel Cells with Exceptionally High Power Density for Range Extender Systems". In: 1.6 (2020), p. 100072.

[13] E. Bucher, W. Sitte, F. Klauser, and E. Bertel. "Impact of humid atmospheres on oxygen exchange properties, surface near elemental composition, and surface morphology of $La_{0.6}Sr_{0.4}CoO_{3-\delta}$". In: *Solid State Ionics* 208 (2012), pp. 43–51.

[14] N. I. Karageorgakis, A. Heel, A. Bieberle-Hütter, J. L. Rupp, T. Graule, and L. J. Gauckler. "Flame spray deposition of $La_{0.6}Sr_{0.4}CoO_{3-\delta}$ thin films: Microstructural characterization, electrochemical performance and degradation". In: *Journal of Power Sources* 195.24 (2010), pp. 8152–8161.

[15] I. Garbayo, V. Esposito, S. Sanna, A. Morata, D. Pla, L. Fonseca, N. Sabate, and A. Tarancon. "Porous $La_{0.6}Sr_{0.4}CoO_{3-\delta}$ thin film cathodes for large area micro solid oxide fuel cell power generators". In: *Journal of Power Sources* 248 (2014), pp. 1042–1049.

[16] C. Benel, A. J. Darbandi, R. Djenadic, A. Evans, R. Tolke, M. Prestat, and H. Hahn. "Synthesis and characterization of nanoparticulate $La_{0.6}Sr_{0.4}CoO_{3-\delta}$ cathodes for thin-film solid oxide fuel cells". In: *Journal of Power Sources* 229 (2013), pp. 258–264.

[17] A. Evans, S. Karalic, J. Martynczuk, M. Prestat, R. Tolke, Z. Yang, and L. J. Gauckler. "$La_{0.6}Sr_{0.4}CoO_{3-\delta}$ Thin Films Prepared by Pulsed Laser Deposition as Cathodes for Micro-Solid Oxide Fuel Cells". In: *ECS Transactions* 45.1 (2012), pp. 333–336.

[18] T. Horita, K. Yamaji, N. Sakai, H. Yokokawa, A. Weber, and E. Ivers-Tiffe. "Oxygen reduction mechanism at porous $La_{1-x}Sr_xCoO_{3-\delta}$ cathodes/$La_{0.8}Sr_{0.2}Ga_{0.8}Mg_{0.2}O_{2.8}$ electrolyte interface for solid oxide fuel cells". In: *Electrochimica Acta* 46.12 (2001), pp. 1837–1845.

[19] M. Shiono, K. Kobayashi, T. Lannguyen, K. Hosoda, T. Kato, K. Ota, and M. Dokiya. "Effect of CeO_2 interlayer on ZrO_2 electrolyte/La(Sr)CoO_3 cathode for low-temperature SOFCs". In: *Solid State Ionics* 170.1-2 (2004), pp. 1–7.

[20] V. V. Srdic, R. P. Omorjan, and J. Seydel. "Electrochemical performances of (La,Sr)CoO_3 cathode for zirconia-based solid oxide fuel cells". In: *Materials Science and Engineering: B* 116.2 (2005), pp. 119–124.

[21] S. Kogler, A. Nenning, G. M. Rupp, A. K. Opitz, and J. Fleig. "Comparison of Electrochemical Properties of $La_{0.6}Sr_{0.4}FeO_{3-\delta}$ Thin Film Electrodes: Oxidizing vs. Reducing Conditions". In: *Journal of The Electrochemical Society* 162.3 (2015), F317–F326.

[22] Y. Huang, J. M. Vohs, and R. J. Gorte. "Fabrication of Sr-Doped LaFeO YSZ Composite Cathodes". In: *Journal of The Electrochemical Society* 151.4 (2004), A646.

Die approbierte gedruckte Originalversion dieser Dissertation ist an der TU Wien Bibliothek verfügbar.
The approved original version of this doctoral thesis is available in print at TU Wien Bibliothek.
TU WIEN Bibliothek Your knowledge hub

[23] F. Bidrawn, S. Lee, J. M. Vohs, and R. J. Gorte. "The Effect of Ca, Sr, and Ba Doping on the Ionic Conductivity and Cathode Performance of $LaFeO_3$". In: *Journal of The Electrochemical Society* 155.7 (2008), B660.

[24] W. Preis. "Oxygen exchange kinetics of $La_{0.4}Sr_{0.6}FeO_3$ by simultaneous application of conductivity relaxation and carrier gas coulometry". In: *Solid State Ionics* 175.1-4 (2004), pp. 393–397.

[25] A. Schmid, G. M. Rupp, and J. Fleig. "Voltage and partial pressure dependent defect chemistry in (La,Sr)$FeO_{3-\delta}$ thin films investigated by chemical capacitance measurements". In: *Physical Chemistry Chemical Physics* 20.17 (2018), pp. 12016–12026.

[26] G. M. Rupp, A. Schmid, A. Nenning, and J. Fleig. "The Superior Properties of $La_{0.6}Ba_{0.4}CoO_{3-\delta}$ Thin Film Electrodes for Oxygen Exchange in Comparison to $La_{0.6}Sr_{0.4}CoO_{3-\delta}$". In: *Journal of The Electrochemical Society* 163.6 (2016), F564–F573.

[27] R. Amin and K. Karan. "Characterization of $La_{0.5}Ba_{0.5}CoO_{3-\delta}$ as a SOFC Cathode Material". In: *Journal of The Electrochemical Society* 157.2 (2010), B285.

[28] F. Baumann, J. Maier, and J. Fleig. "The polarization resistance of mixed conducting SOFC cathodes: A comparative study using thin film model electrodes". In: *Solid State Ionics* 179.21-26 (2008), pp. 1198–1204.

[29] H. Fukunaga. "Reaction model of dense $Sm_{0.5}Sr_{0.5}CoO_{3-\delta}$ as SOFC cathode". In: *Solid State Ionics* 132.3-4 (2000), pp. 279–285.

[30] J.-C. Chang, M.-C. Lee, R.-J. Yang, Y.-C. Chang, T.-N. Lin, C.-H. Wang, W.-X. Kao, and L.-S. Lee. "Fabrication and characterization of $Sm_{0.2}Ce_{0.8}O_{2-\delta}$ $Sm_{0.5}Sr_{0.5}CoO_{3-\delta}$ composite cathode for anode supported solid oxide fuel cell". In: *Journal of Power Sources* 196.6 (2011), pp. 3129–3133. ISSN: 0378-7753.

[31] H. Wang, K. J. Yakal-Kremski, T. Yeh, G. M. Rupp, A. Limbeck, J. Fleig, and S. A. Barnett. "Mechanisms of Performance Degradation of (La,Sr)(Co,Fe)$O_{3-\delta}$ Solid Oxide Fuel Cell Cathodes". In: *Journal of The Electrochemical Society* 163.6 (2016), F581–F585.

[32] E. Bucher and W. Sitte. "Long-term stability of the oxygen exchange properties of $(La,Sr)_{1-z}(Co,Fe)O_3$ in dry and wet atmospheres". In: *Solid State Ionics* 192.1 (2011), pp. 480–482.

[33] W. Wang and M. Mogensen. "High-performance lanthanum-ferrite-based cathode for SOFC". In: *Solid State Ionics* 176.5-6 (2005), pp. 457–462.

[34] E. N. Armstrong, K. L. Duncan, D. J. Oh, J. F. Weaver, and E. D. Wachsman. "Determination of Surface Exchange Coefficients of LSM, LSCF, YSZ, GDC Constituent Materials in Composite SOFC Cathodes". In: *Journal of The Electrochemical Society* 158.5 (2011), B492.

Die approbierte gedruckte Originalversion dieser Dissertation ist an der TU Wien Bibliothek verfügbar.
The approved original version of this doctoral thesis is available in print at TU Wien Bibliothek.
TU Bibliothek Your knowledge hub WIEN

[35] H. J. Hwang, J.-W. Moon, S. Lee, and E. A. Lee. "Electrochemical performance of LSCF-based composite cathodes for intermediate temperature SOFCs". In: *Journal of Power Sources* 145.2 (2005), pp. 243–248.

[36] D. Beckel, U. Muecke, T. Gyger, G. Florey, A. Infortuna, and L. Gauckler. "Electrochemical performance of LSCF based thin film cathodes prepared by spray pyrolysis". In: *Solid State Ionics* 178.5-6 (2007), pp. 407–415.

[37] W. Jung and H. L. Tuller. "A New Model Describing Solid Oxide Fuel Cell Cathode Kinetics: Model Thin Film $SrTi_{1-x}Fe_xO_{3-d}$ Mixed Conducting Oxides-a Case Study". In: *Advanced Energy Materials* 1.6 (2011), pp. 1184–1191.

[38] S. Molin, W. Lewandowska-Iwaniak, B. Kusz, M. Gazda, and P. Jasinski. "Structural and electrical properties of $Sr(Ti,Fe)O_{3-\delta}$ materials for SOFC cathodes". In: *Journal of Electroceramics* 28.1 (2012), pp. 80–87.

[39] S.-L. Zhang, H. Wang, M. Y. Lu, C.-X. Li, C.-J. Li, and S. A. Barnett. "Electrochemical performance and stability of $SrTi_{0.3}Fe_{0.6}Co_{0.1}O_3$ infiltrated $La_{0.8}Sr_{0.2}MnO_3Zr_{0.92}Y_{0.16}O_2$ oxygen electrodes for intermediate-temperature solid oxide electrochemical cells". In: *Journal of Power Sources* 426 (2019), pp. 233–241.

[40] W. Jung and H. L. Tuller. "Investigation of Cathode Behavior of Model Thin-Film $SrTi_{1-x}Fe_xO_{3-\delta}$ (x=0.35 and 0.5) Mixed Ionic-Electronic Conducting Electrodes". In: *Journal of The Electrochemical Society* 155.11 (2008), B1194.

[41] Y. Li, L. M. Wong, C.-C. Yu, S. Wang, and P.-C. Su. "Pulsed laser deposition of $Ba_{0.5}Sr_{0.5}Co_{0.8}Fe_{0.2}O_{3-\delta}$ thin film cathodes for low temperature solid oxide fuel cells". In: *Surface and Coatings Technology* 320 (2017), pp. 344–348.

[42] L. Wang, R. Merkle, G. Cristiani, B. Stuhlhofer, H.-U. Habermeier, and J. Maier. "PLD-deposited $Ba_xSr_{1-x}(CoyFe_{1-y})O_{3-\delta}$ Thin-Film Microelectrodes: Structure Aspects and Oxygen Incorporation Kinetics". In: *ECS Transactions* 13.26 (2019), pp. 85–95.

[43] Q. Liu, K. Khor, and S. Chan. "High-performance low-temperature solid oxide fuel cell with novel BSCF cathode". In: *Journal of Power Sources* 161.1 (2006), pp. 123–128.

[44] D. Chen, Z. Guan, D. Zhang, L. Trotochaud, E. Crumlin, S. Nemsak, H. Bluhm, H. L. Tuller, and W. C. Chueh. "Constructing a pathway for mixed ion and electron transfer reactions for O_2 incorporation in $Pr_{0.1}Ce_{0.9}O_{2-\delta}$". In: *Nature Catalysis* 3.2 (2020), pp. 116–124.

[45] C. Nicollet, C. Toparli, G. F. Harrington, T. Defferriere, B. Yildiz, and H. L. Tuller. "Acidity of surface-infiltrated binary oxides as a sensitive descriptor of oxygen exchange kinetics in mixed conducting oxides". In: *Nature Catalysis* 3.11 (2020), pp. 913–920.

Die approbierte gedruckte Originalversion dieser Dissertation ist an der TU Wien Bibliothek verfügbar.
The approved original version of this doctoral thesis is available in print at TU Wien Bibliothek.
TU Bibliothek Your knowledge hub WIEN

[46] N. Tsvetkov, Q. Lu, Y. Chen, and B. Yildiz. "Accelerated Oxygen Exchange Kinetics on $Nd_2NiO_{4+\delta}$ Thin Films with Tensile Strain along c Axis". In: *ACS Nano* 9.2 (2015), pp. 1613–1621.

[47] K. J. Lee, J. H. Chung, M. J. Lee, and H. J. Hwang. "Chromium Poisoning of Neodymium Nickelate $Nd_2NiO_{4+\delta}$ Cathodes for Solid Oxide Fuel Cells". In: *Journal of the Korean Ceramic Society* 56.2 (2019), pp. 160–166.

[48] Y. Shen, H. Zhao, X. Liu, and N. Xu. "Preparation and electrical properties of Ca-doped $La_2NiO_{4+\delta}$ cathode materials for IT-SOFC". In: *Physical Chemistry Chemical Physics* 12.45 (2010), p. 15124.

[49] G. T. Kim, S. Wang, A. J. Jacobson, Z. Yuan, and C. Chen. "Impedance studies of dense polycrystalline thin films of $La_2NiO_{4+\delta}$". In: *Journal of Materials Chemistry* 17.13 (2007), p. 1316.

[50] J. Fleig. "Solid Oxide Fuel Cell Cathodes: Polarization Mechanisms and Modeling of the Electrochemical Performance". In: *Annu. Rev. Mater. Res.* 33.1 (2003), pp. 361–382.

[51] J. Fleig, F. S. Baumann, V. Brichzin, H.-R. Kim, J. Jamnik, G. Cristiani, H.-U. Habermeier, and J. Maier. "Thin Film Microelectrodes in SOFC Electrode Research". In: *Fuel Cells* 6.3-4 (2006), pp. 284–292.

[52] M. Siebenhofer, C. Riedl, A. Schmid, A. Limbeck, A. K. Opitz, J. Fleig, and M. Kubicek. "Investigating oxygen reduction pathways on pristine SOFC cathode surfaces by in situ PLD impedance spectroscopy". In: *Journal of Materials Chemistry A* 10.5 (2022), pp. 2305–2319.

[53] S. B. Adler. "Factors Governing Oxygen Reduction in Solid Oxide Fuel Cell Cathodes". In: *Chemical Reviews* 104.10 (2004), pp. 4791–4844.

[54] S. Miyoshi, A. Takeshita, S. Okada, and S. Yamaguchi. "Rate-determining elementary step of oxygen reduction reaction at (La,Sr)CoO_3-based cathode surface". In: *Solid State Ionics* 285 (2016), pp. 202–208.

[55] M. Mosleh, M. Sogaard, and P. V. Hendriksen. "Kinetics and Mechanisms of Oxygen Surface Exchange on $La_{0.6}Sr_{0.4}FeO_{3-\delta}$ Thin Films". In: *Journal of The Electrochemical Society* 156.4 (2009), B441.

[56] M. Kunitski, N. Eicke, P. Huber, J. Köhler, S. Zeller, J. Voigtsberger, N. Schlott, K. Henrichs, H. Sann, F. Trinter, L. P. H. Schmidt, A. Kalinin, M. S. Schöffler, T. Jahnke, M. Lein, and R. Dörner. "Double-slit photoelectron interference in strong-field ionization of the neon dimer". In: *Nature Communications* 10.1 (2019).

[57] S. Adler, X. Chen, and J. Wilson. "Mechanisms and rate laws for oxygen exchange on mixed-conducting oxide surfaces". In: *Journal of Catalysis* 245.1 (2007), pp. 91–109.

Die approbierte gedruckte Originalversion dieser Dissertation ist an der TU Wien Bibliothek verfügbar.
The approved original version of this doctoral thesis is available in print at TU Wien Bibliothek.
TU WIEN Bibliothek Your knowledge hub

[58] F. S. Baumann, J. Fleig, H. U. Habermeier, and J. Maier. "Impedance spectroscopic study on well-defined (La,Sr)(Co,Fe)$O_{3-\delta}$ model electrodes". In: *Solid State Ionics* 177.11-12 (2006), pp. 1071–1081.

[59] A. Schmid and J. Fleig. "The Current-Voltage Characteristics and Partial Pressure Dependence of Defect Controlled Electrochemical Reactions on Mixed Conducting Oxides". In: *Journal of The Electrochemical Society* 166.12 (2019), F831–F846.

[60] M. Backhaus-Ricoult, K. Adib, T. St.Clair, B. Luerssen, L. Gregoratti, and A. Barinov. "In-situ study of operating SOFC LSM/YSZ cathodes under polarization by photoelectron microscopy". In: *Solid State Ionics* 179.21-26 (2008), pp. 891–895.

[61] A.-K. Huber, M. Falk, M. Rohnke, B. Luerssen, L. Gregoratti, M. Amati, and J. Janek. "In situ study of electrochemical activation and surface segregation of the SOFC electrode material". In: *Phys. Chem. Chem. Phys.* 14.2 (2012), pp. 751–758.

[62] I. Yasuda. "Oxygen tracer diffusion coefficient of La,$SrMnO_{3+\delta}$". In: *Solid State Ionics* 86-88 (1996), pp. 1197–1201.

[63] E. Navickas, Y. Chen, Q. Lu, W. Wallisch, T. M. Huber, J. Bernardi, M. Stöger-Pollach, G. Friedbacher, H. Hutter, B. Yildiz, and J. Fleig. "Dislocations Accelerate Oxygen Ion Diffusion in $La_{0.8}Sr_{0.2}MnO_{3-\delta}$ Epitaxial Thin Films". In: *ACS Nano* 11.11 (2017), pp. 11475–11487.

[64] T. Huber, A. Opitz, and J. Fleig. "Oxygen reduction via grain boundary transport in thin film platinum electrodes on yttria stabilized zirconia". In: *Solid State Ionics* 273 (2015), pp. 8–12.

[65] M. Dhallu and J. A. Kilner. "Oxygen Transport in YSZ/LSM Composite Materials". In: *Journal of Fuel Cell Science and Technology* 2.1 (2004), pp. 29–33.

[66] A. M. Saranya, D. Pla, A. Morata, A. Cavallaro, J. Canales-Vazquez, J. A. Kilner, M. Burriel, and A. Tarancon. "Engineering Mixed Ionic Electronic Conduction in $La_{0.8}Sr_{0.2}MnO_{3-\delta}$ Nanostructures through Fast Grain Boundary Oxygen Diffusivity". In: *Advanced Energy Materials* 5.11 (2015), p. 1500377.

[67] Y. Li, K. Gerdes, T. Horita, and X. Liu. "Surface Exchange and Bulk Diffusivity of LSCF as SOFC Cathode: Electrical Conductivity Relaxation and Isotope Exchange Characterizations". In: *Journal of The Electrochemical Society* 160.4 (2013), F343–F350.

[68] Y. Li, K. Gerdes, and X. Liu. "Oxygen Transport Kinetics in Infiltrated SOFCs Cathode by Electrical Conductivity Relaxation Technique". In: *Journal of The Electrochemical Society* 160.6 (2013), F554–F559.

[69] E. Bucher, A. Egger, G. B. Caraman, and W. Sitte. "Stability of the SOFC Cathode Material (Ba,Sr)(Co,Fe)$O_{3-\delta}$ in CO_2-Containing Atmospheres". In: *Journal of The Electrochemical Society* 155.11 (2008), B1218.

Die approbierte gedruckte Originalversion dieser Dissertation ist an der TU Wien Bibliothek verfügbar.
The approved original version of this doctoral thesis is available in print at TU Wien Bibliothek.
TU WIEN Bibliothek Your knowledge hub

[70] R. A. Cox-Galhotra and S. McIntosh. "Electrical conductivity relaxation of polycrystalline $PrBaCo_2O_{5+\delta}$ thin films". In: *Solid State Ionics* 228 (2012), pp. 14–18.

[71] J. Maier. "On the correlation of macroscopic and microscopic rate constants in solid state chemistry". In: *Solid State Ionics* 112.3-4 (1998), pp. 197–228.

[72] D. Chen and H. L. Tuller. "Voltage-Controlled Nonstoichiometry in Oxide Thin Films: $Pr_{0.1}Ce_{0.9}O_{2-\delta}$ Case Study". In: *Advanced Functional Materials* 24.48 (2014), pp. 7638–7644.

[73] S. Darvish, H. Sabarou, S. K. Saxena, and Y. Zhong. "Quantitative Defect Chemistry Analysis and Electronic Conductivity Prediction of $La_{0.8}Sr_{0.2}MnO_{3-\delta}$ Perovskite". In: *Journal of The Electrochemical Society* 162.9 (2015), E134–E140.

[74] A. Schmid, G. M. Rupp, and J. Fleig. "How To Get Mechanistic Information from Partial Pressure-Dependent Current–Voltage Measurements of Oxygen Exchange on Mixed Conducting Electrodes". In: *Chemistry of Materials* 30.13 (2018), pp. 4242–4252.

[75] Z. Cai, M. Kubicek, J. Fleig, and B. Yildiz. "Chemical Heterogeneities on $La_{0.6}Sr_{0.4}CoO_{3-\delta}$ Thin Films Correlations to Cathode Surface Activity and Stability". In: *Chemistry of Materials* 24.6 (2012), pp. 1116–1127.

[76] A. Schmid, A. Nenning, A. Opitz, M. Kubicek, and J. Fleig. "High Oxygen Exchange Activity of Pristine $La_{0.6}Sr_{0.4}FeO_{3-\delta}$ Films and Its Degradation". In: *Journal of The Electrochemical Society* 167.12 (2020), p. 124509.

[77] W. Jung and H. L. Tuller. "Investigation of surface Sr segregation in model thin film solid oxidefuel cell perovskite electrodes". In: *Energy Environ. Sci.* 5.1 (2012), pp. 5370–5378.

[78] Y. Chen, W. Jung, Z. Cai, J. J. Kim, H. L. Tuller, and B. Yildiz. "Impact of Sr segregation on the electronic structure and oxygen reduction activity of $SrTi_{1-x}Fe_xO_{3-\delta}$ surfaces". In: *Energy Environmental Science* 5.7 (2012), p. 7979.

[79] J. C. D. Vero, H. Yokokawa, K. Develos-Bagarinao, S.-S. Liu, H. Kishimoto, T. Ishiyama, K. Yamaji, and T. Horita. "Influence of electrolyte substrates on the Sr-segregation and SrSO4 formation in $La_{0.6}Sr_{0.4}Co_{0.2}Fe_{0.8}O_{3-\delta}$ thin films". In: *MRS Communications* 9.1 (2019), pp. 236–244.

[80] F. Pişkin, R. Bliem, and B. Yildiz. "Effect of crystal orientation on the segregation of aliovalent dopants at the surface of $La_{0.6}Sr_{0.4}CoO_{3-\delta}$". In: *Journal of Materials Chemistry A* 6.29 (2018), pp. 14136–14145.

[81] M. Kubicek, G. M. Rupp, S. Huber, A. Penn, A. K. Opitz, J. Bernardi, M. Stöger-Pollach, H. Hutter, and J. Fleig. "Cation diffusion in $La_{0.6}Sr_{0.4}CoO_{3-\delta}$ below 800 °C and its relevance for Sr segregation". In: *Physical Chemistry Chemical Physics* 16.6 (2014), p. 2715.

Die approbierte gedruckte Originalversion dieser Dissertation ist an der TU Wien Bibliothek verfügbar.
The approved original version of this doctoral thesis is available in print at TU Wien Bibliothek.
TU WIEN Bibliothek Your knowledge hub

[82] W. Lee, J. W. Han, Y. Chen, Z. Cai, and B. Yildiz. "Cation Size Mismatch and Charge Interactions Drive Dopant Segregation at the Surfaces of Manganite Perovskites". In: *Journal of the American Chemical Society* 135.21 (2013), pp. 7909–7925.

[83] I. Rosso, E. Garrone, F. Geobaldo, B. Onida, G. Saracco, and V. Specchia. "Sulphur poisoning of $LaMn_{1-x}Mg_xO_{3-\delta}$ catalysts for natural gas combustion". In: *Applied Catalysis B: Environmental* 30.1-2 (2001), pp. 61–73.

[84] A. Yaremchenko, C. Buysse, V. Middelkoop, F. Snijkers, A. Buekenhoudt, J. Frade, and A. Kovalevsky. "Impact of sulphur contamination on the oxygen transport mechanism through $Ba_{0.5}Sr_{0.5}Co_{0.8}Fe_{0.2}O_{3-\delta}$: Relevant issues in the development of capillary and hollow fibre membrane geometry." In: *Journal of Membrane Science* 428 (2013), pp. 123–130.

[85] I. Rossetti, O. Buchneva, C. Biffi, and R. Rizza. "Effect of sulphur poisoning on perovskite catalysts prepared by flame-pyrolysis". In: *Applied Catalysis B: Environmental* 89.3-4 (2009), pp. 383–390.

[86] E. Bucher, C. Gspan, F. Hofer, and W. Sitte. "Sulphur poisoning of the SOFC cathode material $La_{0.6}Sr_{0.4}CoO_{3-\delta}$". In: *Solid State Ionics* 238 (2013), pp. 15–23.

[87] E. Bucher, C. Gspan, and W. Sitte. "Degradation and regeneration of the SOFC cathode material La0.6Sr0.4CoO3-d in SO2-containing atmospheres". In: *Solid State Ionics* 272 (2015), pp. 112–120.

[88] M. A. R. Niania, A. K. Rossall, J. A. V. den Berg, and J. A. Kilner. "The effect of subsurface strontium depletion on oxygen diffusion in La0.6Sr0.4Co0.2Fe0.8O3-d". In: *Journal of Materials Chemistry A* (2020).

[89] N. Schrödl, E. Bucher, A. Egger, P. Kreiml, C. Teichert, T. Höschen, and W. Sitte. "Long-term stability of the IT-SOFC cathode materials $La_{0.6}Sr_{0.4}CoO_{3-\delta}$ and La_2NiO_4 against combined chromium and silicon poisoning". In: *Solid State Ionics* 276 (2015), pp. 62–71.

[90] E. Bucher, C. Gspan, T. Höschen, F. Hofer, and W. Sitte. "Oxygen exchange kinetics of $La_{0.6}Sr_{0.4}CoO_{3-\delta}$ affected by changes of the surface composition due to chromium and silicon poisoning". In: *Solid State Ionics* 299 (2017), pp. 26–31.

[91] S. C. Paulson and V. I. Birss. "Chromium Poisoning of LSM-YSZ SOFC Cathodes". In: *Journal of The Electrochemical Society* 151.11 (2004), A1961.

[92] M. Perz, E. Bucher, C. Gspan, J. Waldhäusl, F. Hofer, and W. Sitte. "Long-term degradation of $La_{0.6}Sr_{0.4}Co_{0.2}Fe_{0.8}O_{3-\delta}$ IT-SOFC cathodes due to silicon poisoning". In: *Solid State Ionics* 288 (2016), pp. 22–27.

[93] G. M. Rupp, A. K. Opitz, A. Nenning, A. Limbeck, and J. Fleig. "Real-time impedance monitoring of oxygen reduction during surface modification of thin film cathodes". In: *Nature Materials* 16.6 (2017), pp. 640–645.

Die approbierte gedruckte Originalversion dieser Dissertation ist an der TU Wien Bibliothek verfügbar.
The approved original version of this doctoral thesis is available in print at TU Wien Bibliothek.
TU WIEN Bibliothek Your knowledge hub

[94] G. M. Rupp, A. Limbeck, M. Kubicek, A. Penn, M. Stoger-Pollach, G. Friedbacher, and J. Fleig. "Correlating surface cation composition and thin film microstructure with the electrochemical performance of lanthanum strontium cobaltite (LSC) electrodes". In: *J. Mater. Chem. A* 2.19 (2014), pp. 7099–7108.

[95] M. Siebenhofer, T. M. Huber, G. Friedbacher, W. Artner, J. Fleig, and M. Kubicek. "Oxygen exchange kinetics and nonstoichiometry of pristine $La_{0.6}Sr_{0.4}CoO_{3-\delta}$ thin films unaltered by degradation". In: *Journal of Materials Chemistry A* 8.16 (2020), pp. 7968–7979.

[96] Z. Chen, X. Wang, F. Giuliani, and A. Atkinson. "Analyses of microstructural and elastic properties of porous SOFC cathodes based on focused ion beam tomography". In: *Journal of Power Sources* 273 (2015), pp. 486–494.

[97] Y. P. Ivanov, M. Kubicek, M. Siebenhofer, A. Viernstein, H. Hutter, J. Fleig, A. Chuvilin, and Z. Zhang. "Strain-induced structure and oxygen transport interactions in epitaxial $La_{0.6}Sr_{0.4}CoO_{3-\delta}$ thin films". In: *Communications Materials* 1.1 (2020), p. 32. ISSN: 2662-4443.

[98] Z. Cai, Y. Kuru, J. W. Han, Y. Chen, and B. Yildiz. "Surface Electronic Structure Transitions at High Temperature on Perovskite Oxides: The Case of Strained $La_{0.8}Sr_{0.2}CoO_{3-\delta}$ Thin Films". In: *Journal of the American Chemical Society* 133.44 (2011), pp. 17696–17704.

[99] G. M. Rupp, M. Kubicek, A. K. Opitz, and J. Fleig. "In Situ Impedance Analysis of Oxygen Exchange on Growing $La_{0.6}Sr_{0.4}CoO_{3-\delta}$ Thin Films". In: *ACS Applied Energy Materials* 1.9 (2018), pp. 4522–4535.

[100] X. Liu, L. Zhang, Y. Zheng, Z. Guo, Y. Zhu, H. Chen, F. Li, P. Liu, B. Yu, X. Wang, J. Liu, Y. Chen, and M. Liu. "Uncovering the Effect of Lattice Strain and Oxygen Deficiency on Electrocatalytic Activity of Perovskite Cobaltite Thin Films". In: *Advanced Science* 6.6 (2019), p. 1801898.

[101] V. Haanappel, D. Rutenbeck, A. Mai, S. Uhlenbruck, D. Sebold, H. Wesemeyer, B. Röwekamp, C. Tropartz, and F. Tietz. "The influence of noble-metal-containing cathodes on the electrochemical performance of anode-supported SOFCs". In: *Journal of Power Sources* 130.1-2 (2004), pp. 119–128.

[102] J. M. Paige, Y. Cheng, P. A. Pepin, C. D. Curran, D. Sun, M. U. Chen, S. McIntosh, J. M. Vohs, and R. J. Gorte. "Surface modification of SOFC cathodes by Co, Ni, and Pd oxides". In: *Solid State Ionics* 341 (2019), p. 115051.

[103] Y. Cheng, A. S. Raman, J. Paige, L. Zhang, D. Sun, M. U. Chen, A. Vojvodic, R. J. Gorte, and J. M. Vohs. "Enhancing Oxygen Exchange Activity by Tailoring Perovskite Surfaces". In: *The Journal of Physical Chemistry Letters* 10.14 (2019), pp. 4082–4088.

Die approbierte gedruckte Originalversion dieser Dissertation ist an der TU Wien Bibliothek verfügbar.
The approved original version of this doctoral thesis is available in print at TU Wien Bibliothek.
TU WIEN Bibliothek Your knowledge hub

[104] D. W. Smith. "An acidity scale for binary oxides". In: *Journal of Chemical Education* 64.6 (1987), p. 480.

[105] E. J. Crumlin, E. Mutoro, Z. Liu, M. E. Grass, M. D. Biegalski, Y.-L. Lee, D. Morgan, H. M. Christen, H. Bluhm, and Y. Shao-Horn. "Surface strontium enrichment on highly active perovskites for oxygen electrocatalysis in solid oxide fuel cells". In: *Energy Environmental Science* 5.3 (2012), p. 6081.

[106] A. Nenning, A. K. Opitz, C. Rameshan, R. Rameshan, R. Blume, M. Haevecker, A. Knop-Gericke, G. Rupprechter, B. Kloetzer, and J. Fleig. "Ambient pressure XPS study of mixed conducting perovskite-type SOFC cathode and anode materials under well-defined electrochemical polarization". In: *J. Phys. Chem. C* 120.3 (2016), pp. 1461–1471.

[107] Q. Lu, G. Vardar, M. Jansen, S. R. Bishop, I. Waluyo, H. L. Tuller, and B. Yildiz. "Surface Defect Chemistry and Electronic Structure of $Pr_{0.1}Ce_{0.9}O_{2-\delta}$ in Operando". In: *Chemistry of Materials* 30.8 (2018), pp. 2600–2606.

[108] M. Koyama and T. Ishimoto. "First-Principles Study on Oxygen Reduction Reaction over $La_{1-x}Sr_xCoO_{3-\delta}$". In: *ECS Transactions* 77.10 (2017), pp. 75–80.

[109] S. Zhang, N. Han, and X. Tan. "Density functional theory calculations of atomic, electronic and thermodynamic properties of cubic $LaCoO_3$ and $La_{1-x}Sr_xCoO_3$ surfaces". In: *RSC Advances* 5.1 (2015), pp. 760–769.

[110] M. Siebenhofer, T. Huber, W. Artner, J. Fleig, and M. Kubicek. "Substrate stoichiometry changes during pulsed laser deposition: a case study on $SrTiO_3$". In: *Acta Materialia* 203 (2021), p. 116461.

[111] A. K. Opitz and J. Fleig. "Investigation of O_2 reduction on Pt/YSZ by means of thin film microelectrodes: The geometry dependence of the electrode impedance". In: *Solid State Ionics* 181.15-16 (2010), pp. 684–693.

[112] C. Riedl, A. Schmid, A. Nenning, H. Summerer, S. Smetaczek, S. Schwarz, J. Bernardi, A. Optiz, A. Limbeck, and J. Fleig. "Outstanding Oxygen Reduction Kinetics of $La_{0.6}Sr_{0.4}FeO_{3-\delta}$ Surfaces Decorated with Platinum Nanoparticles". In: *Journal of The Electrochemical Society* 167.10 (2020), p. 104514.

[113] U. Lucia. "Overview on fuel cells". In: *Renewable and Sustainable Energy Reviews* 30 (2014), pp. 164–169.

[114] J. Wu and H. Yang. "Platinum-Based Oxygen Reduction Electrocatalysts". In: *Accounts of Chemical Research* 46.8 (2013), pp. 1848–1857.

[115] Y. Takasu, N. Ohashi, X.-G. Zhang, Y. Murakami, H. Minagawa, S. Sato, and K. Yahikozawa. "Size effects of platinum particles on the electroreduction of oxygen". In: *Electrochimica Acta* 41.16 (1996), pp. 2595–2600.

Die approbierte gedruckte Originalversion dieser Dissertation ist an der TU Wien Bibliothek verfügbar.
The approved original version of this doctoral thesis is available in print at TU Wien Bibliothek.
TU WIEN Bibliothek Your knowledge hub

[116] B. Wang. "Recent development of non-platinum catalysts for oxygen reduction reaction". In: *Journal of Power Sources* 152 (2005), pp. 1–15.

[117] A. M. Gomez-Marin and J. M. Feliu. "New Insights into the Oxygen Reduction Reaction Mechanism on Pt(111): A Detailed Electrochemical Study". In: *ChemSusChem* 6.6 (2013), pp. 1091–1100.

[118] R. Usmen, E. Logothetis, and M. Shelef. "Measurement of Pt electrode surface area of automotive ZrO_2 oxygen sensors". In: *Sensors and Actuators B: Chemical* 28.2 (1995), pp. 139–142.

[119] A. K. Opitz, A. Schintlmeister, H. Hutter, and J. Fleig. "Visualization of oxygen reduction sites at Pt electrodes on YSZ by means of ^{18}O tracer incorporation: the width of the electrochemically active zone". In: *Physical Chemistry Chemical Physics* 12.39 (2010), p. 12734.

[120] M. P. Hörlein, A. K. Opitz, and J. Fleig. "On the variability of oxygen exchange kinetics of platinum model electrodes on yttria stabilized zirconia". In: *Solid State Ionics* 247-248 (2013), pp. 56–65.

[121] A. K. Opitz, M. P. Hörlein, T. Huber, and J. Fleig. "Current-Voltage Characteristics of Platinum Model Electrodes on Yttria-Stabilized Zirconia". In: *Journal of The Electrochemical Society* 159.5 (2012), B502–B513.

[122] T. M. Huber, E. Navickas, G. Friedbacher, H. Hutter, and J. Fleig. "Apparent Oxygen Uphill Diffusion in $La_{0.8}Sr_{0.2}MnO_{3-\delta}$ Thin Films upon Cathodic Polarization". In: *ChemElectroChem* 2.10 (2015), pp. 1487–1494.

[123] J. C. D. Vero, K. Develos-Bagarinao, S.-S. Liu, H. Kishimoto, T. Ishiyama, K. Yamaji, T. Horita, and H. Yokokawa. "Sulfur poisoning behavior of $La_{1-x}Sr_xCo_{1-y}Fe_yO_{3-\delta}$ thin films with different compositions". In: *Journal of Alloys and Compounds* 748 (2018), pp. 608–619.

[124] B. Luerßen, E. Mutoro, H. Fischer, S. Günther, R. Imbihl, and J. Janek. "In Situ Imaging of Electrochemically Induced Oxygen Spillover on Pt-YSZ Catalysts". In: *Angewandte Chemie International Edition* 45.9 (2006), pp. 1473–1476.

[125] G. Beck, H. Pöpke, B. Luerßen, and J. Janek. "Microstructure of platinum films on YSZ prepared by pulsed laser deposition". In: *Journal of Crystal Growth* 322.1 (2011), pp. 95–102.

[126] G. Beck, H. Fischer, E. Mutoro, V. Srot, K. Petrikowski, E. Tchernychova, M. Wuttig, M. Ruhle, B. Luersen, and J. Janek. "Epitaxial Pt(111) thin film electrodes on YSZ(111) and YSZ(100) — Preparation and characterisation". In: *Solid State Ionics* 178.5-6 (2007), pp. 327–337.

Die approbierte gedruckte Originalversion dieser Dissertation ist an der TU Wien Bibliothek verfügbar.
The approved original version of this doctoral thesis is available in print at TU Wien Bibliothek.
TU Bibliothek Your knowledge hub WIEN

[127] E. Mutoro, B. Luerssen, S. Günther, and J. Janek. "Structural, morphological and kinetic properties of model type thin film platinum electrodes on YSZ". In: *Solid State Ionics* 179.21-26 (2008), pp. 1214–1218.

[128] S. Heiroth, T. Lippert, A. Wokaun, M. Döbeli, J. Rupp, B. Scherrer, and L. Gauckler. "Yttria-stabilized zirconia thin films by pulsed laser deposition: Microstructural and compositional control". In: *Journal of the European Ceramic Society* 30.2 (2010), pp. 489–495.

[129] A. Infortuna, A. Harvey, and L. Gauckler. "Microstructures of CGO and YSZ Thin Films by Pulsed Laser Deposition". In: *Advanced Functional Materials* 18.1 (2007), pp. 127–135.

[130] T. Ryll, H. Galinski, L. Schlagenhauf, P. Elser, J. L. M. Rupp, A. Bieberle-Hutter, and L. J. Gauckler. "Microscopic and Nanoscopic Three-Phase-Boundaries of Platinum Thin-Film Electrodes on YSZ Electrolyte". In: *Advanced Functional Materials* 21.3 (2010), pp. 565–572.

[131] J. L. Hertz, A. Rothschild, and H. L. Tuller. "Highly enhanced electrochemical performance of silicon-free platinum–yttria stabilized zirconia interfaces". In: *Journal of Electroceramics* 22.4 (2008), pp. 428–435.

[132] J. Mizusaki. "Electrode reaction at Pt, O_2 stabilized zirconia interfaces. Part II: Electrochemical measurements and analysis". In: *Solid State Ionics* 22.4 (1987), pp. 323–330.

[133] Q. Fu, J. Yang, and Y. Luo. "A First Principles Study on the Dissociation and Rotation Processes of a Single O_2 Molecule on the Pt(111) Surface". In: *The Journal of Physical Chemistry C* 115.14 (2011), pp. 6864–6869.

[134] J. M. Bray and W. F. Schneider. "Potential Energy Surfaces for Oxygen Adsorption, Dissociation, and Diffusion at the Pt(321) Surface". In: *Langmuir* 27.13 (2011), pp. 8177–8186.

[135] E. Navickas, T. M. Huber, Y. Chen, W. Hetaba, G. Holzlechner, G. Rupp, M. Stöger-Pollach, G. Friedbacher, H. Hutter, B. Yildiz, and J. Fleig. "Fast oxygen exchange and diffusion kinetics of grain boundaries in Sr-doped $LaMnO_3$ thin films". In: *Physical Chemistry Chemical Physics* 17.12 (2015), pp. 7659–7669.

[136] J. D. Rogers, V. S. Sundaram, G. G. Kleiman, S. G. C. Castro, R. A. Douglas, and A. C. Peterlevitz. "High resolution study of the M45N67N67and M45N45N67Auger transitions in the 5d series". In: *Journal of Physics F: Metal Physics* 12.9 (1982), pp. 2097–2102.

[137] G. M. Bancroft, I. Adams, L. L. Coatsworth, C. D. Bennewitz, J. D. Brown, and W. D. Westwood. "ESCA study of sputtered platinum films". In: *Analytical Chemistry* 47.3 (1975), pp. 586–588.

Die approbierte gedruckte Originalversion dieser Dissertation ist an der TU Wien Bibliothek verfügbar.
The approved original version of this doctoral thesis is available in print at TU Wien Bibliothek.
TU WIEN Bibliothek Your knowledge hub

[138] P. Hjalmarsson, M. Søgaard, and M. Mogensen. "Electrochemical performance and degradation of $(La_{0.6}Sr_{0.4})_{0.99}CoO_3$ as porous SOFC-cathode". In: *Solid State Ionics* 179.27-32 (2008), pp. 1422–1426.

[139] H. Wang and S. A. Barnett. "Degradation Mechanisms of Porous $La_{0.6}Sr_{0.4}Co_{0.2}Fe_{0.8}O_3$ Solid Oxide Fuel Cell Cathodes". In: *Journal of The Electrochemical Society* 165.7 (2018), F564–F570.

[140] J. Jamnik and J. Maier. "Generalised equivalent circuits for mass and charge transport: chemical capacitance and its implications". In: *Phys. Chem. Chem. Phys.* 3.9 (2001), pp. 1668–1678.

[141] G. J. Brug, A. L. van den Eeden, M. Sluyters-Rehbach, and J. H. Sluyters. "The analysis of electrode impedances complicated by the presence of a constant phase element". In: *J. Electroanal. Chem.* 176.1-2 (1984), pp. 275–295.

[142] F. S. Baumann, J. Fleig, G. Cristiani, B. Stuhlhofer, H.-U. Habermeier, and J. Maier. "Quantitative Comparison of Mixed Conducting SOFC Cathode Materials by Means of Thin Film Model Electrodes". In: *J. Electrochem. Soc.* 154.9 (2007), B931–B941.

[143] G. M. Rupp, H. Tellez, J. Druce, A. Limbeck, T. Ishihara, J. Kilner, and J. Fleig. "Surface chemistry of $La_{0.6}Sr_{0.4}CoO_{3-\delta}$ thin films and its impact on the oxygen surface exchange resistance". In: *J. Mater. Chem. A* 3.45 (2015), pp. 22759–22769. ISSN: 2050-7488.

[144] M. Escudero, A. Aguadero, J. Alonso, and L. Daza. "A kinetic study of oxygen reduction reaction on La_2NiO_4 cathodes by means of impedance spectroscopy". In: *Journal of Electroanalytical Chemistry* 611.1-2 (2007), pp. 107–116.

[145] D. Chen, S. R. Bishop, and H. L. Tuller. "Praseodymium-cerium oxide thin film cathodes: Study of oxygen reduction reaction kinetics". In: *Journal of Electroceramics* 28.1 (2012), pp. 62–69.

[146] A. Egger, E. Bucher, M. Yang, and W. Sitte. "Comparison of oxygen exchange kinetics of the IT-SOFC cathode materials $La_{0.5}Sr_{0.5}CoO_{3-\delta}$ and $La_{0.6}Sr_{0.4}CoO_{3-\delta}$". In: *Solid State Ionics* 225 (2012), pp. 55–60.

[147] Z. Gao, X. Liu, B. Bergman, and Z. Zhao. "Investigation of oxygen reduction reaction kinetics on $Sm_{0.5}Sr_{0.5}CoO_{3-\delta}$ cathode supported on $Ce_{0.85}Sm_{0.075}Nd_{0.075}O_2$ electrolyte". In: *Journal of Power Sources* 196.22 (2011), pp. 9195–9203.

[148] Y.-L. Huang, C. Pellegrinelli, and E. D. Wachsman. "Reaction Kinetics of Gas–Solid Exchange Using Gas Phase Isotopic Oxygen Exchange". In: *ACS Catalysis* 6.9 (2016), pp. 6025–6032.

[149] A. C. Luntz, M. D. Williams, and D. S. Bethune. "The sticking of O_2 on a Pt(111) surface". In: *The Journal of Chemical Physics* 89.7 (1988), pp. 4381–4395.

Die approbierte gedruckte Originalversion dieser Dissertation ist an der TU Wien Bibliothek verfügbar.
The approved original version of this doctoral thesis is available in print at TU Wien Bibliothek.
TU WIEN Bibliothek Your knowledge hub

[150] C. T. Rettner and C. B. Mullins. "Dynamics of the chemisorption of O_2 on Pt(111): Dissociation via direct population of a molecularly chemisorbed precursor at high incidence kinetic energy". In: *The Journal of Chemical Physics* 94.2 (1991), pp. 1626–1635.

[151] L. Jacobse, A. den Dunnen, and L. B. F. Juurlink. "The molecular dynamics of adsorption and dissociation of O_2 on Pt(553)". In: *The Journal of Chemical Physics* 143.1 (2015), p. 014703.

[152] A. Nenning, L. Volgger, E. Miller, L. V. Mogni, S. Barnett, and J. Fleig. "The Electrochemical Properties of Sr(Ti,Fe)O_3,for Anodes in Solid Oxide Fuel Cells". In: *Journal of The Electrochemical Society* 164.4 (2017), F364–F371.

[153] A. K. Opitz, A. Nenning, C. Rameshan, R. Rameshan, R. Blume, M. Hävecker, A. Knop-Gericke, G. Rupprechter, J. Fleig, and B. Kloetzer. "Enhancing Electrochemical Water-Splitting Kinetics by Polarization-Driven Formation of Near-Surface Iron(0): An In-Situ XPS Study on Perovskite-Type Electrodes". In: *Angewandte Chemie International Edition* 54.9 (2014), pp. 2628–2632.

[154] C. Riedl, M. Siebenhofer, A. Nenning, G. Friedbacher, M. Weiss, C. Rameshan, J. Bernardi, A. Limbeck, M. Kubicek, A. K. Opitz, and J. Fleig. "Performance modulation through selective, homogenous surface doping of lanthanum strontium ferrite electrodes revealed by in situ PLD impedance measurements". In: *Journal of Materials Chemistry A* 10.6 (2022), pp. 2973–2986.

[155] L. Hutton, M. E. Newton, P. R. Unwin, and J. V. Macpherson. "Amperometric Oxygen Sensor Based on a Platinum Nanoparticle-Modified Polycrystalline Boron Doped Diamond Disk Electrode". In: *Analytical Chemistry* 81.3 (2009), pp. 1023–1032.

[156] W. Sari, P. Smith, S. Leigh, and J. Covington. "Oxygen Sensors Based on Screen Printed Platinum and Palladium Doped Indium Oxides". In: *Proceedings* 1.4 (2017), p. 401.

[157] J. Sheng, N. Yoshida, J. Karasawa, and T. Fukami. "Platinum doped titania film oxygen sensor integrated with temperature compensating thermistor". In: *Sensors and Actuators B: Chemical* 41.1-3 (1997), pp. 131–136.

[158] T. Mallat and A. Baiker. "Oxidation of alcohols with molecular oxygen on platinum metal catalysts in aqueous solutions". In: *Catalysis Today* 19.2 (1994), pp. 247–283.

[159] K. Yahikozawa, Y. Fujii, Y. Matsuda, K. Nishimura, and Y. Takasu. "Electrocatalytic properties of ultrafine platinum particles for oxidation of methanol and formic acid in aqueous solutions". In: *Electrochimica Acta* 36.5-6 (1991), pp. 973–978.

[160] M. K. Carpenter, T. E. Moylan, R. S. Kukreja, M. H. Atwan, and M. M. Tessema. "Solvothermal Synthesis of Platinum Alloy Nanoparticles for Oxygen Reduction Electrocatalysis". In: *Journal of the American Chemical Society* 134.20 (2012), pp. 8535–8542.

Die approbierte gedruckte Originalversion dieser Dissertation ist an der TU Wien Bibliothek verfügbar.
The approved original version of this doctoral thesis is available in print at TU Wien Bibliothek.
TU WIEN Bibliothek Your knowledge hub

[161] R. L. Borup, A. Kusoglu, K. C. Neyerlin, R. Mukundan, R. K. Ahluwalia, D. A. Cullen, K. L. More, A. Z. Weber, and D. J. Myers. "Recent developments in catalyst-related PEM fuel cell durability". In: *Current Opinion in Electrochemistry* 21 (2020), pp. 192–200.

[162] S. Ott, A. Orfanidi, H. Schmies, B. Anke, H. N. Nong, J. Hübner, U. Gernert, M. Gliech, M. Lerch, and P. Strasser. "Ionomer distribution control in porous carbon-supported catalyst layers for high-power and low Pt-loaded proton exchange membrane fuel cells". In: *Nature Materials* 19.1 (2019), pp. 77–85.

[163] A. Kongkanand, N. P. Subramanian, Y. Yu, Z. Liu, H. Igarashi, and D. A. Muller. "Achieving High-Power PEM Fuel Cell Performance with an Ultralow-Pt-Content Core Shell Catalyst". In: *ACS Catalysis* 6.3 (2016), pp. 1578–1583.

[164] P. D. Nolan, B. R. Lutz, P. L. Tanaka, J. E. Davis, and C. B. Mullins. "Molecularly chemisorbed intermediates to oxygen adsorption on Pt(111): A molecular beam and electron energy-loss spectroscopy study". In: *The Journal of Chemical Physics* 111.8 (1999), pp. 3696–3704.

[165] J. Zhang, Y. Zhao, X. Guo, C. Chen, C.-L. Dong, R.-S. Liu, C.-P. Han, Y. Li, Y. Gogotsi, and G. Wang. "Single platinum atoms immobilized on an MXene as an efficient catalyst for the hydrogen evolution reaction". In: *Nature Catalysis* 1.12 (2018), pp. 985–992.

[166] T. Zhu, H. E. Troiani, L. V. Mogni, M. Han, and S. A. Barnett. "Ni-Substituted Sr(Ti,Fe)O_3 SOFC Anodes: Achieving High Performance via Metal Alloy Nanoparticle Exsolution". In: *Joule* 2.3 (2018), pp. 478–496.

[167] T. Zhu, H. Troiani, L. V. Mogni, M. Santaya, M. Han, and S. A. Barnett. "Exsolution and electrochemistry in perovskite solid oxide fuel cell anodes: Role of stoichiometry in Sr(Ti,Fe,Ni)O_3". In: *Journal of Power Sources* 439 (2019), p. 227077.

[168] R. Glaser, T. Zhu, H. Troiani, A. Caneiro, L. Mogni, and S. Barnett. "The enhanced electrochemical response of $Sr(Ti_{0.3}Fe_{0.7}Ru_{0.07})O_{3-\delta}$ anodes due to exsolved Ru-Fe nanoparticles". In: *Journal of Materials Chemistry A* 6.12 (2018), pp. 5193–5201.

[169] B. D. Madsen, W. Kobsiriphat, Y. Wang, L. D. Marks, and S. Barnett. "SOFC Anode Performance Enhancement through Precipitation of Nanoscale Catalysts". In: *ECS Transactions* 7.1 (2019), pp. 1339–1348.

[170] M. B. Katz, G. W. Graham, Y. Duan, H. Liu, C. Adamo, D. G. Schlom, and X. Pan. "Self-Regeneration of Pd-LaFeO3 Catalysts: New Insight from Atomic-Resolution Electron Microscopy". In: *Journal of the American Chemical Society* 133.45 (2011), pp. 18090–18093.

Die approbierte gedruckte Originalversion dieser Dissertation ist an der TU Wien Bibliothek verfügbar.
The approved original version of this doctoral thesis is available in print at TU Wien Bibliothek.
TU WIEN Bibliothek Your knowledge hub

[171] H. Tanaka, M. Uenishi, M. Taniguchi, I. Tan, K. Narita, M. Kimura, K. Kaneko, Y. Nishihata, and J. Mizuki. "The intelligent catalyst having the self-regenerative function of Pd, Rh and Pt for automotive emissions control". In: *Catalysis Today* 117.1-3 (2006), pp. 321–328.

[172] M. Uenishi, M. Taniguchi, H. Tanaka, M. Kimura, Y. Nishihata, J. Mizuki, and T. Kobayashi. "Redox behavior of palladium at start-up in the Perovskite-type LaFePdOx automotive catalysts showing a self-regenerative function". In: *Applied Catalysis B: Environmental* 57.4 (2005), pp. 267–273.

[173] M. P. Pechini. "Method of preparing lead and alkaline earth titanates and niobates and coating method using the same to form a capacitor". Patent 3330697. 1967.

[174] G. M. Rupp, M. Glowacki, and J. Fleig. "Electronic and ionic conductivity of $La_{0.95}Sr_{0.05}Ga_{0.95}Mg_{0.05}O_{3-\delta}$ (LSGM) single crystals". In: *Journal of The Electrochemical Society* 163.10 (2016), F1189.

[175] R. Rameshan, A. Nenning, J. Raschhofer, L. Lindenthal, T. Ruh, H. Summerer, A. K. Opitz, T. M. Huber, and C. Rameshan. "Novel Sample-Stage for Combined Near Ambient Pressure X-ray Photoelectron Spectroscopy, Catalytic Characterization and Electrochemical Impedance Spectroscopy". In: *Crystals* 10.10 (2020), p. 947.

[176] A. Head and H. Bluhm. "Ambient Pressure X-Ray Photoelectron Spectroscopy". In: *Encyclopedia of Interfacial Chemistry*. Elsevier, 2018, pp. 13–27.

[177] J. Scofield. "Hartree-Slater subshell photoionization cross-sections at 1254 and 1487 eV". In: *Journal of Electron Spectroscopy and Related Phenomena* 8.2 (1976), pp. 129–137.

[178] M. Weiss, C. Riedl, J. Frank, J. Fleig, and A. Limbeck. "Quantitative analysis of the platinum surface decoration on lanthanum strontium iron oxide thin films via online-LASIL-ICP-MS". In: *Microchemical Journal* 166 (2021), p. 106236.

[179] K. S. Kim, N. Winograd, and R. E. Davis. "Electron spectroscopy of platinum-oxygen surfaces and application to electrochemical studies". In: *Journal of the American Chemical Society* 93.23 (1971), pp. 6296–6297.

[180] T. Kawada, J. Suzuki, M. Sase, A. Kaimai, K. Yashiro, Y. Nigara, J. Mizusaki, K. Kawamura, and H. Yugami. "Determination of Oxygen Vacancy Concentration in a Thin Film of $La_{0.6}Sr_{0.4}CoO_{3-\delta}$ by an Electrochemical Method". In: *Journal of The Electrochemical Society* 149.7 (2002), E252.

[181] H. Tanaka, M. Taniguchi, M. Uenishi, N. Kajita, I. Tan, Y. Nishihata, J. Mizuki, K. Narita, M. Kimura, and K. Kaneko. "Self-Regenerating Rh- and Pt-Based Perovskite Catalysts for Automotive-Emissions Control". In: *Angewandte Chemie International Edition* 45.36 (2006), pp. 5998–6002.

Die approbierte gedruckte Originalversion dieser Dissertation ist an der TU Wien Bibliothek verfügbar.
The approved original version of this doctoral thesis is available in print at TU Wien Bibliothek.
TU WIEN Bibliothek Your knowledge hub

[182] C. Ahamer, A. K. Opitz, G. M. Rupp, and J. Fleig. "Revisiting the Temperature Dependent Ionic Conductivity of Yttria Stabilized Zirconia (YSZ)". In: *Journal of The Electrochemical Society* 164.7 (2017), F790–F803.

[183] L. Zhang, G. Chen, R. Dai, X. Lv, D. Yang, and S. Geng. "A review of the chemical compatibility between oxide electrodes and electrolytes in solid oxide fuel cells". In: 492 (2021), p. 229630.

[184] G. J. la O, S.-J. Ahn, E. Crumlin, Y. Orikasa, M. D. Biegalski, H. M. Christen, and Y. Shao-Horn. "Catalytic Activity Enhancement for Oxygen Reduction on Epitaxial Perovskite Thin Films for Solid-Oxide Fuel Cells". In: *Angewandte Chemie International Edition* 49.31 (2010), pp. 5344–5347.

[185] R. D. Shannon. "Revised effective ionic radii and systematic studies of interatomic distances in halides and chalcogenides". In: *Acta Crystallographica Section A* 32.5 (1976), pp. 751–767.

[186] M. Niania, R. Podor, T. B. Britton, C. Li, S. J. Cooper, N. Svetkov, S. Skinner, and J. Kilner. "In situ study of strontium segregation in $La_{0.6}Sr_{0.4}Co_{0.2}Fe_{0.8}O_{3-\delta}$ in ambient atmospheres using high-temperature environmental scanning electron microscopy". In: *Journal of Materials Chemistry A* 6.29 (2018), pp. 14120–14135.

[187] J. Druce, T. Ishihara, and J. Kilner. "Surface composition of perovskite-type materials studied by Low Energy Ion Scattering (LEIS)". In: *Solid State Ionics* 262 (2014), pp. 893–896.

[188] M. Kubicek, A. Limbeck, T. Fromling, H. Hutter, and J. Fleig. "Relationship between Cation Segregation and the Electrochemical Oxygen Reduction Kinetics of La0.6Sr0.4CoO3 Thin Film Electrodes". In: *Journal of The Electrochemical Society* 158.6 (2011), B727.

[189] C. Berger, E. Bucher, C. Gspan, A. Menzel, and W. Sitte. "Impact of SO_2 on the Oxygen Exchange Kinetics of the Promising SOFC/SOEC Air Electrode Material $La_{0.8}Ca_{0.2}FeO_{3-\delta}$". In: *Journal of The Electrochemical Society* 164.10 (2017), F3008–F3018.

[190] C. Berger, E. Bucher, C. Gspan, A. Menzel, and W. Sitte. "Long-term stability of oxygen surface exchange kinetics of Pr0.8Ca0.2FeO3-d against SO2-poisoning". In: *Solid State Ionics* 326 (2018), pp. 82–89.

[191] H. Tanaka, I. Tan, M. Uenishi, M. Kimura, and K. Dohmae. "Regeneration of Palladium Subsequent to Solid Solution and Segregation in a Perovskite Catalyst: An Intelligent Catalyst". In: *Topics in Catalysis* 16/17.1/4 (2001), pp. 63–70.

[192] C. Riedl, M. Siebenhofer, A. Nenning, A. Schmid, M. Weiss, C. Rameshan, A. Limbeck, M. Kubicek, A. K. Opitz, and J. Fleig. "Insitu techniques reveal the true capabilities of SOFC cathode materials and their sudden degradation due to omnipresent sulfur trace impurities". In: *Journal of Materials Chemistry A* 10.28 (2022), pp. 14838–14848.

Die approbierte gedruckte Originalversion dieser Dissertation ist an der TU Wien Bibliothek verfügbar.
The approved original version of this doctoral thesis is available in print at TU Wien Bibliothek.
TU WIEN Bibliothek Your knowledge hub

[193] B. Koo, K. Kim, J. K. Kim, H. Kwon, J. W. Han, and W. Jung. "Sr Segregation in Perovskite Oxides: Why It Happens and How It Exists". In: *Joule* 2.8 (2018), pp. 1476–1499.

[194] Y. Xiong, K. Yamaji, T. Horita, H. Yokokawa, J. Akikusa, H. Eto, and T. Inagaki. "Sulfur Poisoning of SOFC Cathodes". In: *Journal of The Electrochemical Society* 156.5 (2009), B588.

[195] C. Wang and S. P. Jiang. "Mechanism of SO_2 Poisoning on the Electrochemical Activity of LSCF and LSM Electrodes". In: *ECS Transactions* 68.1 (2015), pp. 1023–1029.

[196] T. Daio, P. Mitra, S. M. Lyth, and K. Sasaki. "Atomic-resolution analysis of degradation phenomena in SOFCS: A case study of SO_2 poisoning in LSM cathodes". In: *International Journal of Hydrogen Energy* 41.28 (2016), pp. 12214–12221.

[197] J. A. Schuler, C. Gehrig, Z. Wuillemin, A. J. Schuler, J. Wochele, C. Ludwig, A. Hessler-Wyser, and J. V. herle. "Air side contamination in Solid Oxide Fuel Cell stack testing". In: *Journal of Power Sources* 196.17 (2011), pp. 7225–7231.

[198] T. Kushi. "Effects of sulfur poisoning on degradation phenomena in oxygen electrodes of solid oxide electrolysis cells and solid oxide fuel cells". In: *International Journal of Hydrogen Energy* 42.15 (2017), pp. 9396–9405.

[199] R. A. Budiman, S. S. Liu, K. D. Bagarinao, T. Ishiyama, H. Kishimoto, K. Yamaji, T. Horita, and H. Yokokawa. "Determination of Factors Governing Surface Composition and Degradation of $La_{0.6}Sr_{0.4}Co_{0.2}Fe_{0.8}O_{3-\delta}$ Electrode under Sulfur-Contained Air". In: *Journal of The Electrochemical Society* 166.6 (2019), F414–F422.

[200] C. C. Wang, K. Chen, and S. P. Jiang. "Sulfur Deposition and Poisoning of $La_{0.6}Sr_{0.4}Co_{0.2}Fe_{0.8}O_{3-\delta}$ Cathode Materials of Solid Oxide Fuel Cells". In: *Journal of The Electrochemical Society* 161.12 (2014), F1133–F1139.

[201] F. Wang, K. Yamaji, D.-H. Cho, T. Shimonosono, M. Nishi, H. Kishimoto, M. E. Brito, T. Horita, and H. Yokokawa. "Evaluation of Sulfur Dioxide Poisoning for LSCF Cathodes". In: *Fuel Cells* 13.4 (2013), pp. 520–525.

[202] L. Zhao, N. H. Perry, T. Daio, K. Sasaki, and S. R. Bishop. "Improving the Si Impurity Tolerance of $Pr_{0.1}Ce_{0.9}O_{2-\delta}$ SOFC Electrodes with Reactive Surface Additives". In: *Chemistry of Materials* 27.8 (2015), pp. 3065–3070.

[203] N. Schrödl, A. Egger, J. Lammer, F. Hofer, and W. Sitte. "Long-Term Stability of Pr_2NiO_4 Air Electrodes for Solid Oxide Cells against Chromium Poisoning". In: *Journal of the Electrochemical Society* 168.1 (2021), p. 014509.

[204] R. Kungas, A. S. Yu, J. Levine, J. M. Vohs, and R. J. Gorte. "An Investigation of Oxygen Reduction Kinetics in LSF Electrodes". In: *Journal of The Electrochemical Society* 160.2 (2012), F205–F211.

Die approbierte gedruckte Originalversion dieser Dissertation ist an der TU Wien Bibliothek verfügbar.
The approved original version of this doctoral thesis is available in print at TU Wien Bibliothek.
TU WIEN Bibliothek Your knowledge hub

[205] D. Chen, S. R. Bishop, and H. L. Tuller. "Non-stoichiometry in Oxide Thin Films: A Chemical Capacitance Study of the Praseodymium-Cerium Oxide System". In: *Advanced Functional Materials* 23.17 (2012), pp. 2168–2174.

[206] J. J. Kim, S. R. Bishop, N. J. Thompson, and H. L. Tuller. "Investigation of Redox Kinetics by Simultaneous In Situ Optical Absorption Relaxation and Electrode Impedance Measurements: Pr Doped Ceria Thin Films". In: *ECS Transactions* 57.1 (2013), pp. 1979–1984.

[207] Y. L. Yang, C. L. Chen, S. Y. Chen, C. W. Chu, and A. J. Jacobson. "Impedance Studies of Oxygen Exchange on Dense Thin Film Electrodes of $La_{0.5}Sr_{0.5}CoO_{3-\delta}$". In: *Journal of The Electrochemical Society* 147.11 (2000), p. 4001.

[208] E. J. Crumlin, E. Mutoro, W. T. Hong, M. D. Biegalski, H. M. Christen, Z. Liu, H. Bluhm, and Y. Shao-Horn. "In Situ Ambient Pressure X-ray Photoelectron Spectroscopy of Cobalt Perovskite Surfaces under Cathodic Polarization at High Temperatures". In: *The Journal of Physical Chemistry C* 117.31 (2013), pp. 16087–16094.

[209] K. A. Stoerzinger, W. T. Hong, E. J. Crumlin, H. Bluhm, M. D. Biegalski, and Y. Shao-Horn. "Water Reactivity on the $LaCoO_3$ (001) Surface: An Ambient Pressure X-ray Photoelectron Spectroscopy Study". In: *The Journal of Physical Chemistry C* 118.34 (2014), pp. 19733–19741.

[210] S. Y. Lai, D. Ding, M. Liu, M. Liu, and F. M. Alamgir. "Operando and Insitu X-ray Spectroscopies of Degradation in $La_{0.6}Sr_{0.4}Co_{0.2}Fe_{0.8}O_{3-\delta}$ Thin Film Cathodes in Fuel Cells". In: *ChemSusChem* 7.11 (2014), pp. 3078–3087.

[211] T. Horita. "An Improvement of SOFC Durability by the Mass Transport Analysis at the Interfaces". In: *Energy Technology 2016*. Springer International Publishing, 2016, pp. 163–170.

[212] E. J. Karlsen, M. A. Nygren, and L. G. M. Pettersson. "Comparative Study on Structures and Energetics of NO, SO and CO Adsorption on Alkaline-Earth-Metal Oxides". In: *The Journal of Physical Chemistry B* 107.31 (2003), pp. 7795–7802.

[213] F. Wang, H. Kishimoto, T. Ishiyama, K. Develos-Bagarinao, K. Yamaji, T. Horita, and H. Yokokawa. "A review of sulfur poisoning of solid oxide fuel cell cathode materials for solid oxide fuel cells". In: *Journal of Power Sources* 478 (2020), p. 228763.

[214] M. V. Lebedev, P. A. Dementev, T. V. Lvova, and V. L. Berkovits. "Modification of the p-GaP(001) work function by surface dipole bonds formed in sulfide solution". In: *Journal of Materials Chemistry C* 7.24 (2019), pp. 7327–7335.

[215] R. T. Sanderson. "Electronegativities in inorganic chemistry: (II)". In: *Journal of Chemical Education* 31.1 (1954), p. 2.

Die approbierte gedruckte Originalversion dieser Dissertation ist an der TU Wien Bibliothek verfügbar.
The approved original version of this doctoral thesis is available in print at TU Wien Bibliothek.
TU WIEN Bibliothek Your knowledge hub

[216] L. Kish, Y. Li, J. Solis, W. Marlow, R. Vajtai, C.-G. Granqvist, V. Lantto, J. Smulko, and G. Schmera. "Detecting harmful gases using fluctuation-enhanced sensing with Taguchi sensors". In: *IEEE Sensors Journal* 5.4 (2005), pp. 671–676.

[217] D. Lee, R. Jacobs, Y. Jee, A. Seo, C. Sohn, A. V. Ievlev, O. S. Ovchinnikova, K. Huang, D. Morgan, and H. N. Lee. "Stretching Epitaxial $La_{0.6}Sr_{0.4}CoO_{3-\delta}$ for Fast Oxygen Reduction". In: *The Journal of Physical Chemistry C* 121.46 (2017), pp. 25651–25658.

[218] R. Moreno, J. Zapata, J. Roqueta, N. Bagués, and J. Santiso. "Chemical Strain and Oxidation-Reduction Kinetics of Epitaxial Thin Films of Mixed Ionic-Electronic Conducting Oxides Determined by X-Ray Diffraction". In: *Journal of The Electrochemical Society* 161.11 (2014), F3046–F3051.

[219] M. Kubicek, Z. Cai, W. Ma, B. Yildiz, H. Hutter, and J. Fleig. "Tensile Lattice Strain Accelerates Oxygen Surface Exchange and Diffusion in $La_{1-x}Sr_xCoO_{3-\delta}$ Thin Films". In: *ACS Nano* 7.4 (2013), pp. 3276–3286.

[220] T. Mayeshiba and D. Morgan. "Strain effects on oxygen migration in perovskites". In: *Physical Chemistry Chemical Physics* 17.4 (2015), pp. 2715–2721.

[221] J. Januschewsky, M. Ahrens, A. Opitz, F. Kubel, and J. Fleig. "Optimized $La_{0.6}Sr_{0.4}CoO_{3-\delta}$ Thin-Film Electrodes with Extremely Fast Oxygen-Reduction Kinetics". In: *Advanced Functional Materials* 19.19 (2009), pp. 3151–3156.

[222] T. Degen, M. Sadki, E. Bron, U. König, and G. Nénert. "The highscore suite". In: *Powder diffraction* 29.S2 (2014), S13–S18.

[223] D. Nečas and P. Klapetek. "Gwyddion: an open-source software for SPM data analysis". In: *Open Physics* 10.1 (2012), pp. 181–188.

[224] L. A. Giannuzzi, J. L. Drown, S. R. Brown, R. B. Irwin, and F. A. Stevie. "Applications of the FIB lift-out technique for TEM specimen preparation". In: *Microscopy Research and Technique* 41.4 (1998), pp. 285–290.

[225] T. M. Huber, M. Kubicek, A. K. Opitz, and J. Fleig. "The Relevance of Different Oxygen Reduction Pathways of $La_{0.8}Sr_{0.2}MnO_{3-\delta}$ (LSM) Thin Film Model Electrodes". In: *Journal of The Electrochemical Society* 162.3 (2014), F229–F242.

[226] E. J. Crumlin, S.-J. Ahn, D. Lee, E. Mutoro, M. D. Biegalski, H. M. Christen, and Y. Shao-Horn. "Oxygen Electrocatalysis on Epitaxial $La_{0.6}Sr_{0.4}CoO_{3-\delta}$ Perovskite Thin Films for Solid Oxide Fuel Cells". In: *Journal of The Electrochemical Society* 159.7 (2012), F219–F225.

[227] Z. Shao, W. Zhou, and Z. Zhu. "Advanced synthesis of materials for intermediate-temperature solid oxide fuel cells". In: *Progress in Materials Science* 57.4 (2012), pp. 804–874.

Die approbierte gedruckte Originalversion dieser Dissertation ist an der TU Wien Bibliothek verfügbar.
The approved original version of this doctoral thesis is available in print at TU Wien Bibliothek.
TU WIEN Bibliothek Your knowledge hub

[228] B. Arndt, H. Noei, T. F. Keller, P. Müller, V. Vonk, A. Nenning, A. K. Opitz, J. Fleig, U. Rütt, and A. Stierle. "Structure and stability of Gd-doped CeO_2 thin films on yttria-stabilized zirconia". In: *Thin Solid Films* 603 (2016), pp. 56–61.

[229] X. Chen and T. Grande. "Anisotropic and Nonlinear Thermal and Chemical Expansion of $La_{1-x}Sr_xFeO_{3-\delta}$ (x = 0.3, 0.4, 0.5) Perovskite Materials". In: *Chemistry of Materials* 25.16 (2013), pp. 3296–3306.

[230] D. Marrocchelli, S. R. Bishop, and J. Kilner. "Chemical expansion and its dependence on the host cation radius". In: *Journal of Materials Chemistry A* 1.26 (2013), p. 7673.

[231] V. Kharton, A. Yaremchenko, M. Patrakeev, E. Naumovich, and F. Marques. "Thermal and chemical induced expansion of $La_{0.3}Sr_{0.7}(Fe,Ga)O_{3-\delta}$ ceramics". In: *Journal of the European Ceramic Society* 23.9 (2003), pp. 1417–1426.

[232] D. Marrocchelli, N. H. Perry, and S. R. Bishop. "Understanding chemical expansion in perovskite-structured oxides". In: *Physical Chemistry Chemical Physics* 17.15 (2015), pp. 10028–10039.

[233] Chen, Yu, and S. B. Adler. "Thermal and Chemical Expansion of Sr-Doped Lanthanum Cobalt Oxide $La_{1-x}Sr_xCoO_{3-\delta}$". In: *Chemistry of Materials* 17.17 (2005), pp. 4537–4546.

[234] S. Bishop, D. Marrocchelli, C. Chatzichristodoulou, N. Perry, M. Mogensen, H. Tuller, and E. Wachsman. "Chemical Expansion: Implications for Electrochemical Energy Storage and Conversion Devices". In: *Annual Review of Materials Research* 44.1 (2014), pp. 205–239.

[235] S. Wang. "High temperature properties of $La_{0.6}Sr_{0.4}Co_{0.8}Fe_{0.2}O_{3-\delta}$ phase structure and electrical conductivity". In: *Solid State Ionics* 159.1-2 (2003), pp. 71–78.

[236] H. Lein, K. Wiik, and T. Grande. "Thermal and chemical expansion of mixed conducting $La_{0.5}Sr_{0.5}Fe_{1-x}Co_xO_{3-\delta}$ materials". In: *Solid State Ionics* 177.19-25 (2006), pp. 1795–1798.

[237] S. R. Bishop, K. L. Duncan, and E. D. Wachsman. "Thermo-Chemical Expansion in Strontium-Doped Lanthanum Cobalt Iron Oxide". In: *Journal of the American Ceramic Society* 93.12 (2010), pp. 4115–4121.

[238] N. H. Perry, J. J. Kim, S. R. Bishop, and H. L. Tuller. "Strongly coupled thermal and chemical expansion in the perovskite oxide system $Sr(Ti,Fe)O_{3-\delta}$". In: *Journal of Materials Chemistry A* 3.7 (2015), pp. 3602–3611.

[239] X. Chen and T. Grande. "Anisotropic Chemical Expansion of $La_{1-x}Sr_xCoO_{3-\delta}$". In: *Chemistry of Materials* 25.6 (2013), pp. 927–934.

[240] T. Grande, J. R. Tolchard, and S. M. Selbach. "Anisotropic Thermal and Chemical Expansion in Sr-Substituted $LaMnO_3$: Implications for Chemical Strain Relaxation". In: *Chemistry of Materials* 24.2 (2011), pp. 338–345.

Die approbierte gedruckte Originalversion dieser Dissertation ist an der TU Wien Bibliothek verfügbar.
The approved original version of this doctoral thesis is available in print at TU Wien Bibliothek.
TU Bibliothek Your knowledge hub WIEN

[241] J. Fleig, G. M. Rupp, A. Nenning, and A. Schmid. "(Invited) Towards an Improved Understanding of Electrochemical Oxygen Exchange Reactions on Mixed Conducting Oxides". In: *ECS Transactions* 77.10 (2017), pp. 93–108.

[242] N. Tsvetkov, Q. Lu, L. Sun, E. J. Crumlin, and B. Yildiz. "Improved chemical and electrochemical stability of perovskite oxides with less reducible cations at the surface". In: *Nat. Mater.* 15.9 (2016), pp. 1010–1016.

[243] M. Yang, E. Bucher, and W. Sitte. "Effects of chromium poisoning on the long-term oxygen exchange kinetics of the solid oxide fuel cell cathode materials $La_{0.6}Sr_{0.4}CoO_{3-\delta}$ and $Nd_2NiO_{4+\delta}$". In: *Journal of Power Sources* 196.17 (2011), pp. 7313–7317.

[244] J. Fleig. "On the current–voltage characteristics of charge transfer reactions at mixed conducting electrodes on solid electrolytes". In: *Phys. Chem. Chem. Phys.* 7.9 (2005), pp. 2027–2037.

[245] F. S. Baumann, J. Fleig, M. Konuma, U. Starke, H.-U. Habermeier, and J. Maier. "Strong Performance Improvement of $La_{0.6}Sr_{0.4}Co_{0.8}Fe_{0.2}O_{3-\delta}$ SOFC Cathodes by Electrochemical Activation". In: *Journal of The Electrochemical Society* 152.10 (2005), A2074.

[246] J. Fleig, R. Merkle, and J. Maier. "The p(O2) dependence of oxygen surface coverage and exchange current density of mixed conducting oxide electrodes: model considerations". In: *Physical Chemistry Chemical Physics* 9.21 (2007), p. 2713.

[247] R. A. D. Souza. "A universal empirical expression for the isotope surface exchange coefficients of acceptor-doped perovskite and fluorite oxides". In: *Physical Chemistry Chemical Physics* 8.7 (2006), p. 890.

Die approbierte gedruckte Originalversion dieser Dissertation ist an der TU Wien Bibliothek verfügbar.
The approved original version of this doctoral thesis is available in print at TU Wien Bibliothek.
TU WIEN Bibliothek Your knowledge hub

List of Figures

1.1 Sketch explaining the chemical reation taking place on different types of fuel cells. Operation temperatures are taken from literature [3]. 2

2.1 a) STEM image of a platinum decorated LSF64 electrode. b) magnified TEM image of a single platinum nanoparticle on LSF64. c) FIB-TEM image of a platinum decorated LSF64 electrode. d) SEM image of pristine LSF64 electrode. e) SEM image of a platinum decorated LSF64 electrode after 16 h in 0.25 mbar O_2 at 600 °C. 10

2.2 a) Sample sketch with embedded current collecting Pt grid at the LSF64|YSZ interface and catalytically active Pt nanoparticles on top of LSF64. b) Surface composition of a platinum decorated LSF64 electrode analyzed from XPS spectra measured after heating to 600 °C for 14 hours. c) Section of the XPS spectra showing a pristine LSF64 electrode and a LSF64 electrode decorated with platinum nanoparticles. 11

2.3 (a) - (c) Impedance spectra of symmetrical samples with LSF64 electrodes measured at 600 °C in 0.25 mbar O_2 (a), 10 mbar O_2 (b) and 210 mbar O_2 (c) before and after platinum decoration. The impedance data are normalized to the active electrode area and divided by two (to reveal ASR values of one electrode). Symbols are measured data, lines are fits to the equivalent circuits shown in the insets. (d) Bar chart showing the area specific resistance of LSF64 electrodes at 600 °C before and after platinum decoration. Times written on the bars indicate degradation times. 12

2.4 a) Impedance spectra of a sample with LSF64 electrodes decorated with Pt particles, measured at different pO_2, revealing faster oxygen incorporation at lower pO_2. b) ASR vs. pO_2 on a -log/log-scale for a pristine sample with LSF64 electrodes (orange data points) from reference[25] and a sample with platinum decorated LSF64 electrodes (blue data points), all measured at 600 °C. 14

Die approbierte gedruckte Originalversion dieser Dissertation ist an der TU Wien Bibliothek verfügbar.
The approved original version of this doctoral thesis is available in print at TU Wien Bibliothek.
TU WIEN Bibliothek Your knowledge hub

2.5 a) Impedance spectra of four different LSF64 electrodes decorated with different amounts of platinum and measured at 600 °C in 10 mbar pO_2. b) Bar chart summarizing the effect of different amounts of platinum on the polarisation resistance of LSF64 electrodes. c) Surface composition of all investigated samples from a) measured by XPS. 16
2.6 Sketch explaining the suggested reaction mechanism for oxygen incorporation on a platinum decorated MIEC (a) and a pristine MIEC (b). 19
2.7 Diffraction pattern of LSF64 thin film decorated with Pt particles, measured in gracing incidence geometry (GID); LSF64 target measured in Bragg-Bretano geometry. 22
2.8 BSE images of all samples decorated with different amounts of platinum. . . 23
2.9 Results of XPS measurements on LSF64 electrodes decorated with different amounts of Pt. a) XPS spectra of La, b) XPS spectra of Pt, c) XPS spectra of Sr, d) XPS spectra of Fe. 24
2.10 Surface composition of samples with LSF64 electrodes decorated with different amounts of platinum determined by XPS measurements. 25
2.11 EIS spectra of a) a sample with STF73 electrodes in 0.25 mbar and b) with LSF64 electrodes in humidified H2 measured in 600 °C before and after Pt decoration.. 26

3.1 A) Sketch of the *i*-PLD heater. B) Sketch of the multi-layer structure of the *i*-PLD sample grown on YSZ or LSGM single electrodes. This nomenclature is identical in figures 3.1, 3.6, 3.7 and the numbers are also mentioned in the text. 31
3.2 AFM image of the measured multilayer electrodes grown on LSGM (A) and YSZ (B) with a top layer made of LSF-Pt2 (10 nm). Please note the different scale bars. 32
3.3 Diffractogram of pristine LSF (green), LSF-Pt1 (orange) and LSF-Pt2 (blue) thin films deposited on YSZ single crystals. The inset shows a magnification of the 211 reflex. 33
3.4 A) HAADF-STEM and B) TEM image of a multilayer electrode (top layer: LSF-Pt2). No exsolutions of platinum nanoparticles are visible on the electrode surface. 34
3.5 Results of ambient pressure XPS (AP-XPS) measurements on a LSF-Pt2 electrode under open circuit voltage and with polarization. Observed binding energies of platinum and distribution of the platinum oxidation states under different working electrode overpotentials η. 35

Die approbierte gedruckte Originalversion dieser Dissertation ist an der TU Wien Bibliothek verfügbar.
The approved original version of this doctoral thesis is available in print at TU Wien Bibliothek.
TU WIEN Bibliothek Your knowledge hub

3.6 Measured impedance spectra from a *i*-PLD multi-layer experiment grown on YSZ (A,C,E) and LSGM (B,D,F) single crystals. Symbols are measured data, lines are fits to the equivalent circuit shown. (A) and (B) Initial deposition of the LSF, LSF-Pt1, LSF-Pt2 electrodes (10 nm each). (C) and (D) Stepwise deactivation of a LSF-Pt2 electrode by depositing LSF on its surface. (E) and (F) Stepwise surface activation of a LSF electrode by growing LSF-Pt2 on top. The obtained area specific resistances of the electrode surface are summarized in figure 3.7. The encircled numbers refer to certain steps in the course of the *i*-PLD experiment and details of the individual steps are explained in the text. 37

3.7 Area specific resistance of *i*-PLD multi-layer electrodes grown on YSZ (triangles, top row) and LSGM (squares, bottom row) calculated from the spectra shown in figure 3.6. Green symbols and lines display deposition of LSF, blue symbols and lines display deposition of LSF-Pt2, orange symbols and lines display deposition of LSF-Pt1. 40

3.8 (A) Surface-ASR of LSF (green) and LSF-Pt2 (blue) (two different samples) versus the oxygen partial pressure plotted as log/log diagram. The numbers next to the symbols are the mean ASR values in Ωcm^2. Lines are a guide for the eye. (B) Area specific resistance plotted versus inverse temperature for LSF (green), LSF-Pt2 deposited on top of LSF (blue) and LSC (grey). Data for LSC are taken from reference[95] for comparison. 41

3.9 A) Degradation behaviour of LSF and LSF-Pt2 during *i*-PLD measurements at 600 °C in synthetic air. B) AFM image of a pristine LSF-Pt1 electrode directly after PLD deposition C) AFM image of a LSF-Pt1 electrode annealed for 16 h in synthetic air at 600 °C. The inset in figure B), C) shows the observed surface composition with platinum measured with XPS. 48

3.10 *ex-situ* XPS measurements (1) pristine LSF-Pt1 (2) pristine LSF-Pt1 heated up to 450 °C in UHV chamber directly before XPS measurements (3) LSF-Pt1 annealed for 16 h in synthetic air, (4) LSF-Pt1 annealed for 16 h in synthetic air, heated up to 450 °C in UHV directly before XPS measurements. 49

3.11 Calculated surface composition from *Ex-situ* XPS measurements on (1) pristine LSF-Pt1 (2) pristine LSF-Pt1 heated up to 450 °C in UHV chamber directly before XPS measurements (3) LSF-Pt1 annealed for 16 h in synthetic air, (4) LSF-Pt1 annealed for 16 h in synthetic air, heated up to 450 °C in UHV directly before XPS measurements. 50

3.12 A) SEM image of a pristine LSF-Pt1 electrode directly after deposition B) SEM image of a LSF-Pt1 electrode, which was annealed for 16 h at 600 °C in synthetic air. C) AFM image of a pristine LSF-Pt1 electode directly after deposition D) AFM image of a LSF-Pt1 electrode,which was annealed for 16 h in synthetic air. 51

Die approbierte gedruckte Originalversion dieser Dissertation ist an der TU Wien Bibliothek verfügbar.
The approved original version of this doctoral thesis is available in print at TU Wien Bibliothek.
TU WIEN Bibliothek Your knowledge hub

3.13 Platinum grid used for electrode contacting. Images from reflected light and secondary electron microscope. 51
3.14 Surface composition of a LSF-Pt2 electrode measured at 600 °C and 1 mbar O_2 52
3.15 Distribution of the platinum oxidation states at OCV and upon application of -300 mV and +300 mV of overpotential. 52

4.1 Sketch of the *i*-PLD setup (l.h.s) and the AP-XPS setup (r.h.s) with simultaneous electrochemical characterization. 57
4.2 A) Surface-related polarization resistance of the investigated electrodes, determined by *i*-PLD measurements, plotted over the electrode thickness. At first, 40 nm of LSC were deposited, followed by different other electrode materials (LSF (green), Pt doped LSF (orange), STF (pink) and PCO (purple)). B), C) Bar charts of calculated area specific surface resistances of the electrodes at 0.04 mbar and 1000 mbar O_2. 58
4.3 Electrode surface resistances from the present study at 0.04 mbar and 1000 mbar O_2 compared with values from figures published in literature: PCO [44, 205, 206] STF [37, 40] LSF [21, 28, 112] LSC [26, 75, 95, 207]. Numbers next to the resistance values in the plot indicate the oxygen partial pressure in mbar, at which the respective electrodes were measured. 59
4.4 Surface related polarization resistance of an LSC electrode (blue rectangles) measured first by *i*-PLD and subsequently during AP-XPS. Red triangles represent sulfur oxide species detected on the surface of the electrode (in SO_4^{x-} per (surface) unit cell of the perovskite.) 61
4.5 Spectra of the binding energy area of O1s and S2p at different conditions during AP-XPS measurements. 63
4.6 A) Surface related polarization resistance of LSC and PCO electrodes measured in the *i*-PLD in synthetic air, in an *ex-situ* measurement setup in synthetic air, and *ex-situ* with purified synthetic air. Values are shown for pristine electrodes and the same electrodes annealed for 10 h at 600 °C in the corresponding gas ("degraded"). B) Sulfur compounds found in the measurement feed gas by ICP-MS measurements without purification, after purification with the described setup, and after being passed through the PLD chamber. . 64
4.7 Sketch showing how adsorption of SO_4^{x-} on a LSC electrode surface hamper oxygen adsorption by a) steric effects and b) by a charge transfer from the electrode to sulfate adsorbates (b) thus forming a space charge beneath. . . . 67
4.8 Linear correlation between the S 2p peak area (relative to La + Sr + Co) plotted versus the O 1s (SO_4) area (relative to La + Sr + Co). The observed slope corresponds well with the stoichiometric ratio of SO_4 70
4.9 Spectra in the Sr 3d binding energy region of the LSC electrode. 70

Die approbierte gedruckte Originalversion dieser Dissertation ist an der TU Wien Bibliothek verfügbar.
The approved original version of this doctoral thesis is available in print at TU Wien Bibliothek.
TU WIEN Bibliothek Your knowledge hub

4.10 Spectra of O 1s and S 2p binding energy of an LSC and PCO electrode directly after *i*-PLD measurements. 71
4.11 Analysis of powder scraped from the PLD wall. 72

5.1 Sample sketch showing the morphology of LSF electrodes grown on YSZ, LSGM and YSZ-GDC. Lattice parameters of substrates are taken from literature. [174, 227, 228] 77
5.2 a) θ-2θ scans of LSF on LSGM, YSZ-GDC and YSZ showing oriented growth on LSGM and GDC/YSZ and polycrystalline growth on YSZ b)Reciprocal space map of an LSF thin film (50 nm) grown on LSGM. 78
5.3 AFM images of LSF thin films grown on LSGM, YSZ-GDC and YSZ. Please note the different height scale bars for LSF thin films grown on LSGM and YSZ-GDC vs. LSF thin films grown on YSZ. 78
5.4 Impedance spectra (Nyquist plot) of LSF thin films after 2000 and 6000 pulses of LSF deposited on the different substrates LSGM, YSZ-GDC and YSZ, measured at 600 °C in 0.04 mbar O_2. The inset displays the equivalent circuit used for fitting; CPE = constant phase element. $R_1||CPE_1$ was only required for some of the spectra. The oxygen exchange reaction (OER) resistance R_2 was analyzed in more detail. 79
5.5 Thickness dependent area-specific oxygen exchange resistance (ASR) of dense LSF thin films on LSGM, YSZ/GDC and YSZ substrates measured by *i*-PLD, at 600 °C and 0.04 mbar oxygen partial pressure. Lines are a guide to the eye. 80
5.6 A) pO_2 dependence of the area specific oxygen exchange resistance of polycrystalline LSF (purple) compared with LSF grown in epitaxial structure on GDC (red) at 600 °C. B) Determination of the activation energy at an oxygen partial pressure of 0.04 mbar of epitaxial LSF (grown on LSGM (orange) and GDC (red)) and polycrystalline LSF (purple). 81
5.7 A) HRTEM image of the interface region between LSGM and LSF B) HRTEM image of the LSF thin film (surface near region visible). 82
5.8 A) Lattice parameter in the *in-plane* (100) direction 5 nm from the LSGM interface (blue) and 35 nm from the LSGM interface (orange). B) Lattice parameter in the *out-of-plane* (010) direction 5 nm from the LSGM interface (blue) and 35 nm from the LSGM interface (orange). 83
5.9 EDX line scan of a LSF thin film grown on a LSGM substrate with a Pt protection layer. 83

Die approbierte gedruckte Originalversion dieser Dissertation ist an der TU Wien Bibliothek verfügbar.
The approved original version of this doctoral thesis is available in print at TU Wien Bibliothek.
TU WIEN Bibliothek Your knowledge hub

5.10 a) Lattice parameters of LSF obtained from literature [229] (powder diffraction) B) Comparison of the *in-plane* and *out-of-plane* lattice parameters of LSF grown on LSGM measured by HRTEM with the lattice parameter of LSF grown on YSZ measured by XRD are shown. C) Comparison of the lattice volume of polycrystalline vs. epitaxial grown LSF and the measured ASR. . . 84
5.11 A) Calculation of defect concentrations and inverse reaction rates of LSF for different values of ΔH_{ox}; calculation of the concentration amended activation energy ($E_a^{conc.}$) and simulation of the increase of the concentration contribution to the reaction rate (ASR ~ $1/k_q$), B) Sketch explaining the conducted calculations 88
5.12 Area-specific resistance of a dense LSF thin film electrode grown on YSZ/GDC. Straight lines are a guide to the eye. 90
5.13 FFT analysis of LSF thin film. Red circles in the FFT patterns highlights the half-integer reflections indicating the presence of the brownmillerite phase. 91
5.14 Rietveld analysis of LSF thin film grown on YSZ. Red line: XRD recorded in GID geometry, Blue line: Rietveld refinement Green line: background 92

6.1 Sketch of the multilayer sample applied for *i*-PLD measurements. Sketch of the *i*-PLD measurement setup. 96
6.2 A) Resistance ratio compared to pure PCO10 after decoration with acidic oxides (TiO_2, SnO_2); B) Resistance ratio compared to pure PCO10 after decoration with basic oxides (SrO, CaO); All measurements were conducted at 600 °C and 0.04 mbar O_2. C) Resistance ratio compared to pure PCO10 after decoration with the respective binary oxides plotted versus the Smith acidity[104] D) Graphic displaying that a "reset" of the polarization resistance to initial values is possible after decorating the electrode surface with 2 ML of the respective binary oxides by depositing 20 nm of PCO10. 97
6.3 A) Impedance spectra of a PCO10 electrode decorated with increasing amounts of TiO_2. B) Impedance spectra of a PCO10 electrode decorated with increasing amounts of SrO. C) Equivalent circuit used for fitting the spectra shown in A) and B). Lines shown are fits conducted with the equivalent circuits shown. 98
6.4 A) pO_2 dependence of the polarization resistance on pure and decorated PCO10 electrodes at 600 °C B) Determination of the activation energy on pure and decorated PCO10 electrodes at 0.04 mbar O_2 99

Die approbierte gedruckte Originalversion dieser Dissertation ist an der TU Wien Bibliothek verfügbar.
The approved original version of this doctoral thesis is available in print at TU Wien Bibliothek.
TU WIEN Bibliothek Your knowledge hub

6.5 A) Pr^{4+}/Pr^{3+} ratio on PCO10 pure, PCO10 decorated with 2 ML SrO, PCO10 decorated wit 2 ML SnO_2 at OCV, under cathodic bias (-0.4 V) and under anodic bias (0.4 V) B) Polaron area on PCO10 decorated with 2 ML SnO2 or 2 ML SrO under OCV and cathodic (-0.4 V) and anodic polarisation (0.4 V) C) Difference between oxygen gas phase and O 1s bulk binding energy of pure PCO10, PCO10 decorated with 2 ML SnO_2, PCO10 decorated with 2 ML SrO and PCO10 decorated with 2 ML SrO and contaminated with sulphur D) Surface potential measured correlated with the Smith acidity. 102

6.6 Sketch explaining the possible different effects of surface decoration on the PCO10 electrode. It affects directly the surface potential at the site of the decorations χ_0, d, but also slightly extends its effect electrostatically along the free surface χ_0, f. 105

6.7 Sketch explaining the effect of surface decoration on the surface potential. Smith acidity of the binary oxides deposited compared to the PCO10 electrode. Data taken from [45]. 106

Die approbierte gedruckte Originalversion dieser Dissertation ist an der TU Wien Bibliothek verfügbar.
The approved original version of this doctoral thesis is available in print at TU Wien Bibliothek.
TU WIEN Bibliothek Your knowledge hub

Acknowledgements

After four exciting years at the research group "Festkörperelektrochemie" and eight years at TU Wien my journey at university finally comes to an end. I am glad to look back to three busy, but also very successful, exciting, instructive and eventful years during my PhD with only the cancellation of almost all conferences being the major downside. In the following I would like to express my gratitude all people that supported me in the past years.

First of all, I would like to thank Juergen for giving me the possibility to conduct my PhD thesis in his research group, for always taking the time to discuss my measurement results with me and for spending hours reading and correcting my manuscripts. Of course, I also would like to express my gratitude to Markus and AlexO for all the hours spent explaining me many concepts of solid state ionics and all their helpful comments regarding conducting my measurements or writing my manuscripts.

I also would like to thank Christoph Rameshan for allowing me to conduct measurements at his AP-XPS and Andreas Limbeck for offering me funding from the FWF online-LASIL project.

Secondly, I really would like to thank Matthäus for the close cooperation in the last years. You definitely sparked my enthusiasm for understanding the OER mechanism on the MIEC electrode surfaces. Thanks for introducing me to the *i*-PLD technique, designing and conducting many measurements with me and for the many hours we spent together trying to understand our (strange) measurement results. I could not imagine a better colleague to work with!

A big thanks also goes to Claudia, Harald and AlexS for sharing the office room with me (the coldest and darkest room on the floor) and the many interesting (both scientific and non-scientific) talks we had. I also would like to thank AlexS for the many hours he took explaining me the defect chemistry of LSF and its interplay with the OER reaction.

Also many thanks to AndiN for conducting many AP-XPS measurements with me and for always having a solution when I encountered a problem in the lab, Tobias for constructing fancy measurement equipment (especially thanks for the quartz balance), Christin for being the organized person in the *i*-PLD project, always remembering all appointments and having

Die approbierte gedruckte Originalversion dieser Dissertation ist an der TU Wien Bibliothek verfügbar.
The approved original version of this doctoral thesis is available in print at TU Wien Bibliothek.
TU WIEN Bibliothek Your knowledge hub

notes about all experiments in her lab book, Joseph for a lot of senseless fun conversation, AndiB for cutting me a FIB lamaelle - which saved my fourth publication - and Martin for his funny humor, when something was again not working in our research group.

Finally I would like to thank my parents and my brothers for their continuous support over the last years. In the end, also my girlfriend Jimena - despite not understanding my passion for the oxygen exchange reaction - deserves my deep gratitude for her support and understanding in the last years, especially for the many hours I spent working "in her time" on my thesis in the evenings and weekends.

Die approbierte gedruckte Originalversion dieser Dissertation ist an der TU Wien Bibliothek verfügbar.
The approved original version of this doctoral thesis is available in print at TU Wien Bibliothek.
TU WIEN Bibliothek Your knowledge hub